Alkaloids and Diarylheptanoids of *Hippobroma longiflora* and *Pellacalyx saccardianus*: Structure and Bioactivity

Chan Zi Yang

School of Pharmacy

University of Nottingham Malaysia

Thesis submitted to the University of Nottingham for the Degree of Doctor of Philosophy

July 2020

Preface

This thesis is submitted for the degree of *Doctor of Philosophy* at the University of Nottingham. The study herein was conducted under the supervision of Dr. Lim Kuan Hon and Prof. Ting Kang Nee of the Faculty of Science and Engineering, University of Nottingham Malaysia.

This work is to the best of my knowledge original, except where acknowledgement and references are made to previous studies. This thesis has not been submitted for any degree and is not concurrently submitted in candidature of any other degree.

Part of this work has been presented in the following publication:

Chan, Z. Y.; Govindaraju, K.; Krishnan, P.; Low, Y. Y.; Chong, K. W.; Yong, K. T.; Ting, K. N.; Lim, K. H. *Phytochem. Lett.* **2019**, *30*, 93–98.

Acknowledgements

I would like to express my deepest gratitude to the following people for their continual support throughout my research.

Dr. Lim Kuan Hon, my academic supervisor has offered me valuable advice and guidance. He granted me resources that made this research feasible. Besides, I am grateful to my co-supervisor, Prof. Ting Kang Nee and her team, Dr. Lee Mei Kee and Dr. Kayatri Govindaraju for conducting the antispasmodic bioassays. I am also indebted to my senior colleague, Mr. Premanand Krishnan, who assisted me in the acquisition of materials and apparatus.

I would like to thank our collaborators from the University of Malaya for their assistance in acquiring most of the spectroscopic data. My deepest appreciation goes to Prof. Kam Toh Seok, Dr. Low Yun Yee, Dr. Lim Siew Huah and fellow PhD graduates Dr. Dawn Sim, Dr. Chong Kam Weng as well as PhD student Mr. Wong Soon Kit (Department of Chemistry, Faculty of Science, UM). In particular, I would like to acknowledge Dr. Low Yun Yee for performing the X-ray crystallography analyses. I am also grateful to Dr. Yong Kien Thai (Institute of Biological Sciences, Faculty of Science, UM) who identified the plant specimens of this research.

I sincerely acknowledge Dr. Mai Chun Wai, Dr. Hii Ling Wei and Dr. Leong Chee Onn from the Department of Life Sciences and the Department of Pharmaceutical Chemistry, School of Pharmacy, International Medical University (IMU), who conducted the cytotoxic bioassays.

My appreciation also goes to a few undergraduate students (School of Pharmacy, University of Nottingham Malaysia) who were involved in parts of my research. They are Mr. Sayed Mohammadhossein Modaresi, Mr. Kevin Zhan Song Ming, Ms. Gan Shang Yen and Ms. Leong Zi Xin.

Last but not least, I am grateful to my parents, my partner and my friends for their unceasing support and encouragement. For those I might have left out inadvertently, I offer my apologies.

Abstract

Plant secondary metabolites such as alkaloids and diarylheptanoids play a crucial role in drug discovery due to their high structural diversity and useful biological activity. The present research aims to isolate and elucidate bioactive alkaloids and/or diarylheptanoids from two understudied Malaysian angiosperms, i.e., *Hippobroma longiflora* (L.). G. Don. (Campanulaceae) and *Pellacalyx saccardianus* Scort. (Rhizophoraceae). *H. longiflora* is a naturalised herb with ethnobotany suggestive of neuroactive alkaloids, while *P. saccardianus* is a rainforest tree that exhibited remarkable cytotoxic activity.

Phytochemical investigation into the whole plant of *H. longiflora* yielded three new diphenethylpiperidine alkaloids, hippofoline A (**1**), hippofoline B (**2**) and (–)-*cis*-2′,2′′-diphenyllobelidiol *N*-oxide (**5**), along with two known alkaloids (–)-lobeline (**3**) and (–)-cis-2′,2′′-diphenyllobelidiol (**4**). The absolute configurations of alkaloid **1** and **2** were established based on experimental and calculated ECD data, while those of **3** and **4** were confirmed by X-ray crystallography. Alkaloids **2** – **4** were shown to induce concentration-dependent relaxation effects on rat isolated tracheal segments that were pre-contracted with carbachol, with **3** being especially potent (EC_{50} 1.2 ± 0.2 nM). The antispasmodic activity of alkaloids **2** – **4** was postulated to involve the antagonism of muscarinic acetylcholine receptors. This novel pharmacological aspect justifies the diphenethylpiperidine alkaloids as antispasmodic drug leads.

From the leaves and bark of *P. saccardianus*, seven new nortropane alkaloids were characterised, i.e., 3α-cinnamoyloxy-*N*-phloretoylnortropane (**6**), 3α-cinnamoyloxy-*N*-formylnortropane (**7**), 3α-phenylacetoxy-*N*-formylnortropane (**8**), 3α-

benzoyloxy-*N*-formylnortropane (**9**), 3α-acetoxy-*N*-formylnortropane (**10**), (±)-bissaccardine (**13**) and (±)-trissaccardine (**14**). Their chemical structures (including the relative configuration of **13**) were elucidated by comprehensive spectroscopic analyses. Two known nortropane alkaloids, 3α-cinnamoyloxynortropane (**11**) and 3α-benzoyloxynortropane (**12**), were co-isolated in high yields. Through semi-synthesis experiments, the novel oligomers **13** and **14** were deduced to be natural aza-Michael adducts of the monomer **11**. Alkaloids **13** and **14** also exhibited potent cytotoxicity towards a panel of pancreatic cancer cell lines (AsPC-1, SW1990, BxPC-3 and PanC-1), with IC_{50} values ranging from 1.13 – 10.85 μM. The unprecedented discovery of the cytotoxic tropane alkaloids **13** and **14** was highlighted. Additionally, alkaloids **6**, **9**, and **11** – **13** were shown to induce weak relaxation effects on rat isolated tracheal rings that were pre-contracted with carbachol. Analyses of their structure activity relationships with respect to antimuscarinic activity (atropine as positive control) suggested plausible weak receptor-binding interactions that may diminish antispasmodic activity.

On the other hand, two pairs of enantiomeric diarylheptanoid-phenylpropanoid adducts bearing a cyclohexenone core, (±)-saccardianones A and B (**15** and **16**), an alkaloidal diarylheptanoid-phenylpropanoid adduct bearing a 4-piperidone core (±)-saccardianine A (**17**), a pair of enantiomeric dimeric diarylheptanoid alkaloids bearing a tetrahydropyridine core, (±)-saccardianine B (**18**), a suspected degradation product, saccardianine C (**19**), together with a diarylheptanoid derived spirocompound, pellaspirone (**20**), and a diarylheptanoid-rutinoside, saccardianoside (**21**) were obtained and characterised from the leaves of *P. saccardianus*. Two known diarylheptanoids, platyphyllenone (**22**) and (±)-5-hydroxy-1,7-bis-(4-hydroxyphenyl)-3-heptanone (**23**) were co-isolated in high

yields. The relative configuration of **15** was elucidated by X-ray crystallography, while that of **18** was determined by NOESY analysis. The absolute configuration of **21** was determined by chemical derivatisation coupled to HPLC and spectroscopic analyses. Through semi-synthesis experiment, **20** was deduced to be an experimental artifact. The biogenetic pathways of **15** – **18** were proposed with **23** as a common precursor, which underwent aldol condensation and/or transamination steps to afford the novel alicyclic cores. Compounds **16** and **20** exhibited moderate but selective cytotoxicity towards pancreatic AsPC-1 (IC_{50} 15.47 μM) and breast MDA-MB-231 (IC_{50} 13.32 μM) cancer cell lines, respectively.

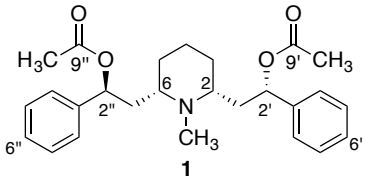

1

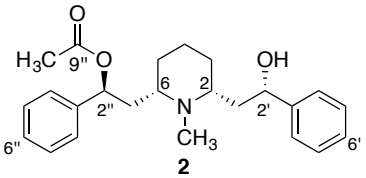

2

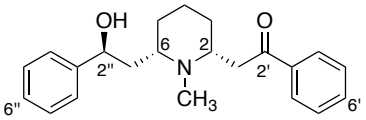

3

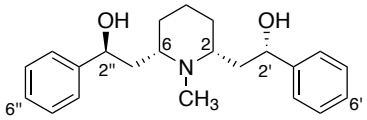

4

5 *N*-oxide

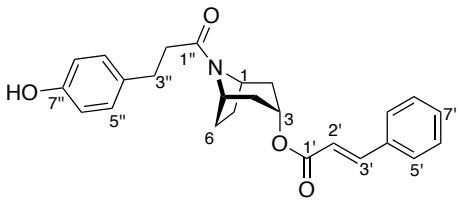

6

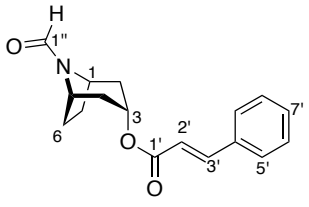

7

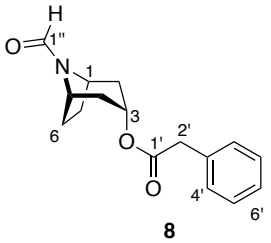

8

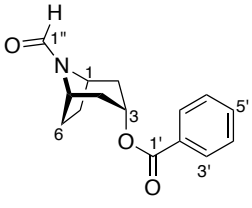

9

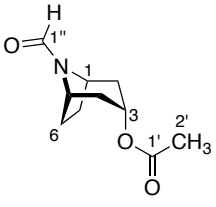

10

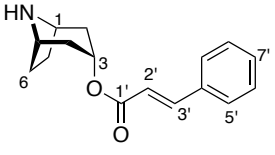

11

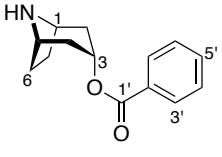

12

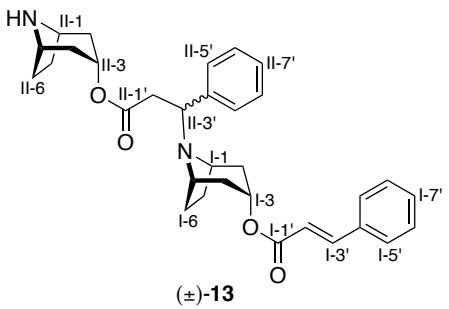

(±)-**13**

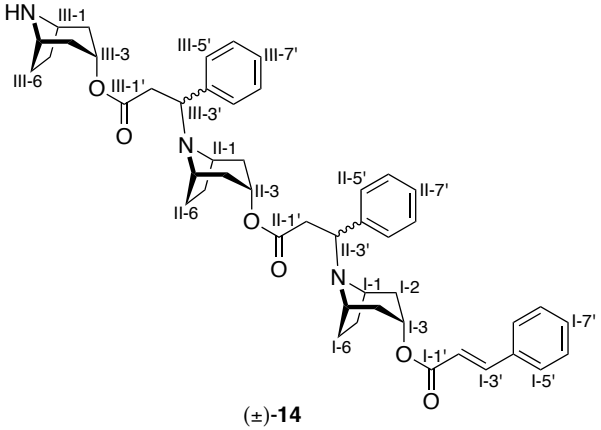

(±)-**14**

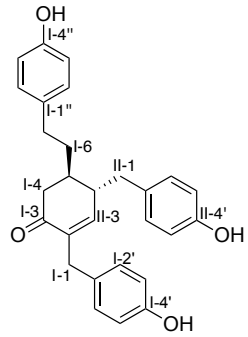

(±)-**15**

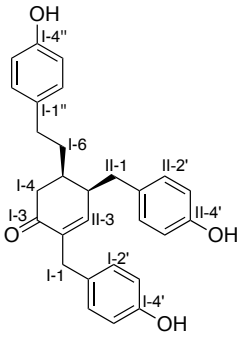

(±)-**16**

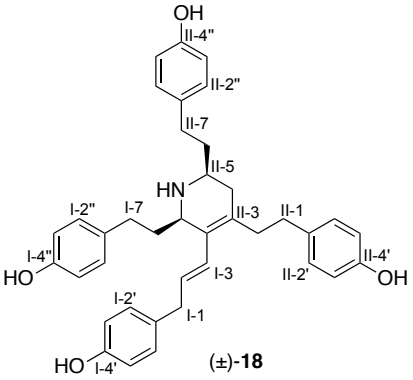

(±)-**18**

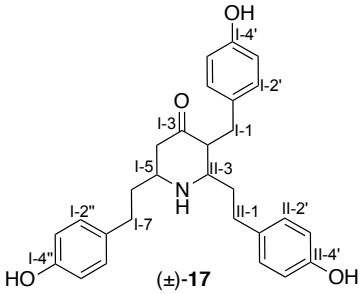

(±)-**17**

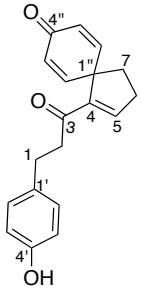

20

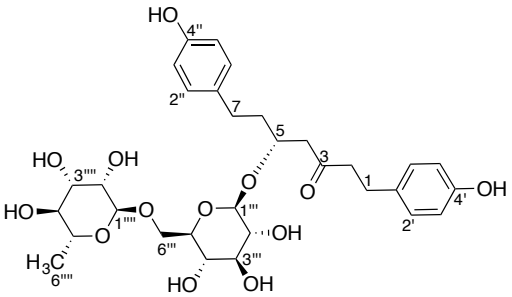

21

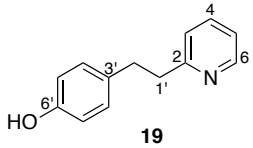

19

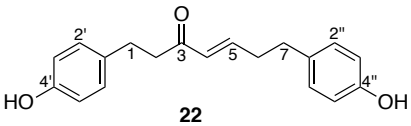

22

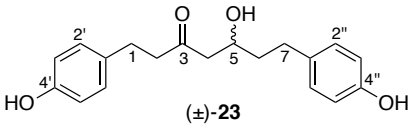

(±)-**23**

Table of Contents

List of Abbreviations

Ar	aryl group
ACh	acetylcholine
ACN	acetonitrile
br	broadened (NMR signal)
CD_3OD	deuterated methanol
$CDCl_3$	deuterated chloroform
$(CD_3)_2CO$	deuterated acetone
$CHCl_3$	chloroform
COSY	Correlation Spectroscopy
CTLC	Centrifugal Thin Layer Chromatography
c	concentration
ca.	*Circa*, approximately
cm	centimeter
CRC	Concentration Response Curve
d	doublet
dd	doublet of doublets (NMR multiplicity)
dt	doublet of triplets (NMR multiplicity)
DCM	dichloromethane
DEA	diethylamine
DMEM	Dulbecco's Modified Eagle's medium (cell culture)
DMSO	dimethylsulfoxide
ECD	electronic circular dichroism
E_{max}	maximal efficacy
EC_{50}	half maximal effective concentration
EtOH	ethanol
Et_2O	diethyl ether
EtOAc	ethyl acetate
e.g.	*exempli gratia*, for example
etc	*et cetera*, and so forth
Fig.	Figure
HCl	hydrochloric acid
HPLC	High Pressure Liquid Chromatography
HMBC	Heteronuclear Multiple Bond Correlation Spectroscopy
HRESIMS	High Resolution Electron Spray Ionisation Mass Spectrometry
HRDARTMS	High Resolution Direct Analysis in Real Time Mass Spectrometry
HSQC	Heteronuclear Single Quantum Coherence Spectroscopy
Hz	Hertz
h	hour
IC_{50}	half maximal inhibitiory concentration
IR	Infrared
IUPAC	International Union of Pure and Applied Chemistry
i.e.	*id est*, namely

J	coupling constant
kg	kilogram
L	litre
m	multiplet (NMR multiplicity)
M	Molar
mp	melting point
m/z	mass-to-charge ratio
Me	methyl
MeOH	methanol
MHz	megahertz
mAChR	muscarinic acetylcholine receptor
mL	mililitre
mM	milimolar
min	minute
NaOH	sodium hydroxide
NMR	Nuclear Magnetic Resonance
NOESY	Nuclear Overhauser Effect Spectroscopy
nAChR	nicotinic acetylcholine receptor
nm	nanometer
nM	nanoMolar
OH	hydroxyl group
ppm	parts per million
PDA	photodiode array
PSL	*Pellacalyx saccardianus* Leaf (crude extract code)
PSB	*Pellacalyx saccardianus* Bark (crude extract code)
PSF	*Pellacalyx saccardianus* Fraction (chromatograpy fraction code)
q	quartet (NMR multiplicity)
RPMI	Roswell Park Memorial Institute (cell culture medium)
R_f	retention factor
R_t	retention time
rtp	room temperature and pressure
s	singlet (NMR multiplicity)
sp.	unspecified species
spp.	several species
sx	sextet (NMR multiplicity)
SEM	standard error of the mean
SD	standard deviation
t	triplet (NMR multiplicity)
THF	tetrahydrofuran
TLC	Thin Layer Chromatography
TMS	tetramethylsilane
UV	ultraviolet
viz.	*videlicet*, which is

List of Figures

List of Tables

List of Appendices

Chapter 1: Introduction

1.0 Chapter Overview

Natural products can be defined as any chemical substances produced by a living organism that can be purified and isolated. Throughout the course of human evolution, natural products have been extensively exploited as food, medicine, entheogen and poison. Owing to their immense structural diversity, natural products provide important chemical leads for drug discovery. The 2015 Nobel Prize in medicine was awarded for the discoveries of two natural products, avermectin and artemisinin, which offered cure for parasitic diseases affecting hundreds of millions of people annually. Currently in the fight against the COVID-19 coronavirus pandemic, small molecule natural products such as emodin[1] (anthraquinone), colchicine[2] (alkaloid) and ivermectin[3] (macrolide) emerge as antiviral or immunomodulatory drugs. Plant based natural products are particularly diverse and bioactive. Of interest for this research, *Hippobroma longiflora* and *Pellacalyx saccardianus* are two understudied plant species that elaborate valuable natural products, namely, alkaloids and diarylheptanoids.

In Chapter 1, an overview of the phytochemistry of alkaloids is outlined in Section 1.1. In Section 1.2, specific focus is given to the chemistry and the neuropharmacology of lobeline (**3**), since **3** is a bioactive piperidine alkaloid of *H. longiflora*. Subsequently, Sections 1.3 and 1.4 provide a general review on tropane alkaloids and diarylheptanoids, which are known to occur in *P. saccardianus*. Notably, Sections 1.3.2, 1.3.3 and 1.4.3 highlight the immense structural diversity of the tropane alkaloids and diarylheptanoids reported to date, which enables valuable comparison to the novel compounds obtained in the present study.

Finally, the two plant species investigated in the present study are detailed in Sections 1.5 and 1.6, with emphasis on their understudied phytochemistry along with the associated biological activity and research gaps.

1.1 Alkaloids

1.1.1 Introduction and History

Alkaloids are secondary metabolites that occur naturally in plants and fungi, but to a lesser extent can be found in some animals, sea sponges and bacteria. Alkaloids are generally defined as heterocyclic organic molecules containing one or more nitrogen atoms.[4,5] The word alkaloid is derived from 'alkali', eluding to its general ability to act as a chemical base. Many alkaloids have pronounced physiological effects, leading to their use in modern medicine. The expression of alkaloids is scattered across the evolutionary tree. Not all organisms produce alkaloids, as most alkaloids can only be found in specific taxa of organism. True to secondary metabolites, alkaloids are not directly essential to an organism's survival or reproduction. It is widely accepted that living organisms produce alkaloids as chemical defence against predators because alkaloids are generally poisonous. In some remarkable instances, innocuous organisms such as grasses of the genus *Lolium* enhance their survival fitness by harbouring symbiotic relationship with endophytic fungi (*Neothypodium* spp.) that produce anti-herbivorous pyrrolizidine alkaloids (loline).[6] On the other hand, other researchers suggested that plant alkaloids serve as transport or storage molecules for certain organic acids.[4] Some alkaloids like strychnine was even shown to confer cytoprotective effects by quenching singlet oxygen.[4,7] Considering the huge diversity of alkaloids in the

kingdom of life, no common functions of alkaloids can be easily identified. The biochemical roles of alkaloids remain debatable.

Since early human history, plant alkaloids were widely exploited as herbal remedies, psychedelic drugs and poisons. The Sumerians had been cultivating opium poppy for its painkilling effect since 3,400 B.C.[4] Early Italian ladies instilled plant juices containing atropine to dilate their pupils. Numerous plants and fungi containing alkaloids are also taken during tribal rituals to produce psychotropic effects. The famous South American entheogenic brew Ayahuasca is actually a mixture of two plants, one containing tryptamine alkaloids (from *Psychotria viridis*), while the other contains beta-carboline alkaloids (from *Banisteriopsis caapi*).[8] This combination of alkaloids acts synergistically to produce a hallucinogenic effect, but would otherwise be ineffective if taken individually.[8] It remains a mystery as to how the ancient tribesman discovered the effects of Ayahuasca. Besides, plant alkaloids have long been indicated as poisons in hunting, murders or accidental mass poisonings. The neuromuscular blocking drug tubocurarine was initially discovered from poison arrows made from a South American vine, *Chondrodenron tomentosum.*[4,5] The controversial philosopher Socrates was executed by a decoction made of the poison hemlock plant (*Conium maculatum*).[4,5] Accidental ingestion of cereals contaminated by ergot alkaloids produced by fungi such as *Claviceps purpurea* resulted in epidemics of poisonings throughout human history, often attributed to supernatural forces.[4,9] Ironically, the same vasoconstricting effect of ergot alkaloids that caused dry gangrenes were later exploited as anti-migraine drugs.

It was not until the nineteenth century that Friedrich Sertürner, a German chemist first isolated an alkaloid he named morphine from opium in 1816.[4] Other

alkaloids were subsequently isolated, including strychnine (in 1817), caffeine (in 1819) and quinine (in 1820), predominantly by two French chemists Pierre Pelletier and Joseph Caventou.[4] Simple alkaloid structure like that of coniine was first elucidated by Hugo Schiff in 1870 via chemical degradation studies, followed by its total synthesis in 1889.[4] Complex alkaloid structures like that of strychnine would continue to elude chemists for many years until the twentieth century, when modern spectroscopic techniques were in place. Notably, the structure of strychnine (once regarded as a chemical impossibility, Table 1.2) was finally elucidated by Robert Robinson in 1946 and confirmed by Robert Woodward in 1947, with more than 400 publications attributed to the subject matter.[10] Woodward later achieved the total synthesis of strychnine in 1954.[10] For their work in elucidating the structures of complicated alkaloids, Robinson and Woodward were each awarded the Nobel Prize in Chemistry in 1947 and 1965, respectively. Since then, tens of thousands of alkaloids were discovered from natural sources.

1.1.2 Chemical and Physical Properties

Most alkaloids exist as crystalline solids at room temperature and pressure, with the exception of nicotine and hyoscine, which are oily liquids in their free-base form.[4,5] Alkaloids usually appear white or colourless, but may be intensely coloured when they contain multiple conjugated systems, e.g., sanguinarine.[4] Many alkaloids like strychnine and quinine are very bitter in taste, probably a result of evolutionary chemoreception as a warning for poison.[11] An alkaloid may occur naturally in plants in the form of a free-base, salt (of an acid), amide or *N*-oxide. The solubility of alkaloids varies depending on their molecular structure as well as the ionisation and oxidation state. In general, most alkaloids in their free-base form

are soluble in organic solvents, while alkaloid salts and alkaloid *N*-oxides are preferentially soluble in water.

The chemistry of alkaloids is predominantly accentuated in the electron lone pair of its nitrogen atom. In a broader sense, an alkaloid can be considered as a molecule containing one or more amine functions. There are currently known alkaloids with primary (e.g., mescaline), secondary (e.g., ephedrine), tertiary (e.g., atropine) and quaternary (e.g., muscarine) amine group (Table 1.1, Table 1.2). Primary, secondary and tertiary alkaloids can undergo acid-base reaction to produce a salt, viz., protonated amine. In contrast, the nitrogen atom of a quaternary alkaloid carries a permanent positive charge and is non-basic. Some alkaloids also contain an amine function that is π-conjugated, which significantly decreases its basicity. In a similar effect, alkaloids with an amide function such as piperine and colchicine (Table 1.2) are essentially non-basic. The amine function of alkaloids can act as a nucleophile and participate in intermolecular and/or intramolecular condensation reactions, e.g., Mannich reaction. The Mannich reaction occurs when an iminium ion (formed via nucleophilic attack of an amine to an activated carbonyl group) undergoes an electrophilic addition with an enol function. This is a crucial step in the biogenetic pathways of many alkaloids (Fig. 1.4b, Fig. 1.8).[5,17]

Tertiary alkaloids are liable to oxidation into *N*-oxides, which may arise as artifacts due to prolonged exposure to oxygen and light. All alkaloid *N*-oxides contain the functional group R_3-N^+-O^-. As a result, they are highly polar and mostly insoluble in organic solvents. The physical, chemical, spectroscopic and pharmacological properties of alkaloid *N*-oxides may differ significantly from the parent alkaloid. However, the highly polar property of alkaloid *N*-oxides often

precludes their isolation by conventional extraction procedures using organic solvents.

1.1.3 Chemical Tests for Alkaloids

Many alkaloids produce insoluble precipitates with heavy metal or triiodide complexes, useful as qualitative or quantitative tests for alkaloids. The precipitated alkaloids may be amorphous or crystalline solids. Examples include the Meyer's reagent (potassium iodomercuric chloride) and the Wagner's reagent (iodine in potassium iodide), which produce white or yellowish precipitates with most alkaloids.[4] The latter was historically used to quantify the concentration of caffeine in tea extracts.[12] On the other hand, more sensitive alkaloid precipitating reagent such as the Dragendorff's reagent is used as a spray to detect alkaloids in planar chromatography such as TLC. The Dragendorff's reagent provides an alkaloid detection range of 0.01 – 1.0 μg.[13] It contains a mixture of bismuth oxynitrate in acidified potassium iodide solution, affording bismuthtetraiodide ions (BiI_4^-).[4,13] Most secondary and tertiary alkaloids will be protonated under the acidic environment and produce bright red or orange precipitates by complexing with BiI_4^-. It should be noted that primary alkaloids, amino acids, as well as alkaloids that do not contain basic amine groups seldom stain or stain poorly with the Dragendorff's reagent. Furthermore, the non-specificity of the Dragendorff's reagent should be cautioned. Purine alkaloids such as caffeine do not stain under the Dragendorff's reagent whereas organic compounds containing conjugated ketones or lactone groups (e.g., chalcones and cardiac glycosides) may stain prominently.[14] False-positive stains of the Dragendorff's reagent tend to decolourise over time, typically less than 24 hours on standing (personal observation). Last but not least, many alkaloids tend to form insoluble crystalline

salts with picric acid (Hager's reagent) and picrolonic acid, both of which are polynitrated phenols.[15] These reagents offer the advantage of recovering the original alkaloid by warming the precipitate with diluted sulfuric acid.[15]

1.1.4 Alkaloid Nomenclature and Classification

Alkaloids are almost exclusively named with the suffix "-ine", in combination with the Latin name of the organism from which they are derived. Alternatively, an alkaloid may be named after its discoverer or its physiological effects. For instance, the piperidine alkaloid lobeline was named after its biological origin, the Indian tobacco plant (*Lobelia inflata)*.

In general, alkaloids can be classified into two main groups, i.e., heterocyclic and non-heterocyclic alkaloids. Non-heterocyclic alkaloids (also called atypical alkaloids) are less common in plants as they contain nitrogen atoms that are not part of a ring system.[4] In contrast, the more diverse heterocyclic alkaloids (typical alkaloids) can be classified according to their ring structure. A summary of the different classes of alkaloids with relevant examples and their biological origin is shown in Table 1.1 and Table 1.2.

Table 1.1: Examples of non-heterocyclic alkaloids. [4,5]

Alkaloid/Structure	Biological origin
Ephedrine (Phenylethylamine, coloured red) 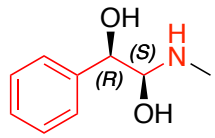 (1*R*,2*S*)-(-)-ephedrine 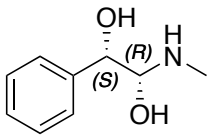 (1*S*,2*R*)-(+)-ephedrine 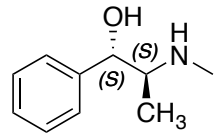 (1*S*,2*S*)-(+)-pseudoephedrine 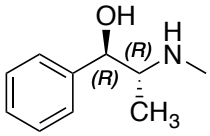 (1*R*,2*R*)-(-)-pseudoephedrine	*Ephedra* spp. (Ephedraceae)
Mescaline (Phenylethylamine) 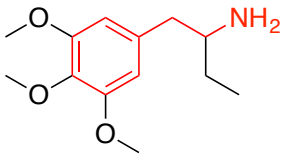	*Lophophora* spp. (Cactaceae)
Colchicine 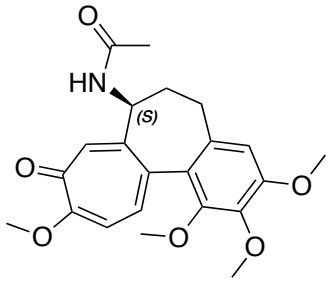 Note: Colchicine has an amide function and is relatively non-basic.	*Colchicum* spp., *Gloriosa* spp. (Liliaceae)
(–)-Erythromycin 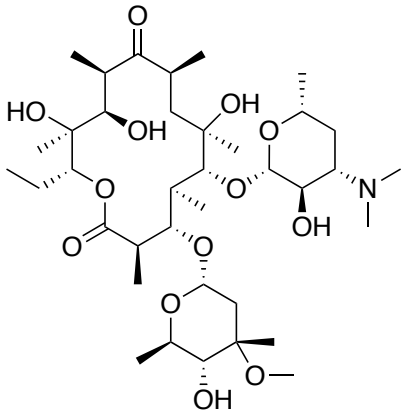	*Streptomyces erythreus* (Bacteriophyta, Actinomycetales)

Paclitaxel 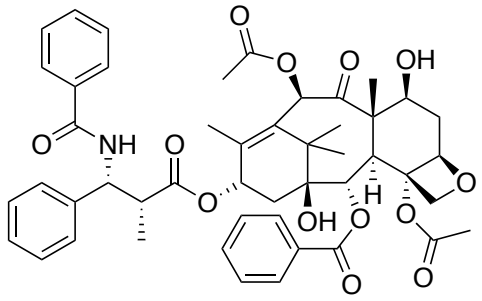 	*Taxus brevifolia* (Taxaceae)
Muscarine 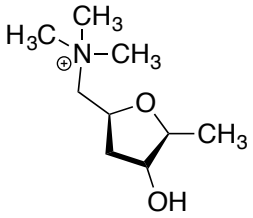 Note: Muscarine is a quaternary alkaloid.	*Inocybe* spp.*,* *Clitocybe* spp. (Fungi)

Table 1.2: Examples of heterocyclic alkaloids.[4,5]

Heterocyclic skeleton	Specific example and (biological origin)
Pyrrolidine 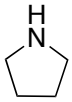 	Hygrine (*Erythroxylum* spp.*)* 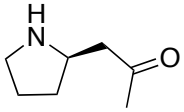
Pyrrolizidine 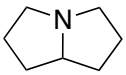 	Senecionine (*Senecio* spp.) 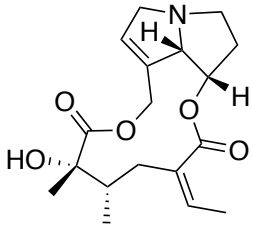
Pyridine  	Trigonelline (*Trigonella foenum-gracum*) 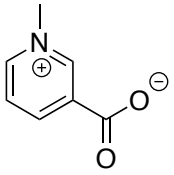
Piperidine 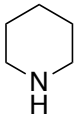 	Piperine (*Piper nigrum*)

	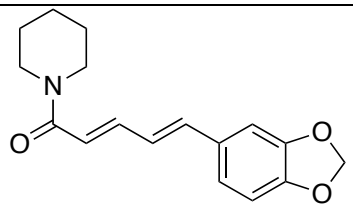
Pyridine and piperidine	Anabasine (*Nicotiana* spp.) 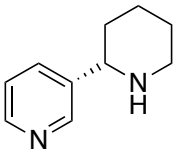
Pyridine and pyrrolidine	Nicotine (*Nicotiana* spp.) 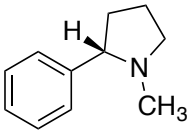
Tropane 	Section 1.7 (*vide infra*)
Quinoline 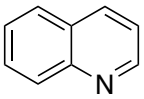	Quinine (*Cinchona* spp.) 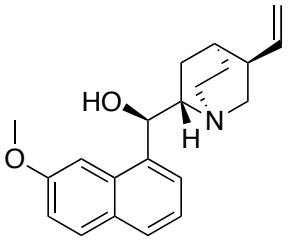
Isoquinoline 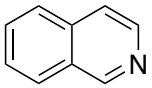	Morphine (*Papaver somniferum*) 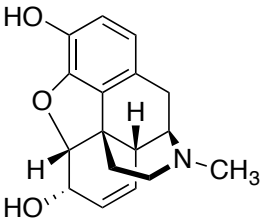
Aporphine 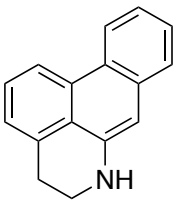	Anonaine (*Annona* spp.) 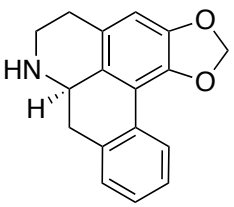

Indole 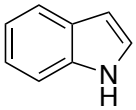	Yohimbine (*Pausinystalia yohimbe*) 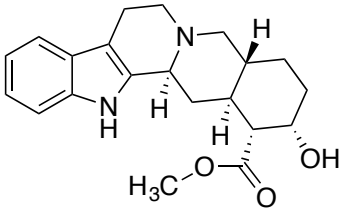 Strychnine (*Strychnos* spp.) 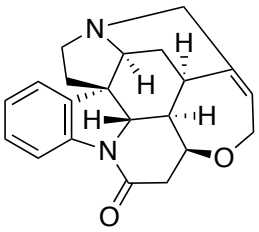 Ergotamine (*Claviceps purpurea*) 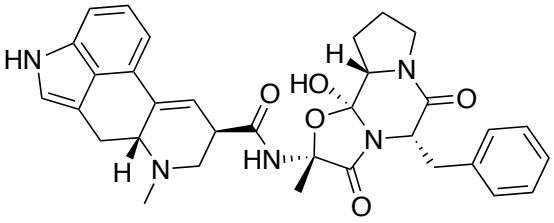
Indolizidine 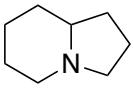	Castanospermine (*Castanospermum* spp.) 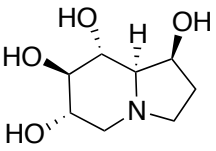
Imidazole 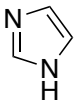	Pilocarpine (*Pilocarpus* spp.) 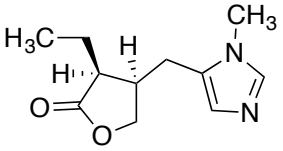
Purine 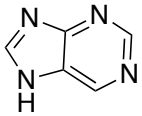	Caffeine (*Coffea* spp.) 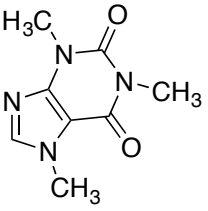

1.1.5 Alkaloid Biosynthesis

The biosynthesis of alkaloids in plants involves a complicated series of biochemical reactions. Broadly, primary metabolites are processed and reconstructed into alkaloids by various enzymes, which are in turn regulated by multiple genes and signal transduction pathways. These genes and enzymes are often species specific, forming the basis of chemotaxonomy.[16,17] The majority of plant alkaloids are biosynthesised from amino acids (Table 1.3). In this case, there is usually a decarboxylation step on the precursor amino acid, followed by direct incorporation of its nitrogen atom into the alkaloidal skeleton.[4,5,16,17] In contrast, some alkaloids do not originate from amino acids and have their nitrogen atom incorporated via a transamination step during the later stages of biosynthesis, e.g., coniine, ephedrine, capsaicin, terpenoid and steroidal alkaloids.[5]

Table 1.3: Precursor amino acids of common alkaloids.

Precursor amino acids	Alkaloid skeleton (see Table 1.1 and Table 1.2 for skeletal structures)
Tryptophan 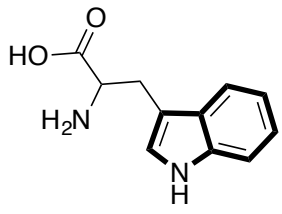	Simple indole (serotonin-type), terpenoid-indole, β-carboline, pyrroloindole (physostigmine), ergotamine-type and quinoline.
Tyrosine 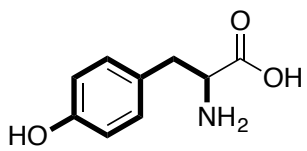	Phenethylamine, isoquinoline, benzylisoquinoline, aporphine, phenethylisoquinoline (colchicine) and phenanthrene (Amaryllidaceae alkaloids).

Histidine 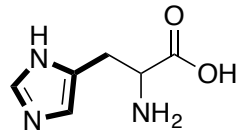	Imidazole (pilocarpine).
Ornithine 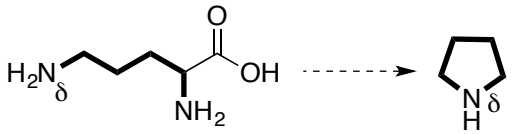	Pyrrolidine, pyrrolizidine and tropane.
Lysine 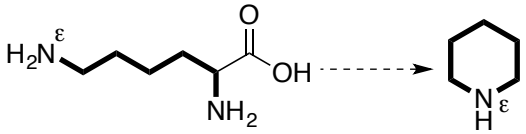	Piperidine, quinolizidine and indolizidine.

1.1.6 Bioactivity of Alkaloids

The bioactivity of an alkaloid depends on the intermolecular interactions between the alkaloid and its drug target. A drug target can be any cellular receptors, ion channels, enzymes, proteins or nucleic acids.[18,19] The binding of an alkaloid to a drug target would induce conformational changes that lead to downstream effects and biological responses. It should be noted that many alkaloids undergo first pass metabolism via the liver, which may result in altered bioactivity depending on the routes of administration. The detailed study of an alkaloid's bioactivity and mechanism of action relies on various methodologies such as computerised quantitative structural activity relationship (QSAR), X-ray crystallography (of the alkaloid with its receptor), as well as radio-ligand binding assays. Some notable examples of known alkaloids with useful bioactivity are shown in Table 1.4.

Table 1.4: Bioactivity, mechanism of action and medicinal usage of selected known alkaloids.[4,5,18,19]

Alkaloid/ biological source	Mechanism of action	Medicinal or ethnobotanical usage
Aconitine *Aconitum* spp.	Prolonged sodium-ion channel activation	Topical herbal analgesic
Ajmaline *Rauwolfia serpentina*	Sodium-ion channel blocker	Antiarrhythmic drug
Arecoline *Areca catechu*	Nicotinic acetylcholine receptor agonist	Herbal stimulant
Atropine *Atropa* spp., *Datura* spp.	Section 1.3.5 (*vide infra*)	Section 1.3.5 (*vide infra*)
Berberine *Berberis* spp.	AMP-activated protein kinase activator, stimulate glycolysis	Potential antidiabetic agent
Cocaine *Erythroxylum* spp.	Section 1.3.5 (*vide infra*)	Section 1.3.5 (*vide infra*)
Caffeine *Coffea* spp.	Adenosine receptor antagonist	Wakefulness promoting stimulant
Colchicine *Colchicum* spp., *Gloriosa* spp.	Binding to tubulin protein, inhibits microtubule formation during cell division, highly cytotoxic	Anti-mytotic agent; treatment of gout
Emetine *Carapichea ipecacuanha*	Protozoa protein synthesis inhibitor	Antiprotozoal agent
Ergotamine *Claviceps purpurea* (Fungi)	Serotonin $5HT_{1D}$ receptor agonist, vasoconstriction of capillaries around trigeminal nucleus	Anti-migraine drug
Erythromycin *Streptomyces erytreus* (Actinobacteria)	Binding to bacteria 23s rRNA, bacterial protein synthesis inhibitor	Antibacterial drug

Galantamine *Galanthus* spp.	Acetylcholinesterase (enzyme) inhibitor	Symptomatic treatment of Alzheimer's disease
Harmala alkaloids *Peganum harmala*	Monoamine oxidase (MAO) (enzyme) inhibitor	Psychedelic entheogen
Ibogaine *Tabernanthe iboga*	Various neurotransmitter receptors interactions	Anti-opioid addiction, psychedelic entheogen
Morphine *Papaver somniferum*	Opioid receptor agonist	Strongly addictive analgesic; derivatives such as loperamide are antispasmodic
Nicotine *Nicotiana* spp.	Nicotinic acetylcholine receptor agonist	Strongly addictive stimulant; insecticide
Physostigmine *Physostigma venenosum*	Acetylcholinesterase inhibitor	Treatment of glaucoma
Quinine *Cinchona* spp.	Inhibits the ability of *Plasmodium* to digest hemoglobin.	Antimalarial drug
Reserpine *Rauwolfia serpentina*	Vesicular Monoamine Transporter (VMAT) blocker, decreases the degradation of noradrenaline and serotonin	Antihypertensive, antipsychotic
Strychnine *Strychnos* spp.	Glycine receptor antagonist; neurotoxic convulsant	Rodenticide
Taxol (Paclitaxel) *Taxus brevifolia*	Microtubule stabilization, prohibits mitotic division	Anticancer drug
Tubocurarine *Chondrodendron* spp.	Nicotinic acetylcholine receptor antagonist; neuromuscular blocker	Paralytic agent in general anaesthesia
Vincristine, vinblastine *Catharanthus roseus*	Tubulin protein binding; inhibits microtubule	Anticancer drug

	formation and mitosis; highly cytotoxic	
Yohimbine *Pausinystalia yohimbe*	Alpha 2-adrenoreceptor antagonist	Stimulant, treatment of erectile dysfunction

1.2 (−)-Lobeline and Its Derivatives

1.2.1 Chemistry of (−)-Lobeline

(−)-Lobeline, also known as 2*R*,6*S*,2′′*S*-lobeline or *cis*-lobeline (**3**), is a piperidine alkaloid that is chemotaxonomically exclusive to the plant family Campanulaceae, which includes *Hippobroma longiflora*.[4,5,20] Alkaloid **3** features a distinctive *N*-methyl piperidine nucleus with two phenethyl (C_6–C_2) substituents at the C-2 and C-6 positions (Fig. 1.1). Well-known natural derivatives of **3** (mostly isolated from *Lobelia* spp.) include lobelanine, norlobelanine, lobelanidine and norlobelanidine (Fig. 1.1).[21] All these derivatives of **3** can be interconverted via oxidation, reduction and/or demethylation reactions. Of all the *Lobelia* alkaloids, **3** is regarded as the most biologically active and thus, most widely studied. It was first isolated and characterised by Wieland in 1929 and subsequently had its absolute configuration confirmed via total synthesis.[21]

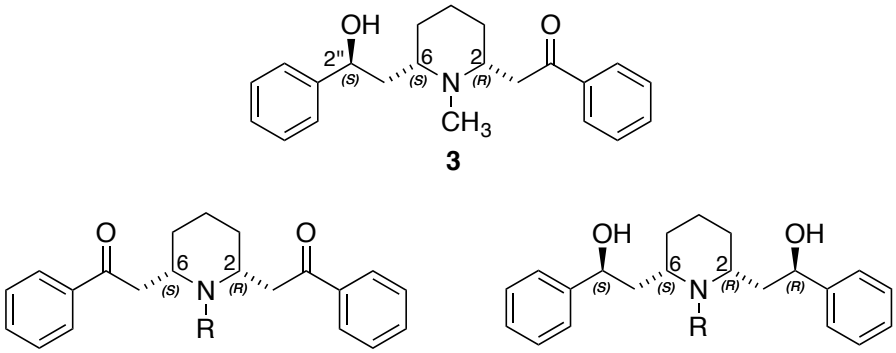

Lobelanine R= CH_3
Norlobelanine R= H

Lobelanidine R= CH_3
Norlobelanidine R= H

Figure 1.1: Chemical structures of (−)-lobeline and its derivatives.

The stereochemistry of **3**, as with most molecules containing a β-aminoketone moiety, is configurationally unstable. Under neutral and anhydrous conditions, pure (−)-lobeline exists approximately 100% in the 2*R*,6*S* configuration. The hydrogen atoms bonded to C-2 and C-6 are in a 1,3-diaxial (*cis*) configuration. However, under base-catalysed conditions or as a solution in hydrophilic solvents, **3** readily undergoes epimerisation at its C-2 position into its 2*S*,6*S*-*trans*-isomer via a retro aza-Michael reaction (Figure 1.2).[22] It was reported that the epimerisation reaction reaches an equilibrium in chloroform solution when the *cis*:*trans* ratio approaches 45:54.[22] As the retro aza-Michael reaction is likely base-catalysed, strongly acidic condition (pH < 3.0) was reported to quench the epimerisation of **3**.[22]

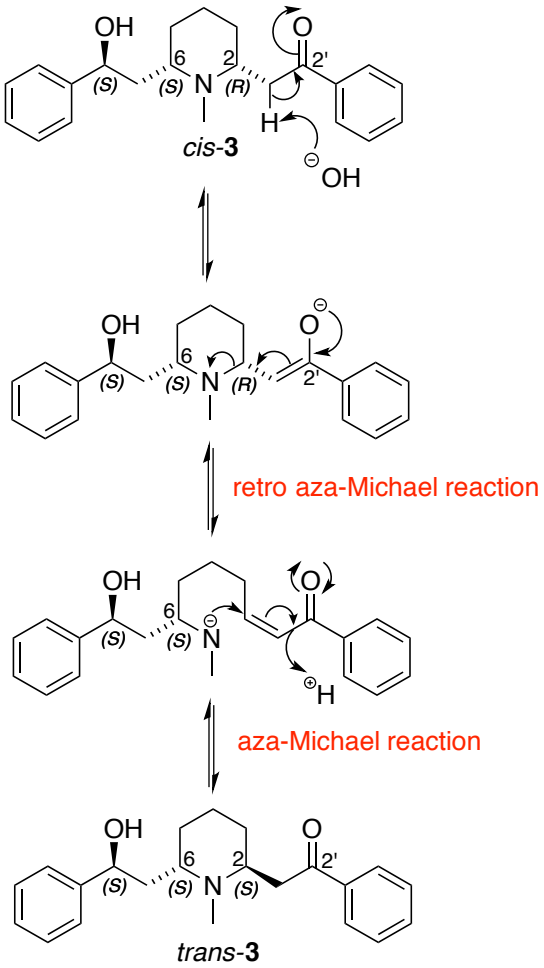

Figure 1.2: Epimerisation of 2*R*,6*S*,2′′*S*-lobeline to 2*S*,6*S*,2′′*S*-lobeline via retro aza-Michael reaction.

The β-aminoketone moiety of **3** also predisposes it to chemical degradation via a retro Mannich reaction, to give acetophenone and a sedamine-type alkaloid (Fig. 1.3).[22] Since the retro Mannich reaction requires the availability of a nitrogen lone pair in the piperidine ring, **3** will not decompose under acidic conditions (nitrogen atom is protonated) or as an ionic salt like lobeline sulfate. Other lobeline derivatives lacking a β-aminoketone moiety such as lobelanidine are chemically stable.

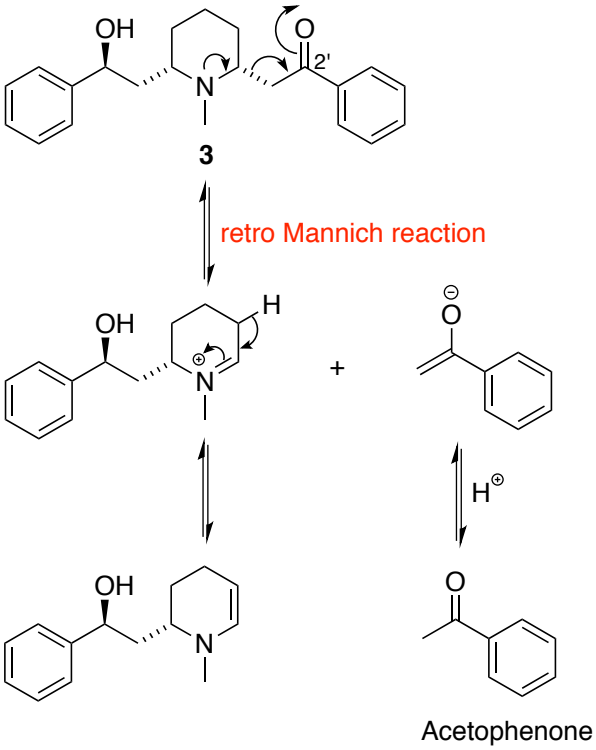

Figure 1.3: Chemical decomposition of (–)-lobeline via retro Mannich reaction.

It is also worth noting that the symmetrical lobelanine and lobelanidine (Fig. 1.1) are optically inactive because they are meso compounds. However, an optically active epimer of lobelanidine exists, i.e., (−)-*cis*-2′,2′′-diphenyllobelidiol (**4**),[20] as the two only differ in the configuration at C-2′. Many other lobeline derivatives with unknown stereochemistry were reported (mainly from *Lobelia inflata*)[21] and they demand further structural elucidation.

1.2.2 Biosynthesis of (–)-Lobeline

The biosynthetic pathways of **3** were widely studied, albeit incomplete. It is accepted that both the amino acids, L-lysine and L-phenylalanine, serve as the precursors to **3.**[4,5,21] Evidently, radiolabelled L-lysine yielded radioactive **3** through feeding experiments in *Lobelia syphilita.*[21] In common with most piperidine alkaloids, L-lysine is thought to furnish the piperidine nucleus, viz., C-2 and C-6 of L-lysine constitute C-2 and C-6 of **3**, respectively. As shown in Figure 1.4a, L-lysine is first biotransformed into 5-aminopentanal, which undergoes ring-closure to give 2,3,4,5-tetrahydropyridine via intramolecular iminium ion formation. This intermediate was previously isolated from radiolabelled tracer studies in *Lobelia inflata.*[21] The substituents that would later be incorporated into C-2 and C-6 of the piperidine nucleus are derived from L-phenylalanine.[21] L-Phenylalanine is bio-transformed into *trans*-cinnamic acid via the enzyme Phenylalanine Ammonia Lyase (PAL).[5,21] β-Oxidation of cinnamic acid would afford benzoylacetic acid, which furnishes the two diphenethyl moieties of **3**.

In the subsequent pathway (Fig. 1.4b), Mannich reaction of two molecules of benzoylacetic acid (enolate anion) with 2,3,4,5-tetrahydropyridine yields norlobelanine. *N*-Methylation of norlobelanine affords lobelanine, which on reduction yields **3**. It is notable that the enzymatic incorporation of the two diphenethyl substituents is highly stereospecific, resulting in the formation of the totally symmetrical 2*R*,6*S*-norlobelanine.[21] However, the carbonyl function at C-2′′ in lobelanine would be stereospecifically reduced into a 2′′*S* chiral center, giving the asymmetrical **3**.[21] The biosynthetic pathways for other lobeline derivatives are less studied, but it is conceivable that they arise from modifications of **3** as the parent alkaloid.

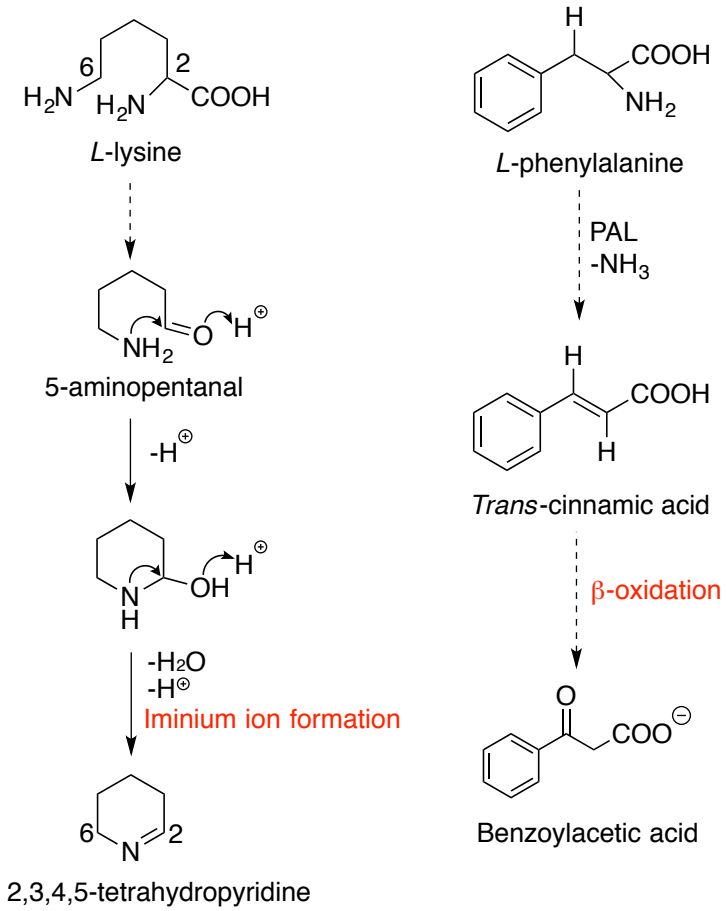

Figure 1.4a: Biosynthetic pathway of (–)-lobeline (part I).

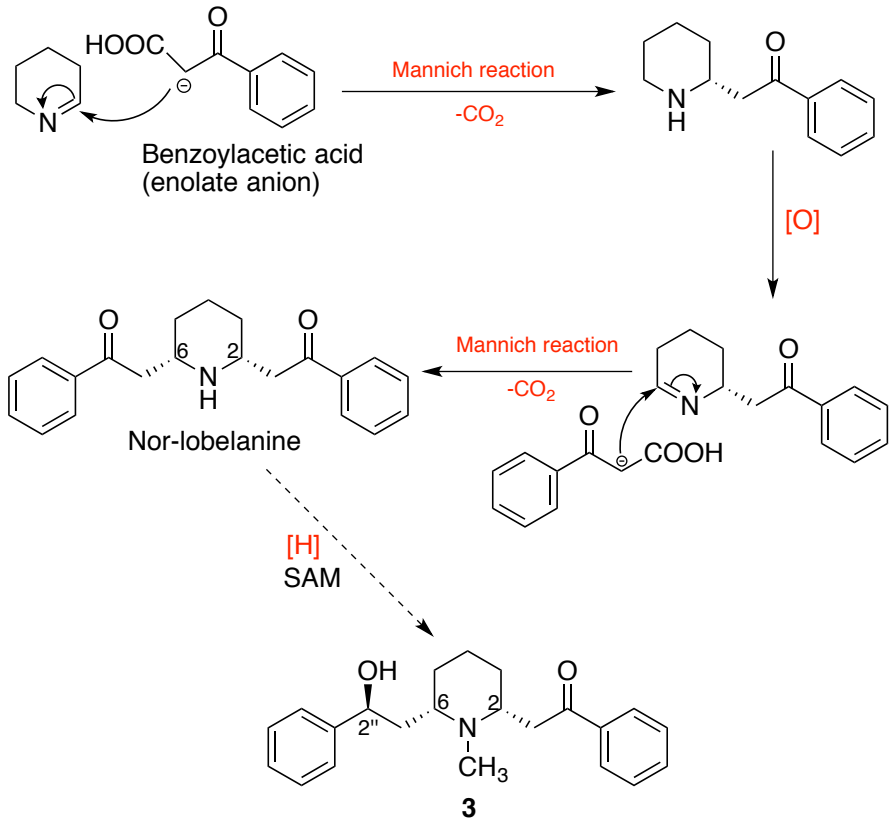

Figure 1.4b: Biosynthetic pathway of (–)-lobeline (part II).

1.2.3 Pharmacology of (–)-Lobeline

(–)-Lobeline (**3**) is an alkaloid with well-known biological activities. It was previously used as a respiratory stimulant to treat asthma and bronchitis.[4,5,21] Alkaloid **3** was shown to activate the carotid and aortic body chemoreceptors, causing relaxation in airway muscles as well as promoting mucous expectoration.[21] Various *Lobelia* species (particularly *L. inflata*) were used in herbal remedies to alleviate symptoms of asthma and respiratory illnesses. However, **3** is considered to be quite toxic due to its unpredictable side effects.[4,5,21] Safer yet more effective agents have superseded its use in modern medicine. Nonetheless, recent pharmacological studies have uncovered new mechanism of action and therapeutic potentials of **3**. It was demonstrated in animal models that **3** could reverse psychostimulant addiction,[23] improve memory as well as decrease anxiety.[21] There are renewed interests regarding the use of **3** as a novel agent in the treatment of neurological diseases such as drug dependency, Alzheimer's disease and hyperactive disorders.[21]

The biological effects of **3** are often compared to those of nicotine, as both alkaloids act on the same biological target, i.e., nicotinic acetylcholine receptors (nAChRs). In general, **3** and nicotine evoke a stimulatory effect on the autonomic ganglia (innervated with nAChRs), leading to tachycardia, hypertension and increased respiration rate.[5,21] In toxic doses, they result in central nervous system depression, respiratory paralysis and death.[21] nAChRs have been extensively studied and elucidated over the years. It is classified as a ligand gated ion channel, which consists of a pentameric protein structure that has a combination of α (α2-α9) and β (β2-β4) subunits.[18,19] Different subtypes of nAChRs exist mainly in the brain (central nervous system), the autonomic nervous system as well as the

neuromuscular junction.[18,19] The binding of the endogenous neurotransmitter acetylcholine (ACh) or agonists like nicotine to nAChRs opens the ion channel, which allows an influx of extracellular cations such as Na^+. This initial depolarisation, also known as an excitatory post-synaptic potential (EPSP) would attain certain threshold such that voltage gated ion-channels become activated. As a result, neuronal action potential (membrane depolarisation) can be transmitted, leading to a physical response. nAChRs as a whole are known to modulate human cognitive, locomotor and behavioral responses.[19]

In contrast to nicotine, the mechanism of action of **3** has remained ambiguous. Alkaloid **3** is currently considered as a mixed agonist or even an antagonist at nAChRs.[21] Considering the varied subtypes of nAChRs, it is plausible that **3** interacts differently with individual nAChR subtypes. This could explain the differences between the actions of **3** and nicotine (full agonist). Besides, it was proposed that **3** may act as an allosteric modulator of nAChR to inhibit dopamine release from rat striatum.[21] An alternative mechanism suggested that **3** inhibits dopamine uptake by binding to vesicular monoamine transporter (VMAT2).[22,23] Nevertheless, the indirect antagonism of **3** on dopamine transmission makes it a promising anti-addiction drug lead.[23]

The biological activity of natural lobeline derivatives are under-examined, although some synthetic structural analogues were investigated. These studies provided essential clues to their potential structural activity relationships. It was shown that both C-2 and C-6 substituents of the piperidine nucleus in **3** are just as essential as its piperidine nucleus.[21] Removal of the piperidine ring or either substituents would result in a big decrease of affinity to nAChR.[21] Besides, at least one oxygen atom (either carbonyl or hydroxyl at C-2′ or C-2′′) is essential for

maintaining lobeline's affinity to nAChR.[21] The asymmetrical **3** produced higher affinity than its symmetrical stereoisomers.[21] This phenomena suggests that the binding of **3** to its receptors is stereospecific, as both hydroxyl and ketone moiety (in their asymmetrical position) are crucial in providing receptor recognition.

1.3 Tropane Alkaloids

1.3.1 Introduction and History

Present in *Pellacalyx saccardianus*, the tropane alkaloids are a group of structurally diverse secondary metabolites featuring a characteristic 8-azabicyclo[3.2.1] nucleus (Fig. 1.5). Approximately 200 tropane alkaloids have been characterised to date, predominantly occurring in the angiosperm families Solanaceae and Erythroxylaceae.[24–26] Being quintessential examples of pharmacologically active natural products, tropane alkaloids such as atropine and hyoscine are widely exploited in herbal remedies as well as modern medicine as antimuscarinic drugs. In contrast, the psychostimulant tropane alkaloid cocaine negatively impacts human health, while its derivatives are widely used as anaesthetic drugs. Considering the immense structural diversity of tropane alkaloids, Sections 1.3.1 – 1.3.5 aim to provide a general review of their chemotaxonomy, biosynthesis and bioactivity. Notably, Section 1.3.3 highlights the characteristic NMR spectroscopic properties of tropane alkaloids in relation to stereochemistry, which were observed in this research (Chapter 3). Finally, Section 1.3.6 focuses on the lesser known oligomeric tropane alkaloids, because similar compounds were encountered in this research (Chapters 3.8 and 3.9).

The discovery of tropane alkaloids was largely pioneered by German chemists. The first tropane alkaloid, atropine was isolated by Mein in 1831 from the roots of *Datura* sp., although he did not publish his results.[26,27] In 1833, Geiger and Hesse published the isolation of atropine from *Atropa belladonna*[26] and provided a sample to Liebig for analysis, who established its empirical formula.[27] Kraut and Lossen later discovered that atropine could be hydrolysed by a strong base into an alcohol (tropine) and an organic acid (tropic acid).[26,27] About 50 years later, they established the stereochemical relationship between atropine and (–)-hyoscyamine.[26] In 1879, Ladenburg achieved the total synthesis of atropine via esterification of tropine and tropic acid.[26,27] On the other hand, cocaine was first isolated by Gaedecke in 1855, while its structure was determined by Lossen in 1862.[27] It was not until 1954 that the stereochemistry of (–)-cocaine was resolved by the Swiss chemists, Hardegger and Ott.[27]

1.3.2 Nomenclature and Chemotaxonomy of Tropane Alkaloids

The tropane ring is a bicyclic system, i.e., 8-azabicyclo[3.2.1], that incorporates a fused pyrrolidine-piperidine moiety (Fig. 1.5). Its various equivalent representations are depicted in Figure 1.5. Herein, the tropane ring nomenclature is adopted as per recommendation by the IUPAC.[28] The numbering of C-1 starts clockwise at the 'back' of the tropane ring, with C-3 facing right (Fig. 1.5, case **a**). However, depending on the substituents at C-6 and/or C-7, C-1 may start anti-clockwise at the 'front' of the tropane ring such that the substituent with a higher priority bears the lowest numbering (Fig. 1.5, cases **d**, **e** and **f**). It should be noted that only case **a** is encountered in this research.

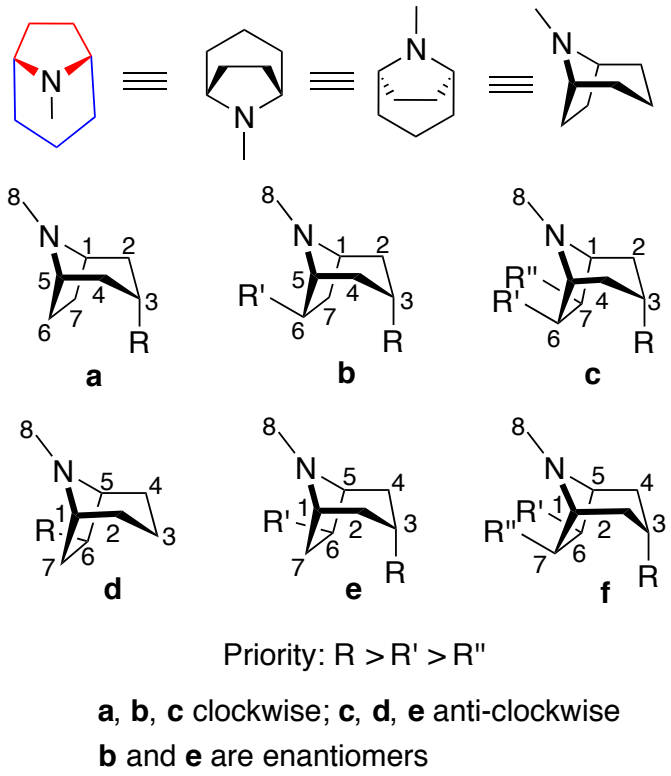

Figure 1.5: Representations of the tropane ring and its IUPAC nomenclature.

In general, plant-derived tropane alkaloids can be classified into three main categories based on their biosynthetic intermediates, i.e., 3α-tropine (c.f., atropine), 3β-tropine (c.f., calystegines) and methylecgonine (c.f., cocaine) (Table 1.5). Tropane alkaloids originating from 3α-tropine are best represented by atropine, its laevorotary enantiomer (–)-hyoscyamine and (–)-hyoscine (scopolamine), all of which are exclusive to the plant family Solanaceae (tribes *Datureae*, *Solandreae*, *Solaneae*, *Mandragorea*, *Hyoscyameae*, and *Cestroideae*).[5,25,29] Atropine and (–)-hyoscyamine are C-3α monosubstituted tropane esters, while hyoscine has an additional epoxide function at C-6 and C-7. In the tribe *Salpiglossidae* (Solanaceae), which includes the genus *Schizanthus*, 3α-tropine esters of senecoic acid, tiglic acid, angelic acid as well as the dicarboxylic acids (itaconic acid, citraconic acid and mesaconic acid) are widely elaborated (c.f., schizanthines and grahamines).[29–31] On the other hand, methylecogine-derived tropane alkaloids are of the cocaine-type, which feature an acetate group at C-2, alongside a C-3β configured ester

substituent.[5,25,29] (–)-Cocaine is chemotaxonomically exclusive to several species of the genus *Erythroxylum* (Erythroxylaceae), most notably the South American coca plant, *Erythroxylum coca*.[25,29] In the third category, the calystegines are a group of nortropane derivatives with polyhydroxyl substituents, which include a characteristic 3β-OH group.[25,29,32] They were first isolated from *Calystegia sepium* (Convolvulaceae), but can also be found in the roots of many Solanaceae plants.[25,29] Interestingly, a group of unusual pyranotropane alkaloids (bellendine and darlingine) were characterised from certain plants in the family Proteaceae, which are confined to Australia.[25,29,33] 3α-Tropine esters can also be found sporadically in the angiosperm families Convolvulaceae and Rhizophoraceae.[25,29] For instance, a novel dithiolane tropane ester, brugine, was isolated from *Bruguiera sexangula*.[25,29] A summary of the chemotaxonomy of plant-derived tropane alkaloids is shown in Table 1.5. Apart from the plant kingdom, tropane alkaloid homologues are present in cyanobacteria and the tricolour poison-dart frog.[5]

Table 1.5: Chemotaxonomy of plant-derived tropane alkaloids.[5,25,29–37]

Plant family/ representative genera	**Selected examples of tropane alkaloids** (Known absolute stereochemistry are shown)
Solanaceae Tribe *Datureae* (*Datura* spp.*, Brugmansia* spp.) Tribe *Solandreae* (*Solandra* spp.) Tribe *Solaneae* (*Atropa* spp., *Latua* spp., *Acristus* spp.) Tribe *Mandragoreae* (*Mandragora* spp.) Tribe *Hyoscyameae* (*Scopolia* spp., *Hyoscyamus* spp., *Physochlaina* spp., *Anisodus* spp., *Przewalskia* spp.) Tribe *Cestroideae* (*Duboisia* spp., *Anthocercis* spp.)	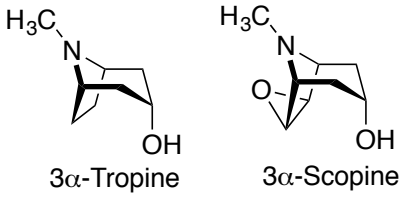 3α-Tropine 3α-Scopine 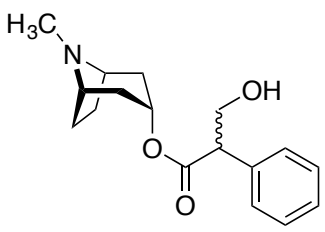 Atropine 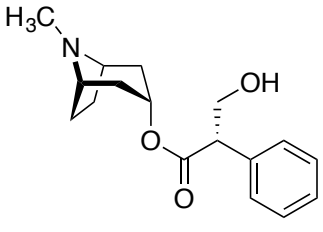 (–)-Hyoscyamine 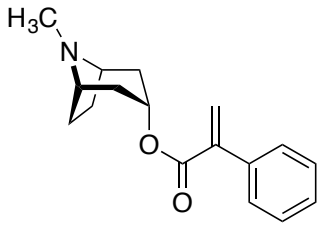 Apoatropine Atropic acid ester 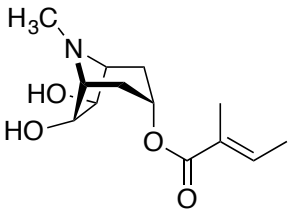 Meteloidine Tiglic acid ester 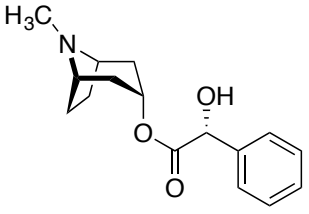 Littorine (*R*)-Phenyllactic acid ester 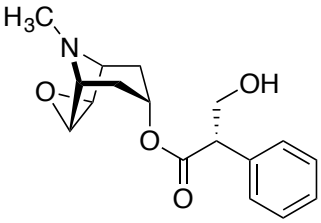 Hyoscine (scopolamine) 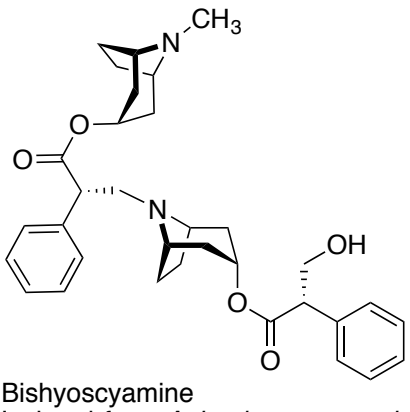 Bishyoscyamine Isolated from *Anisodus acutangulus*

Tribe *Salpiglossidae* (*Schizanthus* spp.)	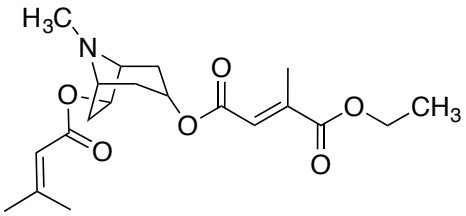 Schizanthine A 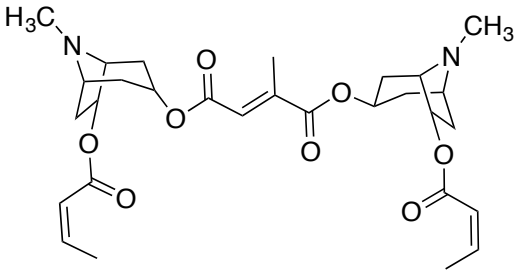 Schizanthine B (ditropane diester of mesaconic acid) 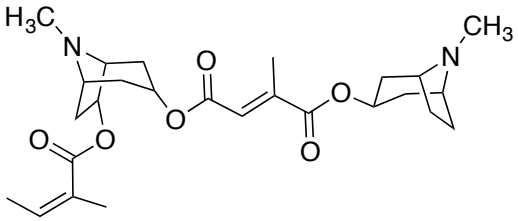 Schizanthine C (ditropane diester of mesaconic acid) 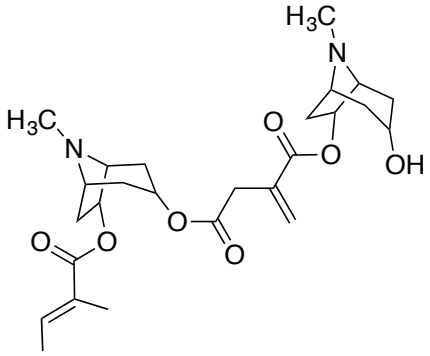 Schizanthine E (ditropane diester of itaconic acid) 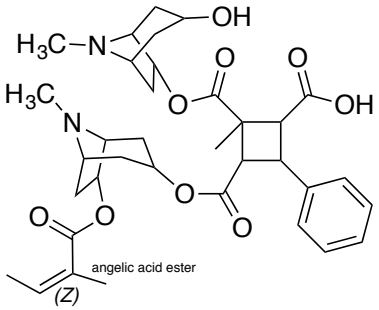 Grahamine A

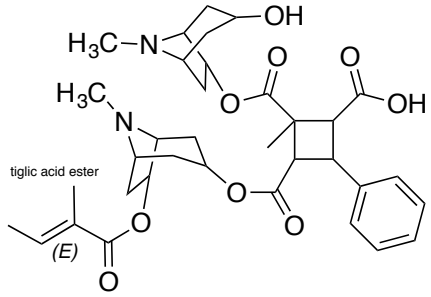

Grahamine B

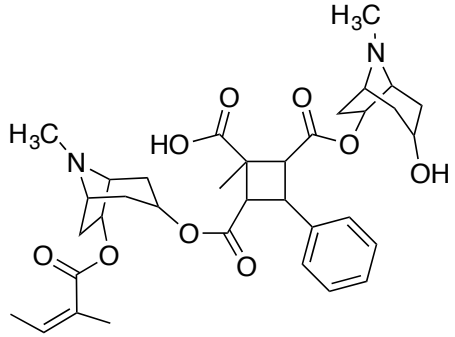

Grahamine C

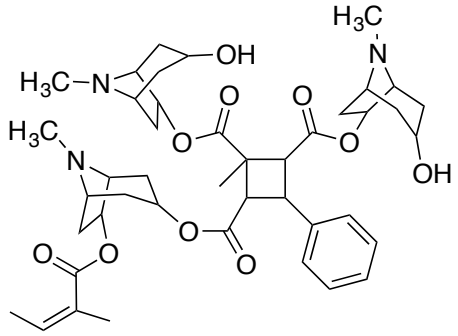

Grahamine D

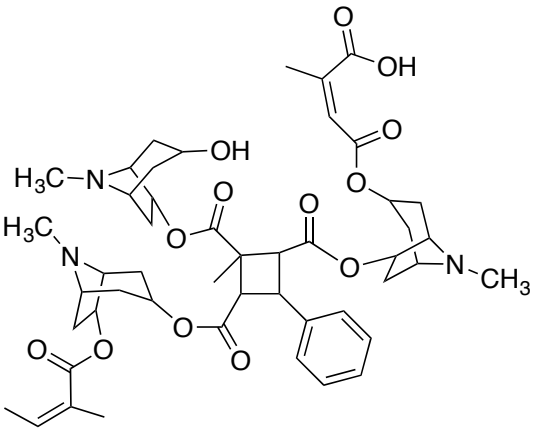

Grahamine E

	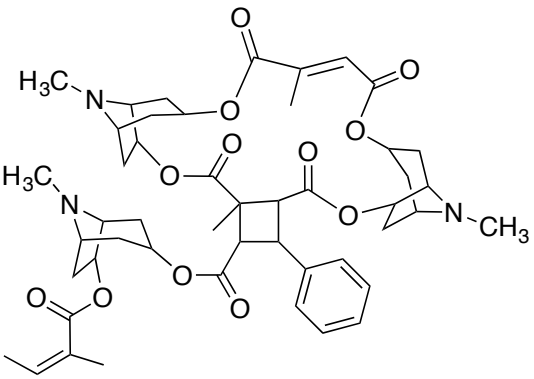 Grahamine
Erythroxylaceae *Erythroxylum* spp., in particular *E. coca*, *E. hypericifolium*, *E. moonii*, *E. novogranatense* and *E. pervillei.*	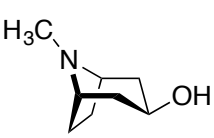 3β-Tropine 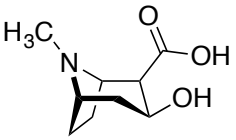 Ecogine 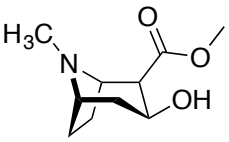 Methylecogine 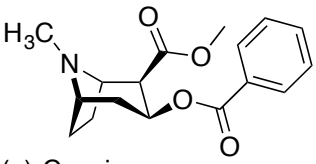 (–)-Cocaine 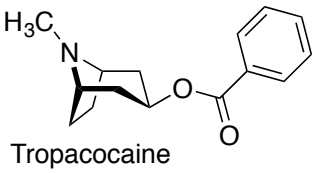 Tropacocaine 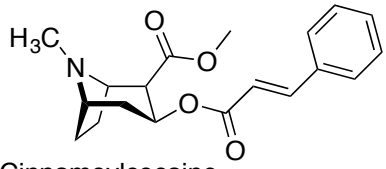 Cinnamoylcocaine 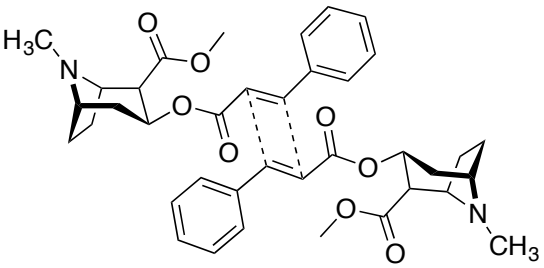 2 X Cinnamoylcocaine hv 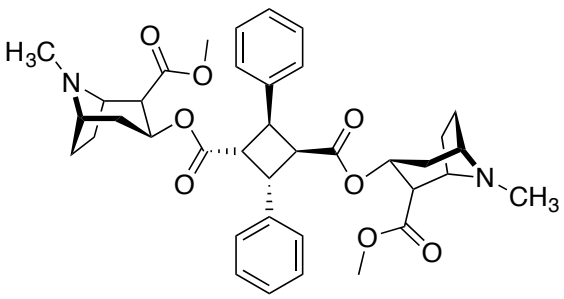 α-Truxilline

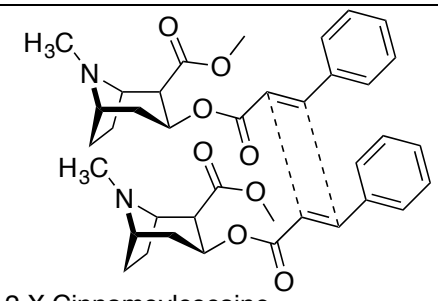

2 X Cinnamoylcocaine

hv

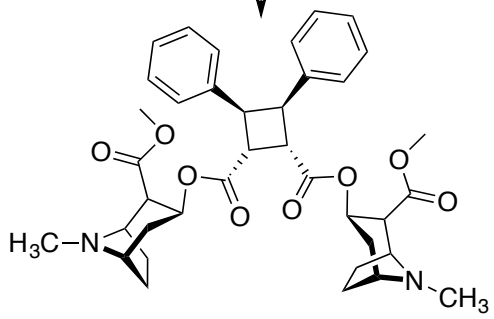

β-Truxilline

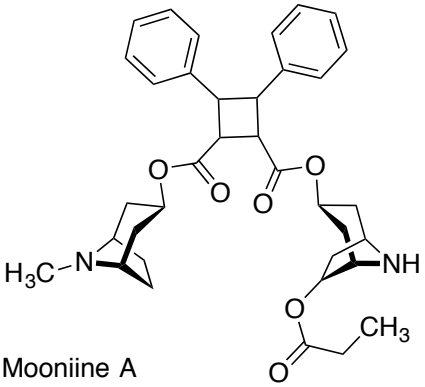

Mooniine A

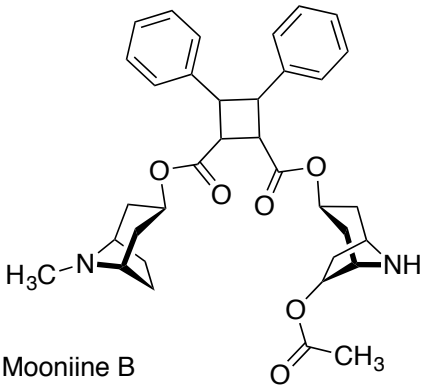

Mooniine B

Protaceae *Bellandena montana*, *Darlingia* spp., and *Knightia* spp.	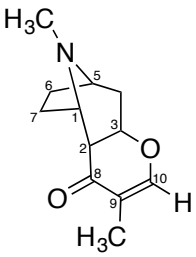 Bellendine 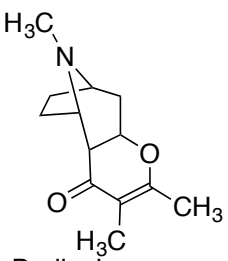 Darlingine 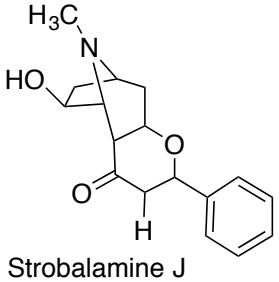 Strobalamine J 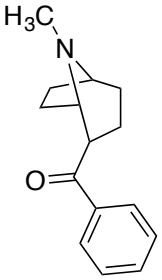 Ferrugine 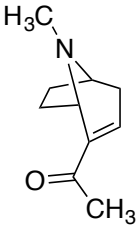 Ferruginine 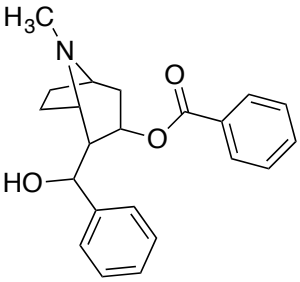 Alkaloid DF Isolated from *Darlingia ferruginea*
Convolvulaceae *Convolvulus* spp., *Erycibe* spp., *Calystegia* spp., and *Merremia* spp.	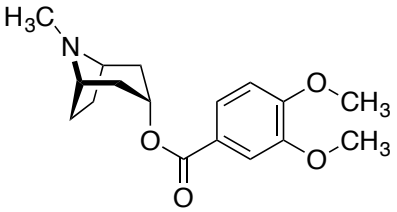 Convolvine Tropine-3α-veratrate 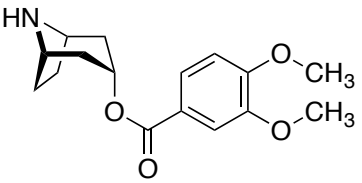 Convolamine Nortropine-3α-veratrate 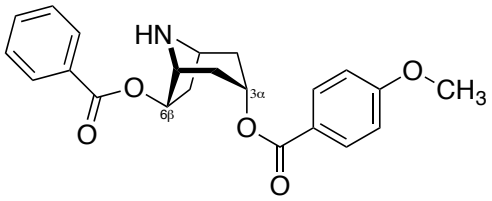 Merredissine

	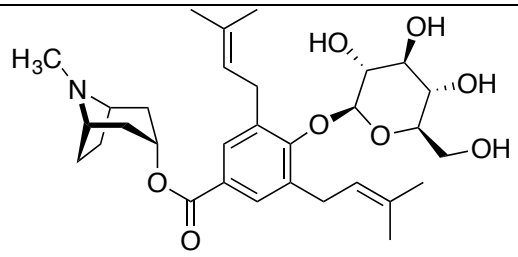 Merresectine B 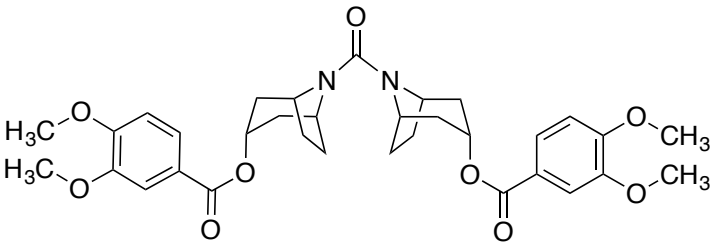 Subhirsine (isolated from *Convolvulus subhirsutus*) 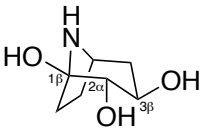 Calystegine A_3 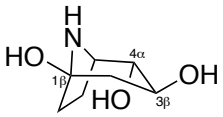 Calystegine A_5 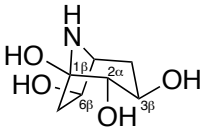 Calystegine B_1 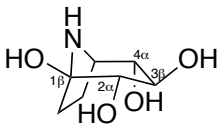 Calystegine B_2 Note: Calystegines are also found in many species of Solanaceous plants.
Rhizophoraceae *Bruguiera* spp., *Crossostylis* spp., and *Pellacalyx* spp.	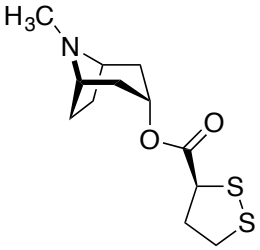 Brugine Isolated from *Bruguiera sexangula* 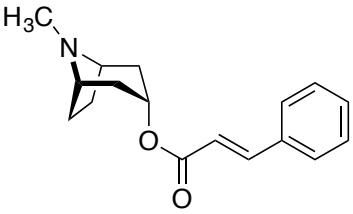 Tropine-3α-cinnamate

	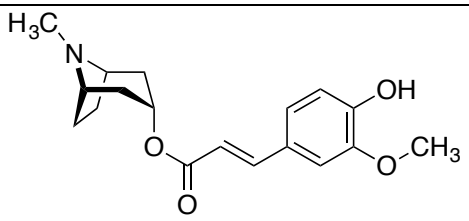 Tropine-3α-ferulate

1.3.3 Chemistry and Stereochemistry of Tropane Alkaloids

Almost all plant-derived tropane alkaloids can be considered as esters comprising of tropine (tropane alcohol) and an organic acid, e.g., tropic acid, benzoic acid, cinnamic acid etc. Demethylation of the *N*-Me group of tropane alkaloids gives nortropane derivatives. Naturally occurring tropane alkaloids are usually secondary or tertiary amines, which can react as a chemical base or a nucleophile. Tropane alkaloids are reliably stained by the Dragendorff's reagent. Reactive functionalities associated with the ester moiety can also contribute to the chemical reactivity of tropane alkaloids. In a classical example, acid-base catalysed keto-enol tautomerisation of the tropic ester moiety of (–)-hyoscyamine results in its racemisation into atropine (Fig. 1.6).

The stereochemistry of tropane alkaloids is diverse, often ambiguous in literature and is worthy of emphasis. A plain or unsubstituted tropane ring is considered as a meso-compound because a longitudinal axis of symmetry bisects the molecule through C-3 and the N atom, *viz*., a mirror plane of symmetry. Hence, tropane and tropine are optically inactive and possess chemically equivalent ^{1}H and ^{13}C NMR signals.[28,38] Similarly, C-3 monosubstituted tropane esters share this element of symmetry and are optically inactive. They typically show five discrete sets of ^{13}C NMR signals attributed to C-3 (most downfield), C-1/C-5, C-2/C-4, C-6/C-7 (most upfield) and *N*-Me group.[38] However, it should be noted that hydrogen bonding between certain functionalities such as C=O and OH in the organic acid

moiety of tropane esters may induce an unsymmetrical element and results in the splitting of the otherwise equivalent ^{13}C NMR signals into fine doublets.[38] Besides, two epimers exist for tropine and monosubstituted tropane esters at the C-3 position. The OH or ester groups may be α-configured (*endo* to the tropane ring) or β-configured (*exo* to the tropane ring). This is due to stereoselective biogenetic pathways as described in Section 1.3.4. Where applicable, analysis of the ^{1}H NMR coupling constant of H-3 is useful to determine the configuration of C-3 on the basis of the Karplus relationship. Typically, a triplet of ca. J = 5 Hz is observed for H-3β (C-3α) as the dihedral angle between H-3 and H-2/H-4 is around 60°.[39] In contrast, H-3α (C-3 β) generally exhibits a larger coupling constant of ca. J = 10 Hz due to a dihedral angle of about 180° between H-3 and H-2_{ax}/H-4_{ax}, i.e., *trans*-diaxial coupling.[39] The Karplus relationship can also be applied to establish the relative configuration of C-6 and/or C-7 substituted tropane esters.[85] For instance, H-6α would not show vicinal coupling to H-5 due to a dihedral angle of close to 90°, implying a 6β-configuration of the substituent.[85] It is also notable that disubstituted and trisubstituted tropane esters (although not encountered here) are non-symmetrical, optically active and exhibit non-chemically equivalent NMR signals.[28] The enantiomers of disubstituted and trisubstituted tropane esters are numbered differently according to the IUPAC nomenclature (Fig. 1.5). Determination of their absolute configurations can be challenging and requires ECD spectroscopy, X-ray crystallography or chemical derivatisation with chiral auxiliary reagents like Mosher's acid (α-methoxy-α-trifluoromethylphenylacetic acid, MTPA), followed by NMR analysis.[28] The use of LCMS or polarimetry alone to elucidate tropane ester enantiomers is currently considered as unreliable.[28]

The tropane ring is widely accepted to adopt two stable conformations, i.e., chair (C-3 *endo* to C-6/C-7) and boat (C-3 *exo* to C-6/C-7) (Fig. 1.7).[34,40] X-ray crystallography analyses of tropane alkaloids showed that the boat conformation is favored, particularly when there is intramolecular hydrogen bonding between the *N*-Me or *N*-H group with the ester or hydroxyl substituent at C-3 of the tropane ring.[39,40] Besides, the *N*-Me group of tropane alkaloids can equilibrate between the axial or the equatorial positions. An equatorial *N*-Me group is usually favoured given that there are no substituents on C-6 and C-7.[5]

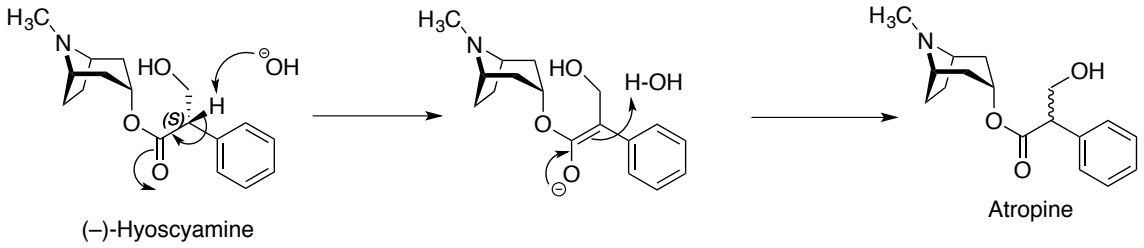

Figure 1.6: Base catalysed racemisation of (–)-hyoscyamine.

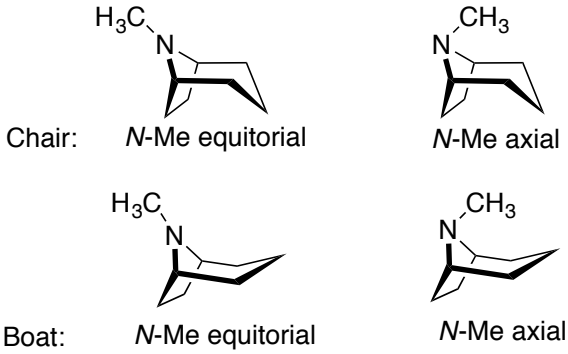

Figure 1.7: Four stable conformations of the tropane nucleus.

1.3.4 Biosynthesis of Tropane Alkaloids

The biosynthetic pathways of plant-derived tropane alkaloids are well-studied. In principle, they are derived from L-ornithine, which is in turn produced by the transamination of L-glutamic acid, an intermediate of the Krebs cycle. L-Ornithine consists of a five-carbon backbone with an α and δ amino group. It is the

nitrogen atom from the δ amino functionality that is incorporated into the tropane ring. A summary of the biosynthetic pathways of the two major classes of tropane alkaloids, i.e., atropine and (–)-cocaine, are compiled based on published literatures,[4,5,24,26] and depicted in Figure 1.8.

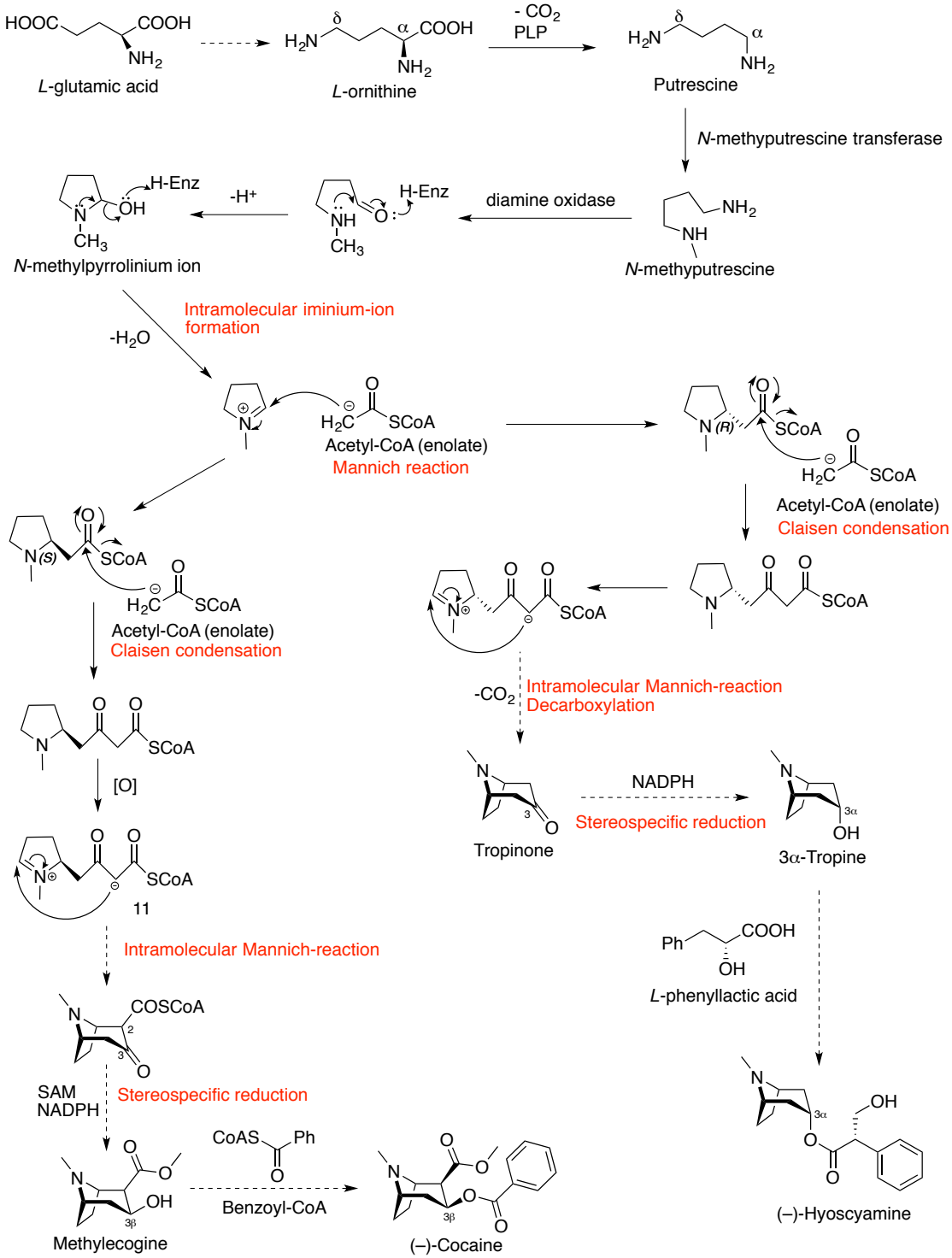

Figure 1.8: Biosynthetic pathways of tropane alkaloids.

Firstly, L-orithine is converted into putrescine via pyridoxal-5′-phosphate (PLP) catalysed decarboxylation. Putrescine is then methylated at the δ-N position into *N*-methylputrescine by the enzyme putrescine *N*-methyltransferase. This is followed by oxidative deamination of the α-NH_2 group via diamine oxidase, producing an aminoaldehyde intermediate which undergoes intramolecular ring-closure (iminium ion formation) to give a *N*-methyl-pyrrolinium cation. Mannich reaction of the *N*-methyl-pyrrolinium cation with one unit of acetyl-CoA generates a hygrine-type pyrrolidine alkaloid precursor (C_4N), comprising of the *R* and *S*-stereoisomers, which diverge into two separate downstream pathways. In both pathways, side-chain lengthening occurs as another molecule of acetyl-CoA is added via Claisen condensation, producing the piperidine (C_5N) component of the tropane ring. Subsequently**,** a new *N*-methyl-pyrrolinium cation is generated, followed by an intramolecular ring-closure Mannich reaction, which furnishes a tropanyl ring. The *S*-addition product retains its acetoacetyl side chain and is transformed into methylecogine after methyl ester formation at C-2 (by SAM) and reduction of its C-3 carbonyl group. (–)-Cocaine is produced by esterification of methylecogine with benzoyl-CoA. Notably, stereospecific reduction of C-3 results in exclusively the 3β–configured cocaine-type alkaloids. In contrast, decarboxylation of the acetoacetyl group at C-2 of the *R*-addition product generates tropinone, while a stereospecific reduction of C-3 produces 3α-tropine. Subsequent esterification of 3α-tropine with L-phenyllactic acid (arising from L-phenylalanine), followed by a rearrangement process would produce (–)-hyoscyamine. In turn, 6β-hydroxylation of (–)-hyoscyamine followed by epoxidation via 2-oxoglutarate dependent dioxygenase generates (–)-hyoscine.

1.3.5 Pharmacology of Tropane Alkaloids

Plants containing tropane alkaloids were used since ancient times as medicine, psychoactive drug and poison. In particular, the genus *Datura* (Solanaceae), with some nine species is known to be cultivated throughout tropical and temperate regions of the world, owing to its medicinal and often toxic properties.[24,26,29] In fact, *stramonium* (dried leaves of *Datura stramonium*), *belladonna* (dried leaves of *Atropa belladonna*), and *hyoscyamus* (dried leaves of *Hyoscyamus niger*) are still listed in old American and European pharmacopoeias as valid prescription drugs.[4] Other high alkaloid-yielding Solanaceae plants such as *Brugmansia sanguinea* and *Duboisia* spp. are cultivated by the pharmaceutical industry to produce tropane alkaloids.[5]

Atropine, (–)-hyoscyamine and hyoscine antagonise the central and peripheral effects of acetylcholine on muscarinic acetylcholine receptors (mAChRs). They are classified as competitive antagonists, which block acetylcholine from binding to mAChRs. Different from the nicotinic acetylcholine receptors (Section 1.2.3), mAChRs are metabotropic and function on G-protein signal transduction. Five subtypes of mAChRs (M1 – M5) are currently characterised from the human body.[18,19] Collectively, they mediate the parasympathetic nervous system as well as the cognitive and memory processes of human brain. The parasympathetic nervous system promotes salivation, lachrymation, digestion and excretion. Drugs that antagonise mAChRs will result in anti-secretion, anti-micturition, bronchodilation, mydriasis, cycloplegia and tachycardia, *viz*., physiological responses that are useful in treating various pathological conditions. Besides, antagonism of mAChRs in the central nervous system causes marked excitation (prominent in atropine), followed by sedation

(prominent in hyoscine), amnesia or in toxicity, delirium and death by medullary paralysis.[5,18] Currently, intravenous atropine is indicated for the treatment of bradycardia, hypersalivation, abnormal bronchial secretions and organophosphate pesticide poisoning.[5,24] Hyoscine is formulated as a transdermal patch for the treatment of motion-sickness.[5,24] Semi-synthetic derivatives of atropine such as homatropine, tropicamide and cyclopentolate are widely used as mydriatics for ophthalmological examinations (Fig. 1.9).[5,24] Low-dose atropine eyedrop is also used to retard the progression of childhood myopia.[41] Quaternised tropane alkaloids are particularly valued because they cannot cross the blood-brain barrier, hence devoid of undesirable central nervous system side effects. For example, hyoscine butylbromide is widely used as a gastrointestinal antispasmodic, ipratropium and oxitropium bromide are potent antiasthamatic drugs, while glycopyrrolate is used to counteract the parasympathomimetic side effects of neostigmine in general anesthesia (Fig. 1.9).[5,24] To date, atropine remains the gold standard antimuscarinic drug in pharmaceutical research.

In contrast, the illicit drug (–)-cocaine is a tropane alkaloid of great burden to the global society, with an estimated 14 million cocaine users worldwide.[42] Consumption of cocaine is associated with a wide range of medical, psychiatric and socioeconomic morbidity, e.g., death by overdose, HIV infection and drug-related crimes.[42,43] Cocaine inhibits the VMAT (vesicular monoamine transporter) protein of presynaptic neurons, which recycles monoamine neurotransmitters like dopamine, serotonin and noradrenaline into storage vesicles.[5,18] This causes prolonged stimulatory effects and addiction in the human brain. There is currently no proven pharmacotherapy for cocaine addiction as the search for cocaine-antagonising drugs continues.[24,42] Cocaine also produces a numbing effect on the

mucosa and was once used as a local anaesthetic drug, especially for ophthalmic applications.[5,24] This is due to cocaine's ability to block sodium ion-channels of sensory neurons, inhibiting the transmission of electrical signals that lead to all sensations.[5,18,24] Various synthetic analogues were later developed based on the structure of cocaine, often omitting its tropane moiety. This is because the key pharmacophore was determined to be an aromatic ester linked to an amine group.[5,18,24] Nevertheless, cocaine derived anaesthetics are specifically named with the suffix '-caine', e.g. lidocaine, procaine etc. They are extensively used in local and regional anaesthesia, as well as antiarrhythmic drugs (Fig. 1.9).

Other plant-derived tropane alkaloids such as calystegines are less studied. They are non-centrally active due to their highly polar characteristics.[5] However, calystegines A_3 and B_2 (Table 1.5) were shown to inhibit glycosidase, potentially useful as anti-diabetic and anti-viral drugs.[5,25,32] In contrast, non-plant-based tropane alkaloid homologues are very toxic. The cyanobacteria derived anatoxin-*a* (Fig. 1.10) is highly poisonous, often causing mass fatalities in algal blooms. It binds to nAChRs with high affinity as an agonist, making it a useful pharmacological probe for studying nAChRs.[5] On the other hand, the amphibian derived epibatidine (Fig. 1.10) was once investigated as a lead compound for analgesic drug, which is hundreds of times more potent than morphine.[5,18] Epibatidine binds to specific subtypes of nAChRs that lead to the conduction of pain signals, but its excessive toxicity on the mammalian system poses a limitation.[5,18] Considering the high structural diversity of tropane alkaloids, exciting new findings on their bioactivities are anticipated.

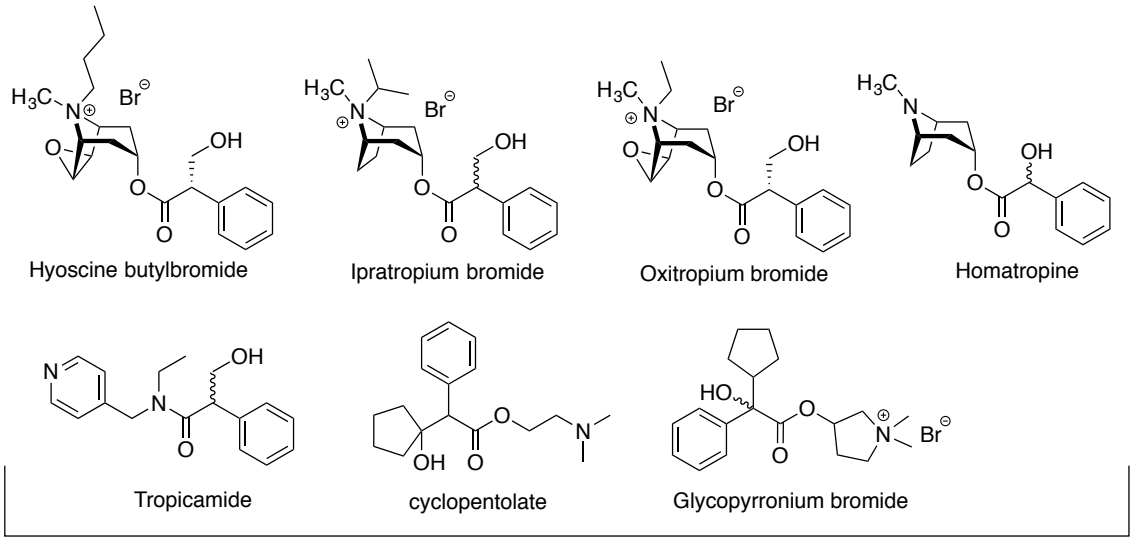

Synthetic and semi-synthetic derivatives of atropine and hyoscine.

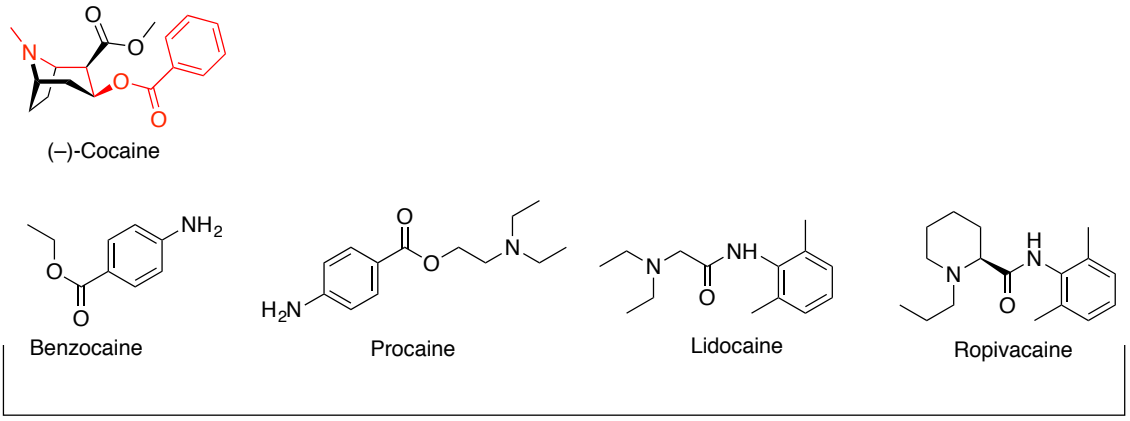

Synthetic derivatives of cocaine.
Note: Pharmacophore of the anaesthetic activity of cocaine is highlighted in red.

Figure 1.9: Synthetic and semi-synthetic tropane alkaloid derivatives used in modern medicine.[5,18,24]

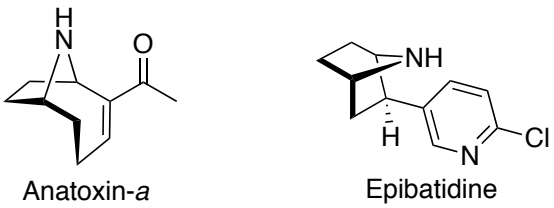

Figure 1.10: Biologically active non-plant-derived tropane alkaloid homologues.

1.3.6 Oligomeric Tropane Alkaloids

Oligomeric (mostly dimeric) tropane alkaloids have been occasionally isolated from plants in the family Solanaceae, Erythroxylaceae and Convolvulaceae.

In this review, four types of oligomeric tropane alkaloids are identified. The first type, represented by the truxillins and mooniines[35] are proposed to arise via a [2+2] photocatalysed cycloaddition of two cinnamoylcocaine monomers, resulting in a dimerised cyclobutane skeleton (c.f., α-truxillin and β-truxillin, mooniines A and B, Table 1.5). Depending on the orientation of the two olefinic functionalities, either the *syn*- or *anti*-addition products are formed. In common with this structure are grahamines A (dimer), B (dimer), C (dimer), D (trimer) and E (trimer), which were elucidated from *Schizanthus grahamii* (Solanaceae) (Table 1.5). The absolute stereochemistry of the grahamines are complicated and remain unresolved.[31] Nonetheless, it is argued that their absence from the roots of *Schizanthus* spp. supported the photocyclisation hypothesis.[31] In contrast, the second type of dimeric tropane alkaloid is condensed via intermolecular esterification of two 3α-tropine moieties with a dicarboxylic acid (e.g., schizanthines B, C and E, Table 1.5).[30] The third type of dimeric tropane alkaloid, i.e., subhirsine,[36] features two tropane moieties condensed via an amide bond (Table 1.5). Subhirsine was reported from the roots of *Convolvulus subhirsutus* (Convolvulaceae), and is currently the sole example of its type.[36] Last but not least, the fourth type of dimeric tropane alkaloid is coupled via a direct N–C bond. This includes bishyoscyamine,[34] which was isolated from the roots of *Anisodus acutangulus* (Solanaceae) (Table 1.5). The absolute stereochemistry of bishyoscyamine was resolved by ECD spectroscopy, while its bioactivity remains unexplored.[34] In view of the structural diversity of dimeric tropane alkaloids in addition to their under-studied biological activity, further phytochemical research is warranted.

1.4 Diarylheptanoids

1.4.1 Introduction and History

Also present in *Pellacalyx saccardianus*, the diarylheptanoids are a group of plant secondary metabolites with a distinctive 1,7-diphenylheptane skeleton. Approximately 400 diarylheptanoids have been characterised to date, occurring in either linear or cyclic forms, while occasionally coupled with other secondary metabolites such a flavonoids, terpenes and glycosides.[43,44] Diarylheptanoids exhibit a sporadic distribution in the plant kingdom but are predominantly elaborated by the families Zingiberaceae, Betulaceae and Juglandaceae.[43–45] Several species from Zingiberaceae, such as the ginger (*Zingiber officinale*), galangal (*Alpinia spp.*), tumeric (*Curcuma longa*) and cardamom (*Elettaria spp.* and *Ammomum spp.*), are widely cultivated as spices or medicinal herbs with huge economic value. In fact, many diarylheptanoids are physiologically active, exhibiting remarkable anti-cancer, anti-inflammation, anti-oxidant and anti-microbial activities.[43–46] Given the high structural diversity of diarylheptanoids, a general review of their chemistry, biosynthesis, and bioactivity is outlined in Sections 1.4.1 – 1.4.5. Notably, Section 1.4.3 underscores the unusual type IV and type V linear diarylheptanoids (Table 1.6), which offer valuable structural comparison to the novel diarylheptanoids obtained herewith (Chapters 4.1 – 4.4).

The first diarylheptanoid, curcumin, was isolated from turmeric (*Curcuma longa*) as a 'yellow-dye' by German scientists, Vogel and Pelletier in 1815.[43,44] Its chemical structure was established by Milobedzka via degradation experiments in 1910 and later confirmed by Lempe in 1913 via total synthesis.[44] In 1953, an Indian chemist Srinivasan separated curcumin as three closely related compounds by

chromatography (curcumin, demethoxycurcumin and bis-demethoxycurcumin) and showed that they exist in kenol-enol tautomeric forms (Table 1.6).[47] Since then, no other diarylheptanoids were reported until 1964, when linear diarylheptanoids such as yashabushiketol (Table 1.6) was elucidated by the Japanese chemist, Asakawa.[43] In the coming 21st century, more than 300 diarylheptanoids have been discovered as they continue to emerge as structurally diverse and biologically active natural products.

1.4.2 Physical and Chemical Properties

Many diarylheptanoids exist as oily liquids at room temperature and pressure. Some diarylheptanoids like curcumin are strongly coloured due to high degree of π-conjugation. The presence of aromatic rings in diarylheptanoids enables their easy detection under short-wave UV light (254 nm), or in the region of 225 – 260 nm by PDA detector. Diarylheptanoids are generally hydrophobic and soluble in various organic solvents like acetone and chloroform. However, diarylheptanoids with polyphenolic or glycosidic substituents tend to be more soluble in polar solvents such as alcohol and water.

The chemical properties of diarylheptanoids are predominated by reactive functionalities within their aryl or heptane group. Diarylheptanoids containing phenol moieties can essentially react as weak acids because the corresponding phenoxide anions are resonance stabilised. In the present study, the acidic property of phenol-containing diarylheptanoids is exploited for their extraction via acid-base chemical partitioning (Section 6.9). Solvents containing formic acid or trifluoroacetic acid (0.1% v/v as additives) were also used to enhance the resolution of phenolic diarylheptanoids under normal phase and reverse phase chromatography. Diarylheptanoids with conjugated diketo substituents like

curcumin can undergo keto-enol tautomerisation under different pH environments. In fact, curcumin was used as a pH indicator because at high pH (> 8.4), the reddish enol form of curcumin is favoured, while at pH <7.4, the orange keto-form predominates.[48] Curcumin is also a well-known complexometric indicator of boron, as it produces a bright red complex (rosocyanine) with boric acid.[48] For the chemical detection of diarylheptanoids in TLC, the use of general staining reagents with strong oxidising property such as iodine or alkaline potassium permanganate is preferred. This is because many diarylheptanoids contain oxidisable olefinic bonds or hydroxyl groups in their heptane chain.

1.4.3 Diarylheptanoid Classification and Natural Occurrence

According to the comprehensive review of naturally occurring diarylheptanoids by Lv and She,[43] diarylheptanoids can be classified into two main classes, i.e, linear and cyclic. Linear diarylheptanoids are further divided into five sub-groups, i.e., types I – V, depending on their substituents or connectivity of the heptane chain. In contrast, cyclic diarylheptanoids are biphenyls or diaryl-ethers, which can be classified into meta-metacyclophanes or meta-paracyclophanes (types VI and VII, respectively). A summary of the seven types of diarylheptanoids is shown in Table 1.6.

Diarylheptanoids exhibit a sporadic distribution in the plant kingdom. Linear diarylheptanoids (types I – V) are predominantly elaborated by the angiosperm families Aceracea, Betulaceae and Zingiberaceae.[43–45] Quantification of species-specific linear diarylheptanoids was even adopted as chemotaxonomic marker to distinguish different *Alnus* species (Betulaceae).[49] Besides, structurally unusual linear diarylheptanoids (types IV and V) are almost exclusively characterised from the genus *Alpinia*, i.e., *A. blepharocalyx* and *A. officinarum*

(Zingiberaceae).[43,50–52] 1,3– and 1,5–Diarylheptanoids are only known from the seaweed *Cymodocea nodosa* (Cymodoceaceae).[43] On the other hand, cyclic diarylheptanoids (types VI and VII) are mainly isolated from the families Betulaceae, Juglandaceae and Myricaceae.[43–45,53] The occurrence of diarylheptanoid types based on plant families is summarised in Table 1.7.

Table 1.6: Classification of linear and cyclic diarylheptanoids.[43–45,50–53]

Type	Feature	Example (known absolute stereochemistry are shown)
I	Linear diarylheptanoids that are saturated, unsaturated, with carbonyl groups and/or olefinic bonds and/or kavain and/or glycoside moiety.	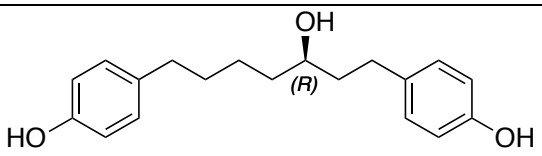 (–)-Centrolobol Isolated from *Betula pendula* 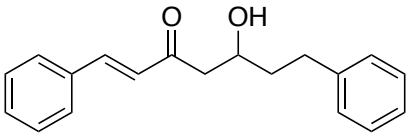 Yashsbushiketol Isolated from *Alnus firma* 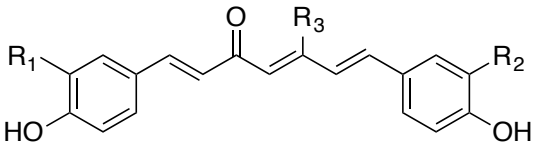 Curcumin I, R_1: OCH_3 R_2 : OCH_3 R_3 : OH Curcumin II, R_1: OCH_3 R_2 : H R_3 : OH Curcumin III, R_1: H R_2 : H R_3 : OH Isolated from *Curcuma longa*

		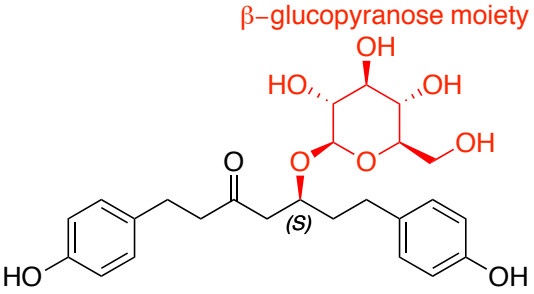 Platyphylloside Isolated from *Alnus hirsuta* 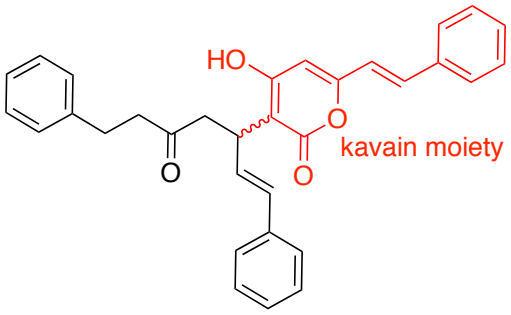 Katsumadin B Isolated from *Alpinia katsumadai*
II	Linear diarylheptanoids consisting of pyran ring with 1,5–oxy bridge or furan ring with 3,6–oxybridge.	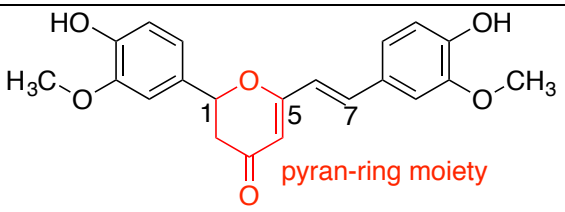 Cyclocurcumin Isolated from *Curcuma longa* 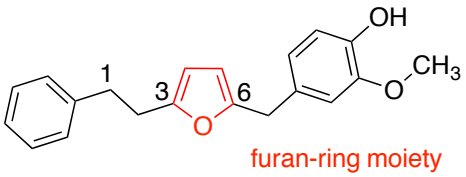 2-methoxy-4-((5-phenethylfuran-2-yl)methyl)phenol Isolated from *Alpinia officinarum*

III	Linear diarylheptanoids with chalcone, flavanone, isoflavanone or flavanol substituents.	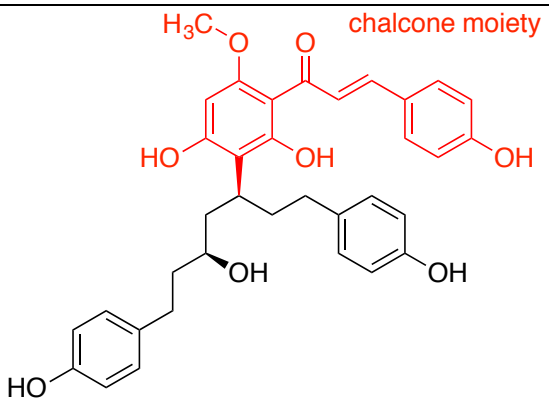 Deoxycalyxin A Isolated from *Alpinia blepharocalyx* 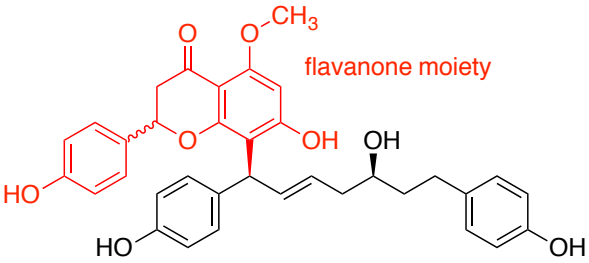 Calyxin C Isolated from *Alpinia blepharocalyx* 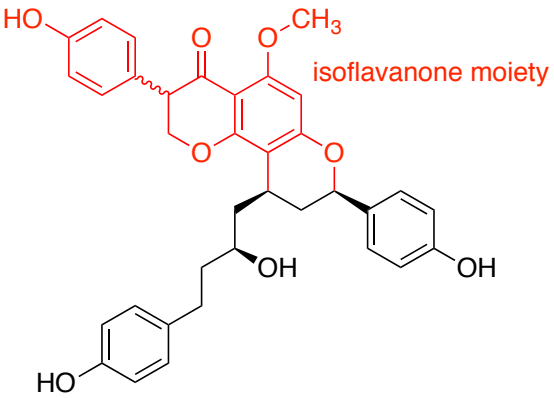 Calyxin M Isolated from *Alpinia blepharocalyx*

		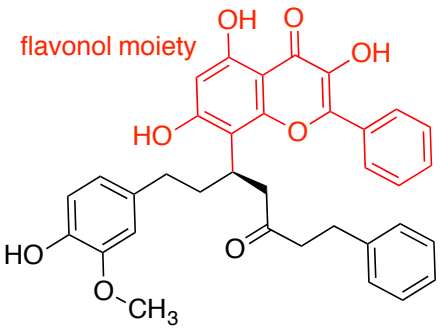 Officinin A Isolated from *Alpinia officinarum*
IV	Dimeric linear diarylheptanoids linked via epoxy-rings, phenyl group, chalcone or pyridine moiety. Note: monomeric units are highlighted in red and blue.	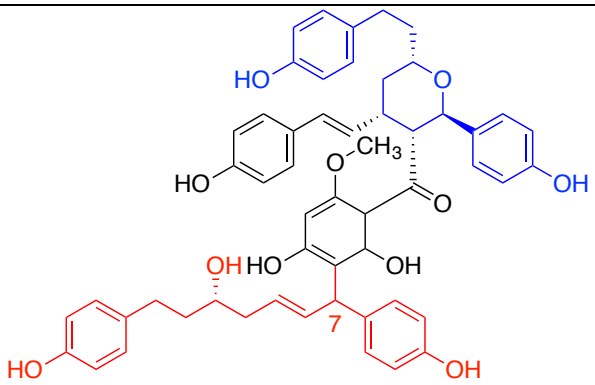 Blepharocalyxin A: 7*S* Blepharocalyxin B: 7*R* 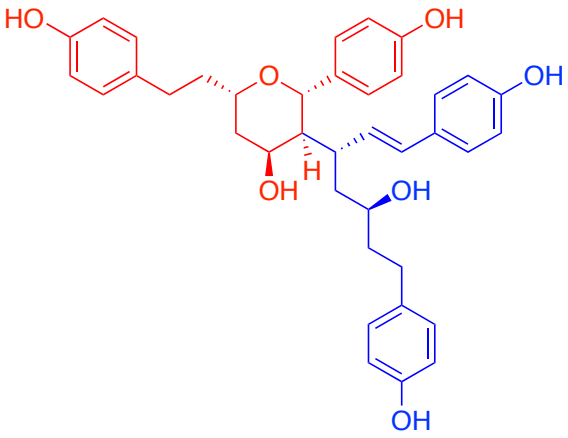 Blepharocalyxin C

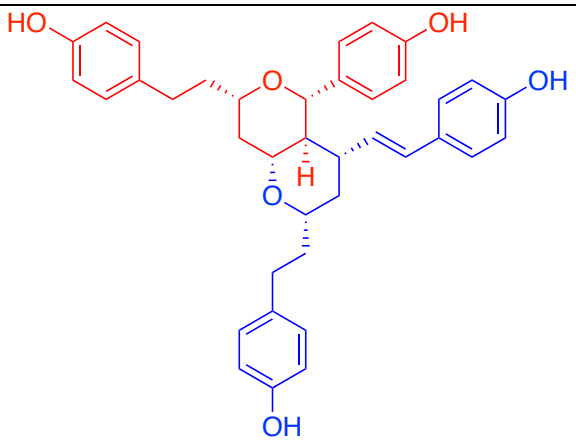

Blepharocalyxin D

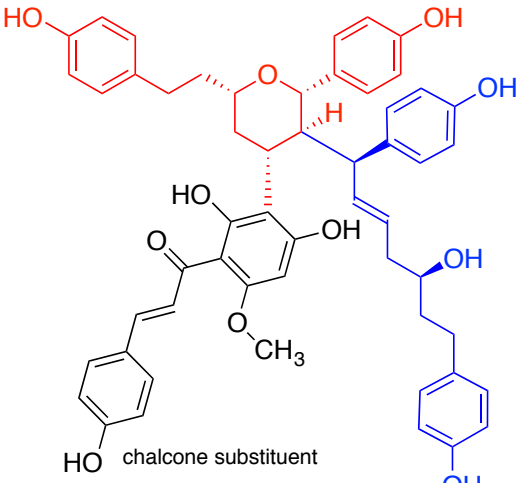

Blepharocalyxin E

Note: Bleparocalyxins A–E were isolated from *Alpinia blepharocalyx*

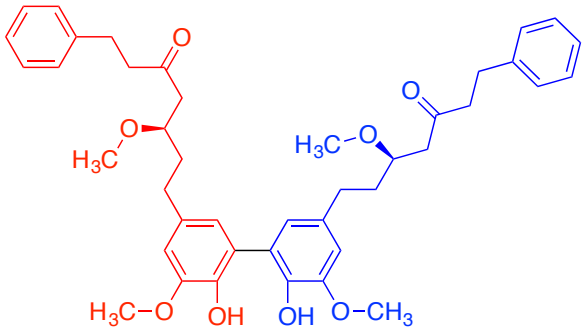

Alpinoid A
Isolated from *Alpinia officinarum*

		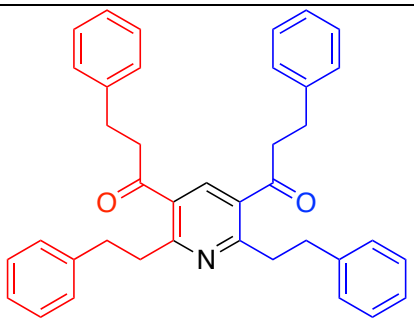 Officinaruminane A 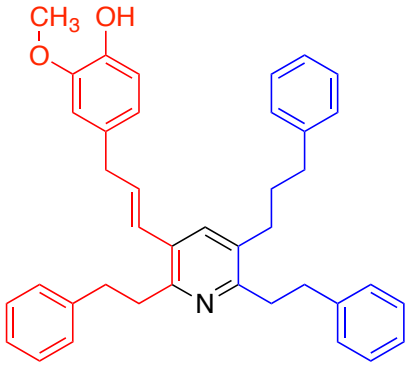 Officinine B Note: Officinaruminane A and officinine B were isolated from *Alpinia officinarum.*
V	Unusual 1,3– or 1,5–linear diarylheptanoids with varying degree of unsaturation, and 1,7–linear diarylheptanoid-terpene or sesquiterpene adducts.	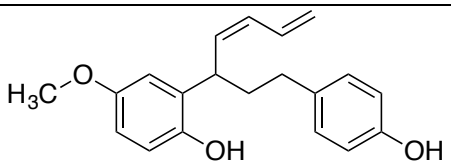 Cymodiene Isolated from *Cymodocea nodosa* 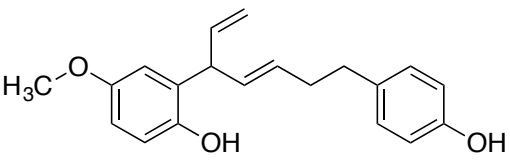 Isocymodiene Isolated from *Cymodocea nodosa* 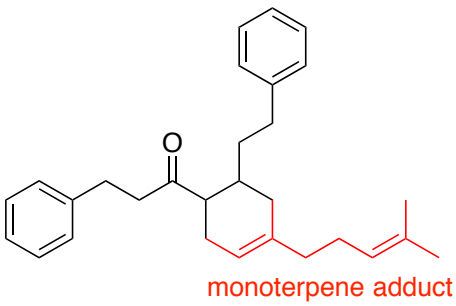 monoterpene adduct Officinaruminane B (unknown stereochemistry)

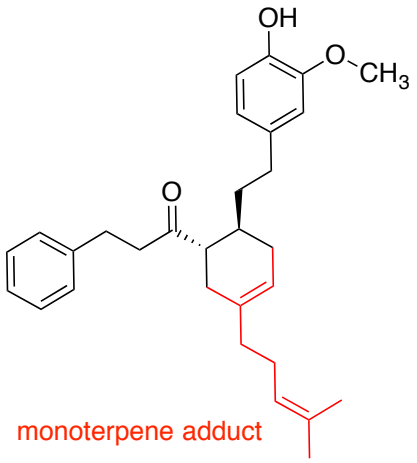

Alpinoid A (racemate)

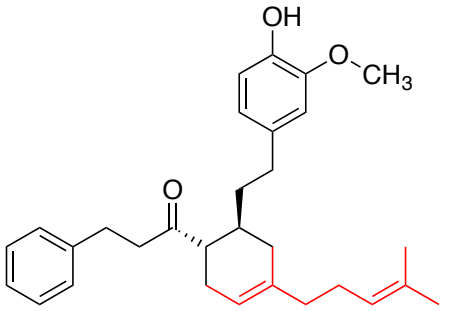

Alpinoid B (racemate)

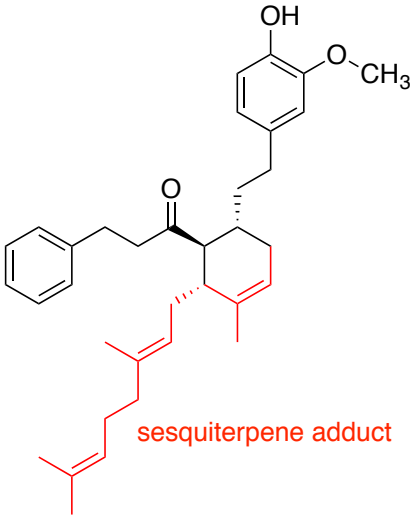

Alpinoid C (racemate)

		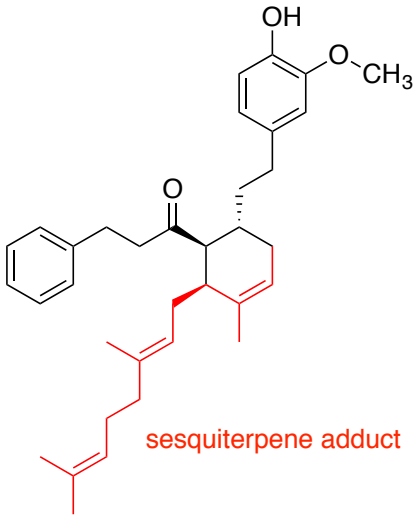 Alpinoid D (racemate) 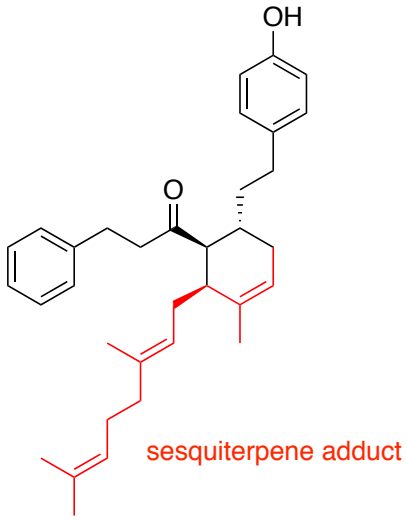 Alpinoid E (racemate) Note: Officinaruminane B and Alpinoid A–E were isolated from *Alpinia officinarum.*
VI	Meta-paracyclophanes linked via diaryl-ether bonds. Contain saturated or unsaturated aliphatic chain, with one or more carbonyls.	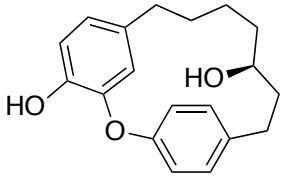 Acerogenin A Isolated from *Acer nikoense* 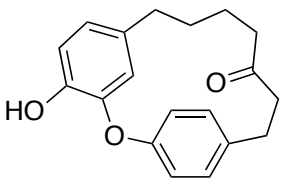 Acerogenin C Isolated from *Acer nikoense*

		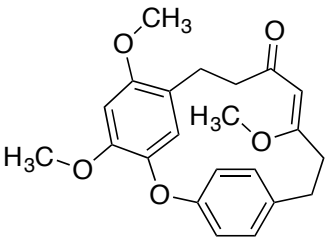 Garuganin I Isolated from *Garuga pinnata*
VII	Meta-metacyclophanes linked at two phenyl groups. Contain saturated or unsaturated aliphatic chain, with one or more carbonyls. Include some unusual examples with ether linkage or *p*-benzoquinonyl moiety.	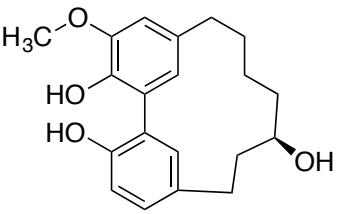 Juglanin B Isolated from *Juglans regia* 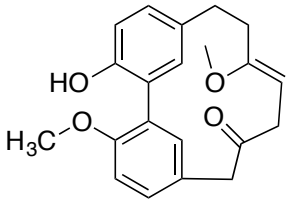 Garuganin V Isolated from *Garuga pinnata* 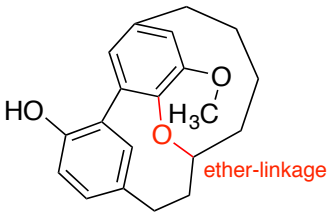 Myricarborin (stereochemistry unknown) Isolated from *Myrica arborea* 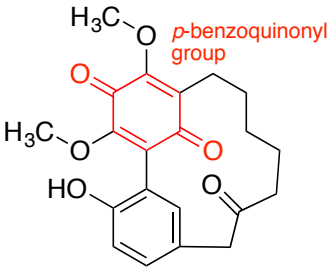 Rubanone Isolated from *Myrica rubra*

Table 1.7: The occurrence of diarylheptanoid types based on plant families.[43-46]

Family	Genus	Linear diarylheptanoid					Cyclic diarylheptanoid	
		Type I	Type II	Type III	Type IV	Type V	Type VI	Type VII
Aceraceae	*Acer*	+	-	-	-	-	+	+
Actinidiaceae	*Clematoclethra*	-	-	-	-	-	-	+
Betulaceae	*Alnus*	+	+	-	-	-	-	-
	Betula	+	-	-	-	-	+	+
	Carpinus	-	-	-	-	-	-	+
Burseraceae	*Garuga*	-	-	-	-	-	+	-
Cymodoceacea	*Cymodocea*	-	-	-	-	+	-	+
Dioscoreaceae	*Dioscorea*	-	+	-	-	-	-	-
	Tacca	+	-	-	-	-	-	-
Fabaceae	*Centrolobium*	+	+	-	-	-	-	-
Juglandaceae	*Juglans*	+	+	-	-	-	+	+
	Platycarya	-	-	-	-	-	+	-
	Rhoiptelea	+	-	-	-	-	-	-
Myricaceae	*Myrica*	-	-	-	-	-	+	+
Zingiberaceae	*Alpinia*	+	+	+	+	+	-	-
	Curcuma	+	+	-	-	-	-	-
	Zingiber	+	+	-	-	-	-	-

1.4.4 Diarylheptanoid Biosynthesis

The biosynthesis of diarylheptanoids is widely accepted to involve the shikimate pathway, with two possible routes starting from the amino acid L-phenylalanine.[44] In the first proposed pathway[44] (Fig. 1.11), L-phenylalanine is biotransformed into cinnamoyl CoA via the enzyme phenylalanine ammonia lyase (PAL). Cinnamoyl CoA then undergoes Claisen condensation with one unit of malonyl CoA to produce a diketide intermediate (cinnamoylacetyl CoA), which contains a phenylpentane skeleton. The cinnamoylacetyl CoA enolate anion then undergoes Claisen condensation with another unit of cinnamoyl CoA, with concomitant decarboxylation to generate a diketo-diarylheptanoid. This pathway

agrees to the general observation that linear diarylheptanoids often have carbonyl groups at C-3 and C-5 on their heptane chain, while the olefinic bonds are located at C-1 and C-6, *viz*., two cinnamate units linked by a center malonyl carbon. As empirical support, ^{14}C labelled phenylalanine, acetate and malonate were shown to impart radioactivity into curcumin a few days following their injection into turmeric.[44] In contrast, an alternative biosynthetic pathway[44] (Fig. 1.12) suggests that cinnamoyl CoA undergoes Claisen condensation with five units of malonyl CoA, resulting in a pentaketide intermediate with a phenyldodecene backbone. The pentaketide intermediate then undergoes intramolecular cyclisation to generate a proto-diarylheptanoid containing a cyclohexatrione moiety, which undergoes consecutive reduction and elimination reactions to yield a diarylheptanoid with a *p*-hydroxyphenyl substituent. Only one unit of cinnamoyl CoA is required in the second pathway, although further experiments are required to validate it.

On the other hand, cyclic diarylheptanoids are proposed to arise from linear diarylheptanoids via phenolic oxidative coupling, which involves the formation of free radicals (Fig. 1.13).[53] Due to the delocalisation of the unpaired electrons into each phenol ring, different cyclised products can arise from different resonance forms of the free radical. For instance, *C–O* coupling would lead to the formation of meta-paracyclophanes with a diarylether linkage, while ortho-ortho coupling would result in the formation of meta-metacyclophanes.

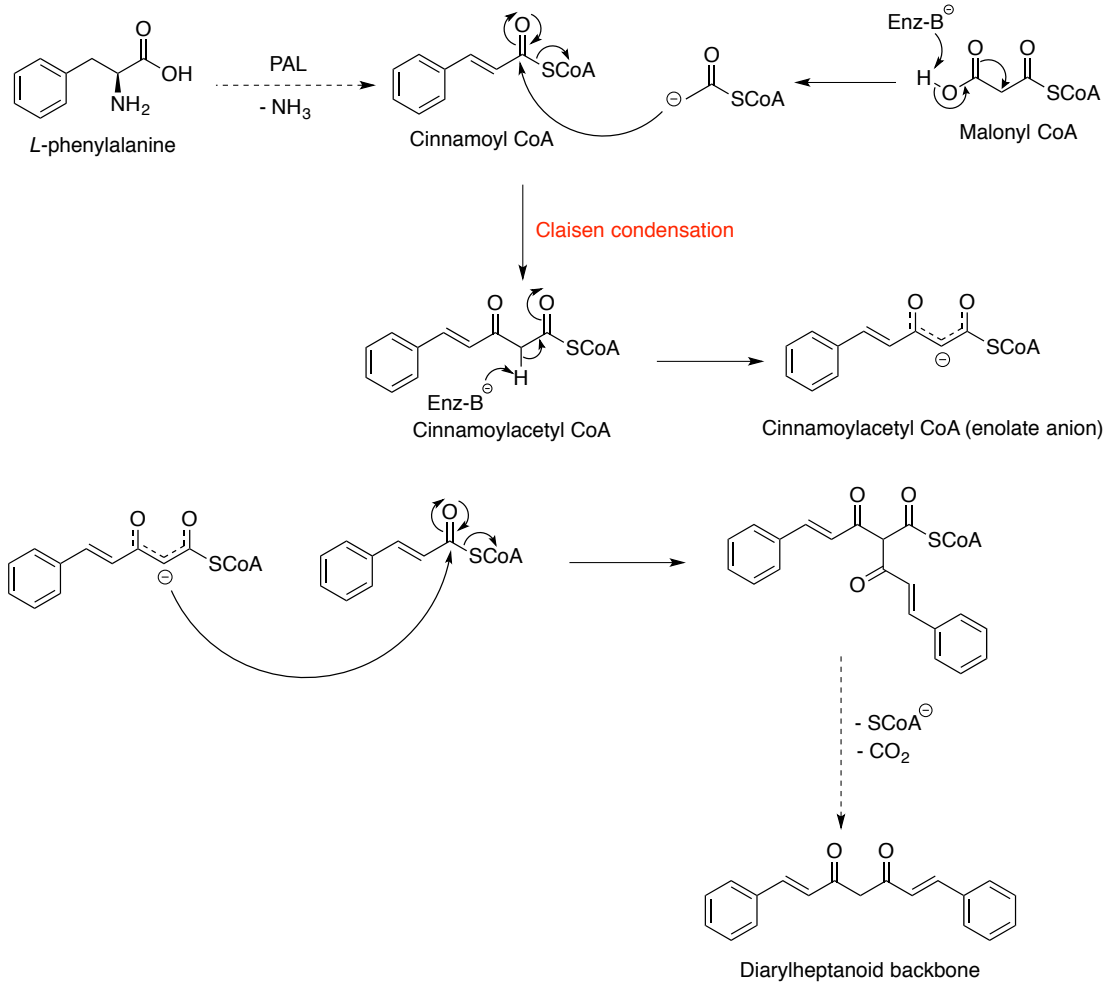

Figure 1.11: Biosynthetic pathway of linear diarylheptanoid.

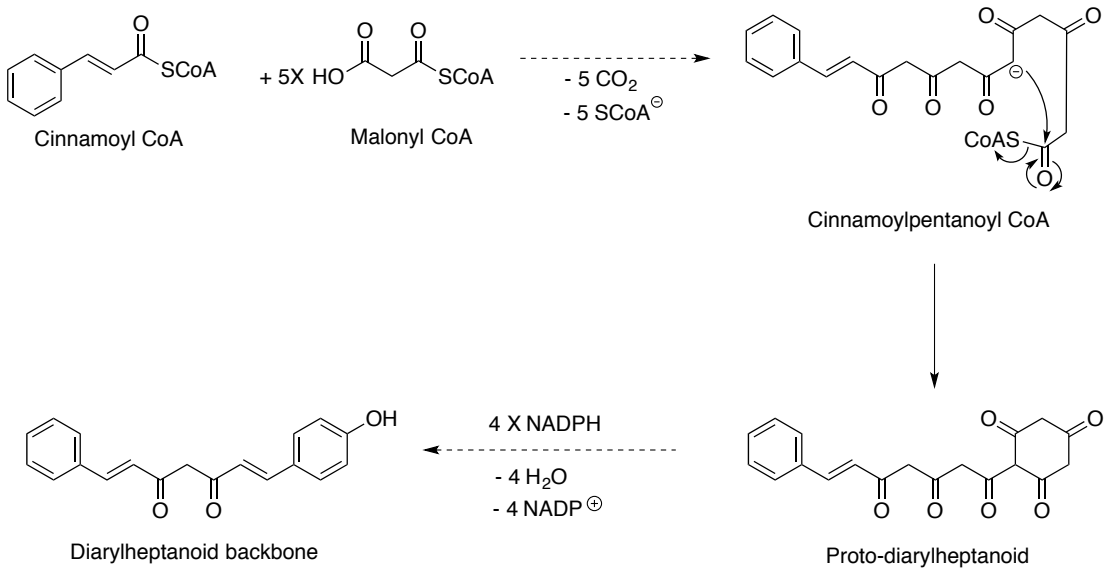

Figure 1.12: Alternative biosynthetic pathway of linear diarylheptanoid.

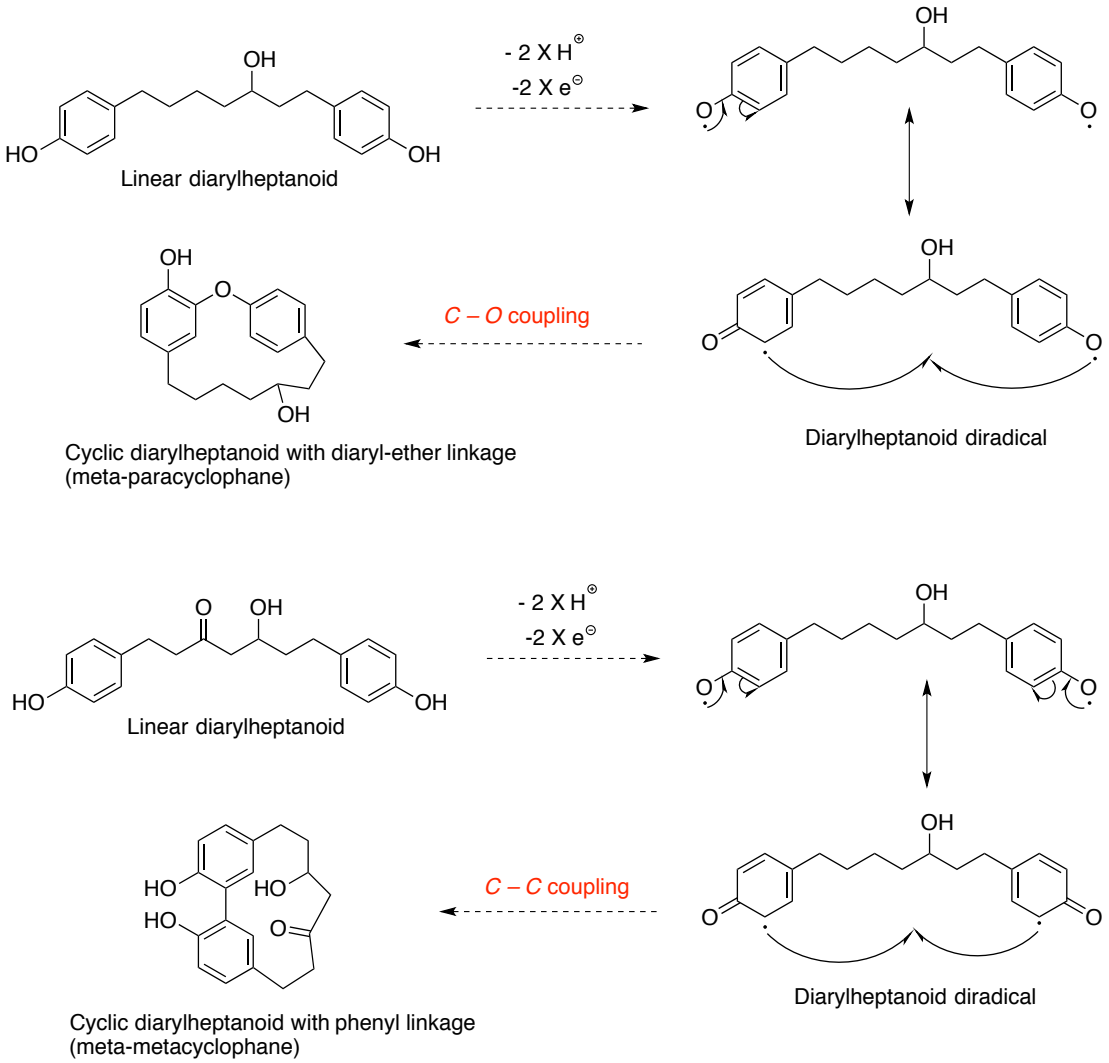

Figure 1.13: Biosynthetic pathway of cyclic diarylheptanoid.

1.4.5 Bioactivity of Diarylheptanoids

Many plants containing diarylheptanoids such as turmeric (*Curcuma longa*), gingers, galangals (*Alpinia*, *Etlingera* and *Zingiber* spp.), maples (*Acer* spp.) and walnuts (*Juglans* spp.) are used since ancient times as spices or traditional herbs, to treat ailments such as indigestion, gastritis or conditions that generally involve inflammation of the human body.[43,44,46] The ethnopharmacy of diarylheptanoids provides a strong contrast to alkaloids, which are often psychoactive and poisonous (Section 1.1.6). Nonetheless, bioactive diarylheptanoids have gained interest since the 1900s, beginning with the isolation of curcumin, which is the

most widely studied diarylheptanoid to date. Curcumin is well-known to have a pleiotropic effect, capable of producing many therapeutic responses such as anti-cancer, anti-inflammation, anti-diabetic, anti-microbial and anti-coagulation both *in vitro* and *in vivo*.[43,44,46,54] It has even reached phase I and phase II human clinical trials to treat various cancers and inflammatory diseases.[54] However, there are also counter-evidences to suggest that curcumin is unstable, has low-bioavailability and causes non-specific interactions that lead to false-positive results in many bioassays, i.e., a pan-assay interference compound (PAINS).[55] In spite of the controversial biological effects of curcumin, the huge structural diversity of diarylheptanoids ensures continued research into their bioactivities. A summary of the known bioactivity of selected diarylheptanoids is shown in Table 1.8.

Table 1.8: Examples of natural diarylheptanoids with known bioactivity.

Bioactivity	Compound structure/ botanical source	Remarks
Cytotoxic activity Note: A pure compound with IC_{50} of < 10 μM is considered as cytotoxic when tested against a cancer cell line (ACS standard).	Curcumin (Table 1.6)/ *Curcuma longa*	Reached phase I and phase II clinical trials for human colorectal cancer, pancreatic cancer, breast cancer, prostate cancer, multiple myeloma and lung cancer.[54] Shown to lower cancer marker levels, improve precancerous lesions and provide symptomatic relief.[54] Generally safe and well-tolerated.
	Platyphylloside (Table 1.6)/ *Betula papyrifera*	Moderate *in vitro* cytotoxicity on A-549 lung cancer and DLD-1 colorectal cancer cell lines, IC_{50}: 10.3–13.8 μM.[43]

	Blepharocalyxin D (Table 1.6)/ *Alpinia blepharocalyx*	Potent *in vitro* cytotoxicity on 26-L5 colorectal cancer cell lines, IC_{50}: 3.16 μM.[43]
	Blepharocalyxin E (Table 1.6)/ *Alpinia blepharocalyx*	Moderate *in vitro* cytotoxicity on HT-1080 fibrosarcoma cancer cell lines, IC_{50}: 9.02 μM.[43]
Antimicrobial activity	Hirsutenone/ *Alnus hirsuta* 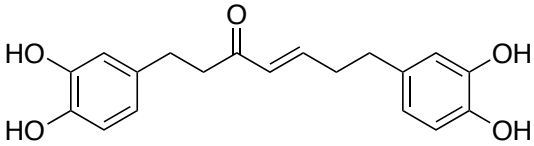	Antiviral effect on SARS coronavirus via inhibition of papain-like viral protease. Also inhibits the growth of methicillin resistant *Staphylococcus aureus* (MRSA) bacteria, MIC: 31.25–250 μg/mL.[56]
	Platyphyllone (synonymous with platyphyllonol)/ *Alnus japonica* 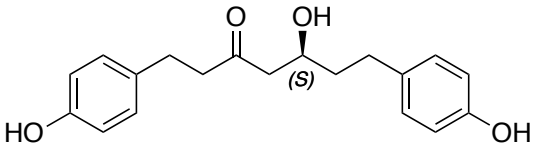	Strong anti-influenza activity activity against KBNP-0028 (H9N2) avian influenza virus, EC_{50}: 29.9 µM (positive control, Zanamivir, EC_{50}: 16.9 μM).[57]
Antioxidant activity	Curcumin I–III (Table 1.6)/ *Curcuma longa*	Potent peroxynitrite scavenging activity, IC_{50}: 4.0–29.0 μM.[43]
	Acerogenin E and K/ *Acer nikoense* 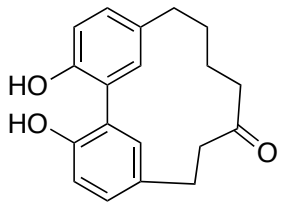 Acerogenin E	Inhibit nitric oxide production in lipopolysaccharide activated macrophages, IC_{50}: 24 μM and 25 μM, respectively (positive control, monomethyl-L-arginine monoacetate (L-NMMA), IC_{50}: 28.0 μM).[58]

	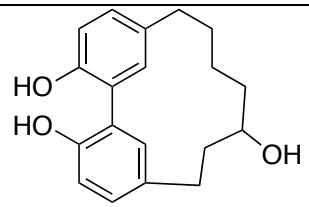 Acerogenin K Note: Unknown stereochemistry	
Anti-Alzheimer's activity	Myricanol/ *Myrica cerifera* 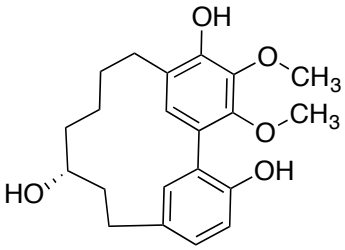 Myricanol	Lower tau-protein activity in *ex-vivo* brain slices of murine model.[59]
Antiemetic activity	5-hydroxy-7-(4-hydroxyphenyl)-1-phenyl-3-heptanone/ *Alpinia officinarum* 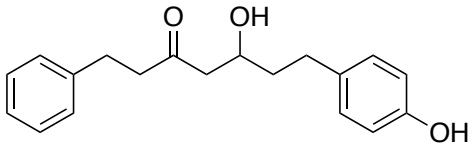 Note: Unknown stereochemistry	Inhibited copper sulphate induced retching response of chicks via a dose-dependent manner. Major anti-emesis constituent in the rhizomes of *A. officinarum*.[60]
	Katsumadain A/ *Alpinia katsumadai* 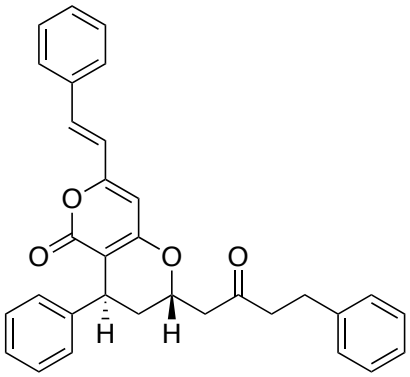 Katsumadain B/ *Alpinia katsumadai*	

1.5 *Hippobroma longiflora* (L.) G. Don

1.5.1 Taxonomy and Molecular phylogeny

Hippobroma longiflora (L.) G. Don is a species of flowering plant belonging to the family Campanulaceae (subfamily Lobelioideae).[61] The genus *Hippobroma* is currently monotypic, with the lectotype specimen *Hippobroma longiflora* (L.) G. Don, Gen. Hist. 3:717. 1834 deposited in the Sloane Herbarium 3:23, upper plant (BM).[61] It was first collected by Sir Hans Sloane during is his voyage to Jamaica (1687-1689) and described by Carl Linnaeus in 1753 as *Lobelia longiflora* L.[61] It was subsequently reclassified as *Hippobroma longiflora* (L.) G. Don by the Scottish botanist, George Don in 1834.[61] The Latin name *Hippobroma longiflora* literally translates as "horse-poison, long-flower".[62]

The plant family Campanulaceae comprises a group of dicotyledonous flowering plants (order Asterales) with cosmopolitan distribution.[63,64] It consists of roughly 84 genera and 2400 species, ranging from small herbs to trees.[63,64] The general synapomorphic characteristics of Campanulaceae include: 5-lobed flowers and calyx, epigynous flowers and lactifers producing milky sap.[63] The family Campanulaceae is further divided into five subfamilies: Campanuloideae, Nemacladoideae, Cyphioideae, Cyphocarpoideae and Lobelioideae, the latter being the largest subfamily consisting of around 1200 species in 30 genera worldwide.[63] Members in the subfamily Lobelioideae are extremely diverse and were subjected to various morphological classifications as well as taxonomic discrepancies. However, recent advancements in molecular biology have revealed the phylogeny and evolutionary trends in Lobelioideae, to the point where molecular data surpassed morphological studies.[63,64] In a higher-level phylogenetic study employing conservative gene markers together with worldwide sampling, Antonelli

(2007) classified the subfamily Lobelioideae into 5 different clades.[63] Of these, *H. longiflora* (L.) G. Don is grouped into clade 5, which also includes the monotypic genus *Downingia* and *Solenopsis.*[63] Besides, there is strong support indicating that *H. longiflora* belongs to a subclade that is geographically confined to the Antilles (West Indies).[63,64] This inference is consistent with the historic records that *H. longiflora* was initially described from Jamaica.

1.5.2 Morphology

Hippobroma longiflora is an evergreen, herbaceous flowering plant that grows to ca. 20 cm in height (Fig. 1.14a). It prefers wet soil and shady area, where it quickly colonises. The leaves of *H. longiflora* are dark green, simple, lanceolate and dentated, usually around 10 cm long. They are sessile (lack petioles and stipules) and spirally arranged. The top of the leaves is glabrous (without hairs), while the bottom is slightly hairy (Fig. 1.14a). The stems of *H. longiflora* are erect and pubescent (with short hairs), also dark green in colour. The flowers are showy, solitary and axillary (arising from the base of the leaf) (Fig. 1.14b). The corolla is 5-lobed, actinomorphic and pure white in colour. The androecium, which consists of 5 stamens, is grouped to one end of the flower. The calyx is also 5-lobed, hairy and tubular, encasing an epigynous ovary (Fig. 1.14c). *H. longiflora* can potentially undergo self-pollination. The fruits are in the form of capsules, also encased in the calyx. The capsules are made up of two compartments when matured, containing numerous small black seeds. All parts of the plant exude a sticky white sap when cut.

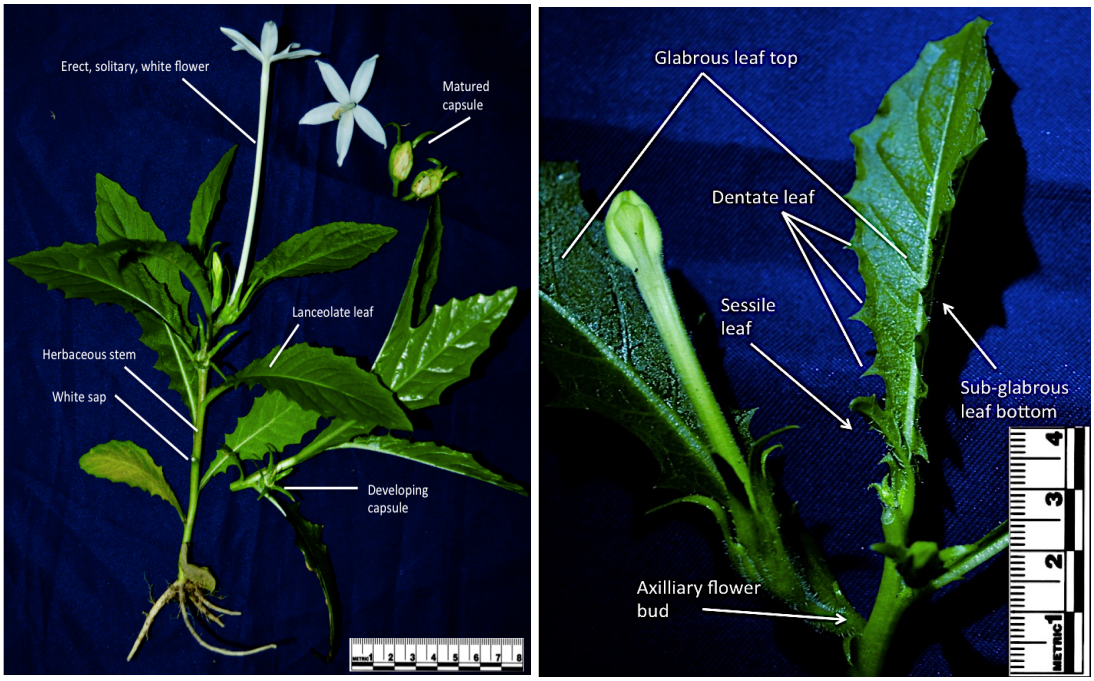

Figure 1.14a: Gross morphology of *H. longiflora.*

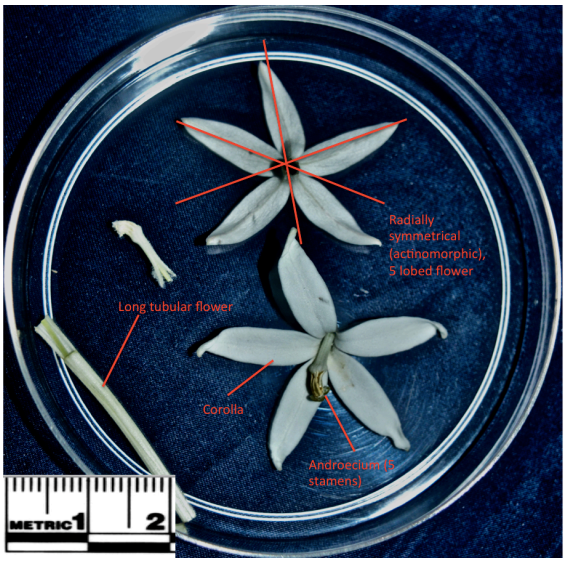

Figure 1.14b: Flower morphology of *H. longiflora.*

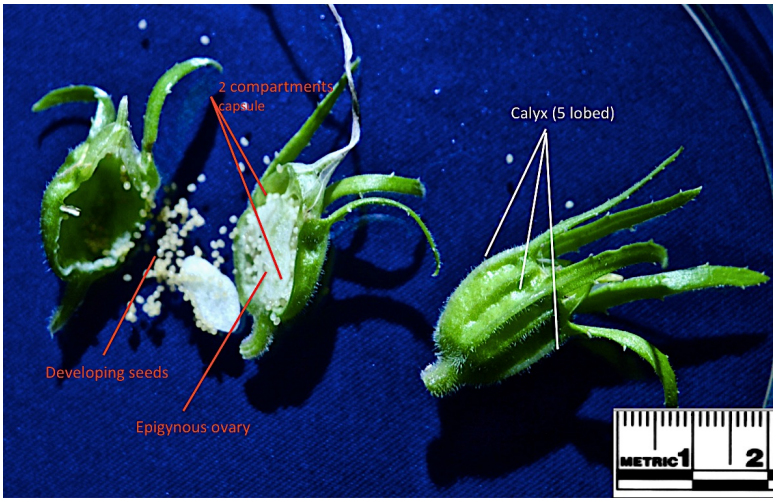

Figure 1.14c: Capsule morphology of *H. longiflora.*

1.5.3 Ethnobotany

As reflected by its Latin name, *Hippobroma longiflora* is widely regarded as a poisonous plant. There are various anecdotal claims elaborating the toxic effects of this species. The sap of *H. longiflora* is said to cause blindness in contact with the eyes, while ingestion may produce symptoms such as vomiting, rapid feeble heart rate and muscle paralysis.[65] Owing to its purportedly highly toxicity, *H. longiflora* is seldom used internally as traditional medicine. In Malaysia, a paste of the plant can be applied topically to achieve counter-irritant and analgesic effects.[65] It is also indicated for treating snakebites and bee stings. As with many poisonous plants in the region, *H. longiflora* is sometimes planted as a repellent for snakes.

1.5.4 Phytochemicals, Bioactivities and Research Gap

To date, scientific literature regarding the phytochemistry of *Hippobroma longiflora* is scarce. Three piperidine alkaloids of the lobeline type were isolated and characterised from the aerial parts of *H. longiflora.*[20,66] In contrast, the roots of *H. longiflora* yielded a polyacetylene glycoside, lobetyolin.[20] A list of known phytochemicals isolated from *Hippobroma longiflora* is shown in Table 1.9. It is

noteworthy that the previous two phytochemical studies on *H. longiflora* were conducted on specimens collected from Denmark[20] and Hong Kong.[66] The phytochemistry of the Malaysian (Southeast Asian) specimens remains unexplored.

Table 1.9: Known phytochemical constituents of *Hippobroma longiflora*.

Compound structure and name	Reference
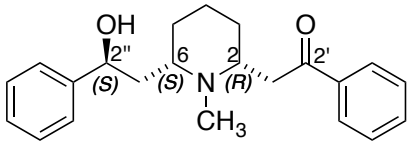 2*R*,6*S*,2′′*S*-Lobeline (**3**)	20
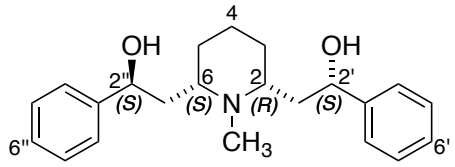 (−)-*cis*-2′,2′′-Diphenyllobelidiol (**4**)	20,66
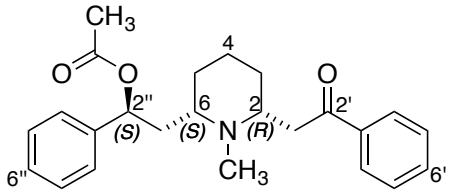 (2*R*,6*S*,2′′*S*)-2′′-*O*-Acetyllobeline	20
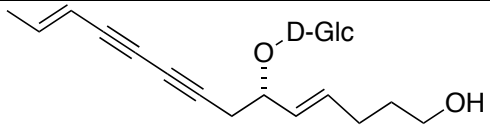 Lobetyolin (polyacetylene glycoside)	20

The biological activity of *H. longiflora* is not well studied. Under the synonym *Isotoma longiflora*, *H. longiflora* was tested for its piscicidal (fish-killing) activity.[65] The alkaloidal extract of the plant, although not characterised, produced high toxicity towards *Tilapia mossambica*, but not *Labistes reticulates.*[67] The crude ethanolic extract of *H. longiflora* also produced toxic effects on the brine shrimp larvae (*Artemia nauplii*), giving a lethal concentration (LC_{50}) of 423 ppm.[68] These preliminary reports concur with the traditional claims that *H. longiflora* is a

poisonous herb, which should be used with caution. Besides, the ethanolic leaf extract of *H. longiflora* exhibited analgesic effects towards acetic acid induced writhing response in the murine model.[69] While the analgesic components were not elucidated, they are possibly due to the presence of neuroactive alkaloids. Indeed, our preliminary TLC-based phytochemical screening on the crude extract of *H. longiflora* revealed a rich presence of multiple alkaloids. Considering the occurrence of new lobeline-type alkaloids in *H. longiflora,* in addition to the valuable bioactivity of lobeline (Section 1.2.3), a detailed phytochemical investigation on this species is warranted. The main research gap to be addressed here is the lack of phytochemical studies into the pure alkaloids of *H. longiflora*.

1.6 *Pellacalyx saccardianus* Scort.

1.6.1 Taxonomy and Molecular Phylogeny

Pellacalyx saccardianus Scort. is a species of deciduous tree belonging to the plant family Rhizophoraceae.[70] It was first described as a new species by the English botanist, Sir Joseph Dalton Hooker (1817-1911) in *Icones Plantarum* in 1886.[70] In its original description, *P. saccardianus* is named after the Italian botanist Benedetto Scortechini (1845-1886). The holotype specimen of *P. saccardianus* was reported by Hooker from the state of Perak and Melaka in Peninsular Malaysia.

The plant family Rhizophoraceae (*sensu lato*) comprises ca. 16–18 genera with 120 species collectively known as the mangroves.[71,72] Swedish botanist Carl Linnaeus (1741-1755) first described this taxon to include a group of trees occurring in tropical mangrove swamps, based on the type species *Rhizophora mangle* L.[71] Plants of the family Rhizophoraceae have a pantropical distribution and

can be found in estuary intertidal zones, inland forests as well as montane habitats. Most members of Rhizophoraceae are trees or shrubs exhibiting pronounced root formations, woody bark and opposite leaves with interpetiolar stipules.[70,71] It is widely recognised that the family Rhizophoraceae are divided into four tribes, i.e., Anisophylleae, Gynotrocheae, Macarisieae and Rhizophoreae.[71,72] The Rhizophoreae tribe consists of four genera (*Rhizophora*, *Bruguiera*, *Kandelia* and *Ceriops*), which are mainly trees confined to saltwater intertidal zones.[71] They represent the true mangrove species vital to the estuarine ecosystem and are well-known for bearing remarkable aerial root structures and viviparous fruits. The other tribes Anisophylleae, Gynotrocheae and Macariseae consist of lesser known inland shrubs and trees, with highly variable morphology and complicated taxonomy.[71,72] The genus *Pellacalyx* is currently grouped within the tribe Gynotrocheae together with three other genera, namely, *Carallia*, *Crossostylis* and *Gynotroches*.[71] Recent phylogenetic analyses have erected the tribe Anisophyllaeae into a distinct family, while supporting the genus *Gynotroches* and *Pellacalyx* to be sister taxons.[71] Interestingly, the Rhizophoraceae family is shown to be closely related to the Coca family (Erythroxylaceae) based on both molecular phylogeny and cladistic morphology (floral structure).[73,74] This observation may offer tentalising biogenetic basis for the occurrence of tropane alkaloids in both plant families.

The genus *Pellacalyx* Korth. was first described by the Dutch botanist, Pieter Willem Korthals in 1836.[70] Currently, it comprises eight taxonomically accepted species, namely, *P. axilliaris*, *P. lobbii*, *P. pustulatus*, *P. symphiodiscus*, *P. parkinsonii*, *P. cristatus*, *P. yunnanensis* and *P. saccardianus*.[70] Of these, *P. axilliaris* and *P. saccardianus* are endemic to Peninsular Malaysia, the latter occurs in secondary

rainforests, while the former is confined to freshwater swamps.[70] The common morphological features of *Pellacalyx* include opposite, decussate leaves, which are often serrulate, prominent interpetiolar stipules, hollow young stems and conspicuous oblong seeds.[70]

1.6.2 Morphology

Pellacalyx saccardianus is a medium sized tree of ca. 15 m tall, with woody trunk measuring a diameter of ca. 25 cm (Fig. 1.15a). The leaf of *P. saccardianus* usually measures around 14 x 5 cm, with 9 – 12 pairs of nerves. They are oblong (long parallel sides) with a short tip, glaborous (without hairs) and serrulated (toothed edges) (Fig. 1.15b). The stipules are ca. 10 mm long, highly conspicuous and sheath the young shoots without overlapping margins (Fig. 1.15c). The flowers are small, 4-merous with filamentous petals, 2 – 8 fascicled (clustered) or on branched glomerules (Fig. 1.15d), abundant during May to December. The calyx and calyx tubes are both densely haired. The fruits are ovate, measure 2.5 x 1 cm, subglaborous, greenish yellow when ripe and abundant from June to November (Fig. 1.15d). The young branches are puberulous (fine, downward pointing hairs) with hollow stems, while the bark is usually reddish in colour. *P. saccardianus* also has a unique colleter (secretory structure on the stipule), which aids in its identification, i.e., multiple irregular triangle shaped colleters along the adaxial (inner) sides and the base of its stipules.[72]

Figure 1.15a: Adult specimen of *P. saccardianus*.

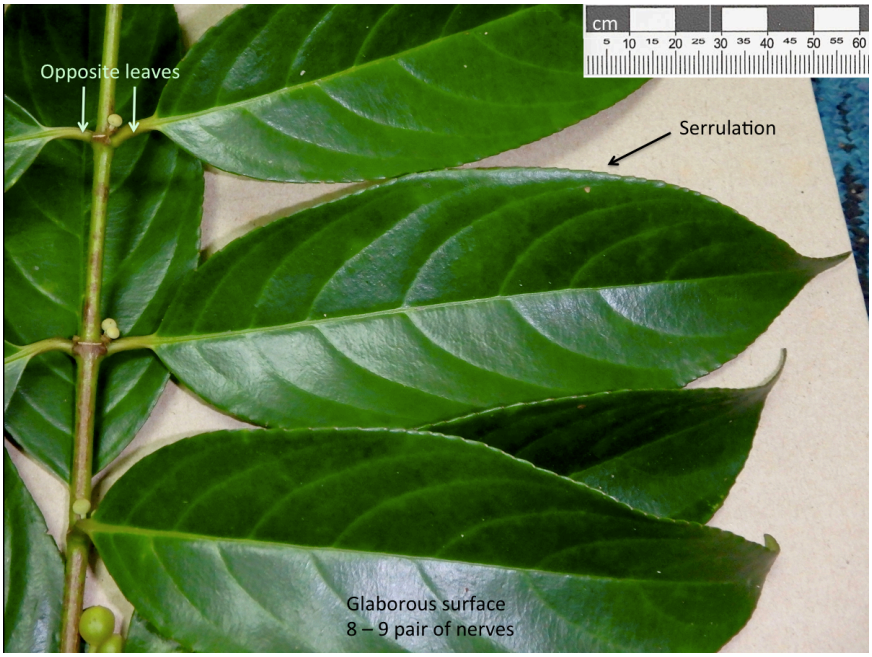

Figure 1.15b: Leaf morphology of *P. saccardianus*.

Figure 1.15c: Interpetiolar stipules of *P. saccardianus*.

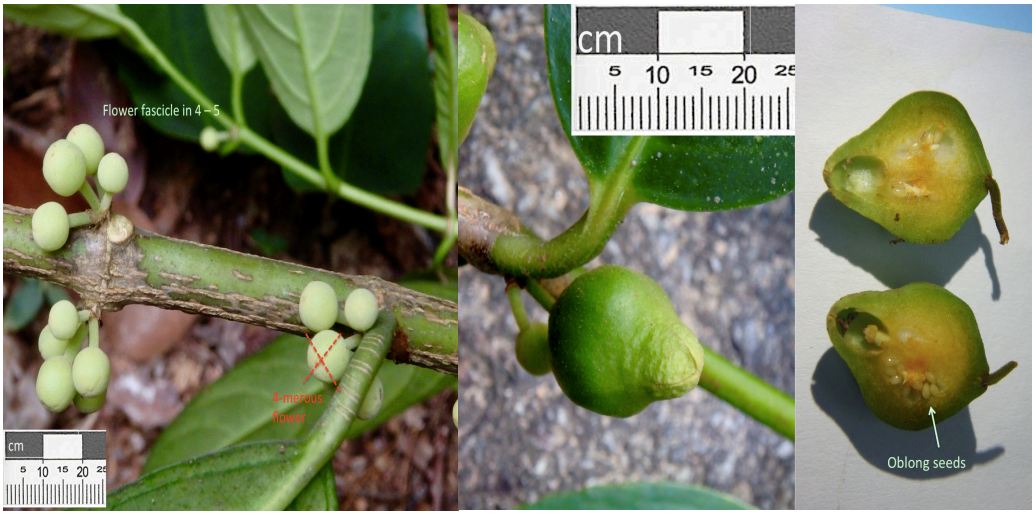

Figure 1.15d: Flower and fruit morphology of *P. saccardianus*.

1.6.3 Ethnobotany

Very little is known about the ethnobotany of *Pellacalyx saccardianus* although it is a common species in Peninsular Malaysia. This is probably because *P. saccardianus* is a relatively large tree, making its cultivation impractical for traditional household usages. A study on the ethnobotany of medicinal plants among the Semai indigenous people of Perak (Malaysia) revealed that post-partum women used the leaves of *P. sccardianus* in a bath.[75] However, it is not clear how the bath would benefit women who had given birth.[75] Other species of *Pellacalyx* are not known to have any ethnobotanic relevance.

1.6.4 Phytochemicals, Bioactivities and Research Gap

The phytochemistry and biological activity of *Pellacalyx saccardianus* are largely understudied. At the time of writing, only one study reported the phytochemicals and bioactivity of *P. saccardianus*.[76,77,78] From the Soxhlet leaf extract of *P. saccardianus*, two new compounds, i.e., pellacalyxin and 1,2-*O*-(1-methylethylidene)fucoside, together with six known compounds were isolated (Table 1.10).[76,77,78] Of these compounds, pellacalyxin is of particular interest because it has a 4-piperidone core that is incorporated into a diarylheptanoid skeleton (Table 1.10). Hence, pellacalyxin can be considered as a novel type V alkaloidal diarylheptanoid (Table 1.6). Moreover, the isolation of simple linear diarylheptanoids such as platyphyllenone and 5*R*-hydroxy-1,7-bis-(4-hydroxyphenyl)-3-heptanone from *P. saccardianus*[76] provided further evidence for the occurrence of diarylheptanoids in the plant. It should be noted that diarylheptanoids are not well-documented to exist in the family Rhizophoraceae. The above study also claimed the occurrence of a tropane alkaloid in *P.*

saccardianus,[76] although its identity was not elaborated. 3α-Cinnamoyloxynortropane (**11**) had been isolated in high yield from a congeneric species, *Pellacalyx axilliaris*.[79] It can therefore be inferred that tropane alkaloids occur in other *Pellacalyx* species including *P. saccardianus*. Besides, simple sterols and fatty acids were also isolated from the leaves of *P. axilliaris* (Table 1.10).[80,81]

Table 1.10: Known phytochemical constituents of *Pellacalyx saccardianus*.[76–78]

Phytochemical type	Compound structure and name (known absolute stereochemistry is shown)
Diarylheptanoid	Platyphyllenone (**22**) 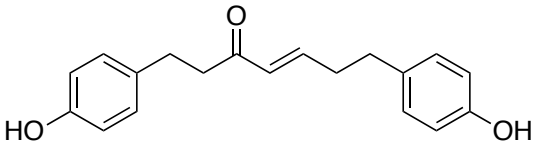 5R-Hydroxy-1,7-bis-(4-hydroxyphenyl)-3-heptanone 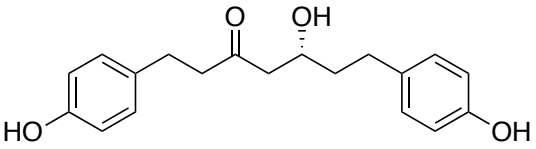 Pellacalyxin (new compound) 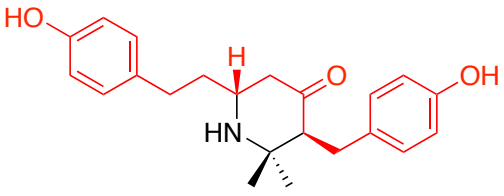
Fucose glycoside 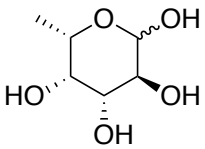 L-Fucose	1,2-O-(1-Methylethylidene)fucoside (new compound) 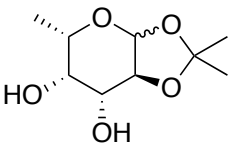

	Methyl-L-fucoside 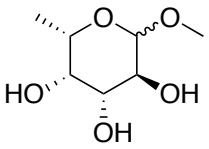 Note: Absolute stereochemistry of the anomeric carbon was not reported for both glycosides.
Triterpene	24*S*-Ethylcholesta-5,22,25-trien-3β-ol 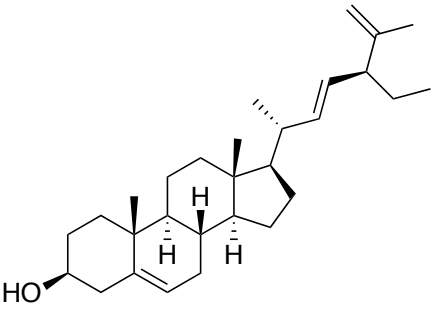 Note: Also present in *Pellacalyx axilliaris*[80] β-amyrin palmitate 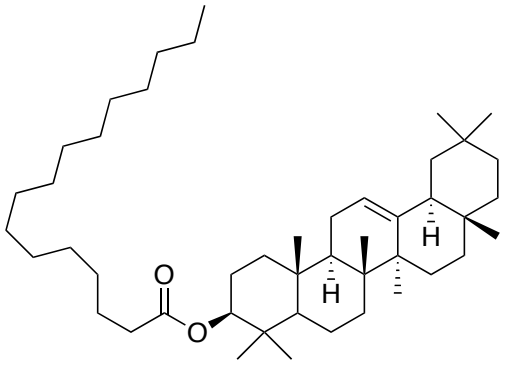 Note: Also present in *Pellacalyx axilliaris*[80] Squalene 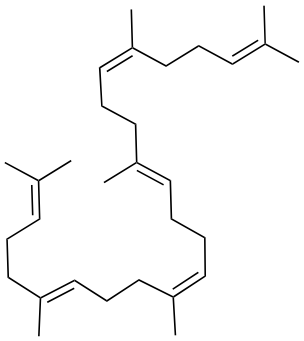

Of the above phytochemicals, β-amyrin palmitate, platyphyllenone (**22**) and pellacalyxin selectively inhibited cyclooxygenase-2 (COX-2) enzyme and reduced prostaglandin synthesis *in vitro*, viz., anti-inflammation response.[76,81] Interestingly, their inhibition of COX-2, while comparable to the positive control, resveratrol (80 – 98% inhibition at all concentrations of 0.01 – 10 μM), was not concentration-dependent (IC_{50} could not be derived).[76] The structural activity relationship was attributed to favorable hydrophobic interactions with a valine pocket (location 523) of COX-2.[76]

In the present research, preliminary TLC-based chemical profiling on the crude leaf and bark extract of *P. saccardianus* have revealed a rich presence of multiple alkaloids and phenolic compounds. The crude leaf extract also demonstrated potent *in vitro* cytotoxicity against different pancreatic and breast cancer cell lines, i.e., 2 – 20% cell viability following treatment with 0.1 mg/mL plant extract for 72 hours (unpublished result, data not shown). Considering the presence of potentially novel diarylheptanoids (like pellacalyxin) and tropane alkaloids in *P. saccardianus,* in addition to its potent *in vitro* cytotoxicity, this species constitutes a worthy research subject. The main research gap to be addressed here is the lack of phytochemical investigation into purified cytotoxic compounds of *P. saccardianus*.

1.7 Research Aim, Objectives and Problem Statement

Chronic and/or infectious diseases impose great healthcare and financial burden to the global society. There is a need to identify novel lead compounds based on the phytochemicals isolated from plants selected through ethnobotanical and/or bioactivity screening. The aim of this research is to conduct a detailed phytochemical exploration into two understudied Malaysian plants, i.e., *Hippobroma longiflora* (L.) G. Don and *Pellacalyx saccardianus* Scort. The specific objectives of the current research are outlined as below:

1. To isolate piperidine alkaloids from the crude extract of *H. longiflora*, as well as diarylheptanoids and tropane alkaloids from the crude extract of *P. saccardianus* via chemical partitioning and chromatographic methods.

2. To elucidate the chemical structures of the pure alkaloids and diarylheptanoids obtained via comprehensive spectroscopic and spectrometric analyses. The absolute configurations of the chiral compounds would be resolved where possible.

3. To analyse the antispasmodic activity of the piperidine and tropane alkaloids obtained, i.e., relaxation activity on rat isolated tracheal smooth muscle.

4. To analyse the cytotoxic activity of the alkaloids and diarylheptanoids obtained from *P. saccardianus* on a panel of human cancer cell lines.

Chapter 2: Diphenethylpiperidine Alkaloids of *Hippobroma longiflora*

2.1 Hippofoline A (1)

Hippofoline A (**1**) was isolated as a yellowish oil with $[\alpha]_D$ = –40.6 (*c* 0.18, $CHCl_3$). The IR spectrum showed a strong absorption band at 1733 cm^{-1} due to the presence of ester function. The molecular formula of **1** was determined to be $C_{26}H_{33}NO_4$ on the basis of HRDARTMS measurements ($[M+H]^+$, *m/z* 424.2488). The proposed structure of **1** is shown in Figure 2.1a.

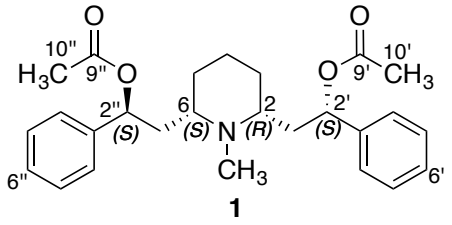

1

Figure 2.1a: Chemical structure of **1**.

The ^{13}C NMR spectrum of **1** (Table 2.1) showed 22 resonances. Two carbonyl carbon resonances associated with two acetate functions were recorded at δ_C 170.12 and 170.31, while the two acetate methyl resonances were observed at δ_C 21.33 and 21.36. There were eight resonances within the aromatic region of δ_C 126.45 – 141.34. Of these, four correspond to four pairs of equivalent aromatic carbons, namely C-4′/8′, C-5′/7′, C-4′′/8′′ and C-5′′/7′′. An *N*-methyl carbon signal was also detected at δ_C 27.44. The ^1H NMR spectrum of **1** (Table 2.1) showed the presence of 10 aromatic protons (H-4′/8′, H-5′/7′ and H-6′; H-4′′/8′′, H-5′′/7′′ and H-6′′), which were heavily merged within the aromatic region of δ_H 7.26 – 7.34. Two distinct methyl singlets (CH_3-10′ and CH_3-10′′) associated to two acetate functions were detected at δ_H 2.050 and 2.051, respectively. Two substantially deshielded signals due to two benzylic oxymethine hydrogens (H-2′ and H-2′′) were also recorded at δ_H 5.86 and 5.83. The splitting pattern for H-2′ and H-2′′

were observed as dd due to vicinal coupling with two diastereotopic protons (H-1′ and H-1′′), with coupling constants of ca. 9 and 6 Hz. The two pairs of diastereotopic hydrogens, i.e., H-1′a/H-1′b and H-1′′a/H-1′′b, were adjacent to two stereocenters, namely C-2/C-2′ and C-6/C-2′′, respectively. The signal of H-1′b was found to show a splitting pattern of ddd, with a geminal coupling constant of $J_{\text{H-1′b-H-1′a}}$ = 14.0 Hz, and two vicinal coupling constants of $J_{\text{H-1′b-H-2′}}$ = 8.8 Hz and $J_{\text{H-1′b-H-2}}$ = 5.5 Hz. A similar ddd splitting pattern was observed for H-1′′b. However, the signal for H-1′a was broadened and overlapped with the *N*-methyl singlet at δ_H 2.20, while the splitting pattern for H-1′′a appeared to be complicated. As such, H-1′a and H-1′′a were denoted as m. Last but not least, two aminomethine hydrogens and an *N*-methyl group were observed at δ_H 2.27 (H-2), 2.47 (H-6) and 2.20 (*N*-Me), respectively. A group of severely overlapped signals due to hydrogens of the propylene fragment [δ_C 24.93 (C-3), 24.53 (C-4), 24.64 (C-5)] was observed at δ_H 1.11 – 1.70.

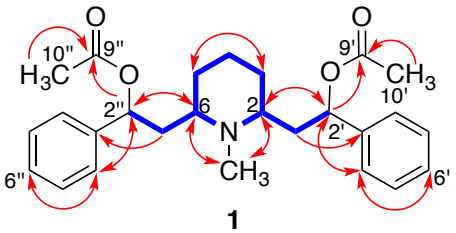

1

(— = COSY; ↷ = HMBC)

Figure 2.1b: Selected COSY and HMBC correlations of **1**.

Analyses of the COSY and HSQC data revealed a partial structure that corresponds to the aliphatic/alicyclic carbon backbone in the structure of **1**, i.e., (O)CHCH$_2$CHCH$_2$CH$_2$CH$_2$CHCH$_2$CH(O) (Fig. 2.1b). In the HMBC spectrum (Fig. 2.1b), three-bond correlations from *N*-Me to C-2 and C-6 established the connectivity between C-2 and C-6 via an *N*-Me group, thus revealing the *N*-methylpiperidine

nucleus of **1**. Finally, the two acetate functions were readily determined to be associated with the two benzylic oxymethines (C-2′ and C-2′′) on the basis of the three-bond correlations from H-2′ to C-9′ and from H-2′′ to C-9′′. Hence, the 2D structure of **1** was elucidated as an *N*-methyl-2,6-diphenethylpiperidine alkaloid with two acetate groups substituted at C-2′ and C-2′′.

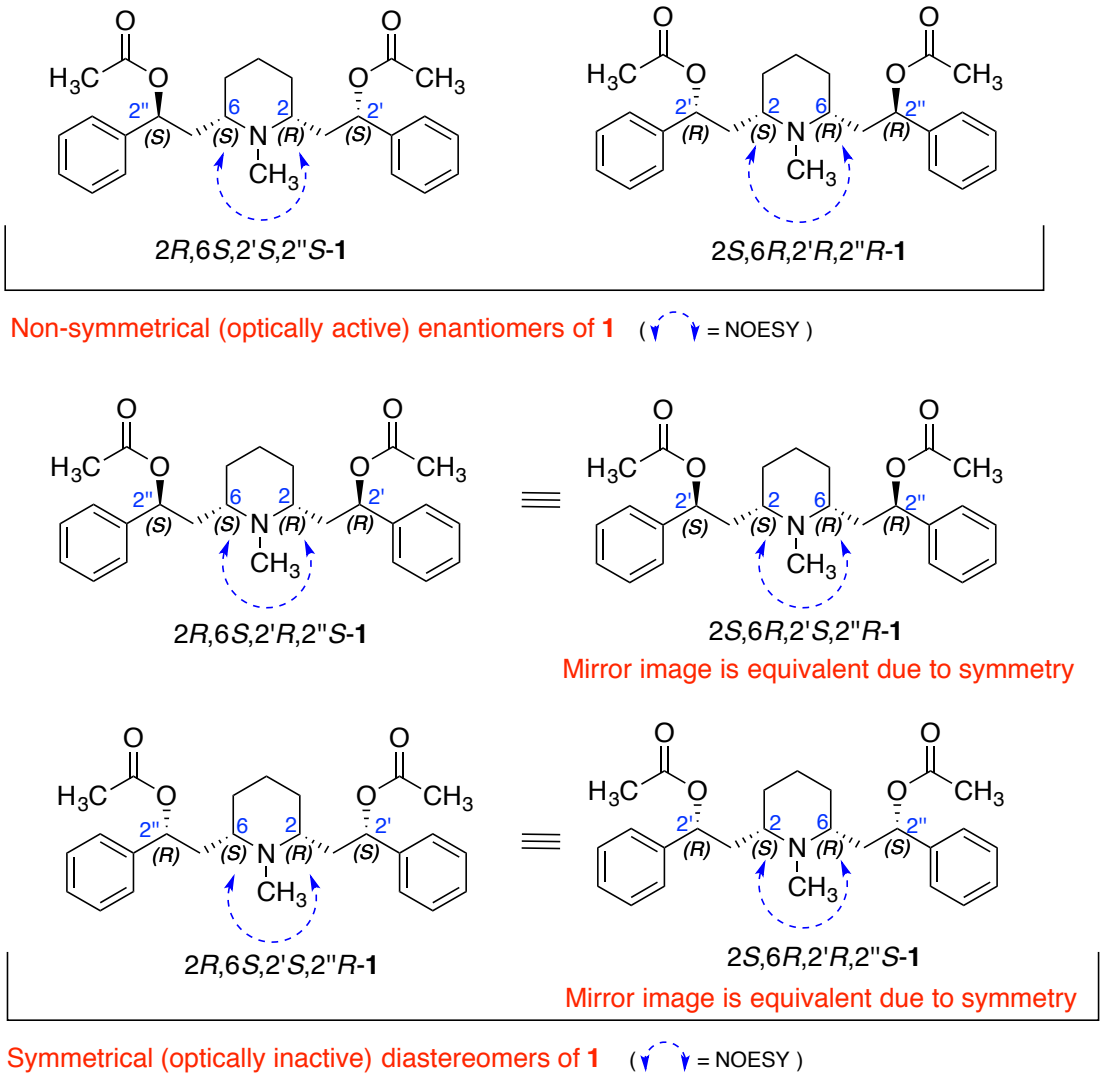

Figure 2.1c: Four possible stereoisomers of **1** with 1,3-diaxial NOESY correlation.

There are four stereocenters in the structure of **1**, i.e., C-2, C-6, C-2′ and C-2′′. The presence of 22 carbon resonances in its ^{13}C NMR spectrum indicated a non-symmetrical 2,6-diphenethylpiperidine structure because a symmetrical one would

produce only 12 carbon resonances. This is also consistent with **1** being an optically active compound. The presence of a NOESY correlation between H-2 and H-6 further indicated a 1,3-diaxial spatial interaction that requires both H-2 and H-6 to be *cis* configured, viz., the relative configuration of either 2*R*,6*S* or 2*S*,6*R* (Fig. 2.1c). Hence, there are only two stereochemical possibilities for **1**, i.e., 2*R*,6*S*,2′*S*,2′′*S* and 2*S*,6*R*,2′*R*,2′′*R*, which are enantiomers (Fig. 2.1c). It should be noted that despite the lack of an element of symmetry in the structure of **1**, it possesses identical acetate moieties at C-2 and C-6. The absolute configuration of **1** was finally established as 2*R*,6*S*,2′*S*,2′′*S* based on comparison of the experimental and calculated electronic circular dichroism (ECD) spectra (Fig. 2.1d). Hippofoline A (**1**) therefore represents a new lobeline-type alkaloid.

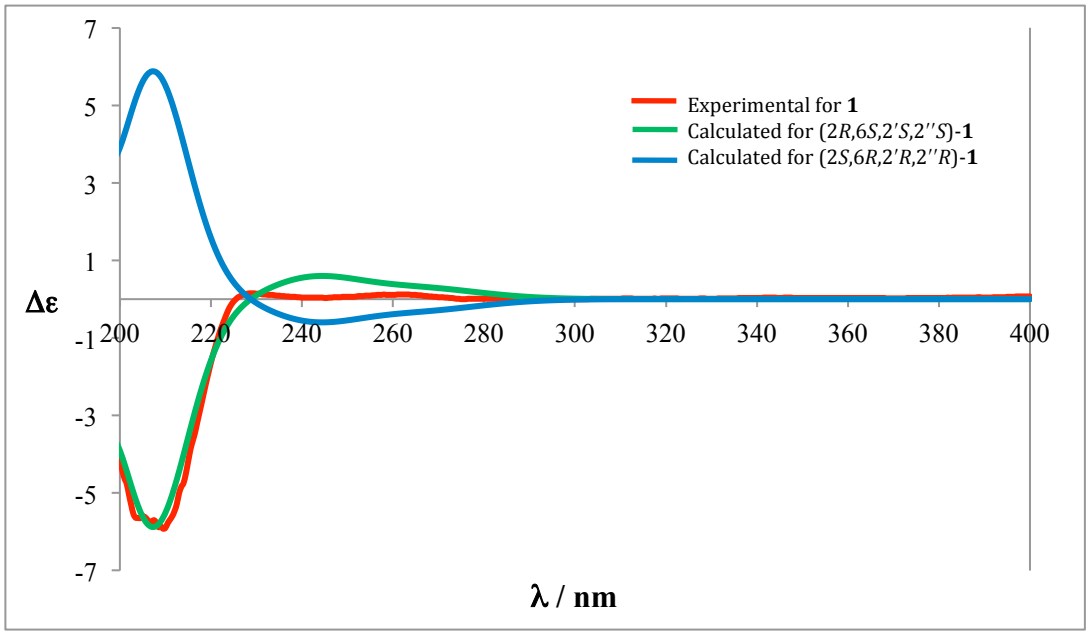

Figure 2.1d: Experimental and calculated ECD spectra of **1** in ACN.

Table 2.1: ^{1}H and ^{13}C NMR data of **1** (600 MHz, $CDCl_3$).[a]

Position	δ_C, type	δ_H (mult., *J* in Hz)
2	58.82, CH	2.27 (m)
3a	24.93[b], CH_2	1.41 (m)
3b		1.70 (m)
4a	24.53[b], CH_2	1.22 (m)
4b		1.11 (m)
5a	24.64[b], CH_2	1.41 (m)
5b		1.70 (m)
6	58.94, CH	2.47 (m)
1'a	40.62, CH_2	2.20 (m)
1'b		1.62 (ddd, 14.0, 8.8, 5.5)
2'	73.82[c], CH	5.86 (dd, 8.9, 6.2)
3'	140.46[d], C	-
4'/8'	126.86[e], 2 x CH	7.34 (m)
5'/7'	128.46[e], 2 x CH	7.31 (m)
6'	127.81[f], CH	7.26 (m)
9'	170.12[g], $\underline{CO}OCH_3$	-
10'	21.33[h], $COO\underline{CH_3}$	2.050 (s)
1''a	41.17, CH_2	1.98 (m)
1''b		1.89 (ddd, 14.5, 8.5, 6.1)
2''	74.00[c], CH	5.83 (dd, 8.8, 5.5)
3''	141.34[d], C	-
4''/8''	126.45[e], 2 x CH	7.34 (m)
5''/7''	128.26[e], 2 x CH	7.31 (m)
6''	127.71[f], CH	7.26 (m)
9''	170.31[g], $\underline{CO}OCH_3$	-
10''	21.36[h], $COO\underline{CH_3}$	2.051 (s)
N-Me	27.44	2.20 (s)

[a] Assignments based on COSY, HSQC and HMBC analyses.
[b-h] Signals are interchangeable within each column.

2.2 Hippofoline B (2)

Hippofoline B (**2**) was isolated as a yellowish oil with $[\alpha]_D$ –61 (*c* 0.17, $CHCl_3$). The IR spectrum showed a prominent ester absorption band at 1732 cm^{-1}, in addition to a broad hydroxyl absorption band at 3264 cm^{-1}. HRDARTMS measurements ($[M+H]^+$, *m/z* 382.2397) established the molecular formula of **2** as $C_{24}H_{31}NO_3$, differing from that of **1** by 42 mass units. This suggested the replacement of a $OCOCH_3$ group in **1** with an OH group in **2**, as there were only 19

carbon resonances in the ^{13}C NMR spectrum of **2** (Table 3.2). Indeed, the ^{13}C and ^{1}H NMR spectra (Table 3.2) of **2** largely resembled those of **1**, except that one instead of two acetate groups was detected in **2** [δ_H 2.07 (3H, s, H-10′′), δ_C 170.27 (C-9′′) and 21.29 (C-10′′)]. The proposed structure of **2** is shown in Figure 2.2a.

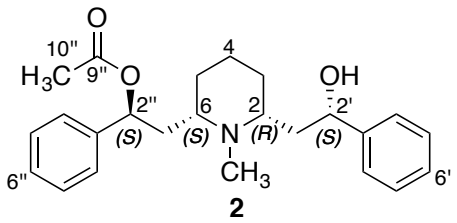

2

Figure 2.2a: Chemical structure of **2**.

Further analyses of the COSY and HSQC data of **2** revealed the presence of an identical diphenethylpiperidine backbone as **1**, except that **2** was deduced to be an *O*-deacetyl derivative of **1** (Fig. 2.2b). This deduction is consistent with the observation of an OH absorption band in the IR spectrum of **2**. The acetate group of **2** was determined to be attached at C-2′′ on the basis of three-bond HMBC correlation from H-2′′ to C-9′′ (Fig. 2.2b).

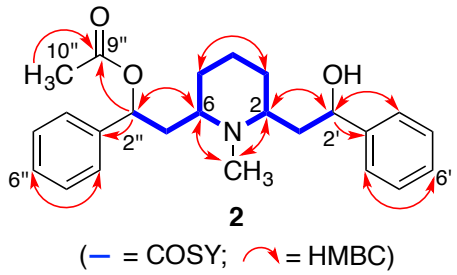

2

Figure 2.2b: Selected COSY and HMBC correlations of **2**.

Similar to alkaloid **1**, the NOESY correlation between H-2 and H-6 in **2** indicated that both hydrogens are *cis* to each other. However, due to the different substituents at C-2′ and C-2′′, four possible non-symmetrical stereoisomers (two pairs of enantiomers) exist for **2** (Fig. 2.2c). The experimental ECD spectrum of **2** (Fig. 2.2d, negative Cotton effect at 216 nm) showed a similar curve to the ECD

spectra calculated for 2*R*,6*S*,2′*S*,2′′*S* and 2*S*,6*R*,2′*S*,2′′*S*, inferring that only the configurations at C-2′ and C-2′′ could be determined with certainty. Since the configurations at C-2 and C-6 in alkaloids **1**, **3** and **4** were established as *R* and *S*, respectively, the absolute configurations for **2** was therefore deduced, based on biogenetic grounds, to be 2*R*,6*S*,2′*S*,2′′*S*. Hippofoline B (**2**) is therefore 2′-*O*-deacetylhippofoline A.

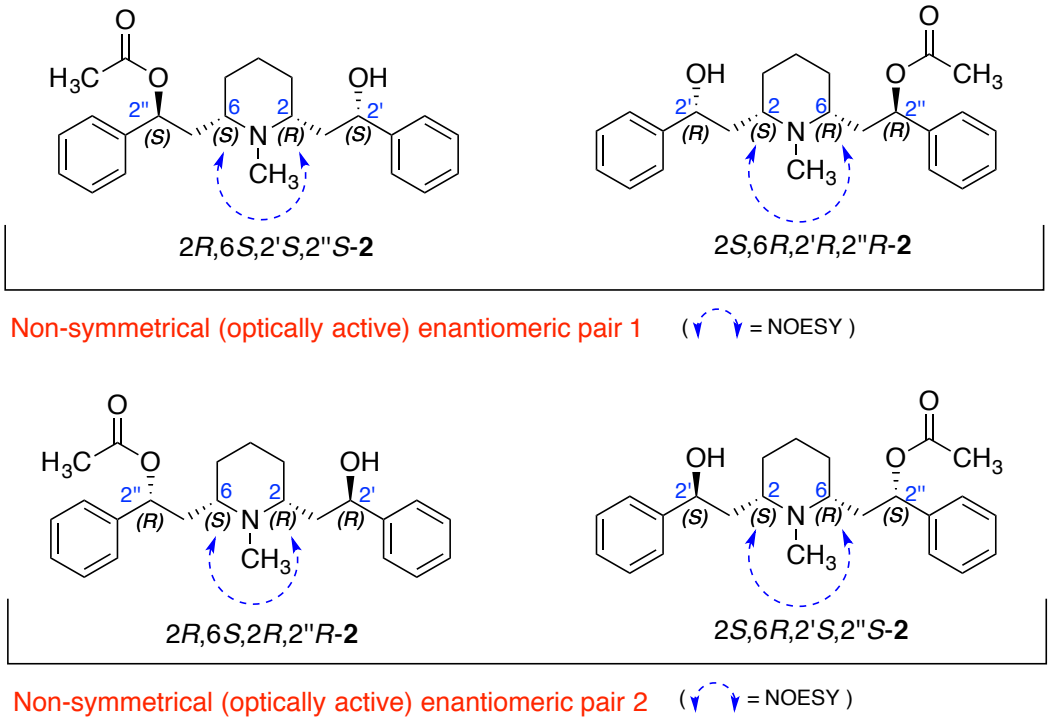

Figure 2.2c: Non-symmetrical stereoisomers of **2** with 1,3-diaxial NOESY correlation.

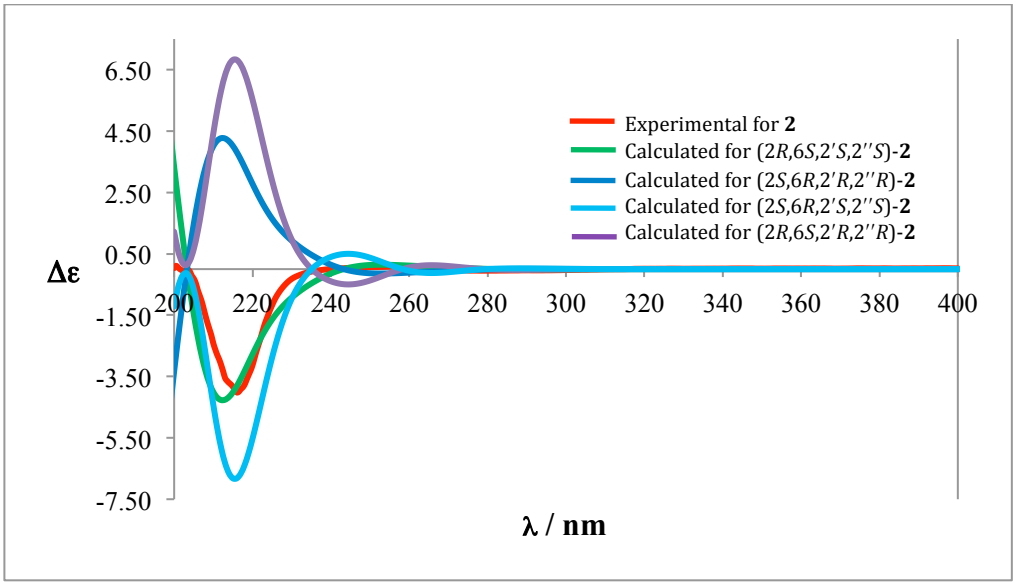

Figure 2.2d: Experimental and calculated ECD spectra of **2** in ACN.

Table 2.2: ^{1}H and ^{13}C NMR data of **2** (600 MHz, $CDCl_3$).[a]

Position	δ_C, type	δ_H (mult., *J* in Hz)
2	60.74, CH	2.68 (br t, 8.0)
3	25.67, CH_2	1.20 – 1.80 (m)
4	24.32, CH_2	1.20 – 1.80 (m)
5	26.61, CH_2	1.20 – 1.80 (m)
6	59.76, CH	2.36 (m)
1'a	39.25, CH_2	1.98 (m)
1'b		1.74 (m)
2'	72.16, CH	5.08 (dd, 7.2, 4.1)
3'	145.55, C	-
4'/8'	125.55, 2 x CH	7.30 (m)
5'/7'	128.58, 2 x CH	7.30 (m)
6'	126.64, CH	7.22 (m)
1''a	41.00, CH_2	2.31 (dt, 14.2, 7.1)
1''b		1.74 (m)
2''	73.88, CH	5.83 (t, 7.1)
3''	140.08, C	-
4''/8''	126.90, 2 x CH	7.41 (m)
5''/7''	128.10, 2 x CH	7.37 (m)
6''	128.14, CH	7.33 (m)
9''	170.27, $\underline{CO}OCH_3$	-
10''	21.29, $COO\underline{CH_3}$	2.07 (s)
N-Me	Not observed	2.41 (s)

[a] Assignments based on COSY, HSQC and HMBC analyses.

2.3 (–)-Lobeline (3)

(–)-Lobeline or (2*R*,6*S*,2′′*S*)-lobeline (**3**, Fig. 1.1) was isolated as orange block crystals from dichloromethane (mp 111-113 ˚C), with $[\alpha]_D$ = –33.5 (*c* 0.76, $CHCl_3$). The IR spectrum showed absorption bands at 1683 and 3357 cm^{-1} due to the presence of ketone and hydroxyl functionalities. The molecular formula of **3** was determined to be $C_{22}H_{27}NO_2$ on the basis of HRDARTMS measurements ($[M+H]^+$, *m/z* 338.2120). The absolute configuration of **3** was previously determined as 2*R*,6*S*,2′′*S* based on its hydrobromide salt.[82] Since suitable crystals of **3** in the free base form were obtained, Cu Kα radiation X-ray diffraction analysis was conducted, which confirmed the absolute configuration as 2*R*,6*S*,2′′*S* (Fig. 2.3).

The ^1H and ^{13}C NMR spectra of **3** (Table 2.3) were mostly comparable to literature values.[20] It should be noted that apart from the resonances due to **3**, the spectra were complicated by resonances due to minor impurities within the NMR sample solution. This could be due to the partial degradation of **3** via retro-Mannich reaction in the presence of chloroform (Fig. 1.3).

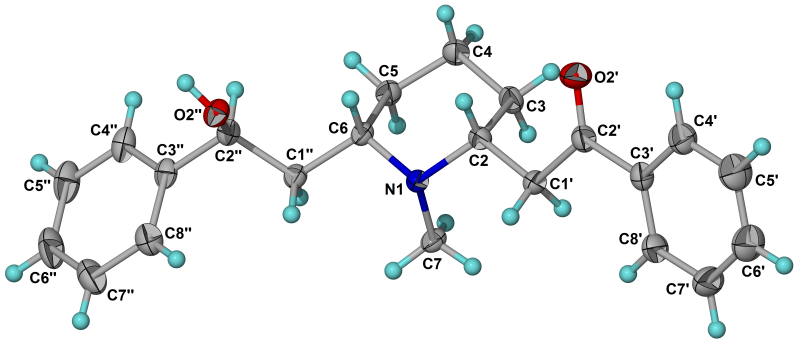

Figure 2.3: X-ray crystal structure of **3**.

Table 2.3: ^{1}H and ^{13}C NMR data of **3** in comparison with literature data.

	3		**Literature Data** [20]	
Position	δ_C,[a] type	δ_H[a] (mult., *J* in Hz) ($CDCl_3$, 600 MHz)	δ_C	δ_H (mult., *J* in Hz) (CD_3OD, 400 MHz)
2	59.01, CH	3.56 (m)	62.3	4.10 (m)
3a	20.49,[b] CH_2	1.62[c] (m)	24.9	1.79 – 1.89 (m)
3b				
4a	24.78,[b] CH_2	1.59 – 1.82[c] (m)	23.7	1.94 (m)
4b				
5a	23.41,[b] CH_2	1.14 – 1.58[c] (m)	25.0	1.79 – 1.89 (m)
5b				
6	64.48, CH	3.22 (br m)	67.0	3.98 (m)
1'a	43.82, CH_2	3.21 (dd, 16.0, 4.9)	39.6	3.61 (m)
1'b		3.02 (dd, 16.0, 8.5)		
2'	198.30, C=O		200.2	
3'	137.02, C		137.1	
4'/8'	128.21, 2 x CH	7.96 (dd, 7.4, 1.2)	129.4	8.07 (m)
5'/7'	128.69, 2 x CH	7.47 (t, 7.8)	130.0	7.54 (m)
6'	133.14, CH	7.57 (tt, 7.4, 1.2)	135.4	7.67 (tt, 7.3, 1.3)
1''a	40.45, CH_2	1.93 (dt, 14.8,	40.2	1.79 – 1.89 (m)
1''b		11.0)		2.18 (ddd, 15.5, 11.1,
		1.45 (m)		10.2)
2''	75.80, CH	4.94 (dd, 10.8, 3.0)	74.9	5.05 (dd, 11.1, 2.8)
3''	145.04, C		145.8	
4''/8''	125.51, 2 x CH	7.36 (t, 7.8)	126.6	7.42 (m)
5''/7''	128.09, 2 x CH	7.31 (t, 7.8)	129.6	7.36 (m)
6''	126.97, CH	7.23 (tt, 7.2, 1.2)	128.8	7.27 (tt, 7.3, 1.3)
N-Me	27.28	2.35 (s)	26.9	2.83 (s)

[a] Assignments based on COSY, HSQC and HMBC analyses.
[b-c] Signals are interchangeable within each column.

2.4 (−)-*Cis*-2′,2′′-Diphenyllobelidiol (4)

(−)-*Cis*-2′,2′′-Diphenyllobelidiol (**4,** Table 1.9)[20,66] was isolated as colourless block crystals from dichloromethane (mp 110-112 ˚C), with $[\alpha]_D$ = −55.8 (*c* 0.34, $CHCl_3$). The IR spectrum showed a broad absorption band at 3390 cm^{-1} due to the presence of OH group. The molecular formula of **4** was determined to be $C_{22}H_{29}NO_2$ on the basis of HRDARTMS measurements ($[M+H]^+$, *m/z* 340.2277). The ^1H and ^{13}C NMR data of **4** (Table 2.4) were mostly identical to literature values.[20] The absolute configuration of **4** was previously proposed as 2*R*,6*S*,2′*S*,2′′*S* based on correlation of the NMR and optical rotation data.[20] In the present research, the absolute configuration of **4** was confirmed for the first time by Cu Kα radiation X-ray diffraction analysis to be 2*R*,6*S*,2′*S*,2′′*S* (Fig. 2.4).

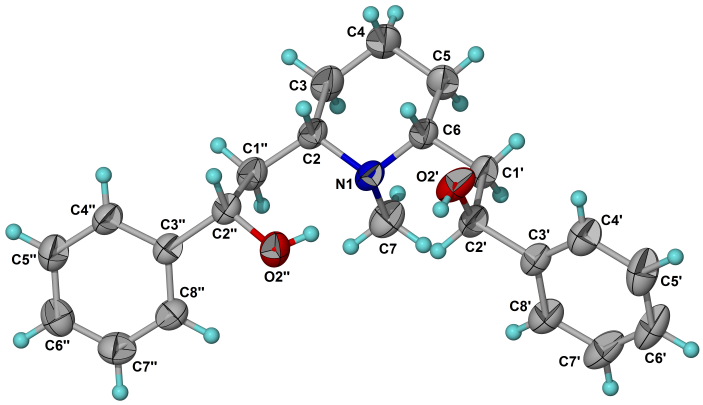

Figure 2.4: X-ray crystal structure of **4**.

Table 2.4: ^{1}H and ^{13}C NMR data of **4** in comparison with literature data.

Position	**4**		**Literature data**[20]	
	δ_C,[a] type	δ_H[a] (mult., *J* in Hz) ($CDCl_3$, 600 MHz)	δ_C	δ_H (mult., *J* in Hz) (CD_3OD, 400 MHz)
2	63.56, CH	3.05 (br t, 8.0)	65.5	3.71 (m)
3a	24.04 – 24.63, CH_2	1.22 – 1.81 (m)	23.7	1.75 (m)
3b				
4a	24.04 – 24.63, CH_2	1.22 – 1.81 (m)	23.3	1.61 (m)
4b				
5a	24.04 – 24.63, CH_2	1.22 – 1.81 (m)	22.2	1.81 (m)
5b				
6	59.40, CH	3.13 (br t, 9.0)	62.0	3.42 (m)
1'a	40.56, CH_2	2.00 (dt, 14.4, 10.3)	38.3	2.15 (ddd, 15.4, 4.6, 4.1)
1'b		1.53 (m)		2.44 (ddd, 15.2, 9.4, 4.7)
2'	75.12, CH	4.92 (dd, 10.0, 3.0)	70.6	5.07 (dd, 4.7, 4.6)
3'	144.86, C		144.3	
4'/8'	125.68,[b] 2 x CH	7.38[e] (d, 7.7)	125.1	7.47 (m)
5'/7'	128.33,[c] 2 x CH	7.34 (m)	128.4	7.41 (m)
6'	127.19,[d] CH	7.24[f] (tt, 7.2, 1.5)	127.3	7.30 (m)
1''a	41.77, CH_2	1.83 (m)	38.9	1.78 (m)
1''b		1.72 (m)		2.18 (ddd, 15.4, 11.3, 11.0)
2''	70.64, CH	4.87 (d, 9.5)	73.3	4.96 (dd, 11.0, 2.77)
3''	145.57, C		143.4	
4''/8''	125.59,[b] 2 x CH	7.33[e] (m)	125.2	7.43 (m)
5''/7''	128.35,[c] 2 x CH	7.31 (m)	128.2	7.36 (m)
6''	127.13,[d] CH	7.25[f] (tt, 7.2, 1.5)	127.4	7.33 (m)
N-Me	30.34	2.31 (s)	25.9	2.90 (s)

[a] Assignments based on COSY, HSQC and HMBC analyses.
[b-f] Signals are interchangeable within each column.

2.5 (–)-*Cis*-2′,2′′-Diphenyllobelidiol *N*-oxide (5)

(–)-*Cis*-2′,2′′-Diphenyllobelidiol *N*-oxide (**5**) was isolated in minute amount as a white amorphous solid, $[\alpha]_D$ = –55.5 (*c* 0.13, $CHCl_3$). The molecular formula of **5** was determined to be $C_{22}H_{29}NO_3$ on the basis of HRDARTMS measurements ($[M+H]^+$, *m/z* 356.2226). Notably, a second *m/z* peak corresponding to **4** (*m/z* = 340.2266) was detected alongside **5**, while the two only differed by 16 mass units, viz., an oxygen atom. The ^1H and ^{13}C NMR spectra of **5** (Table 2.5) were largely similar to those of **4**, except that some ^1H and ^{13}C NMR chemical shift values were considerably downfield shifted. In particular, the carbon resonances of C-2 and C-6 were downfield shifted from δ_C 63.56 and 59.40 in **4** to δ_C 79.64 and 75.75 in **5**, respectively. This indicated that C-2 and C-6 of **5** were attached to an *N*-oxide function. Additionally, a strong NOESY interaction between H-2 and H-6 was clearly observed, suggesting the presence of a 1,3-diaxial interaction between H-2 and H-6 (relative configuration of 2*R*, 6*S*). Alkaloid **5** was thus elucidated as a previously undescribed *N*-oxide derivative of **4** (Fig. 2.5). The possibility of **5** being an artifact produced from **4** during the extraction and isolation procedures could not be excluded (Section 1.1.2).

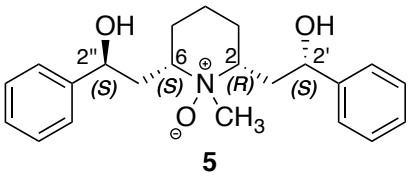

5

Figure 2.5: Chemical structure of **5**.

Table 2.5: ^{1}H and ^{13}C NMR data of **5** (600 MHz, $CDCl_3$).[a]

Position	δ_C, type	δ_H (mult., *J* in Hz)
2	79.64, CH	3.50 (m)
3a	31.71,[b] CH_2	1.85[f] (m)
3b		1.54 (m)
4a	23.02, CH_2	1.67 (m)
4b		1.45 (m)
5a	31.57,[b] CH_2	1.54[f] (m)
5b		1.54 (m)
6	75.75, CH	3.32 (ddd, 9.8, 7.4, 2.4)
1'a	43.53, CH_2	2.41 (ddd, 15.7, 10.8, 7.4)
1'b		1.71 (dt,15.7, 2.0)
2'	72.15, CH	4.79 (br d,10.5)
3'	145.46, C	
4'/8'	125.74,[c] 2 x CH	7.43[g] (br d, 7.0)
5'/7'	128.23,[d] 2 x CH	7.34[h] (t, 7.7)
6'	126.71,[e] CH	7.23[i] (br t,7.2)
1''a	40.28, CH_2	2.76 (ddd, 15.7, 7.5, 4.1)
1''b		1.89 (ddd, 15.8, 4.9, 2.7)
2''	69.43, CH	5.08 (t, 4.5)
3''	144.34, C	
4''/8''	125.86,[c] 2 x CH	7.44[g] (br d, 7.0)
5''/7''	128.30,[d] 2 x CH	7.35[h] (br t, 7.6)
6''	127.10,[e] CH	7.25[i] (t, 7.2)
N-Me	42.00	2.96 (s)

[a] Assignments based on COSY, HSQC and HMBC analyses.
[b-i] Signals are interchangeable within each column.

Chapter 3: Nortropane Alkaloids of *Pellacalyx saccardianus*

3.1 3α-Cinnamoyloxy-*N*-phloretoylnortropane (6)

3α-Cinnamoyloxy-*N*-phloretoylnortropane (**6**) was isolated as a colourless oil, which was optically inactive. The molecular formula of **6** was determined to be $C_{25}H_{27}NO_4$ on the basis of HRDARTMS measurements ($[M+H]^+$, *m/z* 406.2015). The UV spectrum showed three absorption maxima at 216, 223 and 278 nm, while the IR spectrum indicated the presence of α,β-unsaturated ester (1706 cm^{-1}), tertiary amide (1632 cm^{-1}) and hydroxyl (3225 cm^{-1}) functionalities. The proposed structure of **6** is shown in Figure 3.1a.

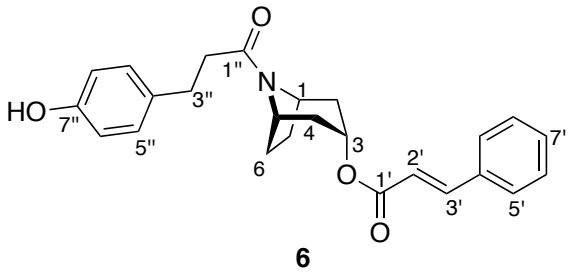

6

Figure 3.1a: Chemical structure of **6**.

The ^1H and ^{13}C NMR spectra of **6** (Table 3.1) exhibited signals characteristic of an *N*-substituted nortropane moiety,[38,83,84] viz., an oxymethine [δ_H 5.12 (1H, t, *J* = 5.1 Hz); δ_C 67.80 (C-3)], two aminomethines [δ_H 4.73 (1H, m), 4.08 (1H, m); δ_C 50.39, 53.85 (C-1/5)], as well as two pairs of diastereotopic methylenes in the piperidine (C-2/4) and pyrrolidine (C-6/7) fragments of the 8-azabicyclo[3.2.1] ring. The ^1H NMR signals of C-2/4 and C-6/7 appeared to be heavily merged within δ_H 1.74 – 2.16 (8H), while the ^{13}C NMR signals of C-2/4 [δ_C 35.90, 37.37] were clearly distinct from C-6/7 [δ_C 26.99, 28.71]. The diastereotopic protons H-2a/4a and H-2b/4b could be assigned via analysis of the COSY and HSQC data (Fig. 3.1b). They were generally observed as doublets with a large coupling constant of ca. 15

Hz. On the other hand, the splitting pattern and coupling constant of H-3 (triplet, J = 5.1 Hz) have established a H-3β configuration of the tropane ring, viz., an *endo* (3α) substituent at C-3. This observation is consistent with literature values,[39,83,85] as explained by the Karplus relationship (Section 1.3.3).

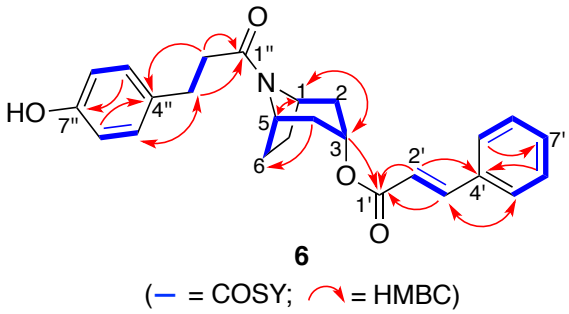

Figure 3.1b: Selected COSY and HMBC correlations of **6**.

Additionally, the NMR spectra of **6** showed characteristic signals due to an α,β-unsaturated ester function [δ_C 166.11 (C-1′); δ_H 6.40, δ_C 118.29 (C-2′); δ_H 7.64, 145.07 (C-3′)] and a phenyl ring [δ_H 7.53 (2H, m) and 7.40 (3H, m); δ_C 134.20 (C-4′), 128.13 X 2 (C-5′/9′), 128.94 X 2 (C-6′/8′), 130.48 (C-7′)]. The large coupling constant observed for δ_H 6.40 and 7.64 (J = 16.0 Hz) indicated a *trans*-disubstituted double bond at C-2′ and C-3′. The presence of a *trans*-cinnamoyloxy moiety was confirmed by the HMBC correlations from H-2′ to C-4′ and from H-3′ to C-1′ and C-5′/9′ (Figure 3.1b). The *trans*-cinnamoyloxy moiety was deduced to be attached to C-3 of the tropane ring based on the HMBC correlation from H-3 to C-1′. Last but not least, the NMR data of **6** revealed signals characteristic of an amide carbonyl [δ_C 168.26 (C-1′′)], a CH_2CH_2 fragment [δ_H 2.97 (2H), 2.57 (2H); δ_C 35.85 (C-2′′), 30.87 (C-3′′)] and a 4-hydroxyphenyl ring [δ_H 7.07 (2H, d, J = 8.0 Hz), 6.78 (2H, d, J = 8.0 Hz); δ_C 132.79 (C-4′′), 129.61 (C-5′′/9′′), 115.43 (C-6′′/8′′), 154.61 (C-7′′)]. These signals lead to the assembly of a phloretoyl (4-hydroxyphenylpropanoyl) group,

which is in agreement with the three-bond HMBC correlations observed from H-3′′ to C-1′′ and C-5′′/9′′; and from H-2′′ to C-4′′ (Fig. 3.1b). Since the phloretoyl moiety was associated with an amide function (IR ν_{max} 1632 cm^{-1}; δ_C 168.26), it must therefore be connected to the N atom of the tropane ring. Taken together, **6** was elucidated as 3α-cinnamoyloxy-*N*-phloretoylnortropane. Considering that amide bond exhibits resonance contributed π-character,[86] two rotamers of **6** exist due to restricted rotation about its amide bond (N–C-1′′) (Fig. 3.1c). Although the two rotamers could readily interconvert and were inseparable, the rotameric effects have caused the NMR signals of C-1/5, C-2/4 and C-6/7 in the otherwise symmetrical tropane ring to become duplicated. Besides, the ^{1}H NMR signal of the aminomethine that was *cis* to the amide carbonyl (δ_H 4.73, combined signals from both rotamers) was downfield shifted by δ_H +0.65 ppm. This was due to a deshielding effect imparted by magnetic anisotropy of the amide group.[86] Similar phenomena had been observed in synthetic as well as natural alkaloids containing amide function.[87,88]

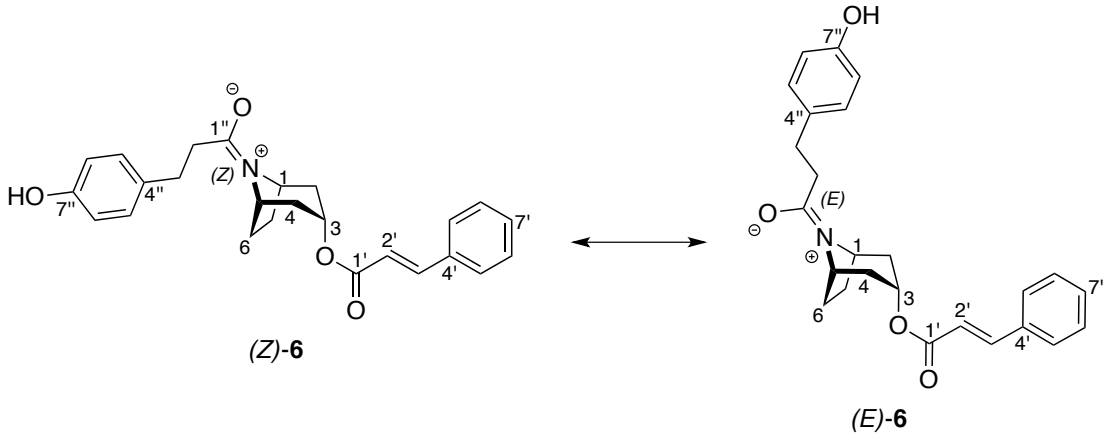

Figure 3.1c: Two interconverting amide rotamers of **6**.

3α-Cinnamoyloxy-*N*-phloretoylnortropane (**6**) represents the first instance where phloretic acid is conjugated with a tropane alkaloid via an amide bond. Notably, simple alkaloids conjugated with *p*-coumaric acid (didehydrophloretic

acid) via an amide linkage were sparsely reported in the literature. Limited examples include baimantuoluoamide A[89] and *N*-*trans*-*p*-coumaroyl tyramine.[90]

Table 3.1: ^{1}H and ^{13}C NMR data of **6** (600 MHz, $CDCl_3$).[a]

Position	δ_C, type	δ_H (mult., *J* in Hz)
1/5	50.39, *N*-CH	4.73 (m)
	53.85, *N*-CH	4.08 (m)
2/4	35.90[b], CH_2	2.16 (dt, 15.3, 4.5)
	37.37, CH_2	1.84 (d, 14.8)
		1.74 (m)
3	67.80, *O*-CH	5.12 (t, 5.1)
6/7	28.71, CH_2	2.11 (m)
	26.99, CH_2	1.90 (m)
1'	166.11, O-C=O	
2'	118.29, C=CH	6.40 (d, 16.0)
3'	145.07, C=CH	7.64 (d, 16.0)
4'	134.20, C	
5'/9'	128.13, 2 X CH	7.53 (m)
6'/8'	128.94, 2 X CH	7.40 (m)
7'	130.48, CH	7.40 (m)
1''	168.26, *N*-C=O	
2''	35.85[b], CH_2	2.57 (m)
3''	30.87, CH_2	2.97 (m)
4''	132.79, C	
5''/9''	129.61, 2 X CH	7.07 (d, 8.0)
6''/8''	115.43, 2 X CH	6.78 (d, 8.0)
7''	154.61, C	

[a] Assignments based on COSY, HSQC and HMBC analyses.
[b] Signals are interchangeable.

3.2 3α-Cinnamoyloxy-*N*-formylnortropane (7)

3α-Cinnamoyloxy-*N*-formylnortropane (**7**) was isolated as an optically inactive colourless oil. The molecular formula of **7** was determined to be $C_{17}H_{19}NO_3$ on the basis of HRESIMS measurements ($[M+Na]^+$, *m/z* 308.1258). The UV spectrum showed three absorption maxima at 216, 223 and 277 nm, while the IR spectrum indicated the presence of tertiary amide (1639 cm^{-1}) and α,β-unsaturated ester (1708 cm^{-1}) functionalities. The proposed structure of **7** is shown in Figure 3.2a.

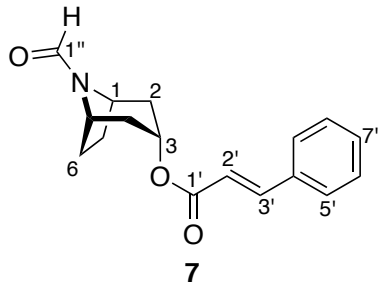

7

Figure 3.2a: Chemical structure of **7**.

The ^1H and ^{13}C NMR spectra of **7** (Table 3.2) exhibited signals that were largely similar to those of **6**, viz., an *N*-substituted nortropane, a *trans*-cinnamate moiety and a β-oriented H-3. However, the phloretoyl fragment in **6** was absent in **7**, replaced instead by a formyl group [δ_H 8.14 (1H, s); δ_C 157.42 (C-1′′)], which was deduced based on analysis of the HSQC data. Further examination of the COSY and HMBC data (Fig. 3.2b) confirmed the presence of a 3α-cinnamoyloxynortropane moiety, which was *N*-substituted to the formyl group based on the three-bond correlation observed from H-1′′ to C-1/5. The presence of a tertiary formamide moiety in **7** was in agreement with the IR spectrum (IR ν_{max} 1639 cm^{-1}). Additionally, the ^1H and ^{13}C NMR resonances associated with C-1/5, C-2/4 and C-6/7 were clearly duplicated as a result of the amide bond induced rotameric effect

(c.f., Fig. 3.1c). Hence, alkaloid **7** was elucidated as 3α-cinnamoyloxy-*N*-formylnortropane.

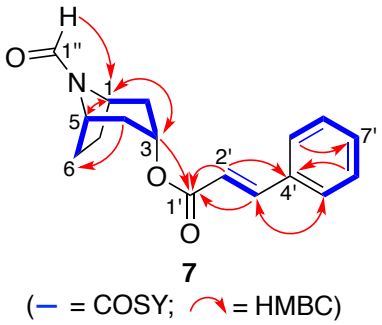

Figure 3.2b: Selected COSY and HMBC correlations of **7**.

Table 3.2: ^{1}H and ^{13}C NMR data of **7** (600 MHz, $CDCl_3$). [a]

Position	δ_C, type	δ_H (mult., *J* in Hz)
1/5	53.54, *N*-CH	4.10 (m)
	48.71, *N*-CH	4.65 (m)
2/4	38.60, CH_2	2.12 (dt, 15.1, 4.5)
		2.03 – 2.09 (m)
	36.00, CH_2	2.22 (m)
		1.96 (d, 15.3)
3	67.75, *O*-CH	5.26 (t, 5.1)
6/7	27.46, CH_2	2.22 (m)
	28.24, CH_2	1.99 – 2.09 (m)
1'	166.01, *O*-C=O	
2'	118.19, C=CH	6.43 (d, 16.0)
3'	145.16, C=CH	7.68 (d, 16.0)
4'	134.18, C	
5'/9'	128.13, 2 X CH	7.55 (m)
6'/8'	128.95, 2 X CH	7.41 (m)
7'	130.52, CH	7.41 (m)
1''	157.42, *N*-CH=O	8.14 (s)

[a] Assignments based on COSY, HSQC and HMBC analyses.

3.3 3α-Phenylacetoxy-*N*-formylnortropane (8)

3α-Phenylacetoxy-*N*-formylnortropane (**8**) was isolated as a colourless oil, which was optically inactive. The molecular formula of **8** was determined to be $C_{16}H_{19}NO_3$ on the basis of HRESIMS measurements ($[M+H]^+$, *m/z* 274.1440). The UV spectrum showed a single absorption maximum at 273 nm, while the IR spectrum indicated the presence of ester (1727 cm^{-1}) and tertiary amide (1663 cm^{-1}) groups. The proposed structure of **8** is shown in Figure 3.3a.

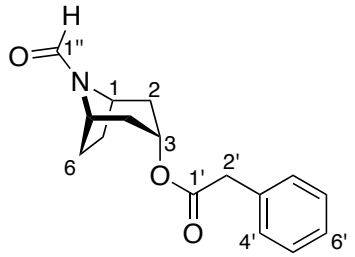

8

Figure 3.3a: Chemical structure of **8**.

Similar to those of **7**, the ^1H and ^{13}C NMR spectra of **8** (Table 3.3) exhibited signals characteristic of an *N*-formylnortropane moiety with a β-oriented H-3. Indeed, analyses of the HSQC and HMBC data revealed an *N*-formyl group [δ_H 9.18, (1H, s); δ_C 179.72 (C-1′′)] that showed three-bond correlations to two nortropanyl aminomethine carbons [δ_C 61.40, 52.81 (C-1/5)] (Fig. 3.3b). The presence of a formamide moiety was further corroborated by the IR spectrum (IR ν_{max} 1663 cm^{-1}) and the duplication of NMR signals for C-1/5, C-2/4 and C-6/7 due to the amide bond induced rotameric effect. By discounting the NMR signals attributed to the *N*-formylnortropane moiety, an ester fragment was left to be assembled from the remaining resonances [δ_C 170.29 (C-1′); δ_H 3.65 (2H, s), δ_C 42.15 (C-2′); δ_H 7.28 – 7.34 (5H), δ_C 133.66 (C-3′), 129.17 (C-4′/8′), 128.75 (C-5′/7′), 127.34 (C-6′)]. In the

HMBC spectrum, the correlations from H-2′ to C-1′, C-3′ and C-4′/8′, as well as from H-4′/8′ to C-2′ and C-6′ confirmed the presence of a phenylacetate ester moiety, which was connected to C-3 based on the three-bond correlation observed from H-3 to C-1′ (Fig. 3.3b). Alkaloid **8** was thus elucidated as 3α-phenylacetoxy-*N*-formylnortropane.

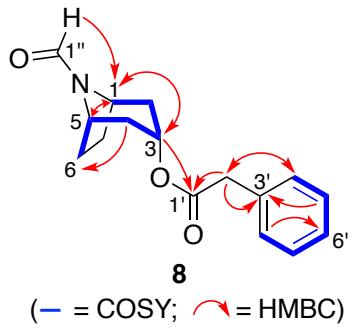

Figure 3.3b: Selective COSY and HMBC correlations of **8**.

Table 3.3: ^{1}H and ^{13}C NMR data of **8** (600 MHz, $CDCl_3$).[a]

Position	δ_C, type	δ_H (mult., *J* in Hz)
1/5	61.40, *N*-CH	4.06 (br s)
	52.81, *N*-CH	5.05 (m)
2/4	38.92, CH_2	2.08 (dt, 15.2, 4.3)
		1.93 (d, 15.1)
	34.98, CH_2	2.33 (dt, 15.3, 4.5)
		1.83 (br d, 15.1)
3	67.52, *O*-CH	5.11 (t, 5.2)
6/7	25.89, CH_2	1.84 – 1.90 (m)
	26.92, CH_2	1.73 (m)
1'	170.29, *O*-C=O	
2'	42.15, CH_2	3.65 (s)
3'	133.66, C	
4'/8'	129.17, 2 X CH	7.28 (m)
5'/7'	128.75, 2 X CH	7.34 (t, 7.3)
6'	127.34, CH	7.28 (m)
1''	179.72, *N*-CH=O	9.18 (s)

[a] Assignments based on COSY, HSQC and HMBC analyses.

3.4 3α-Benzoyloxy-*N*-formylnortropane (9)

3α-Benzoyloxy-*N*-formylnortropane (**9**) was isolated as a colourless oil without optical activity. The molecular formula of **9** was determined to be $C_{15}H_{17}NO_3$ on the basis of HRESIMS measurements ($[M+H]^+$, *m/z* 260.1287). The UV spectrum showed two absorption maxima at 228 and 274 nm, while the IR spectrum indicated the presence of conjugated ester (1712 cm^{-1}) and tertiary amide (1662 cm^{-1}) functionalities. The proposed structure of **9** is shown in Figure 3.4a.

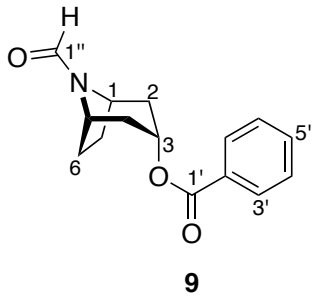

9

Figure 3.4a: Chemical structure of **9**.

The ^1H and ^{13}C NMR spectra of **9** (Table 3.4) gave characteristic signals due to an *N*-formylnortropane moiety with a β-oriented H-3 (c.f., compounds **7** and **8**), viz., a formyl group [δ_H 9.28, (1H, s); δ_C 179.91 (C-1′′)], an oxymethine [δ_H 5.41 (1H, t, *J* = 5.1 Hz); δ_C 67.68 (C-3)], two aminomethines [δ_H 4.23 (1H, dt, *J* = 6.7, 2.8 Hz) and 5.23 (1H, dt, *J* = 6.6, 3.0 Hz); δ_C 61.54 and 52.96 (C-1/5)], and four pairs of alicyclic methylenes [δ_H 2.08 – 2.50 (8H); δ_C 26.42, 27.45 (C-6/7) and 35.26, 39.18 (C-2/4)]. The attachment of the formyl group to the nortropanyl N atom was unambiguously confirmed by the three-bond HMBC correlations observed from H-1′′ to C-1/5 (Fig. 3.4b). Similar to **6** – **8**, the amide bond induced rotameric effect caused duplication of the NMR signals of C-1/5, C-2/4 and C-6/7 in **9**. After discounting the *N*-formylnortropane moiety, there were only five remaining ^{13}C

NMR resonances [δ_C 165.58 (C-1′), 130.08 (C-2′), 129.41 (C-3′/7′), 128.65 (C-4′/6′), 133.32 (C-5′)] to be considered for an aromatic ester group. The observed HMBC correlations from H-3 to C-1′, from H-3′/7′ to C-1′ and C-5, and from H-4′/6′ to C-2′, confirmed the presence of a benzoate ester fragment and its connection to C-3 (Fig. 3.4b). Alkaloid **9** was therefore elucidated as 3α-benzoyloxy-*N*-formylnortropane.

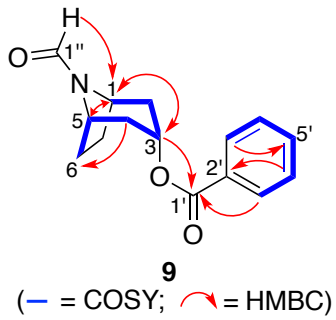

Figure 3.4b: Selected COSY and HMBC correlations of **9**.

Table 3.4: ^{1}H and ^{13}C NMR data of **9** (600 MHz, $CDCl_3$).[a]

Position	δ_C, type	δ_H (mult., *J* in Hz)
1/5	61.54, *N*-CH	4.23 (dt, 6.7, 2.8)
	52.96, *N*-CH	5.23 (dt, 6.6, 3.0)
2/4	39.18, CH_2	2.26 (dt, 15.0, 4.0)
		2.20 (m)
	35.26, CH_2	2.50 (dt, 15.4, 4.5)
		2.08 (d, 14.7)
3	67.68, *O*-CH	5.41 (t, 5.1)
6/7	26.42, CH_2	2.41 (m)
		2.31 (m)
	27.45, CH_2	2.20 (m)
1'	165.58, O-C=O	
2'	130.08, C	
3'/7'	129.41, 2 X CH	8.03 (dd, 8.0, 1.1)
4'/6'	128.65, 2 X CH	7.49 (t, 7.60)
5'	133.32, CH	7.61 (m)
1''	179.91, *N*-CH=O	9.28 (s)

[a] Assignments based on COSY, HSQC and HMBC analyses.

3.5 3α-Acetoxy-*N*-formylnortropane (10)

3α-Acetoxy-*N*-formylnortropane (**10**) was isolated as a colourless oil, which was optically inactive. The molecular formula of **10** was determined to be $C_{10}H_{15}NO_3$ on the basis of HRESIMS measurements ($[M+H]^+$, *m/z* 198.1129). The UV spectrum showed a single absorption maximum at 273 nm, while the IR spectrum indicated the presence of ester (1730 cm^{-1}) and tertiary amide (1659 cm^{-1}) functionalities. The proposed structure of **10** is shown in Figure 3.5a.

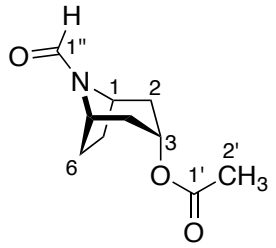

10

Figure 3.5a: Chemical structure of **10**.

The ^1H and ^{13}C NMR spectra of **10** (Table 3.5) exhibited resonances attributed to an *N*-formylnortropane moiety with a β-oriented H-3, similar to those in alkaloids **7** – **9**. However, there were no NMR resonances within the olefinic or aromatic region. The three-bond HMBC correlations from H-3 and CH_3-2′ to C-1′ established the presence of an acetyl group [δ_H 2.10 s (3H); δ_C 169.97 (C-1′), 21.48 (C-2′)] being linked to C-3 (Fig. 3.5b). Hence, **10** was readily elucidated as 3α-acetoxy-*N*-formylnortropane.

Alkaloids **7** – **10** are rare instances of *N*-formylnortropane esters. To our best knowledge, confolidine (Fig. 3.5c) is the only other precedent of an *N*-formylnortropane alkaloid that was previously reported from *Convolvulus subhirsutus* (Convolvulaceae).[91] The elucidation of compounds **7** – **10** thus confirmed the spectroscopic characteristics and provided structural diversity to the relatively rare *N*-formylnotropane esters. While naturally occurring *N*-formyl

alkaloids of the aporphine,[87] tropane,[91] indole,[92] phenanthrene[93] and pyrrole[94] skeletons were known to literature (Fig. 3.5c), their biogenetic pathways in plants are not well understood. Although *N*-formyltropinone was previously demonstrated to arise from photolytic oxidation,[95] alkaloids **7** – **10** were unlikely to be artifacts of laboratory extraction given the harsh conditions of the photochemical reaction, i.e., solvents saturated with oxygen in the presence of light.

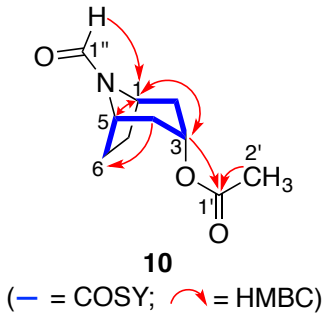

Figure 3.5b: Selected COSY and HMBC correlations of **10**.

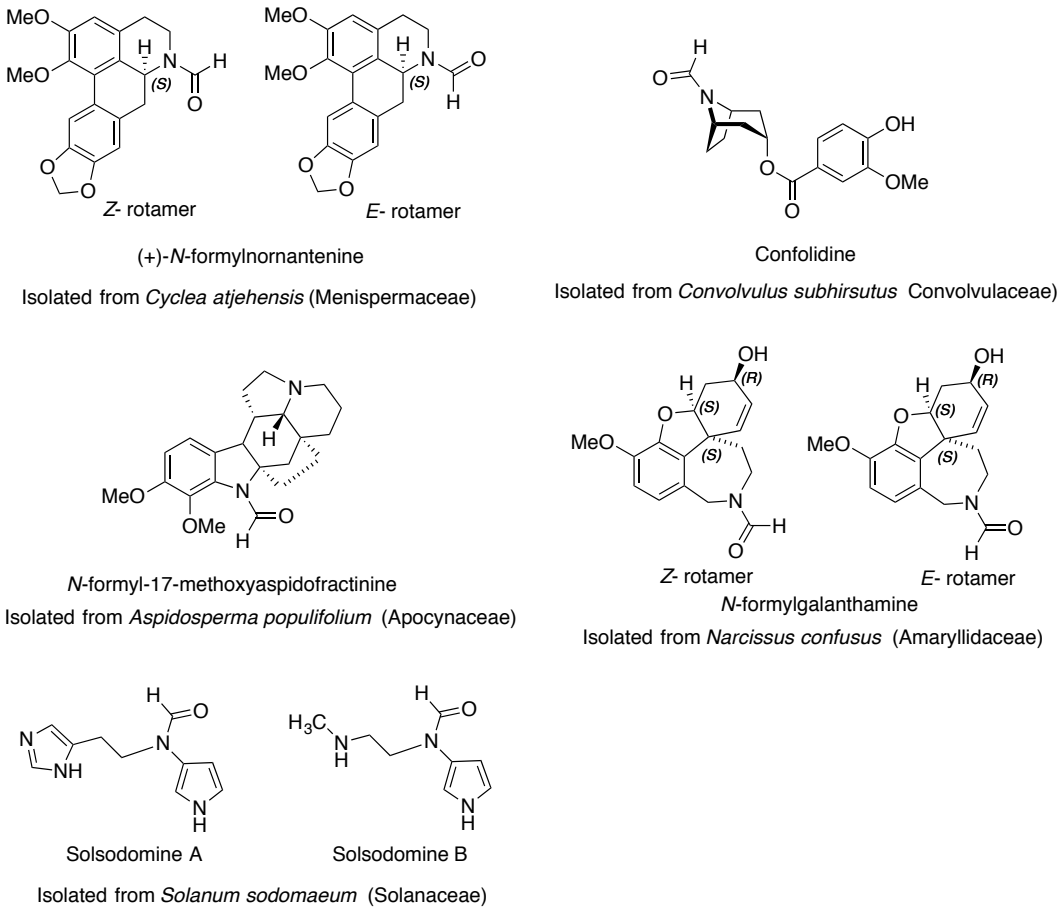

Figure 3.5c: Examples of naturally occurring *N*-formyl alkaloids.[87,91–94]

Table 3.5: ^{1}H and ^{13}C NMR data of **10** (600 MHz, $CDCl_3$).[a]

Position	δ_C, type	δ_H (mult., *J* in Hz)
1/5	61.56, *N*-CH	4.18 (dt, 6.6, 2.6)
	52.96, *N*-CH	5.16 (dt, 6.7, 2.9)
2/4	39.04, CH_2	2.13 (m)
		2.05 (d, 15.4)
	35.11, CH_2	2.38 (dt, 15.4, 4.2)
		1.93 (d, 15.4)
3	67.10, *O*-CH	5.12 (t, 5.1)
6/7	26.18, CH_2	2.25 (td, 12.0, 4.0)
		2.08 (s)
	27.26, CH_2	2.18 (td, 12.0, 4.0)
		2.13 (m)
1'	169.97, O-C=O	
2'	21.48, CH_3	2.10 (s)
1''	179.78, *N*-CH=O	9.24 (s)

[a] Assignments based on COSY, HSQC and HMBC analyses.

3.6 3α-Cinnamoyloxynortropane (11)

3α-Cinnamoyloxynortropane (**11**, Fig. 3.6) was isolated as a yellowish oil. The molecular formula of **11** was determined to be $C_{16}H_{19}NO_2$ on the basis of HRESIMS measurements ($[M+H]^+$, *m/z* 258.14818). The UV spectrum exhibited three absorption maxima at 216, 222 and 276 nm, while the IR spectrum indicated the presence of amine (3406 cm^{-1}) and conjugated ester (1710 cm^{-1}) functionalities. The ^{1}H and ^{13}C NMR data of **11** were compared alongside literature

values[73] in Table 3.6. It is noteworthy that the ^{13}C NMR resonances of C-1/5, C-2/4 and C-6/7 in **11** were equivalent due to symmetry of the nortropinyl ring. Despite being a known alkaloid previously isolated from *Pellacalyx axilliaris*,[79] this is the first instance where **11** was isolated from *P. saccardianus*. Alkaloid **11** was also the most abundant alkaloid present in the leaf and bark extracts of *P. saccardianus*. Furthermore, the co-isolation of **11** provided support to the biogenetic origins of alkaloids **6**, **7**, (±)-**13** and (±)-**14** in *P. saccardianus*.

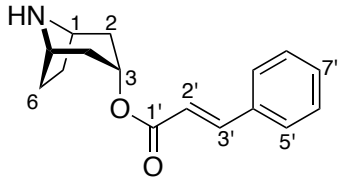

11

Figure 3.6: Chemical structure of **11**.

Table 3.6: ^{1}H and ^{13}C NMR data of **11** in comparison with literature data.

	11		**Literature Data**[79]	
Position	δ_C,[a] type	δ_H [a] (mult., *J* in Hz) (600 MHz, $CDCl_3$)	δ_C	δ_H (mult., *J* in Hz) (300 MHz, $CDCl_3$)
1/5	53.57, *N*-CH	3.92 (br s)	53.34	3.68 (s)
2/4	34.95, CH_2	2.49 (dt, 16.0, 4.0) 2.01 (d, 16.0)	36.56	1.8 – 2.3 (m)
3	66.47, *O*-CH	5.23 (t, 5.0)	67.66	5.21 (t, 4.7)
6/7	27.27, CH_2	2.17 (m)	28.60	1.8 – 2.3 (m)
1'	165.90, *O*-C=O		166.17	
2'	117.99, C=CH	6.41 (d, 16.0)	118.53	6.42 (d, 16.0)
3'	145.35, C=CH	7.67 (d, 16.0)	144.81	7.66 (d, 16.0)
4'	134.15, C		not reported	
5'/9'	128.16, 2 X CH	7.54 (m)	128.11	7.35 – 7.45 (m)
6'/8'	128.96, 2 X CH	7.41 (m)	128.92	7.50 – 7.60 (m)
7'	130.56, CH	7.41 (m)	130.38	7.50 – 7.60 (m)

[a] Assignments based on COSY, HSQC and HMBC analyses.

3.7 3α-Benzoyloxynortropane (12)

3α-Benzoyloxynortropane (**12**, Fig. 3.7) was isolated as a yellowish oil. The molecular formula of **12** was determined to be $C_{14}H_{17}NO_2$ on the basis of HRESIMS measurements ($[M+H]^+$, *m/z* 232.1343). The UV spectrum exhibited a single absorption maximum at 229 nm, while the IR spectrum indicated the presence of amine (3395 cm^{-1}) and conjugated ester (1712 cm^{-1}) functionalities. The ^1H NMR data of **12** was tabulated along with literature values[96] in Table 3.7. 3α-Benzoyloxynortropane was previously characterised from the leaves of *Erythroxylum macrocarpum* and *Erythroxylum sideroxyloides*.[96] It is notable that **12** is the deformyl derivative of alkaloid **9**.

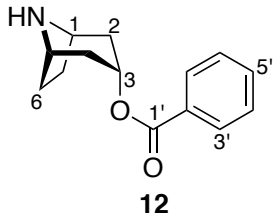

Figure 3.7: Chemical structure of **12**.

Table 3.7: ^1H and ^{13}C NMR data **12** in comparison with literature data.

	12		**Literature Data[96]**
Position	δ_C,[a] type	δ_H[a] (mult., *J* in Hz) (600 MHz, CD_3OD)	δ_H, (mult., *J* in Hz) (250 MHz, $CDCl_3$)
1/5	55.23, *N*-CH	3.96 (br s)	3.49 (m)
2/4	34.97, CH_2	2.31 (m) 2.09 (m)	1.70 – 2.30 (m)
3	67.40, *O*-CH	5.22 (t, 5.0)	5.28 (t, 4.7)
6/7	27.34, CH_2	2.31 (m) 2.09 (m)	1.70 – 2.30 (m)
1'	166.97, *O*-C=O		
2'	134.63, C		
3'/7'	130.48, 2 X CH	7.93 (dd, 7.1, 1.4)	7.95 (m)
4'/6'	129.89, 2 X CH	7.43 (t, 7.7)	7.50 (m)
5'	131.37, CH	7.54 (tt, 7.4, 1.8)	7.50 (m)

[a] Assignments based on COSY, HSQC and HMBC analyses.

3.8 Bissaccardine (13)

(±)-Bissaccardine (**13**) was isolated as a colourless oil, which had no optical activity. The molecular formula of **13** was determined to be $C_{32}H_{38}N_2O_4$ on the basis of HRESIMS measurements ($[M+H]^+$, *m/z* 515.2927). The UV spectrum showed three absorption maxima at 216, 223 and 277 nm, while the IR spectrum indicated the presence of ester (1707 cm^{-1}) and α,β-unsaturated carbonyl (1636 cm^{-1}) functionalities. The proposed structure of **13** is shown in Figure 3.8a.

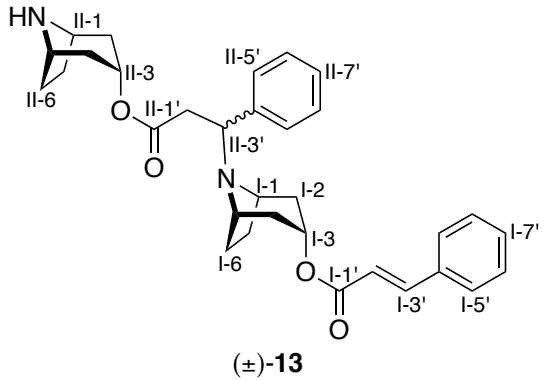

Figure 3.8a: Chemical structure of **13**.

The ^1H and ^{13}C NMR spectra (Table 3.8) of **13** showed numerous signals appearing in pairs, indicative of a dimeric compound that comprises two monomeric halves with very similar structures. Comparison of the ^1H and ^{13}C NMR data of **13** with those of **6**, **7** and **11** readily revealed the presence of a 3α-cinnamoyloxynortropane moiety, which represents the first half of its dimeric structure (unit I). By discounting the signals associated with unit I, analysis of the COSY and HMBC data (Fig. 3.8b) elucidated the second half of the dimeric structure (unit II) to constitute another nortropane moiety, which was connected to a $PhCHCH_2CO_2$ (3-phenylpropanoyloxy) fragment via an ester linkage, as evident from the HMBC correlation observed from H-II-3 to C-II-1′ (Fig. 3.8b). The phenylpropanoate ester fragment was readily assigned by the HSQC data to

comprise an aliphatic ester carbonyl [δ_C 170.84 (C-II-1′)], a benzylic methine [δ_H 3.87 (1H, dd, J = 9.4, 4.9 Hz); δ_C 60.43 (C-II-3′)], an aliphatic methylene [δ_H 2.89 (1H, dd, J = 14.0, 4.8 Hz) and 2.52 (1H, dd, J= 14.0, 9.0 Hz); δ_C 42.67 (C-II-2′)] and a phenyl group [δ_H 7.38 (2H, m), 7.30 (2H, t, J = 7.4 Hz) and 7.25 (1H, m); δ_C 142.13 (C-II-4′), 128.87 X 2 (C-II-5′/9′), 128.45 X 2 (C-II-6′/8′) and 127.66 (C-II-7′)]. Finally, the HMBC correlation observed from H-II-3′ to C-I-1/5 proved that the nortropanyl N atom of unit I was linked to C-II-3′ of unit II. The 2D structure of **13** was thus elucidated as a dimeric 3α-cinnamoyloxynortropane alkaloid.

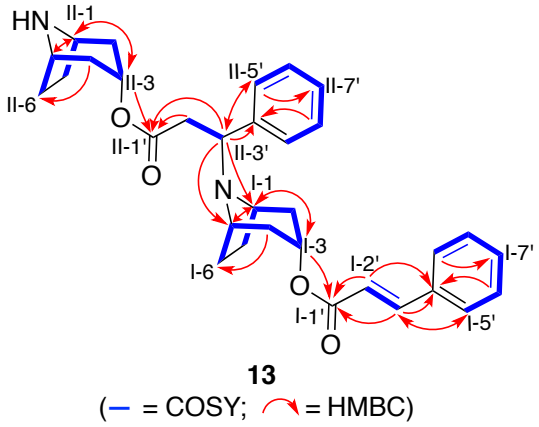

Figure 3.8b: Selected COSY and HMBC correlations of **13**.

It is noted that the ^{1}H and ^{13}C NMR signals for C-1/5, C-2/4 and C-6/7 in units I and II were duplicated. This was possibly due to restricted rotation about the N-I–C-II-3′ bond, which is connected to two bulky fragments on both ends. Despite the presence of a stereocenter at C-II-3, bissacardine (**13**) was shown to be a racemic mixture by chiral-phase HPLC analysis, which resolved the two enantiomeric peaks in 1:1 ratio at R_t 13.35 and 17.36 min (Appendix 45).

Table 3.8: ^{1}H and ^{13}C NMR data of **13** (600 MHz, $CDCl_3$).[a]

Unit	Position	δ_C, type	δ_H (mult., *J* in Hz)
	I-1	55.15[b], *N*-CH	3.33[b] (s)
	I-2a	35.90[c], CH_2	2.18[c] (dt, 15.1, 4.6)
	I-2b		1.76[c] (d, 15.1)
	I-3	68.29, *O*-CH	5.17 (t, 5.4)
	I-4a	35.35[c], CH_2	2.10[c] (m)
	I-4b		1.64[c] (d, 15.1)
	I-5	55.40[b], *N*-CH	3.08[b] (dt, 7.1, 3.2)
	I-6a	26.65[d], CH_2	1.91[d] (d, 6.05)
	I-6b		1.88[d] (br s)
I	I-7a	26.39[d], CH_2	2.08[d] (m)
	I-7b		2.05[d] (m)
	I-1'	166.28, O-C=O	
	I-2'	118.81, C=CH	6.41 (d, 16.0)
	I-3'	144.49, C=CH	7.64 (d, 16.0)
	I-4'	134.36, C	
	I-5'/9'	128.06, 2 X CH	7.53 (m)
	I-6'/8'	128.05, 2 X CH	7.38 (m)
	I-7'	130.27, CH	7.38 (m)
	II-1	52.97[e], *N*-CH	3.62[e] (dt, 7.1, 3.1)
	II-2a	35.23[c], CH_2	2.13[f] (m)
	II-2b		1.67[f] (d, 17.6)
	II-3	66.51, *O*-CH	4.87 (t, 5.2)
	II-4a	35.49[c], CH_2	1.96[f] (m)
	II-4b		1.13[f] (d, 15.1)
	II-5	52.91[e], *N*-CH	3.46[e] (dt, 7.0, 3.1)
	II-6a	27.37[f], CH_2	1.94 – 2.00[g] (m)
	II-6b		1.72[g] (m)
II	II-7a	27.64[f], CH_2	1.90[g] (m)
	II-7b		1.87[g] (m)
	II-1'	170.84, O-C=O	
	II-2'a	42.67, CH_2	2.89 (dd, 14.0, 4.8)
	II-2'b		2.52 (dd, 14.0, 9.0)
	II-3'	60.43, CH	3.87 (dd, 9.4, 4.9)
	II-4'	142.13, C	
	II-5'/9'	128.87, 2 X CH	7.38 (m)
	II-6'/8'	128.45, 2 X CH	7.30 (t, 7.4)
	II-7'	127.66, CH	7.25 (m)

[a] Assignments based on COSY, HSQC and HMBC analyses.

[b - g] Signals are interchangeable within each column.

3.9 Trissaccardine (14)

(±)-Trissaccardine (**14**) was isolated as a colourless oil that was optically inactive. The IR spectrum indicated the presence of amine (3373 cm^{-1}), ester (1733 cm^{-1}) and α,β-unsaturated ester (1636 cm^{-1}) functionalities. HRESIMS measurements ($[M+H]^+$, *m/z* 772.4341) established the molecular formula of **14** as $C_{48}H_{57}N_3O_6$, differing from that of bissaccardine (**13**) and 3α-cinnamoyloxynortropane (**11**) by 257 ($C_{16}H_{19}NO_2$) and 514 ($C_{32}H_{38}N_2O_4$) mass units, respectively. This indicated that **14** is a trimeric alkaloid related to **11** (monomer) and **13** (dimer). The proposed structure of **14** is shown in Figure 3.9a.

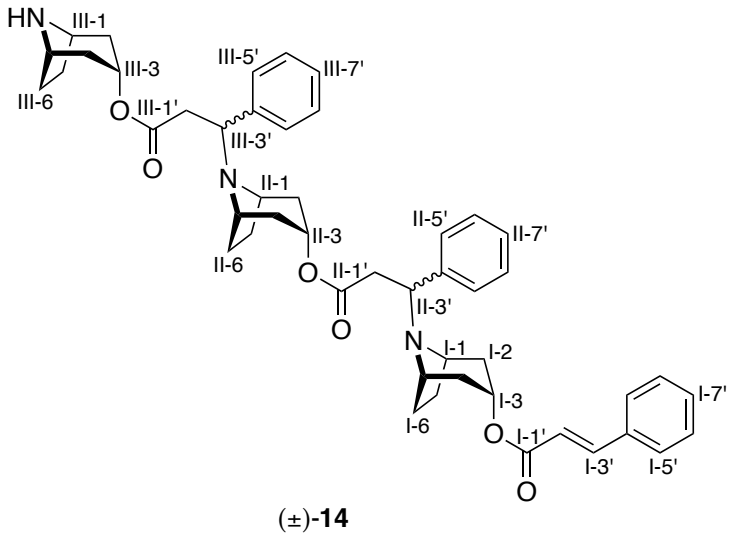

(±)-**14**

Figure 3.9a: Chemical structure of **14**.

The ^1H and ^{13}C NMR spectra of **14** (Table 3.9a) showed the presence of the two nortropane moieties present in **13**, i.e., 3α-cinnamoyloxynortropane (unit I) and 3α-(3-phenylpropanoyloxy)nortropane (unit II). However, there was an additional set of signals (unit III) attributed to a partial structure showing huge resemblance to unit II (Table 3.9b). Most notably, while the ^1H NMR spectrum of **13** showed the presence of two oxymethine signals at δ_H 5.17 (1H, H-I-3) and 4.87 (1H, H-II-3), three oxymethine signals at δ_H 5.16 (1H) and 4.85 (2H) were observed for

14. By analogy with **13**, the two oxymethine signals observed at δ_H 4.85 (2H, t, *J* = 5.0 Hz; H-II-3 and H-III-3) were assignable to a tropane C-3 oxymethine group linking to a 3-phenylpropanoyloxy fragment. Similarly, while the ^{13}C NMR spectrum of **13** showed two ester carbonyl carbon resonances (Table 3.8), three ester carbonyl carbon resonances [δ_C 166.26, 170.69 and 171.04] were observed for **14**. The latter two resonances [δ_C 170.69 (C-II-1′) and 171.04 (C-III-1′)] were each assignable to a carbonyl carbon of the 3-phenylpropanoyloxy fragment. These observations implied that **14** is a trimeric 3α-cinnamoyloxynortropane alkaloid. The presence of one fragment of 3α-cinnamoyloxynortropane (unit I) and two fragments of 3α-(3-phenylpropanoyloxy)nortropane (units II and III) moieties in **14** were further corroborated by analyses of the COSY and HMBC data (Fig. 3.9b). Notably, the N-I–C-II-3′ and N-II–C-III-3′ key linkages were established by the HMBC correlations observed from H-II-3′ to C-I-1/5 and from H-III-3′ to C-II-1/5, respectively. Due to high conformational flexibility of the molecule, the relative configurations at C-II-3′ and C-III-3′ could not be determined via analysis of the NOESY data.

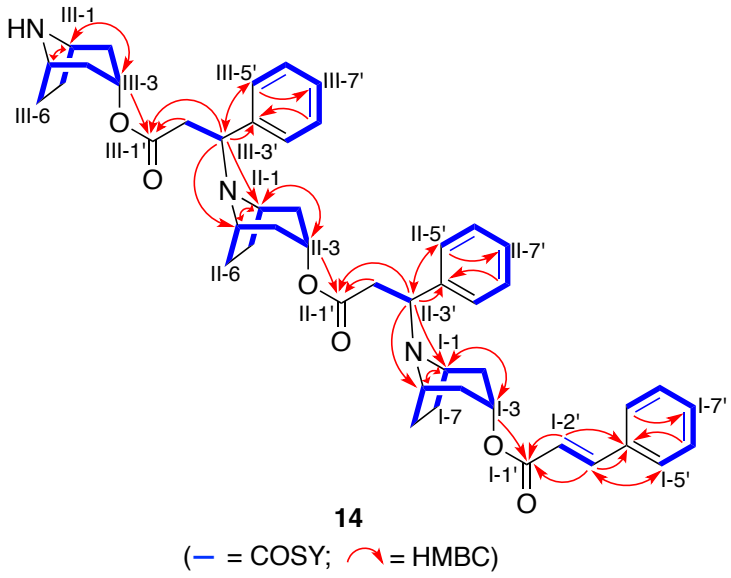

Figure 3.9b: Selected COSY and HMBC correlations of **14**.

Given that **14** was optically inactive, it was suspected to be a racemic mixture. Subsequent chiral-phase HPLC analysis of **14** resolved two enantiomeric peaks in ca. 1:1 ratio at R_t 15.05 and 20.44 min (Appendix 46). Trissaccardine was therefore confirmed to be a racemic mixture.

(±)-Bissaccardine and (±)-trissaccardine (**13** and **14**) represent a rare class of oligomeric tropane alkaloids that is derived via formation of C-N linkages. Only one precedent of such skeleton was previously reported, i.e., bishyoscyamine (Section 1.3.6, Table 1.5), isolated from the roots of *Anisodus acutangulus* (Solanaceae).[34] In contrast, other known examples of dimeric tropane alkaloids are condensed via ester, amide or C–C bonds (Section 1.3.6). Alkaloids **13** was postulated to arise from an aza-Michael addition between two molecules of 3α-cinnamoyloxynortropane (**11**), leading to the formation of the N-I–C-II-3′ linkage (Fig. 3.9c). A subsequent aza-Michael addition involving **13** and a second molecule of **11** furnishes **14** via the formation of the N-II–C-III-3′ linkage.

To investigate whether alkaloids **13** and **14** were artifacts of the acid-base extraction procedure, 3α-cinnamoyloxynortropane (**11**) was independently treated with tartaric acid and ammonia solutions, but no trace of the oligomers **13** and **14** were detected. A similar result was also obtained when **11** was independently treated with three catalysts that are commonly employed to promote aza-Michael addition, i.e., 1,8-diazabicyclo[5.4.0]undec-7-ene (DBU),[97] cerium ammonoium nitrate (CAN),[98] and samarium triflate.[99] On the contrary, gradual decomposition of **13** and **14** into **11** via retro aza-Michael reaction was observed when the compounds were stored in solutions containing bases such as ammonia or diethylamine (particularly prominent during chiral HPLC analysis, Appendix 45 and 46). Hence, (±)-bissaccardine (**13**) and (±)-trissaccardine (**14**)

are reasonably inferred to be natural products formed via biologically catalysed, but non-stereospecific aza-Michael additon of **11**.

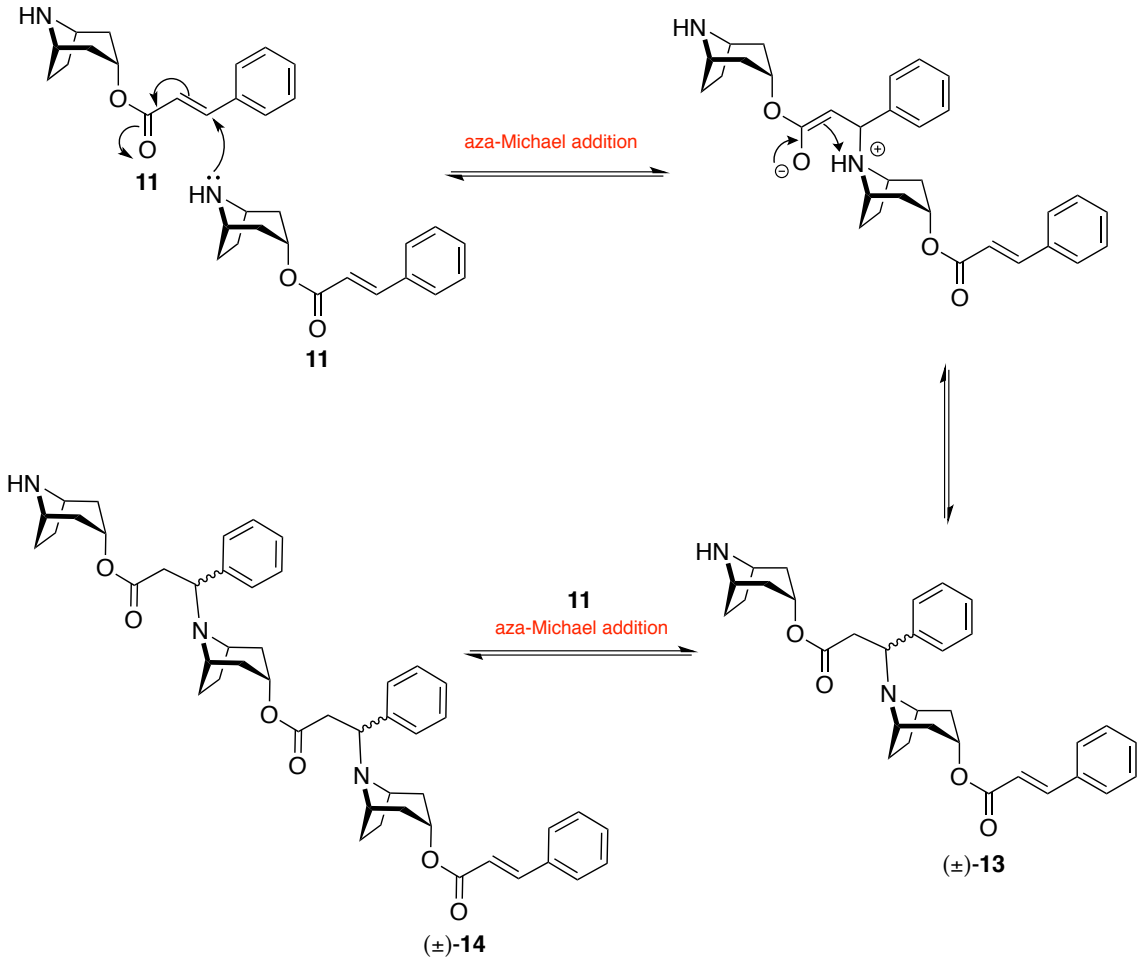

Figure 3.9c: Proposed biosynthetic pathway of **13** and **14**.

Table 3.9a: ^{1}H and ^{13}C NMR data of **14**, unit I and II (600 MHz, $CDCl_3$).[a]

Unit	Position	δ_C, type	δ_H (mult., *J* in Hz)
I	I-1	54.94[b], *N*-CH	3.08[b] (br s)
	I-2a	35.24[c], CH_2	2.09[c] (m)
	I-2b		1.63[c] (d, 15.3)
	I-3	68.35, *O*-CH	5.16 (t, 5.4)
	I-4a	35.97[c], CH_2	2.18[c] (m)
	I-4b		1.74[c] (d, 15.0)
	I-5	55.21[b], *N*-CH	3.31[b] (br s)
	I-6a	26.67[d], CH_2	2.06[d] (m)
	I-6b		2.03[d] (m)
	I-7a	26.17[d], CH_2	1.90[d] (m)
	I-7b		1.79[d] (m)
	I-1'	166.26, *O*-C=O	
	I-2'	118.88, C=CH	6.40 (d, 16.0)
	I-3'	144.44, C=CH	7.63 (d, 16.0)
	I-4'	134.41, C	
	I-5'/9'	128.06, 2 X CH	7.53 (m)
	I-6'/8'	128.87, 2 X CH	7.39 (m)
	I-7'	130.25, CH	7.39 (m)
II	II-1	55.20[b], *N*-CH	2.97[e] (br s)
	II-2a	35.56, CH_2	1.95[f] (m)
	II-2b		1.42[f] (d, 14.5)
	II-3	67.75[e], *O*-CH	4.85 (t, 5.0)
	II-4a	35.56, CH_2	1.88[f] (m)
	II-4b		1.07[f] (d, 14.9)
	II-5	55.42[b], *N*-CH	3.08[e] (br s)
	II-6a	26.17[f], CH_2	1.90[g] (m)
	II-6b		1.79[g] (m)
	II-7a	26.43[f], CH_2	1.82[g] (m)
	II-7b		1.48[g] (m)
	II-1'	170.69[g], O-C=O	
	II-2'a	42.77[h], CH_2	2.86 (dd, 14.3, 5.0)
	II-2'b		2.52 (dd, 14.2, 9.0)
	II-3'	60.42[i], CH	3.87 (dd, 9.0, 5.0)
	II-4'	142.31[j], C	
	II-5'/9'	128.03[k], 2 X CH	7.38 (m)
	II-6'/8'	128.44[l], 2 X CH	7.20 – 7.33 (m)
	II-7'	127.68[m], CH	7.20 – 7.33 (m)

Table 3.9b: ^{1}H and ^{13}C NMR data of **14**, unit III (600 MHz, $CDCl_3$).[a]

Unit	Position	δ_C, type	δ_H (mult., *J* in Hz)
	III-1	52.85[n], *N*-CH	3.51[h] (br s)
	III-2a	34.45[o], CH_2	2.02[i] (m)
	III-2b		1.10[i] (d, 15.7)
	III-3	65.94[e], *O*-CH	4.85 (t, 5.0)
	III-4a	34.56[o], CH_2	2.21[i] (m)
	III-4b		1.66[i] (d, 15.8)
	III-5	52.92[n], *N*-CH	3.69[h] (br s)
	III-6a	27.01[p], CH_2	1.95[j] (m)
	III-6b		1.91[j] (m)
III	III-7a	26.71[p], CH_2	1.71–1.81[j] (m)
	III-7b		1.71–1.81[j] (m)
	III-1'	171.04[g], O-C=O	
	III-2'a	42.57[h], CH_2	2.81 (dd, 14.0, 4.7)
	III-2'b		2.45 (dd, 13.8, 9.7)
	III-3'	60.32[i], CH	3.75 (dd, 9.5, 4.7)
	III-4'	142.02[j], C	
	III-5'/9'	128.03[k], 2 X CH	7.31 (d, 7.4)
	III-6'/8'	128.38[l], 2 X CH	7.20 – 7.33 (m)
	III-7'	127.53[m], CH	7.20 – 7.33 (m)

[a] Assignments based on COSY, HSQC and HMBC analyses.
[b-p] Signals are interchangeable within each column.

Chapter 4: Diarylheptanoids and Derivatives of *Pellacalyx saccardianus*

4.1 Saccardianone A (15)

(±)-Saccardianone A (**15**) was isolated as colourless block crystals from diethyl ether (mp 215 – 216 °C; optically inactive). The molecular formula of **15** was determined to be $C_{28}H_{28}O_4$ on the basis of HRESIMS measurements ($[M-H]^-$, *m/z* 427.1905), amounting to 15 degrees of unsaturation. The UV spectrum showed two absorption maxima at 225 and 278 nm, while the IR spectrum indicated the presence of hydroxyl group (3362 cm^{-1}), α,β-unsaturated ketone (1652 cm^{-1}) and aromatic ring (3031, 1614 and 1514 cm^{-1}). The proposed structure of **15** is shown in Figure 4.1a.

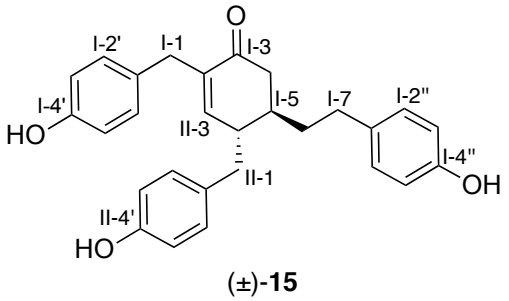

Figure 4.1a: Chemical structure of **15**.

The ^{13}C NMR spectrum of **15** (Table 4.1) showed a total of 22 discrete carbon resonances. Of these, six were due to six pairs of equivalent aromatic methine carbons, namely, C-I-2′/6′, C-I-3′/5′, C-I-2′′/6′′, C-I-3′′/5′′, C-II-2′/6′ and C-II-3′/5′. The total number of carbons in the structure of **15** was therefore determined to be 28, which was consistent with the HRESIMS data. Further analysis of the HSQC data elucidated seven aliphatic carbons (two methine and five methylene carbons), two olefinic carbons (one methine and one quaternary carbon), 18 aromatic carbons (12 methine, three quaternary and three oxygenated

carbons), and one conjugated ketone carbonyl. The presence of a ketone group and three oxygenated aromatic carbons have accounted for all the four oxygen atoms present in the molecular formula of **15**. The 18 aromatic carbons were readily attributed to three 4-hydroxyphenyl groups [δ_C 130.79 (C-I-1′), 130.22 (C-I-2′/I-6′), 115.32 (C-I-3′/I-5′), 155.66 (C-I-4′); δ_C 133.25 (C-I-1′′), 129.56 (C-I-2′′/I-6′′), 115.38 (C-I-3′′/I-5′′), 155.88 (C-I-4′′); and δ_C 130.31 (C-II-1′), 130.60 (C-II-2′/II-6′), 115.41 (C-II-3′/II-5′), 156.06 (C-II-4′)], based on their characteristic ^{13}C NMR chemical shift values.[100] Besides, the two olefinic carbons [δ_C 138.93 (C-I-2) and 150.71 (C-II-3)] were revealed to be a trisubstituted double bond that is conjugated to the ketone group observed at δ_C 200.66 (C-I-3). This was mainly supported by three-bond HMBC correlations from H-II-3 to C-I-3 (Fig. 4.1b). On the other hand, the ^{1}H NMR spectrum of **15** (Table 4.1) exhibited two clusters of three 2H aromatic doublet signals (J = 8.4 Hz) at δ_H 6.65, 6.670, and 6.674 (first cluster); and δ_H 6.84, 6.89, and 6.91 (second cluster), consistent with the presence of three 4-hydroxyphenyl moieties. A vinylic hydrogen doublet at δ_H 6.47 (1H, d, J = 3.4 Hz) was also assigned to the aforementioned trisubstituted olefin C-II-3. Last but not least, a distinct pair of AB doublets were observed at δ_H 3.27 and 3.39 (J = 15.3 Hz), attributable to an isolated benzylic allylic methylene group.

Further examination of the HSQC and COSY data (Fig. 4.1b) revealed the presence of a $CH_2CH_2CH(CH_2)CH(CH=)CH_2$ partial structure that corresponds to the C-I-7–C-I-6–C-I-5(C-I-4)–C-II-2(C-II-3)–C-II-1 fragment in **15**. In the HMBC spectrum (Fig. 4.1b), three-bond correlations from H-II-1 to C-II-2′/6′ and from H-II-2 to C-II-1′ indicated that one of the three 4-hydroxyphenyl moieties was connected to C-II-1. The attachment of the second 4-hydroxyphenyl moiety to the benzylic allylic methylene C-I-1 was established by the three-bond correlations

observed from H-I-1 to C-I-2′/6′, C-I-3 and C-II-3, while the third 4-hydroxyphenyl moiety was connected to C-I-7 based on the correlations observed from H-I-7 to C-I-2′′/6′′ and from H-I-6 to C-I-1′′. After discounting the three aromatic rings, one double bond and one ketone carbonyl group, one more ring remained to be assembled as required by the degrees of unsaturation (*vide supra*). The observed correlations from H-II-3 to C-I-1, C-I-3 and C-I-5, and from H-I-4 to C-I-3 confirmed the presence of a 2-cyclohexenone ring in **15**. The proposed structure of **15** was in full agreement with the 2D NMR data (Fig. 4.1b). Since suitable crystals of **15** were obtained, an X-ray diffraction analysis was conducted, which established the relative configuration of **15** as I-5*R*,II-2*S* (or I-5*S*,II-2*R*), corresponding to an *anti*-configuration at C-I-5 and C-II-2 (Fig. 4.1c). Besides, the X-ray data revealed that **15** crystallised in a centrosymmetric space group, *viz*. racemic crystals. Coupled to the observation that **15** was optically inactive, it was deduced to be a racemic mixture. This was finally confirmed by chiral-phase HPLC analysis**,** which resolved the two enantiomeric peaks in 1:1 ratio at R_t 15.18 and 16.26 min (Appendix 55).

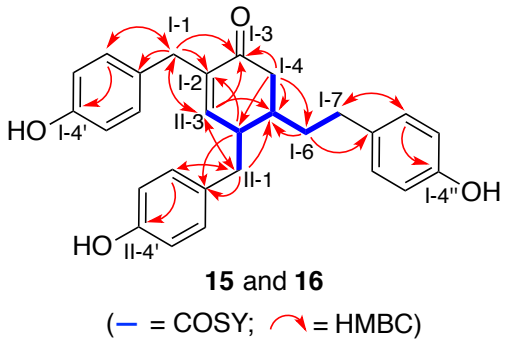

Figure 4.1b: Selected COSY and HMBC correlations of **15** and **16**.

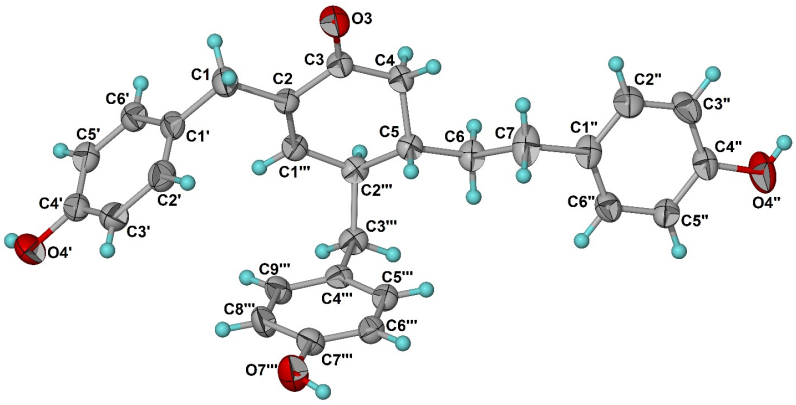

Figure 4.1c: X-ray crystal structure of **15**.

Table 4.1: ^{1}H and ^{13}C NMR data of **15** and **16** (600 MHz, CD_3OD).[a]

Unit	Position	**15**		**16**	
		δ_C, type	δ_H (mult., *J* in Hz)	δ_C, type	δ_H, (mult., *J* in Hz)
I Diaryl-heptanoid	I-1a	34.47, CH_2	3.39 (d, 15.3)	34.52, CH_2	3.42 (d, 15.1)
	I-1b		3.27 (d, 15.3)		3.24 (d, 15.1)
	I-2	138.93, C=C		139.23, C=C	
	I-3	200.66, C=O		200.60, C=O	
	I-4a	41.62, CH_2	2.64 (dd, 16.3, 4.3)	41.18, CH_2	2.48 (m)
	I-4b		2.20 (dd, 16.2, 8.8)		2.38 (dd, 16.9, 4.3)
	I-5	37.53, CH	1.84 (m)	37.74, CH	2.16 (m)
	I-6a	35.79, CH_2	1.87 (m)	32.96, CH_2	1.78 (ddt, 12.9, 9.6, 6.4)
	I-6b		1.57 (m)		1.59 (ddt, 14.2, 8.9, 5.8)
	I-7a	31.99, CH_2	2.57 (m)	32.40, CH_2	2.58 (ddd, 14.9, 9.7, 5.8)
	I-7b		2.43 (ddd, 14.1, 8.9, 6.6)		2.48 (m)
	I-1'	130.79, C		130.62 [b] C	
	I-2'/I-6'	130.22, 2 X CH	6.89 (d, 8.4)	130.22,[c] 2 X CH	6.91 (m)
	I-3'/I-5'	115.32, 2 X CH	6.674 (d, 8.4)	115.28,[d] 2 X CH	6.66[b] (d, 8.5)
	I-4'	155.66, C		155.70,[e] C	
	I-1''	133.25, C		133.26, C	
	I-2''/I-6''	129.56, 2 X CH	6.91 (d, 8.4)	129.46, 2 X CH	6.96 (d, 8.4)
	I-3''/I-5''	115.38, 2 X CH	6.670 (d, 8.4)	115.41,[d] 2 X CH	6.681 (d, 8.4)
	I-4''	155.88, C		155.84,[e] C	
II Phenyl-propanoid	II-1a	37.73, CH_2	2.80 (dd, 13.6, 5.8)	34.65, CH_2	2.81 (m)
	II-1b		2.57 (dd, 13.6, 7.6)		2.51 (m)
	II-2	43.53, CH	2.51 (m)	41.86, CH	2.77 (m)
	II-3	150.71, C=CH	6.47 (d, 3.4)	151.85, C=CH	6.40 (d, 4.5)
	II-1'	130.31, C		130.93,[b] C	
	II-2'/II-6'	130.60, 2 X CH	6.84 (d, 8.5)	130.33,[c] 2 X CH	6.92 (d, 8.4)
	II-3'/II-5'	115.41, 2 X CH	6.65 (m)	115.44,[d] 2 X CH	6.683[b] (d, 8.4)
	II-4'	156.06, C		156.03,[e] C	

[a] Assignments based on COSY, HSQC and HMBC analyses.
[b - e] Signals are interchangeable within each column.

4.2 Saccardianone B (16)

(±)-Saccardianone B (**16**) was isolated as a colourless oil with no optical activity. HRESIMS measurements have established the molecular formula of **16** to be $C_{28}H_{28}O_4$, based on the $[M-H]^-$ peak detected at *m/z* 427.1918. This implied that **16** was an isomer of **15**. The UV and IR spectra of **16** were identical to those of **15**, while the ^1H and ^{13}C NMR spectra showed a general resemblance to those of **15**, apart from minor deviations in their chemical shift values (Table 4.1). Notably, the largest ^{13}C shift differences between **15** and **16** were observed for C-I-6, C-II-1, C-II-2 and C-II-3 (with $|\Delta\delta_C|$ being 2.83, 3.08, 1.67, and 1.14 ppm, respectively), suggesting that **15** and **16** are diastereomers. Subsequent analyses of the 2D NMR data (Fig. 4.1b) confirmed that **16** has an identical planar structure as **15**. Since the structure only has two chiral centers at C-I-5 and C-II-2, **16** must therefore assume a *syn*-configuration at C-I-5 and C-II-2, i.e., I-5*R*,II-2*R* or I-5*S*,II-2*S*. Although **16** could not be crystallised due to paucity of material, it was determined to be a racemic mixture based on chiral-phase HPLC analysis, which resolved the two enantiomeric peaks in 1:1 ratio at R_t 14.55 and 17.86 min (Appendix 56). The proposed chemical structure of saccardianone B is shown in Figure 4.2a.

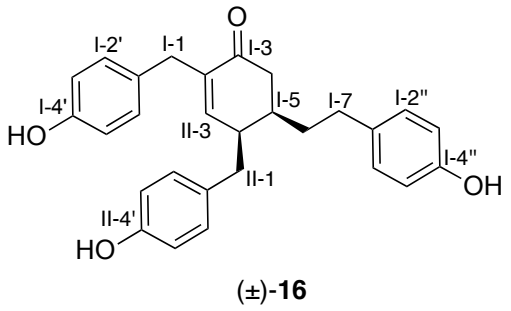

(±)-**16**

Figure 4.2a: Chemical structure of **16**.

The structures of (±)-saccardianones A and B (**15** and **16**) represent the first examples of diarylheptanoid-phenylpropanoid adducts bearing a cyclohexenone

core (c.f., type V linear diarylheptanoid, Table 1.6). A plausible biosynthetic pathway to **15** and **16** starting from 5-hydroxy-1,7-bis-(4-hydroxyphenyl)-3-heptanone (**23**) (co-isolated in the present study, *vide infra*) and *p*-coumaraldehyde is presented in Figure 4.2b. An aldol-like addition of *p*-coumaraldehyde onto the C-I-5 ketone in **23**, followed by a reduction step gives the β-hydroxyaldehyde **A**. A subsequent dehydration then yields the pair of *E*/*Z*-isomers **B**, which on reduction of the C-I-5–C-II-2 double bond and oxidation of the alcohol group at C-I-3, give rise to the *anti*- and *syn*-enantiomeric pairs **C**. Finally, an intramolecular aldol-dehydration reaction yields both **15** and **16** as racemic mixtures.

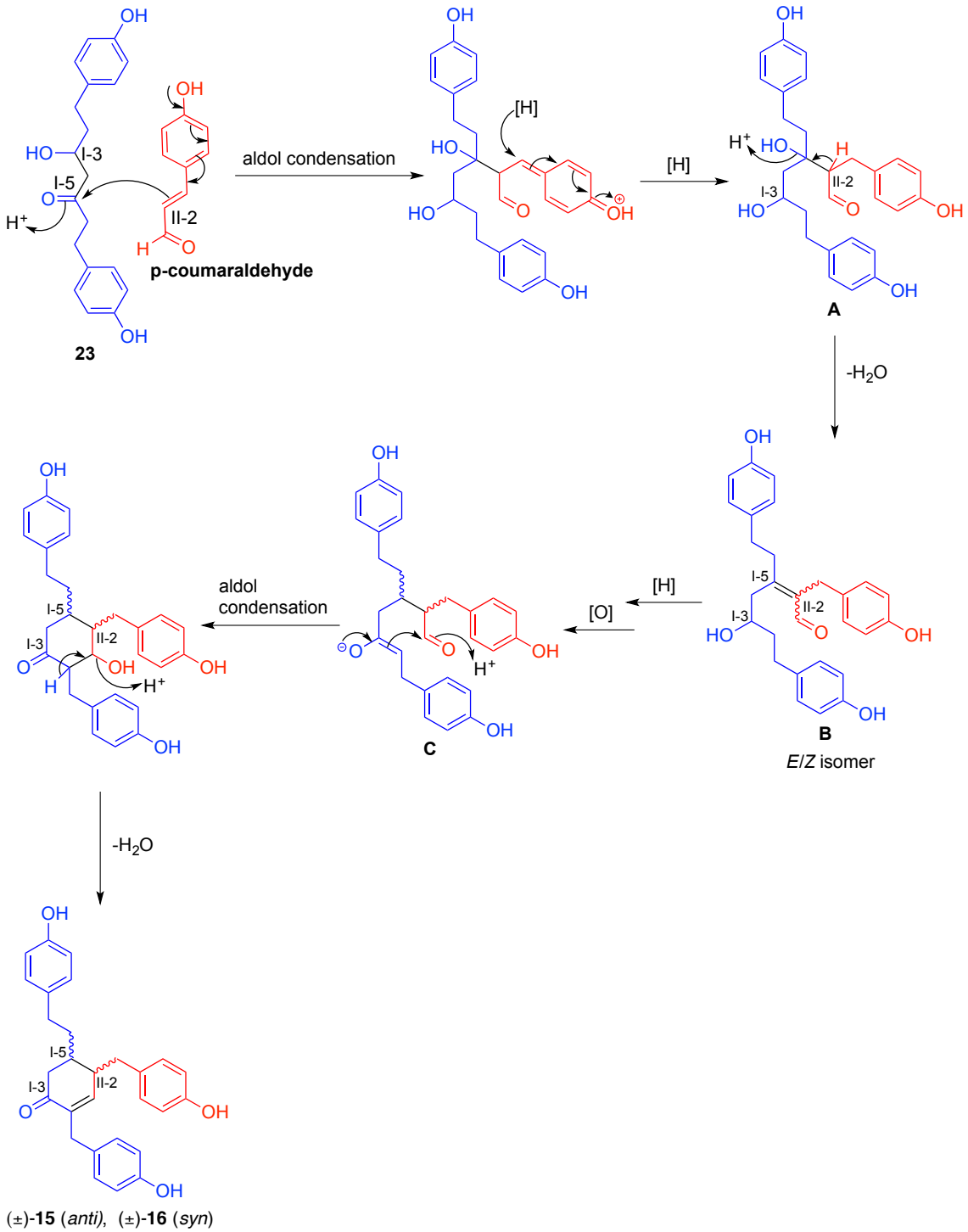

Figure 4.2b: Proposed biosynthetic pathway of **15** and **16**.

4.3 Saccardianine A (17)

(±)-Saccardianine A (**17**) was isolated as a yellowish oil with negligible optical activity. The molecular formula of **17** was determined to be $C_{28}H_{31}NO_4$ on the basis of HRESIMS measurements ($[M+H]^+$, *m/z* 446.2338). The UV spectrum exhibited two absorption maxima at 225 and 279 nm, while the IR spectrum indicated the presence of hydroxyl group (3301 cm^{-1}), ketone group (1699 cm^{-1}), and aromatic ring (3022, 1612 and 1514 cm^{-1}). The proposed 2D-structure of **17** is shown in Figure 4.3a.

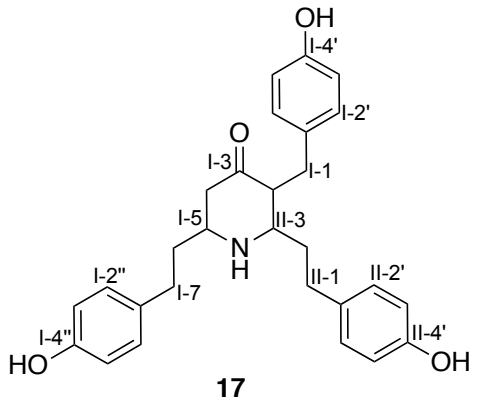

Figure 4.3a: Chemical structure of **17**.

The ^1H and ^{13}C NMR spectra of **17** (Table 4.2) showed a general resemblance to those of saccardianones A and B (**15** and **16**), as there were three sets of resonances corresponding to three 4-hydroxyphenyl moieties. After discounting the three 4-hydroxyphenyl moieties, the ^{13}C and HSQC NMR data (Table 4.2) revealed a total of 10 non-aromatic carbon resonances including six methylenes (C-I-1, C-I-4, C-I-6, C-I-7, C-II-1 and C-II-2), three methines (C-I-2, C-I-5 and C-II-3), and one ketone carbonyl carbon (δ_C 212.14, C-I-3). Analysis of the COSY data (Fig. 4.3b) revealed the presence of CH_2CH, $CH_2CHCH_2CH_2$ and CH_2CH_2CH partial structures, which correspond to the C-I-1–C-I-2, C-I-4–C-I-5–C-I-6–C-I-7 and C-II-1–C-II-2–C-II-3 fragments in **17**. On examination of the HMBC data (Fig. 4.3b), the attachment

of the three 4-hydroxyphenyl moieties to C-I-1, C-I-7 and C-II-1 were deduced based on the three-bond correlations observed from H-I-2′/6′ to C-I-1, H-I-1 to C-I-2′/6′, and H-I-2 to C-I-1′; from H-I-2′′/6′′ to C-I-7, H-I-7 to C-I-2′′/6′′, and H-I-6 to C-I-1′′; from H-II-2′/6′ to C-II-1, H-II-1 to C-II-2′/6′, and H-II-2 to C-II-1′, respectively. Besides, the three-bond correlations from H-I-1 to C-I-3 and C-II-3; and from H-II-3 to C-I-2 indicated attachment of the C-I-1–C-I-2 fragment from C-I-2 to C-I-3. The HMBC correlations from H-I-4 to C-I-2 and C-I-3 further connected the C-I-4–C-I-5–C-I-6–C-I-7 fragment from C-I-4 to C-I-3. On the other hand, HMBC correlations from H-I-1 to C-II-3, and from H-II-3 to C-I-2 allowed the C-II-1–C-II-2–C-II-3 fragment to be connected from C-II-3 to C-I-2. Finally, a 4-piperidone ring was assembled by linking C-I-5 to C-II-3 via an NH group, as supported by the three-bond correlation from H-II-3 to C-I-5. The proposed planar structure of **17** was in full agreement with the 2D NMR (Fig. 4.3b).

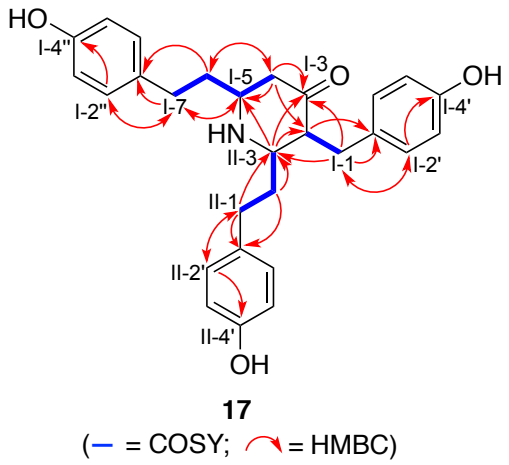

Figure 4.3b: Selected COSY and HMBC correlations of **17**.

Due to severe overlapping of some relevant signals, no useful correlation could be obtained from the NOESY spectrum. The relative configuration of **17** could not be ascertained. Nevertheless, the lack of optical activity of **17** suggested that it was isolated as a racemic mixture. Unfortunately, due to low isolation yield and

sample degradation, further spectroscopic and HPLC analyses of **17** were precluded.

(±)-Saccardianine A (**17**) represents a diarylheptanoid-phenylpropanoid adduct that is related to saccardianones A and B (**15** and **16**). However, **17** incorporated a nitrogen atom embedded within a 4-piperidone core, as it is the second instance where a 4-piperidone-bearing diarylheptanoid was reported from plants (c.f., pellacalyxin, Table 1.10).[76–78] A plausible pathway to **17** starting from **23** and *p*-coumaraldehyde is presented in Figure 4.3c. Transamination of the ketone group in **23**, followed by alcohol oxidation gives the β-aminoketone **D**. An amine-aldehyde condensation reaction between **D** and *p*-coumaraldehyde then gives the iminium ion **E**, which on ring closure via an intramolecular Mannich reaction leads to the 4-piperidone-bearing intermediate **F**. Lastly, reduction of the C-II-1–C-II-2 double bond of **F** furnishes **17**.

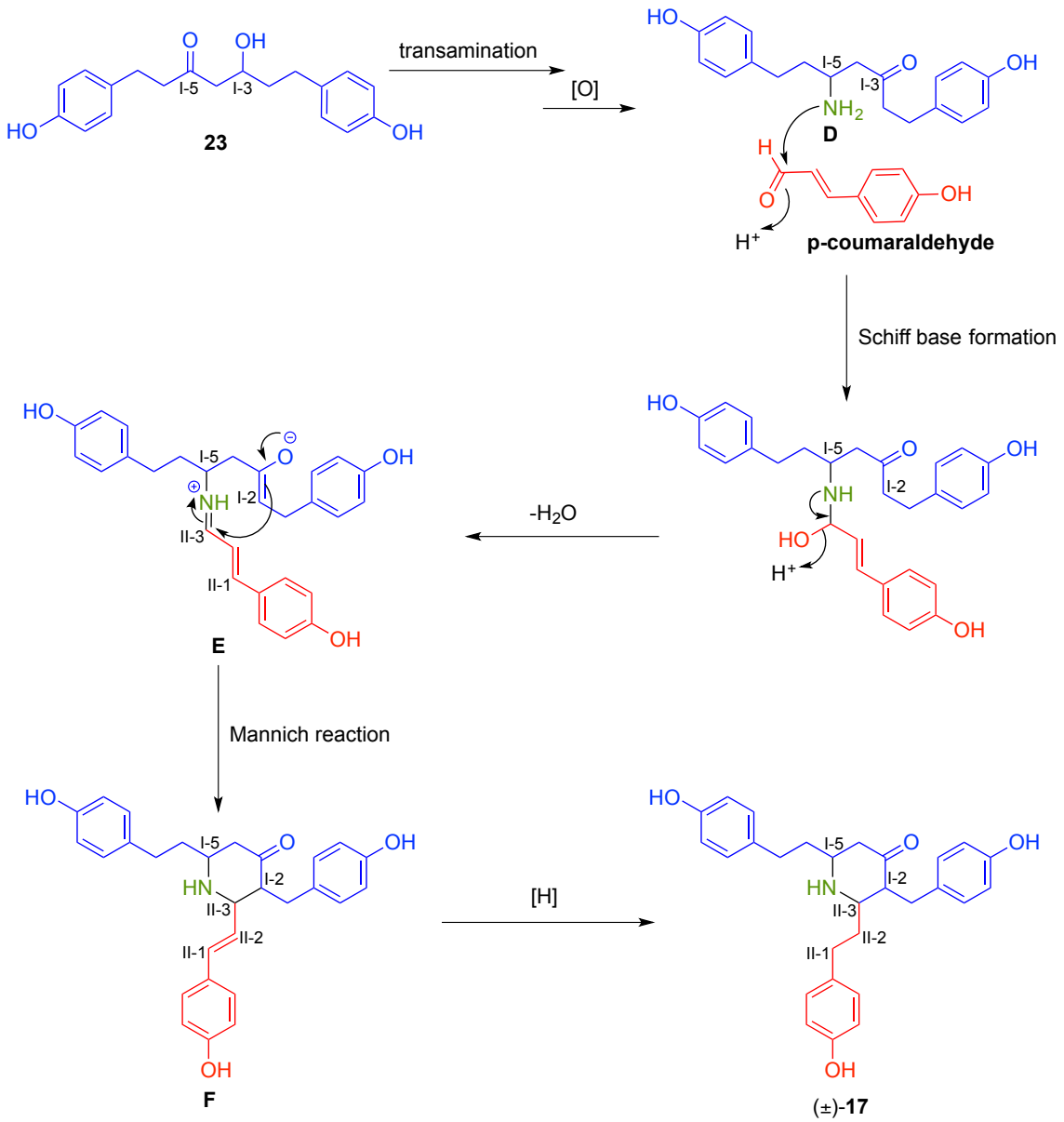

Figure 4.3c: Proposed biosynthetic pathway of **17**.

Table 4.2: ^{1}H and ^{13}C NMR data of **17** (600 MHz, CD_3OD).[a]

Unit	Position	δ_C, type	δ_H, (mult.,*J* in Hz)
I Diarylheptanoid	I-1a	30.98, CH_2	2.86 (dd, 14.5, 6.8)
	I-1b		2.53 (dd, 14.3, 4.3)
	I-2	58.76, CH	2.36 (m)
	I-3	212.14, C=O	
	I-4a	49.15, CH_2	2.30 (dd, 13.5, 3.0)
	I-4b		2.09 (t, 13.0)
	I-5	57.76, *N*-CH	2.59 (m)
	I-6a	39.62, CH_2	1.70 (m)
	I-6b		1.58 (m)
	I-7	32.47, CH_2	2.49 (m)
	I-1'	132.96, C	
	I-2'/I-6'	130.47[c], 2 X CH	6.86 (d, 8.0)
	I-3'/I-5'	116.13[d], 2 X CH	6.54 (d, 8.0)
	I-4'	156.61[e], C	
	I-1''	133.84[b], C	
	I-2''/I-6''	130.53[c], 2 X CH	6.84[b] (d, 8.0)
	I-3''/I-5''	116.17[d], 2 X CH	6.58[c] (d, 8.0)
	I-4''	156.72[e], C	
I Phenylpropanoid	II-1	32.13, CH_2	2.49 (m)
	II-2a	37.32, CH_2	1.94 (m)
	II-2b		1.58 (m)
	II-3	62.03, *N*-CH	2.46 (m)
	II-1'	134.00[b], C	
	II-2'/II-6'	131.32[c], 2 X CH	6.91[b] (d, 8.0)
	II-3'/II-5'	116.38[d], 2 X CH	6.60[c] (d, 8.0)
	II-4'	156.77[e], C	

[a] Assignments based on COSY, HSQC and HMBC analyses

[b - e] Signals are interchangeable.

4.4 Saccardianine B (18)

(±)-Saccardianine B (**18**) was isolated as an optically inactive yellowish oil. HRESIMS measurements ($[M+H]^+$, *m/z* 576.3111) established the molecular formula of **18** as $C_{38}H_{41}NO_4$, amounting to 19 degrees of unsaturation. The UV spectrum exhibited two absorption maxima at 225 and 278 nm, while the IR spectrum indicated the presence of hydroxyl group (3361 cm^{-1}) and aromatic ring (3025, 1615 and 1513 cm^{-1}). The proposed structure of **18** is shown in Figure 4.4a.

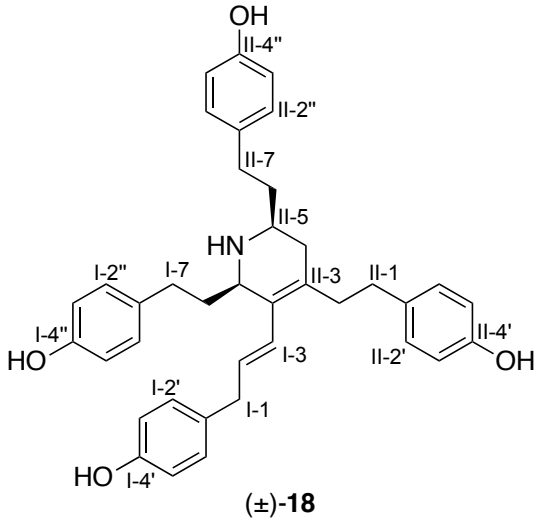

Figure 4.4a: Chemical structure of **18**.

Similar to (±)-saccardianine A (**17**), the ^1H and ^{13}C NMR spectra of **18** (Table 4.3) exhibited resonances due to 4-hydroxyphenyl moieties. However, there were four sets of the associated resonances instead of three, implying that **18** has an additional 4-hydroxyphenyl moiety compared to **17**. Besides, the ^{13}C NMR and HSQC data showed the presence of two olefinic methine carbons (δ_C 131.75 and 127.79) and two quaternary olefinic carbons (δ_C 132.78 and 134.16). The two olefinic methines were also observed in the ^1H NMR spectrum at δ_H 5.30 (dt, J = 16.0, 6.8 Hz) and 5.93 (d, J = 16.0 Hz). Based on the large vicinal coupling constant value of 16.0 Hz, the two olefinic methines were assigned to a *trans*-disubstituted

double bond unit. Additionally, the dt signal observed at δ_H 5.30 indicated that the corresponding olefinic methine was adjacent to a methylene group ($J_{H\text{-}I\text{-}1/H\text{-}I\text{-}2}$ = 6.8 Hz).

The COSY spectrum of **18** (Fig. 4.4b) showed the presence of $CH_2CH{=}CH$, $CHCH_2CH_2$, CH_2CH_2 and $CH_2CHCH_2CH_2$ partial structures, corresponding to the C-I-1–C-I-2–C-I-3, C-I-5–C-I-6–C-I-7, C-II-1–C-II-2 and C-II-4–C-II-5–C-II-6–C-II-7 fragments in **18**, which were further confirmed by the HMBC data (Fig.4.4b). Since the C-I-2–C-I-3 *trans*-disubstituted double bond accounted for two of the four olefinic carbon resonances observed in the ^{13}C NMR spectrum, the two remaining resonances at δ_C 132.78 and 134.16, were therefore assigned to a tetrasubstituted double bond unit. In the HMBC spectrum, three-bond correlations observed from H-I-3 to δ_C 134.16 (C-II-3) and from H-I-2 to δ_C 132.78 (C-I-4) in the HMBC spectrum indicated attachment of the C-I-2–C-I-3 double bond to the C-I-4–C-II-3 tetrasubstituted double bond. Furthermore, the correlations from H-II-1 to C-II-3 and from H-II-2 to C-I-4 allowed the C-II-1–C-II-2 fragment to be connected to the tetrasubstituted double bond at C-II-3 from C-II-2. On the other hand, HMBC correlations from H-I-5 to C-I-4 and C-II-3, and from H-I-3 to C-I-5 enabled the C-I-5–C-I-6–C-I-7 fragment to be connected to C-I-4 from C-I-5, while the correlations from H-II-4 to C-II-2 and from H-II-5 to C-II-3 connected the C-II-4–C-II-5–C-II-6–C-II-7 fragment to C-II-3 from C-II-4. The attachments of the four 4-hydroxyphenyl moieties to C-I-1, C-I-7, C-II-1 and C-II-7 were established based on the three-bond correlations observed from H-I-2′/6′ to C-I-1; from H-I-7 to C-I-2′′/6′′ and H-I-2′′/6′′ to C-I-7; from H-II-2′/6′ to C-II-1 and H-II-1 to C-II-2′/6′; and from H-II-7 to C-II-2′′/6′′ and H-II-2′′/6′′ to C-II-7, respectively. Finally, based on the molecular formula of **18**, an NH group as well as one degree of unsaturation remained to be

accounted for. Since both C-I-5 and C-II-5 were observed at δ_C 57.01 and 53.62, respectively, it was apparent that they were bridged by an NH group, which lead to the assembly of the tetrahydropyridine core. The proposed planar structure of **18** is in complete agreement with the HMBC data (Fig. 4.4b).

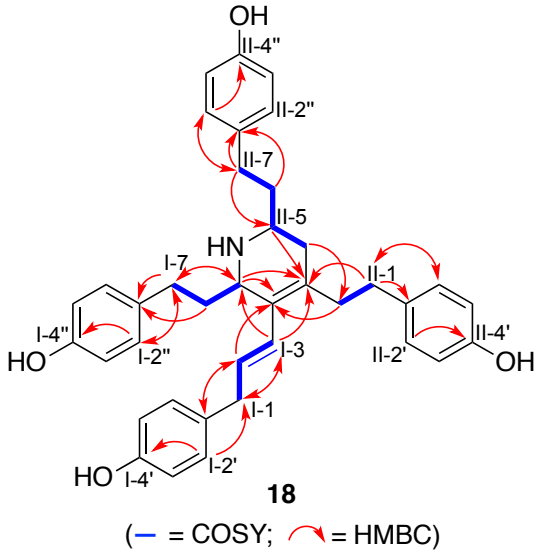

Figure 4.4b: Selected COSY and HMBC correlations of **18**.

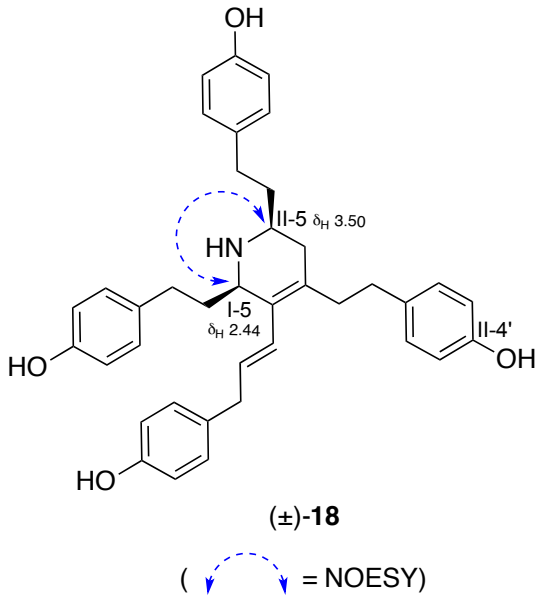

Figure 4.4c: NOESY correlation showing 1,3-diaxial interaction in **18**.

Last but not least, the relative configurations of **18** at C-I-5 and C-II-5 were inferred based on analysis of the NOESY data. The NOESY correlation observed between H-I-5 and H-II-5 required both hydrogens to be in a *syn*-1,3-diaxial configuration (Fig. 4.4c). Hence, the relative configurations at C-I-5 and C-II-5 were determined to be *R* and *S* (or *S* and *R*), respectively. Since **18** showed no optical activity, it was deduced to be isolated as a racemic mixture. This was further confirmed by chiral-phase HPLC analysis of **18**, which gave two the enantiomeric peaks in 1:1 ratio at R_t 15.67 and 16.37 min (Appendix 66).

Saccardianine B (**18**) represents a rare class of dimeric diarylheptanoids in which the two monomeric units are linked not only by a C–C bond but also via an NH group (c.f., type IV diarylheptanoid, Table 1.6). To date, officinaruminane A,[50] officinine B,[51] and alpinidinoid C,[101] were the only other known dimeric diarylheptanoids possessing the same core skeleton as **18**. A plausible dimerisation route to **18** is shown in Figure 4.4d, with diarylheptanoid **23** being proposed as the monomeric precursor. An aldol-dehydration reaction between two molecules of **23** gives the triketo intermediate **G**, which then undergoes a transamination step at C-II-5 to give the amine **H**. A subsequent ring closure via an intramolecular reductive amination of **H** leads to the tetrahydropyridine-bearing intermediate **I**. Finally, ketone reduction at C-I-3, followed by dehydration yields the dimeric **18**.

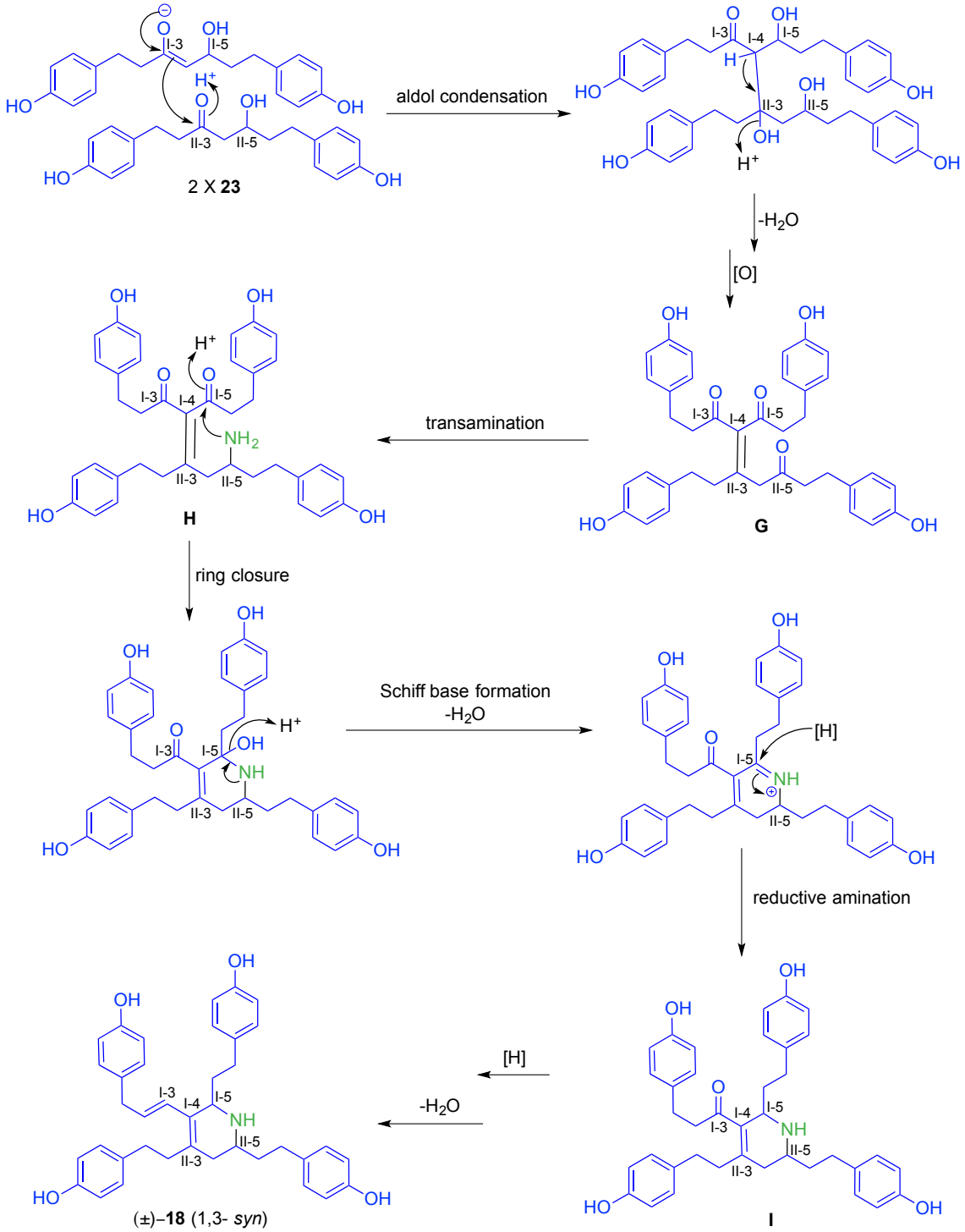

Figure 4.4d: Proposed biosynthetic pathway of **18**.

Table 4.3: ^{1}H and ^{13}C NMR data of **18** (600 MHz, CD_3OD).[a]

Unit	Position	δ_C, type	δ_H, (mult., *J* in Hz)
I	I-1	40.09, CH_2	3.15 (m)
	I-2	131.75, C=CH	5.30 (dt, 16.0, 6.8)
	I-3	127.79, C=CH	5.93 (d, 16.0)
	I-4	132.78, C=C	
	I-5	57.01, CH	3.50 (q, 7.0)
	I-6a	37.46,[e] CH_2	1.86 (m)
	I-6b		1.52 (m)
	I-7	31.65, CH_2	2.28 (m)
	I-I'	132.75, C	
	I-2'/I-6'	130.45,[b] 2 X CH	6.87 (d, 8.5)
	I-3'/I-5'	116.18,[c] 2 X CH	6.61 (d, 8.5)
	I-4'	156.49,[d] C	
	I-1''	134.07,[f] C	
	I-2''/I-6''	130.54,[b] 2 X CH	6.74 (d, 8.5)
	I-3''/I-5''	116.27,[c] 2 X CH	6.55[b] (d, 8.5)
	I-4''	156.62,[d] C	
II	II-1	34.82, CH_2	2.47 (m)
	II-2	37.41,[e] CH2	2.24 (m)
	II-3	134.16, C=C	
	II-4a	38.79, CH_2	1.68 (m)
	II-4b		1.54 (m)
	II-5	53.62, CH	2.44 (m)
	II-6a	38.02, CH_2	1.86 (m)
	II-6b		1.50 (m)
	II-7	32.67, CH_2	2.46 (m)
	II-1'	134.39,[f] C	
	II-2'/II-6'	130.68,[b] 2 X CH	6.79 (d, 8.5)
	II-3'/II-5'	116.38,[c] 2 X CH	6.56[b] (d, 8.5)
	II-4'	156.71,[d] C	
	II-1''	134.74,[f] C	
	II-2''/II-6''	130.80,[b] 2 X CH	6.93 (d, 8.5)
	II-3''/II-5''	116.43,[c] 2 X CH	6.61[b] (d, 8.5)
	II-4''	156.81,[d] C	

[a] Assignments based on COSY, HSQC and HMBC analyses.
[b–f] Signals are interchangeable within each column.

4.5 Saccardianine C (19)

Saccardianine C (**19**) was isolated as an optically inactive yellowish oil. The molecular formula of **19** was determined to be $C_{38}H_{41}NO_4$ on the basis of HRDARTMS measurements ($[M+H]^+$, *m/z* 576.3111). The IR spectrum indicated the presence of aromatic ring (3061, 1596 and 1515 cm^{-1}). The proposed structure of **19** is shown in Figure 4.5a.

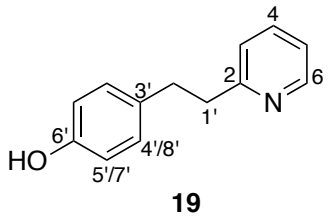

19

Figure 4.5a: Chemical structure of **19**.

The ^1H NMR spectrum (Table 4.4) showed the presence of eight aromatic protons and a distinct pair of 2H triplets attributable to an ethylene group (δ_H 2.96 and 3.08, t, *J* = 8.0 Hz). The ^{13}C NMR spectrum (Table 4.4) showed 11 discrete carbon resonances, two of which were due to two pairs of equivalent aromatic methine carbons, hence totalling 13 carbon atoms. Analysis of the ^{13}C and HSQC NMR data indicated that **19** comprises two aliphatic methylene carbons and 11 aromatic carbons (eight methine, one quaternary, and one nitrogen-bearing and one oxygenated carbon). The presence of a 4-hydroxyphenyl moiety in **19** was readily determined based on the characteristic ^{13}C NMR shifts, i.e., δ_C 132.71 (C-3′), 129.48 (C-4′/8′), 115.37 (C-5′/7′), and 154.54 (C-6′).[100] The remaining aromatic carbons were assigned to a 2-substituted pyridine moiety based on the characteristic ^{13}C NMR shifts and the observed ^1H NMR shifts as well as the corresponding splitting patterns and coupling constants.[102,103] Finally, the 4-hydroxyphenyl and 2-substituted pyridine moieties were bridged via the ethylene

unit based on the HMBC correlations observed from H-1′ to C-3′; from H-2′ to C-4′/8′; from H-2′ to C-2; and from H-1′ to C-3 (Fig. 4.5b). The proposed structure of **19** was in complete agreement with the COSY and HMBC data (Fig. 4.5b).

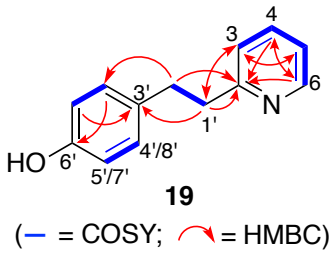

Figure 4.5b: Selected COSY and HMBC correlations of **19**.

Although saccardianine C (**19**) was obtained as a natural product for the first time, it was previously encountered in the structures of hydrangeamines A and B, in which the complete fragment of **19** was conjugated to a secoiridoid glycoside.[103] By comparing the structure of **19** with those of (±)-saccardianine A (**17**), it was speculated that **19** could be a degradation product of **17**. A possible degradation pathway from **17** to **19** involving retro-Michael and retro-aldol reactions is shown in Figure 4.5c.

Table 4.4: ^{1}H and ^{13}C NMR data of **19** (600 MHz, $CDCl_3$).[a]

Position	δ_C, type	δ_H (mult.,*J* in Hz)
2	161.29, C	
3	123.26, CH	7.13 (d, 7.7)
4	136.73, CH	7.60 (td, 7.7, 1.9)
5	121.36, CH	7.14 (dd, 5.0, 7.7)
6	148.72, NH	8.5 d (4.8)
1'	40.13, CH_2	3.08 (t, 8.0)
2'	35.31, CH_2	2.96 (t, 8.0)
3'	132.71, C	
4'/8'	129.48, 2 X CH	6.97 (d, 8.4)
5'/7'	115.37, 2 X CH	6.68 (d, 8.4)
6'	154.54, C	

[a] Assignments based on COSY, HSQC and HMBC analyses.

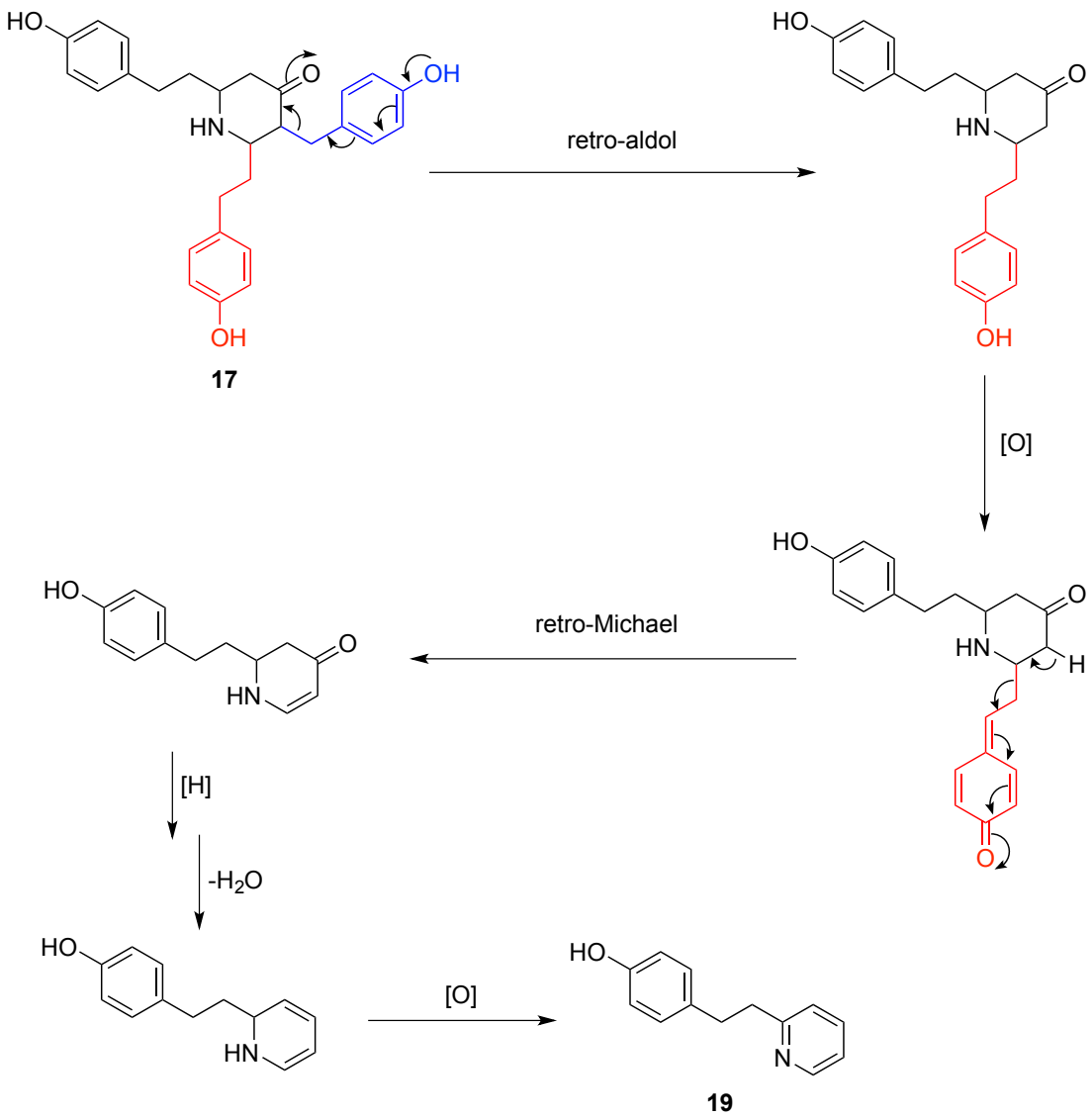

Figure 4.5c: Possible degradation pathway from **17** to **19**.

4.6 Pellaspirone (20)

Pellaspirone (**20**) was isolated as colourless prisms (mp 139 – 140 °C) from chloroform. The molecular formula of **20** was determined to be $C_{19}H_{18}O_3$ on the basis of HRESIMS measurements ($[M-H]^-$, *m/z* 293.1193). The UV spectrum gave a single absorption maximum at 224 nm, while the IR spectrum indicated the presence of hydroxyl (3246 cm^{-1}) and conjugated ketone (1657cm^{-1}) functionalities. The proposed structure of **20** is shown in Figure 4.6a.

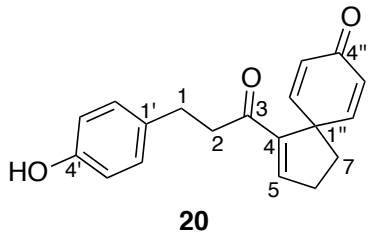

20

Figure 4.6a: Chemical structure of **20**.

The ^1H NMR spectrum of **20** (Table 4.5) showed the presence of nine aromatic/olefinic hydrogens, four aliphatic methylene groups and an OH singlet (δ_H 5.82, br s). The ^{13}C NMR spectrum (Table 4.5) exhibited 15 discrete carbon resonances, four of which were due to four pairs of equivalent aromatic/olefinic methine carbons, giving a sum of 19 carbon atoms. Analysis of the ^{13}C and HSQC NMR data indicated **20** to comprise five aliphatic carbons (four methylene and one quaternary carbon), 12 aromatic/olefinic carbons (nine methine, two quaternary, and one oxygenated carbon), and two conjugated ketone carbonyl carbons (δ_C 186.25 and 196.28). The presence of a 4-hydroxyphenyl moiety in **20** was readily determined based on the characteristic ^{13}C shifts, i.e., δ_C 132.62 (C-1′), 129.45 (C-2′/6′), 115.35 (C-3′/5′) and 154.29 (C-4′).[100] The HSQC and HMBC data also revealed that both the resonances at δ_C 146.03 (C-4) and 147.08 (C-5; δ_H 6.97) were due to a trisubstituted double bond associated with a conjugated ketone

group (Fig. 4.6b). Additionally, HMBC correlations from the olefinic methine resonances observed at δ_H 6.75 (δ_C 152.31) and δ_H 6.30 (δ_C 128.18) to the carbon resonances at δ_C 186.25 (ketone C-4′′) and 53.64 (quaternary C-1′′) indicated the presence of a spirodienone moiety (Fig. 4.6b), which has a relatively rare occurrence in natural products. In comparison, pronuciferine is a spirodienone-containing proaporphine alkaloid,[104] and comparison of the NMR data of **20** with those of pronuciferine confirmed the presence of an unsubstituted spirodienone[104,105] moiety in **20**. Apart from the CH=CH fragments due to the 4-hydroxyphenyl and spirodienone moieties, the COSY data (Fig. 4.6b) also revealed the presence of CH_2CH_2 and $=CHCH_2CH_2$ partial structures, which correspond to the C-1–C-2 and C-5–C-6–C-7 fragments in **20**, respectively. The 4-hydroxyphenyl moiety was deduced to be attached to C-1 based on the three-bond correlations observed from H-1 to C-2′/6′ and from H-2 to C-1′ in the HMBC spectrum, while the attachment of C-2 to C-3 was supported by the correlation from H-1 to C-3. The deduction that the C-5–C-6–C-7 fragment was part of the cyclopentene unit, which was connected to C-3 via C-4, were based on the HMBC correlations observed from H-7 to C-4; and from H-5 to C-1′′ and C-3. Last but not least, the HMBC correlations observed from H-2′′/6′′ to C-4 and C-7; and from H-3′′/5′′ to C-1′′ confirmed C-1′′ as the spirocenter. The proposed structure of **20** was concomitantly proven by X-ray diffraction analysis (Fig. 4.6c).

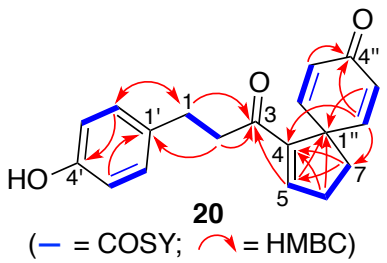

Figure 4.6b: Selected COSY and HMBC correlations of **20**.

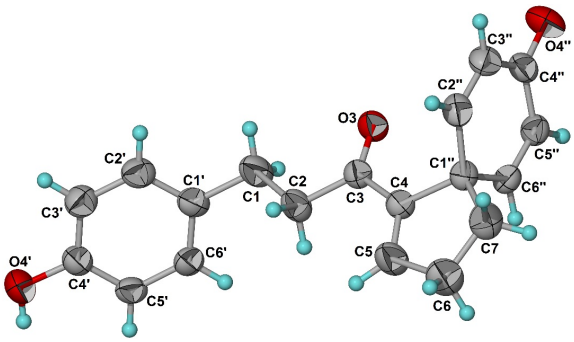

Figure 4.6c: X-ray crystal structure of **20**.

The unusual carbon skeleton of pellaspirone (**20**) suggested that it was derived from a diarylheptanoid that has undergone an intramolecular cyclisation. Platyphyllenone (**22**), which was co-isolated in the present study, was proposed to be the precursor of **20** (Fig. 4.6d). Firstly, oxidation of the C-4–C-5 double bond gives the epoxyketone **J**. A subsequent intramolecular nucleophilic addition of C-1′′ to C-4 leads to epoxide ring-opening and formation of the spirodienone structure, which on a dehydration step yields pellaspirone (**20**).

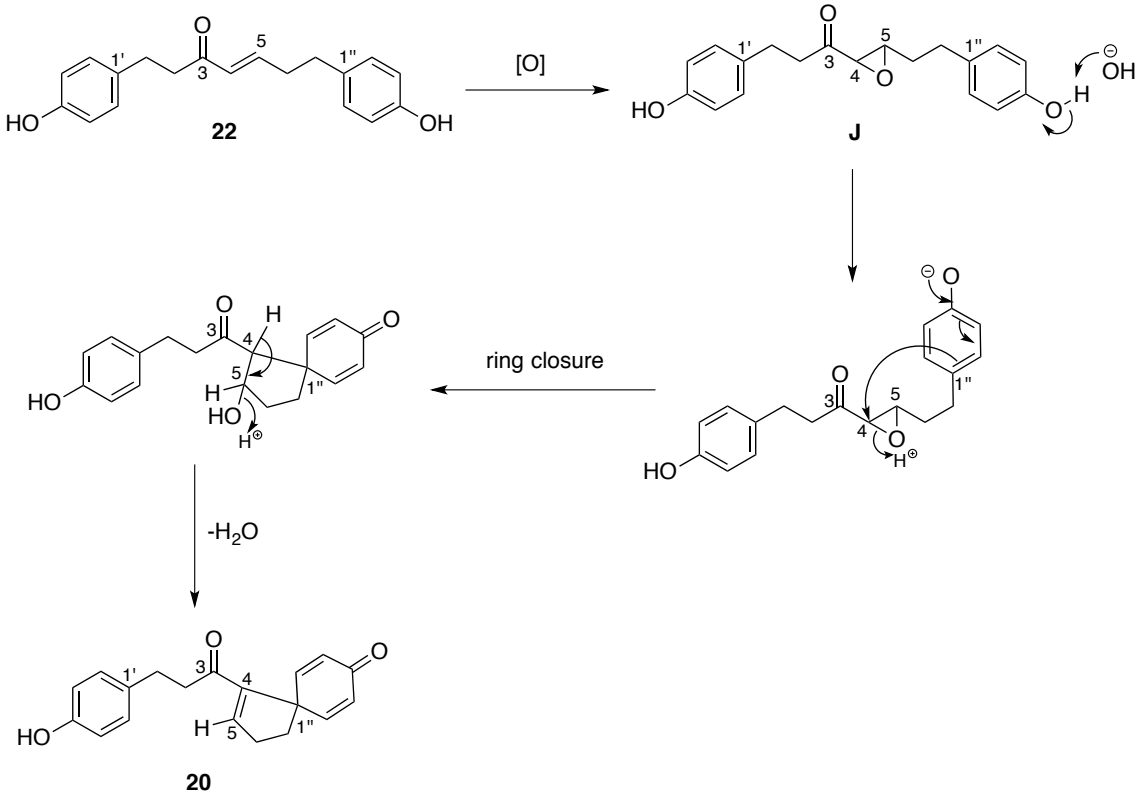

Figure 4.6d: Proposed formation pathway from **22** to **20**.

Having sufficient quantity of **22** in hand, semi-synthesis of **20** was attempted. Platyphyllenone (**22**) was readily converted into epoxyketone **J** via the hydrotalcite-catalysed epoxidation method.[106] The presence of the epoxide functionality[107] in **J** was confirmed by analysis of the ^{1}H and ^{13}C NMR data (Appendix 75). Subsequent treatment of **J** with NaOH resulted in the anticipated product (**20**) in almost quantitative yield. Based on the result of this semi-synthesis, the possibility that **20** being an artifact arising from our acid-base extraction procedure cannot be ruled out. This is despite epoxyketone **J** was not isolated from the crude extract.

Table 4.5: ^{1}H and ^{13}C NMR data of **20** (600 MHz, $CDCl_3$).[a]

Position	δ_C, type	δ_H, (mult., *J* in Hz)
1	29.25, CH_2	2.80 (t, 7.65)
2	41.28, CH_2	2.88 (t, 7.42)
3	196.28, C=O	
4	146.03, C	
5	147.08, CH	6.97 (t, 2.7)
6	31.82, CH_2	2.73 (td, 7.3, 2.7)
7	36.60, CH_2	2.12 (t, 7.32)
1'	132.62, C	
2'/6'	129.45, 2 X CH	6.99 (d, 8.4)
3'/5'	115.35, 2 X CH	6.75 (d, 8.4)
4'	154.29, C	
1''	53.64, C	
2''/6''	152.31, 2 X CH	6.75 (d, 10.0)
3''/5''	128.18, 2 X CH	6.30 (d, 10.0)
4''	186.25, C=O	

[a] Assignments based on COSY, HSQC and HMBC analyses.

4.7 Saccardianoside (21)

Saccardianoside (**21**) was isolated as a colourless oil ($[\alpha]_D$ = –48.45 (MeOH, *c* 0.071)). The molecular formula of **21** was determined to be $C_{31}H_{42}O_{13}$ on the basis of HRESIMS measurements ($[M-H]^-$, *m/z* 621.2547). The UV spectrum showed two absorption maxima at 224 and 278 nm, while the IR spectrum indicated the presence of hydroxyl (3397 cm^{-1}), ketone (1703 cm^{-1}) and aromatic (3014 and 1515 cm^{-1}) functionalities. The proposed structure of **21** is shown in Figure 4.7a.

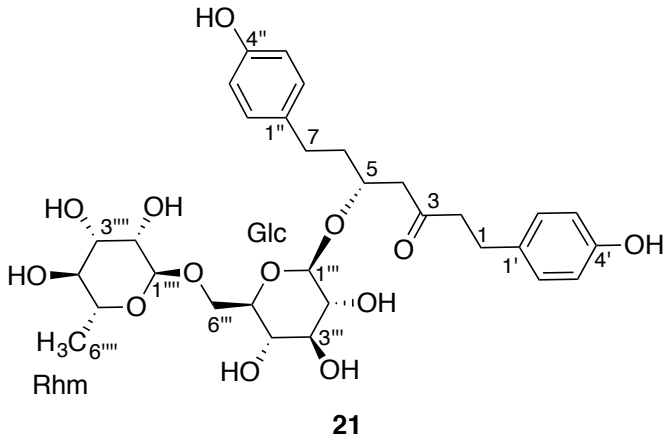

21

Figure 4.7a: Chemical structure of **21**.

The ^{13}C NMR spectrum of **21** (Table 4.6) showed 27 discrete resonances, four of which were due to four pairs of equivalent aromatic methine carbons, thus totalling 31 carbon atoms. There were 12 signals within the aromatic region of δ_C 116.18 – 156.58, which were characteristic of two 4-hydroxyphenyl groups.[100] The ^1H NMR spectrum (Table 4.6) exhibited signals due to eight aromatic hydrogens associated with the aforementioned 4-hydroxyphenyl groups [δ_H 6.68 (2H, d, *J* = 8.3 Hz), 6.69 (2H, d, *J* = 8.3 Hz), 7.00 (2H, q, *J* = 8.3 Hz) and 7.01 (2H, d, *J* = 8.3 Hz)]. Additionally, there were multiple aliphatic methines and methylenes, as well as a distinctive methyl doublet [δ_H 1.24 (3H, d, *J* = 6.2 Hz)]. Analysis of the HSQC data revealed the presence of 18 aliphatic carbon resonances (11 oxygenated methine, 6

methylene and one methyl carbon) and a ketone carbonyl carbon (δ_C 211.87, C-3). Notably, the two substantially downfield methine signals observed at δ_H 4.28 and 4.69 were assigned to two anomeric carbons at δ_C 104.10 (C-1‴) and 102.32 (C-1⁗), respectively. These resonances suggested the presence of two sugar moieties, *viz*., **21** is a glycosidic compound.

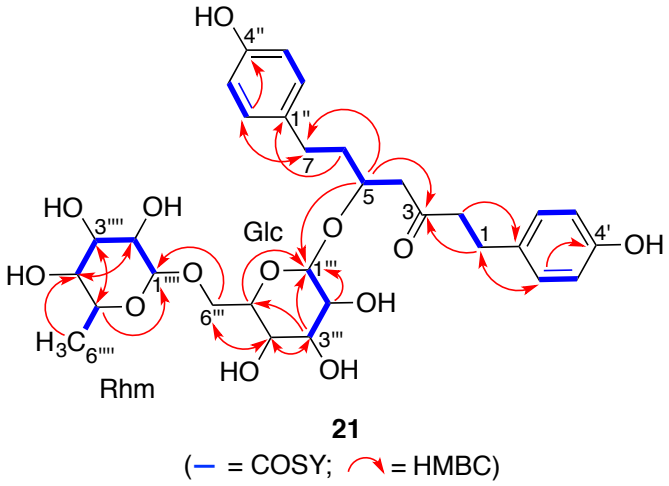

Figure 4.7b: Selected COSY and HMBC correlations of **21**.

Further analysis of the COSY data (Fig. 4.7b) revealed the partial structures CH_2CH_2, $CH_2CHCH_2CH_2$, CHCHCH, CHCHCHCH and CH_3CH, which correspond to the C-1–C-2, C-4–C-5–C-6–C-7, C-1‴–C-2‴–C-3‴, C-1⁗–C-2⁗–C-3⁗–C-4⁗ and C-5⁗–C-6⁗⁗ fragments in the structure of **21**. In the HMBC spectrum (Fig. 4.7b), a 5-*O*-glycated-3-ketodiarylheptanoid moiety[118] was readily determined based on the three-bond correlations observed from H-1 to C-2′/6′ and C-3; from H-5 to C-3 and C-7; and from H-7 to H-2″/6″. The two corresponding pyranose units, namely, glucose (Glc) and rhamnose (Rhm) were assigned based on analyses of the COSY and HMBC data. Their ^1H and ^{13}C NMR chemical shift values were mostly comparable to those of D-glucopyranose and L-rhamnopyranose.[108–110] The three-bond HMBC correlation observed from H-6‴ to C-1⁗ indicated that the Glc unit was connected to the Rhm unit via the C-6‴–O–C-1⁗ bond, implying the presence

of a disaccharide. The absolute configurations of the two sugar moieties were later characterised as D-glucopyranose and L-rhamnopyranose via HPLC analysis of the acid hydrolysate of **21**, following arylthiocarbamoyl-thiazolidine derivatisation (Appendix 82).[111] By analysing the ^{1}H NMR coupling constants of the two anomeric protons (H-1‴ and H-1⁗) according to the Karplus relationship, the configurations of β-D-glucopyranose (diaxial coupling, J = 7.8 Hz) and α-L-rhamnopyranose (equitorial-axial coupling, J = 1.7 Hz) were established.[112] Taken together, the glycosidic moiety of **21** was identified as rutinose, a disaccharide first characterised from the naturally occurring flavonoid-glycoside rutin.[109,113]

Last but not least, the absolute configuration of C-5 in **21** was established as 5*R* by application of the glycosidation shift rule.[114] This was achieved by comparing the ^{13}C NMR chemical shift values of **21** with the co-isolated diarylheptanoid ((±)-**23**) at C-4 ($\Delta\delta_A$ = -1.59) and C-6 ($\Delta\delta_A$ = -2.89), where $\Delta\delta_A = \delta_{C(\text{alcoholic glycoside})} - \delta_{C(\text{alcohol})}$ (Appendices 80 and 81). According to the specified designation (Fig. 4.7c) where the C_α-H bond (H-5) is directed downwards from the paper plane, $\Delta\delta_A$ of the β-CH_2 that is *anti* to the β-D-glucopyranose oxygen (C-6) is always larger than that for the β-CH_2 *syn* to the oxygen (C-4), viz., 5*R* configuration in **21**.[114] Hence, saccardianoside was elucidated as 1,7-bis-(4-hydroxyphenyl)-3-heptanone-5*R*-*O*-rutinoside, the first instance of a diarylheptanoid that is conjugated with rutinose. The natural aglycone of **21** was concomitantly proposed to be 5*R*-hydroxy-1,7-bis-(4-hydroxyphenyl)-3-heptanone [(5*R*)-**23**].[76,115]

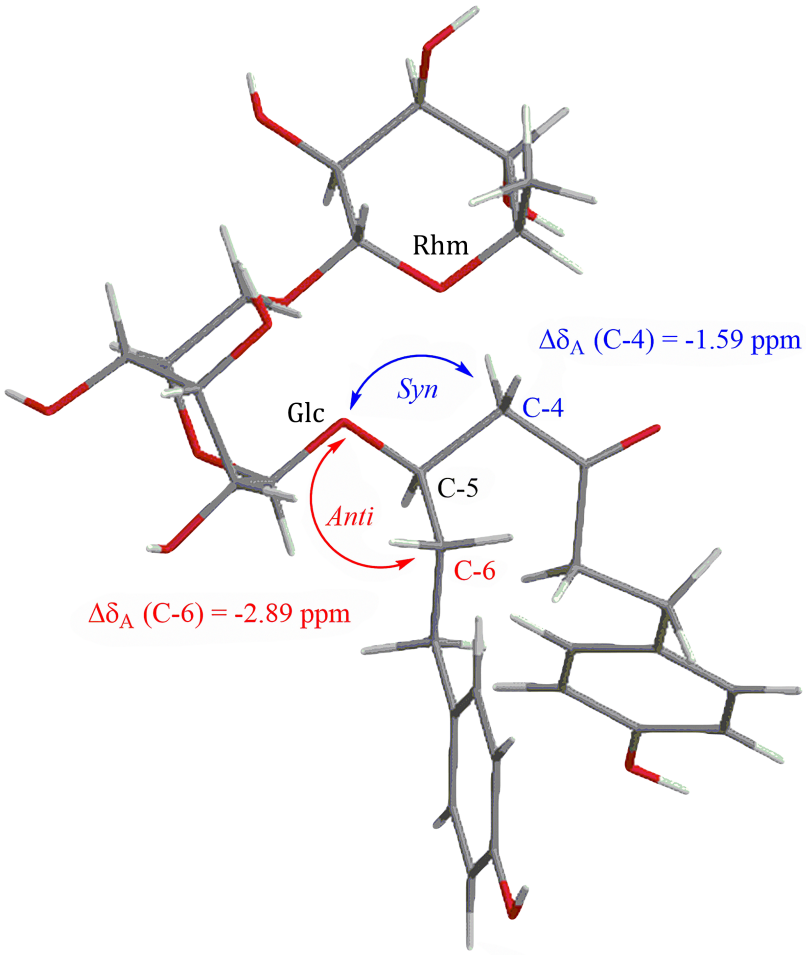

5*R*-**21**

Figure 4.7c: Determination of the absolute configuration of C-5 in **21** by application of the glycosidation shift rule.[114]

Table 4.6**:** ^{1}H and ^{13}C NMR data of **21** (600 MHz, CD_3OD).[a]

Unit	Position	δ_C, type	δ_H (mult., *J* in Hz)
Diarylheptanoid	1	29.82, CH_2	2.75 (m)
	2	46.27, CH_2	2.79 (m)
	3	211.87, C=O	
	4a	50.12, CH_2	2.79 (m)
	4b		2.64 (dd, 15.9, 6.0)
	5	76.77[b], CH	4.07 (p, 6.0)
	6a	38.02, CH_2	1.82 (m)
	6b		1.71 (m)
	7a	31.37, CH_2	2.64 (dd, 15.9, 6.0)
	7b		2.59 (m)
	1'	133.35, C	
	2'/6'	130.41[c], 2 X CH	7.00 (d, 8.3)
	3'/5'	116.18[d], 2 X CH	6.68 (d, 8.3)
	4'	156.39[e], C	
	1''	134.15, C	
	2''/6''	130.44[c], 2 X CH	7.01 (d, 8.3)
	3''/5''	116.23[d], 2 X CH	6.69 (d, 8.3)
	4''	156.58[e], C	
Glc	1'''	104.10, *O*-CH (anomeric)	4.28 (d, 7.8)
	2'''	75.24, CH-OH	3.14 (dd, 9.2, 7.8)
	3'''	78.03, CH-OH	3.33 (s)
	4'''	71.75, CH-OH	3.23 (t, 9.0)
	5'''	76.68[b], *O*-CH	3.31 (m)
	6'''a	68.32, *O*-CH_2	3.89 (dd, 11.2, 1.9)
	6'''b		3.52 (m)
Rhm	1''''	102.32, *O*-CH (anomeric)	4.69 (d, 1.7)
	2''''	72.24, CH-OH	3.82 (dd, 3.5, 1.7)
	3''''	72.40, CH-OH	3.66 (dd, 9.4, 3.3)
	4''''	74.12, CH-OH	3.37 (d, 9.5)
	5''''	69.83, *O*-CH	3.62 (m)
	6''''	18.17, CH_3	1.24 (d, 6.2)

[a] Assignments based on COSY, HSQC and HMBC analyses.
[b - e] Signals are interchangeable.

4.8 Platyphyllenone (22)

Platyphyllenone (**22**, Fig. 4.8) was isolated as a yellowish oil. The molecular formula of **22** was determined to be $C_{19}H_{20}O_3$ on the basis of HRESIMS measurements ($[M-H]^-$, *m/z* 295.13397). The UV spectrum exhibited two absorption maxima at 225 and 278 nm, while the IR spectrum indicated the presence of hydroxyl (3326 cm^{-1}) and α,β-unsaturated ketone (1670cm^{-1}) functionalities. The ^1H and ^{13}C NMR data of **22** are presented alongside literature data[76] in Table 4.7.

Platyphyllenone (**22**) is a type I linear diarylheptanoid that was first isolated from the green bark of *Betula platyphylla* (Betulaceae).[116] It appears to have a wide chemotaxonomic distribution, occurring in various *Alnus* species (Betulaceae)[43,116] as well as *Renealmia alpinia* (Zingerberaceae)[117] and *Pellacalyx saccardianus*[76] (Rhizophoraceae). In the present research, **22** was also the most abundant diarylheptanoid obtained from the leaves of *P. saccardianus*.

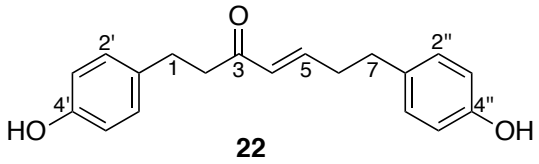

22

Figure 4.8: Chemical structure of **22**.

Table 4.7: ^{1}H and ^{13}C NMR data of **22** in comparison with literature data.

	22		**Literature data[76]**	
Position	δ_C,[a] type	δ_H[a] (mult., *J* in Hz) (600 MHz, $CDCl_3$)	δ_C, type	δ_H (mult., *J* in Hz) (400 MHz, $(CD_3)_2CO$)
1	29.32, CH_2	2.81 (m)	29.1	2.77 (m)
2	41.88, CH_2	2.81 (m)	41.5	2.80 (m)
3	200.30, C=O		198.9	
4	133.10, C=<u>CH</u>	6.08 (dt, 16.0, 1.3)	Not reported	6.10 (dt, 16.0, 1.6)
5	146.92, C=<u>CH</u>	6.82 (dt, 15.8, 6.7)	146.2	6.89 (dt, 16.0, 6.8)
6	34.36, CH_2	2.48 (m)	34.2	2.50 (m)
7	33.46, CH_2	2.69 (t, 7.5)	33.3	2.71 (t, 7.2)
1'	132.63, C		132.1	
2'/6'	129.44,[b] 2 X CH	7.01 (t, 8.0)	129.2	7.05 (dd, 8.4)
3'/5'	115.32, 2 X CH	6.74 (dd, 8.5)	115.1	6.75 (d, 8.4)
4'	153.99,[c] C		155.60	
1''	130.68, C		131.7	
2''/6''	129.43,[b] 2 X CH	7.01 (t, 8.0)	129.2	7.05 (dd, 8.4)
3''/5''	115.29, 2 X CH	6.74 (dd, 8.5)	115	6.75 (d, 8.4)
4''	153.91,[c] C		155.5	

[a] Assignments based on COSY, HSQC and HMBC analyses.

4.9 (±)-5-Hydroxy-1,7-bis-(4-hydroxyphenyl)-3-heptanone (23)

(±)-5-Hydroxy-1,7-bis-(4-hydroxyphenyl)-3-heptanone (**23**, Fig. 4.9) was isolated as a colourless oil that was optically inactive. The molecular formula of **23** was determined to be $C_{19}H_{22}O_4$ on the basis of HRESIMS measurements ($[M-H]^-$, *m/z* 313.14453). The UV spectrum exhibited two absorption maxima at 224 and 279 nm, while the IR spectrum indicated the presence of hydroxyl (3318 cm^{-1}) and ketone (1695cm^{-1}) functionalities. The ^1H and ^{13}C NMR data of **23** were tabulated along with literature values[76] in Table 4.8. Since **23** was optically inactive, it was deduced to be isolated as a racemic mixture.

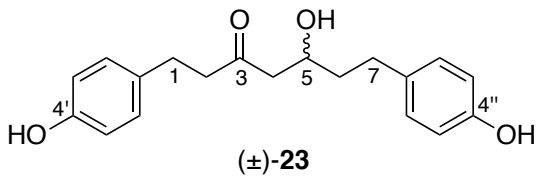

(±)-**23**

Figure 4.9: Chemical structure of **23**.

Interestingly, both of the 5*R* and 5*S* enantiomers of **23** were previously isolated as natural products. 5*S*-**23**, platyphyllonol (Table 1.8) was first isolated alongside **22** from the green bark of *Betula platyphylla* (Betulaceae).[43, 118] Various glucose and xylose glycosides of platyphyllonol were previously characterised from the stem bark of *Alnus hirsuta* (Betulaceae).[118] In contrast, 5*R*-**23** was first isolated from the rhizomes of *Amomum muricarpum* (Zingerberaceae).[115] It was also reported from *P. saccardianus* (Rhizophoraceae).[76] Considering the wide chemotaxonomic distribution of both enantiomers, it is conceivable that **23** may arise naturally as a racemic mixture in *P. saccardianus*. It should be noted that diarylheptanoid **23** was proposed to be the biogenetic precursor to compounds **15** – **18**.

Table 4.8: ^{1}H and ^{13}C NMR Spectroscopic Data for **23** (600 MHz, $(CD_3)_2CO$).[a]

Position	**23**		**Literature data [76]**	
	δ_C,[a] type	δ_H[a] (mult., *J* in Hz) (600 MHz, $(CD_3)_2CO$)	δ_C, type	δ_H (mult., *J* in Hz) (400 MHz, $(CD_3)_2CO$)
1	29.16, CH_2	2.74 (br s)	28.30	2.75 (br s)
2	45.79, CH_2	2.74 (br s)	45.00	2.75 (br s)
3	209.91, C=O		209.10	
4	50.74, CH_2	2.56 (d, 6.2)	49.00	2.56 (d, 6.0)
5	67.58, CH	4.02 (sx, 6.1)	66.00	4.03 (sx, 6.0)
6	40.22, CH_2	1.67 (td, 8.2, 6.4)	39.40	1.68 (dd, 14.0, 6.4)
7a	31.46, CH_2	2.66 (m)	30.60	2.67 (m)
7b		2.54 (br m)		2.55 (m)
1'	132.86, C		132.00	
2'/6'	129.93,[b] 2 X CH	7.02 (d, 8.2)	129.10	7.03 (d, 8.4)
3'/5'	115.80,[c] 2 X CH	6.733[b] (d, 8.4)	115.00	6.74 (d, 8.4)
4'	156.13,[d] C		155.40	8.2
1''	133.71, C		132.90	
2''/6''	129.98,[b] 2 X CH	7.02 (d, 8.4)	129.10	7.03 (d, 8.4)
3''/5''	115.84,[c] 2 X CH	6.730[b] (d, 8.4)	125.00	6.74 (d, 8.4)
4''	156.29,[d] C		155.50	8.2

[a] Assignments based on HSQC analyses.
[b - c] Signals are interchangeable within each column.

Chapter 5: Antispasmodic and Cytotoxic Bioactivity Analysis

As described in Chapter 4, the present research has elucidated five diphenethylpiperidine alkaloids (**1** – **5**) from *H. longiflora*, as well as nine nortropane alkaloids (**6** – **14**) and nine diarylheptanoids (**15** – **23**) from *P. saccardianus*. Considering the known bioactivity of (–)-lobeline (**3**) and tropane alkaloids (Sections 1.2.3 and 1.3.5), in addition to the ethnobotany of *H. longiflora* (Section 1.5.3), alkaloids **1** – **4**, **6**, **9**, **11**, **12** and **13** were tested on an *in vitro* antispasmodic bioassay (Appendices 85 – 88, 90). The antispasmodic bioassay allows the preliminary screening for lead compounds exhibiting muscarinic antagonist, β-adrenoreceptor agonist, and/or calcium channel blocking activity, viz., useful drugs to treat asthma and chronic obstructive pulmonary diseases (COPD).[119–121] On the other hand, the diarylhepatanoids **15**, **16**, **20** and **22** were subjected to an *in vitro* cytotoxic bioassay (Appendices 89 – 91). The rationale was based on their structural resemblance to some type I type V linear diarylheptanoids, e.g., blepharocalyxins, which exhibit pronounced cytotoxic activity (Table 1.8). Indeed, the crude leaf extract of *P. saccardianus* demonstrated potent *in vitro* cytotoxicity against several pancreatic and breast cancer cell lines. The similar cancer cell lines were adopted for further testing with the pure compounds. The antispasmodic and cytotoxic bioassays were successfully conducted by collaborators as acknowledged; the data of which would be discussed here with respect to the preliminary structure activity relationship, proposed mechanism of action, and preclinical relevance.

5.1 Antispasmodic Activity of Diphenethylpiperidine Alkaloids 1 – 4 on Rat Isolated Trachea

The diphenethylpiperidine alkaloids hippofoline A (**1**), hippofoline B (**2**), (–)-lobeline (**3**) and (–)-cis-2′,2′′-diphenyllobelidiol (**4**) were tested for their relaxation activity on rat isolated tracheal segments that were pre-contracted with carbachol (Appendices 85 and 86). Due to paucity of material, (–)-*cis*-2′,2′′-diphenyllobelidiol *N*-oxide (**5**) was not evaluated. Alkaloids **2** – **4** exhibited a concentration-dependent relaxation effect on rat tracheal segments that were pre-contracted with carbachol, a muscarinic receptor (mAChR) agonist (Appendix 85). The alkaloids did not affect the basal tone of the tracheal segments (data not shown), indicating that they were neither stimulatory nor inhibitory in the absence of carbachol. All tested compounds including atropine (positive control for muscarinic antagonist) produced a maximum relaxation (E_{max}) of 110 – 121%, with a rank order of potency (based on EC_{50} values): **3** > atropine > **2** > **4** (Appendix 86). The E_{max} values of all tested compounds were statistically significant when compared to the vehicle control DMSO, viz., alkaloids **2** – **4** exhibited significant antispasmodic activity (Appendix 86). (–)-Lobeline (**3**) was found to be the most potent tracheal smooth muscle relaxant (EC_{50} 1.2 ± 0.2 nM), approximately 10-fold more potent than atropine (IC_{50} 10.1 ± 2.7 nM). On the other hand, hippofoline B (**2**) was approximately 20-fold less potent compared to **3** (EC_{50} 26.0 ± 5.2 nM), while (–)-*cis*-2′,2′′-diphenyllobelidiol (**4**) was the least potent alkaloid tested. Unfortunately, due to the poor solubility of hippofoline A (**1**) in the organ bath buffer, its effect on the tracheal segments could not be determined.

(–)-Lobeline (**3**) is well-known to possess diverse and complicated neuropharmacology (Section 1.2.3). In fact, **3** was previously reported to exhibit an atropine-like (mAChR antagonist) effect on guinea pig ileum and rodent brain.[122,123] It is proposed that the lobeline-type alkaloids (**2** – **4**) antagonised the muscarinic effect of carbachol at tracheal smooth muscles, leading to a loss of contraction. The putative antimuscarinic action of **3** represents a least understood aspect of its cholinergic pharmacology. While the potent antimuscarinic activity of **3** may justify and potentiate its use as an anti-asthmatic drug, the antagonism of other mAChR subtypes may confound neuropharmacological experiments or cause undesirable side effects *in vivo*.

5.2 Antispasmodic Activity of Nortropane Alkaloids 6, 9, 11 – 13 on Rat Isolated Trachea

The nortropane alkaloids 3α-cinnamoyloxy-*N*-phloretoylnortropane (**6**), 3α-benzoyloxy-*N*-formyl-nortropane (**9**), 3α-cinnamoyloxynortropane (**11**), 3α-benzoyloxynortropane (**12**) and (±)-bissacardine (**13**) were tested for their relaxation activity on rat isolated tracheal segments that were pre-contracted with carbachol (Appendices 87 and 88). Due to paucity of material, other nortropane alkaloids were not tested. Alkaloids **6**, **9**, **11** – **13** demonstrated weak relaxation effects on rat isolated tracheal segments that were pre-contracted with carbachol, a muscarinic agonist (Appendix 87). Compared to the positive control atropine, alkaloids **6**, **9**, **11** – **13** were estimated to be many orders of magnitude (at least 600-fold) less potent. However, the EC_{50} values could not be determined because the concentration response curves did not plateau at the highest test concentration. On the other hand, the E_{max} values of the tested compounds ranged from 72 – 106 %, and they were statistically significant when compared to the vehicle control

DMSO (Appendix 88). This implied that alkaloids **6**, **9**, **11** – **13** still exhibited significant antispasmodic activity, despite having very low potency.

The structure activity relationship (SAR) of atropine is well-studied.[18,124,125] Being a non-selective competitive antagonist of mAChRs, atropine blocks acetylcholine (ACh) or agonists like carbachol from binding and activating all subtypes of mAChRs. However, atropine will dissociate from the binding site and can be displaced by an agonist in a concentration dependent manner. Hence, atropine shares the common SAR of ACh, but provides extra binding interactions such that mAChRs are not activated. In general, the SAR of atropine is identified as having tertiary amine bridged by three carbons to an ester group with branched substituents (Fig. 5.1; c.f., Fig. 1.9). The tertiary amine of atropine has to be positively charged (protonated at physiological pH) to allow ionic and cation-π interactions with amino acid residues (aspartate-311 and tryptophan-307) on the ACh *N*-Me+ binding pocket. Quaternised atropine derivatives were shown to exhibit the most potent anti-muscarinic activity.[125] Besides, there needs to be a minimum of two-carbon distance between the amine and ester group to facilitate hydrogen-bonding between the ester carbonyl (H-bond acceptor) and the asparagine-617 residue (H-bond donor) that is crucial in mAChR recognition.[18] The branched component of the ester group is particularly important. It enables extra hydrophobic interactions outside of the ACh binding site, causing a different conformational change such that mAChR is not activated. The lack of branching results in a great reduction of anti-muscarinic activity, indicating that the antagonist binding site is either T-shaped or Y-shaped.[18]

Comparison of the structures of nortropane alkaloids **6**, **9**, **11** – **13** with atropine revealed some shortcomings that may explain their weak anti-muscarinic

activity, including **6** and **9** have amide nitrogens that cannot be protonated. Their interactions with the ACh N^+-Me binding pocket are expected to be very weak if not completely absent. Alkaloids **6**, **9**, **11** – **13** lack branching in their ester component. As a result, hydrophobic interactions with the antagonist binding site of mAChR are expected to be hugely compromised. This is particularly prominent for alkaloids **9** and **12,** which bear a plain benzoate ester group. Alkaloids **6** and **13** have very bulky *N*-substituents, which may lead to weak binding interactions due to steric hindrance. The binding pocket of ACh is often described as a 'tight-fit' because ACh itself is a relatively small molecule.[18] In contrast, alkaloid **11** that contains a tertiary amine and a cinnamate ester group (comparable size to atropine) appeared to be more potent among the tested compounds (Appendix 87). Nonetheless, the weak trachea relaxing activities (presumably anti-muscarinic) of nortropane alkaloids **6**, **9**, **11** – **13** are not expected to be therapeutically useful in the treatment of asthma and COPD.

Interestingly, comparison of the SAR of atropine with the structure of (–)-lobeline (**3**) suggested some similarities that may explain its unexpectedly potent anti-muscarinic activity. In particular, **3** contains a tertiary amine that can be protonated, a three-carbon bridge, a carbonyl group (hydrogen bond acceptor) and two phenyl rings that can be considered as branched due to the 2,6-*syn* configuration of its diphenethyl substituents (Fig. 5.1).

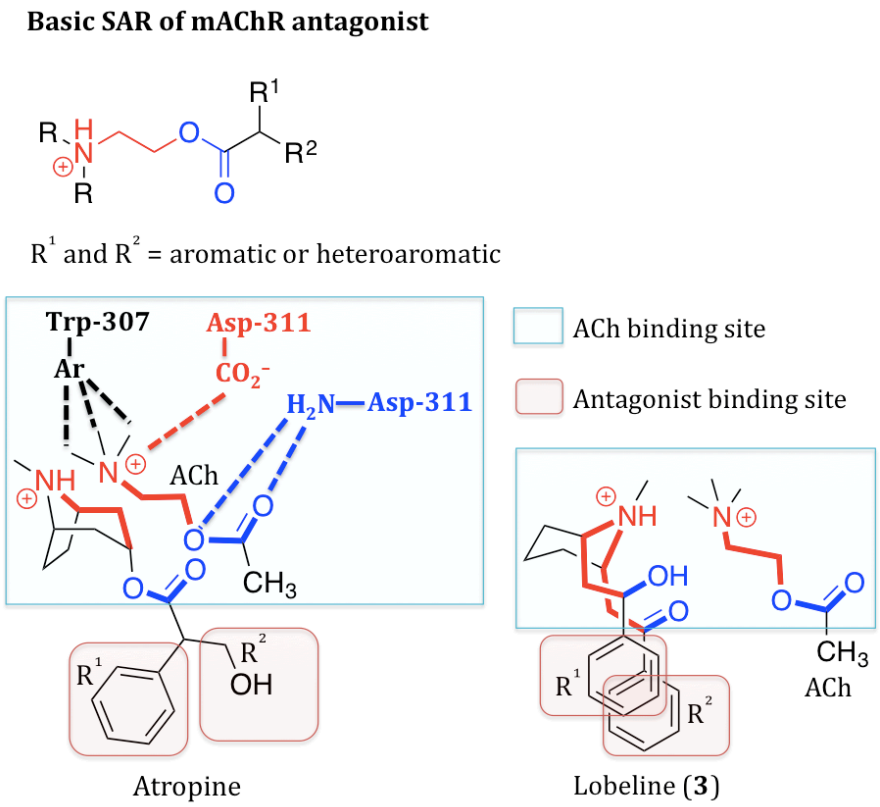

Figure 5.1: SAR comparision between acetylcholine, atropine and (–)-lobeline.

5.3 *In vitro* Cytotoxic Activity of 3α-Cinnamoyloxynortropane (11), Bissaccardine (13) and Trissaccardine (14)

The monomeric, dimeric and trimeric nortropane alkaloids (**11**, **13** and **14**) were evaluated for their cytotoxic effect against a panel of human pancreatic cancer cell lines (Table 5.3). Due to paucity of material, other tropane alkaloids isolated in the present study were not evaluated. (±)-Bissaccardine (**13**) and (±)-trissaccardine (**14**) exhibited pronounced cytotoxicity towards all the four human pancreatic cancer cell lines tested (AsPC-1, BxPC-3, PANC-1 and SW1990), with IC_{50} values ranging from 1.13 – 10.85 μM (Appendix 89). Additionally, **13** was relatively less toxic towards the non-tumorigenic MRC-5 cell line (IC_{50} 11.12 μM). In contrast, **14** did not exhibit selective cytotoxicity despite being the most potent compound,

while 3α-cinnamoyloxynortropane (**11**) was essentially non-cytotoxic (Appendix 89).

At the time of writing, the mechanisms underlying the unprecedented cytotoxic effect of **13** and **14** remain unknown. Given that the monomer **11** was non-cytotoxic**,** it can be inferred that the larger molecules of **13** and **14** would allow extra intermolecular interactions with the relevant biological targets, which were otherwise unattainable by **11**. While the cytotoxic activity of most tropane alkaloids are under-studied, a few C-3, C-6 and/or C-7 di/trisubstituted tropane alkaloids (isolated from *Erythroxylum pervillei* and *Erythroxylum rotundiflorum*) were shown to reverse multi-drug resistance of cancer cells towards vincristine.[126,127] In particular, pervilleine A competitively inhibited ATP-dependent binding of [^{3}H]-vincristine onto p-glycoprotein efflux pumps of multi-drug resistant KB-V1 cell (cervical carcinoma), restoring its sensitivity towards vincristine with IC_{50} values of 0.02 – 0.36 μM.[126] It should be noted that pervilleine A does not have intrinsic cytotoxic activity.[126] Nevertheless, gross comparison of the chemical structures of pervilleine A with **13** and **14** suggested some similarities, i.e., the presence of *trans*-cinnamate moiety and aryl ester substituent in the tropane ring (Fig. 5.2). By inferring that these structures could potentially interact with proteins on cancer cell membrane, the potent cytotoxic mechanism of **13** and **14** demands further biochemical investigations. The cytotoxic selectivity of **13** towards pancreatic cancer cells is particularly favorable, whereas the large molecular size of **14** (MW >500) and its lack of selectivity render it less desirable as an anticancer lead compound.

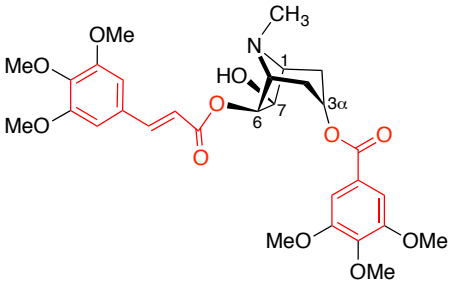

Pervilleine A

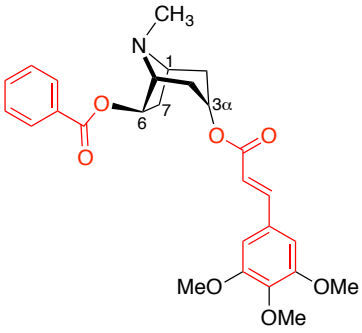

6β-Benzoyloxy-3α-(*E*)-(3,4,5-trimethoxycinnamoyloxy)-tropane

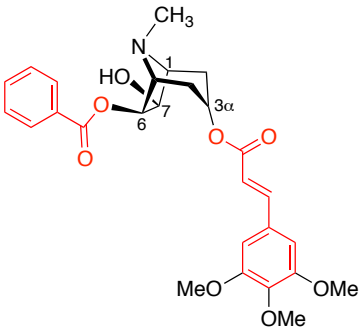

6β-Benzoyloxy-3α-(*E*)-(3,4,5-trimethoxycinnamoyloxy)-tropane-7β–ol

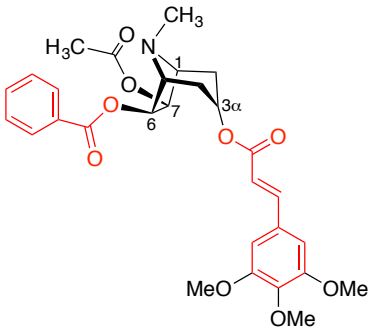

7β-Acetoxy-6β-benzoyloxy-3α-(*E*)-(3,4,5-trimethoxycinnamoyloxy)tropane

Tropane alkaloids that can reverse multidrug resistance of cancer cells towards vincristine.

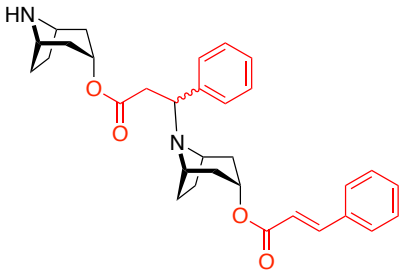

(±)-**13**

Comparison of the chemical structure of **13** with pervilleine A and its derivatives. Similarities are highlighted in red.

Figure 5.2: Comparison of the structure of **13** with those of pervilleine A and its derivatives.[126,127]

5.4 *In vitro* Cytotoxic Activity of Diarylheptanoids 15, 16, 20 and 22

The diarylheptanoids (±)-saccardianone A (**15**), (±)-saccardianone B (**16**), pellaspirone (**20**) and platyphyllenone (**22**) were evaluated for their cytotoxic effect against a panel of human pancreatic and breast cancer cell lines (Appendix 89). Due to paucity of material, compounds **17**, **18** and **19** were not evaluated. (±)-Saccardianone B (**16**) and platyphyllenone (**22**) exhibited moderately potent cytotoxicity towards pancreatic AsPC-1 (IC_{50} 15.47 μM) and PANC-1 (IC_{50} 14.9 μM) cancer cell lines, respectively (Appendix 89). On the other hand, pellaspirone (**20**) was moderately potent towards breast MDA-MB-468 (IC_{50} 16.62 μM) and MDA-MB-231 (IC_{50} 13.32 μM) cancer cell lines (Appendix 89). (±)-Saccardianone A (**15**) was regarded as non-cytotoxic since its IC_{50} values were generally > 20 μM.

Notably, compounds **16** and **22** appeared to show selective cytotoxicity depending on the molecular subtypes of the pancreatic cancer cell lines tested. Compound **16** was most active against the AsPC-1 cell line, which is classified as progenitor pancreatic cancer cells, while platyphyllenone (**22**) was most active against the PANC-1 cell line (IC_{50} 14.9 μM),[128] which along with BxPC-3 and SW1990, were classified as squamous pancreatic cancer cells.[129] The squamous subtype of pancreatic cancer is associated with the poorest prognosis.[130] Additionally, the cytotoxic effects of **16** and **22** were also more pronounced compared to curcumin and gemcitabine (positive controls) for the respective pancreatic cancer cell lines. Although gemcitabine is often used as a first-line chemotherapeutic drug in pancreatic cancer treatment, the development of resistance towards it in pancreatic cancer cells has limited its therapeutic effectiveness.[131,132] Furthermore, unlike gemcitabine, both **16** and **22** did not show significant toxicity towards the non-tumorigenic breast epithelial cell line (MCF-

10A), suggesting their potential to induce tumor-specific cell death in pancreatic cancer cells without harming the normal cells. While the precise mechanisms of the compounds are yet to be elucidated, their selective cytotoxicity makes them attractive therapeutic candidates for pancreatic cancer treatment, which warrant further development. On the other hand, pellaspirone (**20**) appeared to exhibit selective cytotoxicity towards the MDA-MB-468 and MDA-MB-231 breast cancer cell lines, which are classified as triple-negative breast cancer (TNBC).[133] TNBC accounts for approximately 10 – 15% of all breast cancers and it is usually associated with a poor prognosis.[134,135] TNBC does not express hormonal receptors like estrogen receptor (ER), progesterone receptor (PR) and/or human epidermal growth factor receptor 2 (HER-2). There is currently a lack of drug targets available for TNBC, which does not respond to the standard hormonal or herceptin-based approach of breast cancer chemotherapy.[134,135] Hence, the selective cytotoxicity of **20** towards TNBC cell lines is valuable and it demands further biochemical investigation.

Interestingly, diarylheptanoids containing one or more α,β-unsaturated ketone group (**15**, **16**, **20, 22** and curcumin) demonstrated significantly higher cytotoxicity compared to those without this functionality, i.e., saccardianoside (**21**) and (±)-5-hydroxy-1,7-bis-(4-hydroxyphenyl)-3-heptanone (**23**) (IC_{50} > 100 μM, data not shown). The present results conformed to the general observations that electrophilic Michael acceptor groups such as α,β-unsaturated ketone improve cytotoxic activity of natural products.[136,137] This is likely due to interactions of the electrophilic α,β-unsaturated ketone with nucleophilic centers present in proteins or DNA bases. Indeed, synthetic diarylheptanoids containing α,β-unsaturated ketone group also demonstrated potent *in vitro* cytotoxicity towards cancer cells.[138]

The mechanism of cytotoxicity was proposed to involve the inhibition of thioredoxin reductase (TrxR), which is an enzyme crucial to carcinogenesis.[138] The presence of a nucleophilic selenolate residue on TrxR makes it vulnerable to electrophilic addition by Michael acceptors such as α,β-unsaturated ketone. The presence of chalcone and/or diarylheptanoid backbone further enhances TrxR inhibition, and the resulting cytotoxic activity.[138]

Chapter 6: Experimental

Note: All chemical solvents and reagents were purchased from Acros Organics, Merck (Sigma-Aldrich), Nacalai Tesque or Tokyo Chemical Industry (TCI), and were used as received from the commercial supplier, unless stated otherwise.

6.1 Processing of Plant Materials

Approximately 10 kg of fresh *Hippobroma longiflora*, including aerial parts and roots were collected in Penang (GPS coordinate: 5°25′28.50″N 100°16′8.08″E). A voucher specimen (KLU49660) was deposited at the Herbarium, University of Malaya (UM). The specimen was identified as *H. longiflora* by Dr. Yong Kien Thai from Institute of Biological Sciences, UM. The whole plant materials inclusive of the aerial parts (leaves, stems, flowers) and roots were promptly sun-dried and grounded with a Waring blender, yielding approximately 1.25 kg of powder.

Fresh leaves and bark of *Pellacalyx saccardianus* were collected from healthy adult specimens located in Jelebu, Negeri Sembilan (GPS coordinate: 5°25′28.50″N 100°16′8.08″E). A voucher specimen (KLU49678) was deposited at the Herbarium, UM. The specimen was identified as *P. saccardianus* by Dr. Yong Kien Thai. The leaves were dried in a Memert™ oven at 45 °C with ventilation for 48 h, whereas the bark was dried for 72 h. The fully dried leaves and bark were grounded separately with a Retsch™ SM100 rotor beater mill, yielding 2.2 kg and 3.8 kg of leaf and bark powders, respectively. Based on TLC profiling, it was decided that the leaf and bark material should be investigated individually.

6.2 Large-scale Solvent Extraction

The dried powder of *H. longiflora* was transferred into two 15 L extraction flasks in roughly equal portions (ca. 600 g per flask). 2 L of 95% ethanol was added into each flask. The grounded plant powder was allowed to percolate in 95% ethanol at 45 °C overnight. Subsequently, the ethanol extract was vacuum filtered and concentrated via rotary-evaporation, while the solvent was recycled for re-extractions. In total, the above procedure was repeated four times to yield a combined crude extract weighing 177.6 g. The grounded leaves and bark powders of *P. saccardianus* were also extracted with similar procedure, yielding a crude ethanol leaf and bark extracts of 200.2 g and 250.8 g, respectively.

6.3 General Experimental Procedures

6.3.1 Acid-base Chemical Separation

The crude ethanol plant extract was heated gently under a water bath until a free-flowing consistency was obtained. It was added drop-wise into a 2 L conical flask containing 3% w/v tartaric acid, at a mass to volume ratio of ca. 1.5 g : 10 mL. The conical flask was equipped with strong magnetic stirring to ensure thorough dispersion of the plant extract in the acidic solution. The mixture was allowed to stir for approximately 10 min and subsequently vacuum filtered through 60 g of Keisulghur in a Buchner funnel, to remove insoluble particulates. The acidic filtrate was promptly cooled under an ice bath, while slowly basified with addition of 28% w/v ammonia until pH 10 (spot-tested with MERCK pH test-strips). The basified mixture was exhaustively extracted with 5 X 500 mL of chloroform using a 2 L separatory funnel. The chloroform layers were combined

and dried over anhydrous sodium sulfate prior to rotary-evaporation. As a result, a crude alkaloid mixture was obtained, which was kept in a –20°C freezer to prevent chemical degradation. The mass and percentage yield (based on dried plant material) of the crude alkaloid extracts obtained for *H. longiflora* and *P. saccardianus* are shown in Table 6.1.

Table 6.1: Yields of crude alkaloid extracts obtained from acid-base separation.

Plant material	Mass of crude alkaloid extract (g)	Percentage yield (%)
Whole plant of *H. longiflora*	5.59	0.45
Leaves of *P. saccardianus*	20.1	0.91
Bark of *P. saccardianus*	10.0	0.26

6.3.2 Thin Layer Chromatography (TLC)

Thin layer chromatography (TLC) was performed to assess the degree of separation after preparative chromatography work. MERCK TLC Silica gel GF-254 was adopted because it contains a fluorescent dye that facilitates the visualisation of separated compounds under short-wave (254 nm) and long-wave (365 nm) UV light. Briefly, TLC plates were cut into appropriate sizes, usually 2 x 10 cm or 5 x 10 cm. A baseline of 1 cm was drawn, to which samples were spotted by using a finely pulled glass capillary tube. The spotted TLC plate was then placed in a sealed glass jar containing 10 mL of freshly prepared eluent. It was left to develop until the solvent front reached 90% of its height. Subsequently, the TLC plate was removed and air-dried before visualisation under UV light. Separated compounds would normally appear as spots that were marked accordingly using a blunt pencil. The retention factor (R_f) value could be calculated by dividing the distance traveled by a spot with the distance of solvent

front. For general screening purposes, an R_f of 0.5 would suffice whereas for choosing solvent systems for preparative chromatography, an R_f of 0.2 – 0.3 was desired. The adjustments could be achieved by changing the polarity or selectivity of the solvent system.

A systematic approach for developing normal phase TLC solvent systems was adopted according to the methods described by Synder.[139] A binary mixture of three solvents comprising of three different selectivity groups were utilised, i.e., chloroform ($CHCl_3$, acidic group), dichloromethane (DCM, dipole group) and diethyl ether (Et_2O, basic group). Concomitantly, the overall polarity could be increased by adding methanol, or decreased by adding hexane until a desirable R_f value was obtained. To reduce tailing of alkaloid spots, a few drops of ammonia solution (NH_3) or diethylamine (DEA) could be added. To improve the resolution of diarylheptanoids containing polyphenolic group, a few drops of formic acid could be incorporated. Alternatively, solvents with different selectivity such as tetrahydrofuran (THF) or ethyl acetate (EA) were employed to improve the separation of compounds, otherwise unresolved via the above three solvents.

2D TLC was occasionally performed to assess the degradation and/or co-elution of separated compounds. The procedures were similar to the above, except that the sample was spotted on a square TLC plate (usually 12 X 12 cm), with two perpendicular baselines. The TLC plate was sequentially developed twice, in directions that were right angle to each other. The developed spots were pencil-marked and a diagonal line was drawn from the corner of the original spot, through the separated spots to the opposite corner of the TLC

plate. Spots observed on the diagonal line were stable (similar R_f), whereas spots that were not had degraded or were unstable on silica.

6.3.3 TLC Staining Reagents

The Dragendorff's reagent (Section 1.1.3) was used in the form of a spray to detect the presence of alkaloids on developed TLC plates. Generally, alkaloid spots were stained dark orange or red in colour. The Dragendorff's reagent was prepared according to the following recipe. A stock solution was constituted by mixing solution A and solution B together. Solution A was made up of 1.7 g bismuth oxynitrate dissolved in 20 mL glacial acetic acid and 80 mL distilled water. Solution B comprised 36 g potassium iodide dissolved in 90 mL distilled water. The stock solution could be stored in an amber glass bottle for a few months. A working reagent was prepared by diluting 10 mL stock solution with 20 mL glacial acetic acid and 70 mL distilled water.

Iodine vapour was utilised as a general purpose stain to detect the presence of diarylheptanoids or non-alkaloidal compounds on TLC. In a typical procedure, 5 – 6 pieces of re-crystallised iodine chips were placed into a glass jar, which was left for a few min to saturate with iodine vapour. A developed TLC plate was placed directly into the jar and monitored continuously for the staining of dark brown or yellowish spots. The TLC plate was removed promptly after adequate staining to prevent corrosion of the aluminium sheet. It should be noted that iodine stained spots were non-recoverable and could fade over time. The iodine charged jar could be reused for multiple occasions.

6.3.4 Column Chromatography

Column chromatography was performed to fractionate crude alkaloid and/or diarylheptanoid extracts obtained from acid-base separation. Prior to column chromatography, a starting solvent system (usually chloroform–hexane mixtures) was chosen based on TLC, which gave an R_f value of approximately 0.2. The loading capacity for normal phase column chromatography was calculated at a mass to mass ratio of 30 – 50 g of silica gel 60 (Merck 9385, 230-400 mesh): 1.0 g of crude sample.

Firstly, a glass column was mounted in a fume hood. A slurry of silica gel constituted in ample quantity of the starting solvent system was vigorously swirled and poured into the glass column. The column was gently tapped at its sides to remove air bubbles and improve packing. Once the silica gel has packed, elution of blank solvent was assisted by a vacuum pump. A layer of anhydrous sodium sulfate of ca. 2 cm thick was added evenly on top of the silica-gel bed. The anhydrous salt would function to dry the eluent as well as ensuring even loading of sample. The sample to be loaded was dissolved in sufficient quantity of starting solvent system and carefully added onto the column via a jumbo pipette. Vacuum-assisted gradient elution was carried out by increasing the concentration of methanol (from 1% to 20% v/v) in the solvent system. Eluted fractions were concentrated via rotary-evaporation and collected into glass specimen tubes. TLC was performed on every fraction to monitor the gradient elution and to combine fractions with similar separation profiles. Finally, the column was flushed with ethanol prior to disassembly.

6.3.5 Centrifugal Thin Layer Chromatography (CTLC)

Centrifugal Thin Layer Chromatography (CTLC) was employed to further fractionate and isolate individual alkaloids and/or diarylheptanoids from major column fractions. The general procedures for CTLC were outlined as below. Firstly, Silica Gel (Merck 7759) was measured according to the plate thickness of 1 mm (40 g), 2 mm (60 g) or 4 mm (80 g). The silica was thoroughly suspended in cold water and poured onto a CTLC glass plate, which was taped around its edges. It was allowed to bake in an oven for 55 ^{o}C overnight and activated at 120 ^{o}C for 1 h before use. The activated CTLC plate was then shaved with steel blades according to the desired thickness and secured onto the Chromatotron™ (Harrison Research), with a sample loaded through a glass Pasteur pipette after the rotor was switched on. The appropriate solvent system was prepared and added into the Teflon holder, which delivered the solvent into the center of the glass plate. The solvent flow rate could be adjusted accordingly. Separation of UV-active compounds was mainly guided under visualisation from short-wave UV light (254 nm). Individual fractions were collected into 100 mL round bottom flasks and concentrated via rotary-evaporation. TLC was conducted for each fraction to assess their purity. Fractions with similar TLC profiles were combined for re-CTLC, while pure samples were subjected to spectroscopic analyses. All CTLC fractions including pure samples were promptly desiccated in glass vials and stored in a -20 ^{o}C freezer to prevent chemical degradation.

6.3.6 High Pressure Liquid Chromatography (HPLC)

High Pressure Liquid Chromatography (HPLC) was employed to achieve three aims, i.e., purification of complex mixtures otherwise unresolved by CTLC, separation of enantiomers on a chiral-phase column and identification of chemically derivatised sugar enantiomers. All HPLC work in the current study were conducted on a Waters ACQUITY®ARC UHPLC instrument, with maximal operating pressure of 9500 psi and equipped with Waters Quaternary Solvent Manager-R, Sample Manager FTN-R, 2998 PDA Detector and WFCIII Fraction Collector. All four units were connected online and controlled by Water's Empower 3 Software. The standard operating procedure for UHPLC was stated as follows. HPLC grade solvents were used for all HPLC experiments.

In a general procedure, samples were dissolved in suitable mobile phase and filtered through a submicron membrane (0.2 μm) prior to injection. All units of the Water's Acquity Arc system including WFCIII Fraction Collector were switched on and connected online via the Empower 3 Software. The 2998 PDA Detector was allowed to warm up and equilibrate for 5 min with blank MeCN at a flow rate of 0.5 mL/min. This was followed by equilibration of the HPLC column for 10 column volumes at an appropriate flow rate. Subsequent injection sequence, mobile phase gradient and flow rate, column temperature as well as fraction collection were manually controlled by Empower 3 Software. A column cleaning sequence of [MeCN–H_2O, 95:5] at appropriate flow rate was initiated at the end of each HPLC experiment. All columns were stored in suitable mobile phases as specified by manufacturer after use. HPLC separated fractions were

promptly concentrated by rotary-evaporation, desiccated in vials and stored in a -20 ^{o}C freezer to prevent chemical degradation.

6.3.7 Melting Point Determination

Melting points of crystals were recorded on a Stuart SMP10 digital melting point apparatus. The melting point apparatus was calibrated with pure vanillin crystals (mp 81 – 83 °C) before use.

6.3.8 Polarimetry

Optical rotation values for pure compounds with chiral centers were measured on a JASCO P-1020 automatic digital polarimeter (Chemistry Department, University of Malaya). Five observed optical rotation values were recorded, from which a mean value was calculated. The specific rotation [α], was calculated for each optically active compound based on the following formula:

$$[\alpha]_{\lambda}^{T} = \frac{100\ a}{l\ c}$$

where **[α]** is the calculated specific rotation in degrees, at wavelength **λ** (589 nm Sodium D-line) under temperature, $\boldsymbol{T}$ of 25 ^{o}C, $\boldsymbol{a}$ represents the mean of measured optical rotation values, $\boldsymbol{l}$ is the path-length in decimeter (standardised at 1 dm) and $\boldsymbol{c}$ is the concentration of sample in g/100 mL.

6.3.9 Ultraviolet (UV) Spectroscopy

The UV spectra of pure compounds containing chromophores were recorded on a PerkinElmer Lamda 35 UV/Vis spectrophotometer. The scanning wavelengths were specified to start from the solvent cut-off limit (MeOH, 210 nm or MeCN, 190 nm) until 400 nm, at a scanning interval of 10 nm/min. Three accumulations were obtained for each UV spectroscopy experiments. The molar absorptivity (ε) values, reported as log ε for each absorption maxima in the UV spectrum were calculated based on the Beer-Lambert Law:

$$A = \varepsilon\, c\, l$$

where A is the UV absorbance (AU), ε is the molar absorptivity, c is the concentration of sample in mol/dm^{-3} and l is the path length in decimeter (standardised at 1 dm).

6.3.10 Electronic Circular Dichroism (ECD) Spectroscopy

ECD spectra were obtained on a Jasco J-815 Circular Dichroism Spectrometer (Malaysia Genome Institute). ECD scanning parameters, spectra processing and smoothening were controlled via the built in *Spectra Manager* interface. The scanning wavelengths were specified to start from the solvent cut-off limit (MeOH, 210 nm or MeCN, 190 nm) until 400 nm, at a scanning interval of 10 nm/min. Three accumulations were obtained for each ECD experiment.

6.3.11 Infrared (IR) Spectroscopy

IR spectra of pure compounds were recorded on a Perkin Elmer ATR-IR spectrometer. 36 scan accumulations were obtained for each experiment, including the background scan. IR spectra were processed using the built-in

Spectrum interface by Perkin Elmer.

6.3.12 Nuclear Magnetic Resonance (NMR) Spectroscopy

1D NMR (^{1}H and ^{13}C) and 2D NMR (COSY, HSQC, HMBC, NOESY) spectra of all pure compounds were obtained in $CDCl_3$, CD_3OD or $(CD_3)_2CO$ (depending on solubility) with tetramethylsilane (TMS) added as an internal standard on a Bruker 600 MHz NMR spectrometer (Chemistry Department, University of Malaya). All NMR samples were promptly recovered after NMR experiments. 1D and 2D NMR spectra were analysed using MestReNova (MNova) Software (Version 11.01-17801). The chemical shift values were stated in δ (ppm) relative to TMS. Solvent residual signals and/or impurity signals (e.g. silicone grease) were marked based on comparison with literature values where applicable.[140, 141]

6.3.13 High-resolution Direct Analysis in Real Time Mass Spectrometry (HRDARTMS)

HRDARTMS measurements were carried out using a JEOL Accu ToF-DART mass spectrometer (Chemistry Department, University of Malaya). Possible molecular formulas were generated from the *m/z* peaks with the highest relative intensities.

6.3.14 High-resolution Electrospray Ionisation Mass Spectrometry (HRESIMS)

Liquid chromatography separation was performed using Thermo Scientific C18 column (Acclaim™ Polar Advantage II, 3 x 150mm, 3um particle size) on an UltiMate 3000 UHPLC system (Chemistry Department, Universiti

Kebangsaan Malaysia). Gradient elution was performed at a flow rate of 0.2 ml/min at 40°C column temperature using H_2O + 0.1% formic acid (A) and 100% MeCN (B) with 22 minutes total run time. The injection volume of sample was 5ul. The gradient started at 5% B (0 – 3 min); 80% B (3 – 10 min); 80% B (10 – 15 min) and 5% B (15 – 22min). HRESIMS was carried out using a MicroTOF QIII Bruker Daltonic mass spectrometer (Chemistry Department, Universiti Kebangsaan Malaysia) using either ESI positive or negative ionisation modes with the following settings, capillary voltage: 3500 V, nebuliser pressure: 3.5 bar, drying gas: 10 L/min at 250°C. The mass range was at 50 – 1000 *m/z*. The accurate mass data of the molecular ions, provided by the TOF analyser, were processed by Compass Data Analysis software (Bruker Daltonik GmbH).

6.4 Isolation of Compounds 1 – 5 from the Whole Plant of *H. longiflora*

5.59 g of the whole plant crude alkaloid extract of *H. longiflora* was initially fractionated by column chromatography (silica gel 60 Merck 9385, gradient elution, DCM–MeOH, 1:0 → 6:4) to give a total of five major fractions, i.e., HLF1 (1.48 g), HLF2 (1.34 g), HLF3 (1.35 g), HLF4 (0.38 g) and HLF5 (1.69 g). Subsequent re-chromatography of these partially separated fractions was carried out by CTLC. Alkaloid **1** (65 mg) was isolated from HLF1 (DCM-MeOH, 9:1), **2** (15 mg) from HLF2 (Et_2O-hexane-MeOH, 1:1:0.2; followed by THF–hexane, 2:3), **3** (70 mg) from HLF3 (DCM-MeOH, 9:1), **4** (20 mg) from HLF4 (DCM- MeOH, 9:1), and **5** (5 mg) from HLF5 (DCM-MeOH, 4:1).

6.5 Isolation of Compounds 6, 7, 13 – 19 from the Leaves of *P. saccardianus*

20.1 g of the leaf crude alkaloid extract of *P. saccardianus* was initially fractionated by vacuum column chromatography under gradient elution ($CHCl_3$–

MeOH, 1:0 → 7:3) to afford five major fractions, i.e., PSF1 – PSF5. The first major fraction PSF1 (570 mg) was subjected to CTLC with $CHCl_3$–MeOH–NH_3 (9.5:0.5:0.1), yielding seven subfractions (PSF1/1 – PSF1/7). Compound **6** (12.0 mg) was isolated by re-CTLC of PSF1/7 (50 mg) under isocratic elution (Et_2O–MeOH, 10:0.4). The second major fraction PSF2 (2.98 g) was re-chromatographed with vacuum column chromatography (similar conditions as the above), yielding six subfractions (PSF2/1 – PSF2/6). CTLC of PSF2/1 (145 mg) under isocratic elution (Et_2O–MeOH, 10:0.4) afforded **7** (8.0 mg). CTLC of PSF2/3 (39.1 mg) under gradient elution (Et_2O–*n*-hexane–MeOH, 6:3:0.2 → 9:1:0.2) yielded **19** (4.5 mg) and **17** (3.0 mg), while the more polar **18** (4.0 mg) was obtained under isocratic elution by DCM–MeOH–NH_3 (9:1:0.05). CTLC of PSF2/6 (185.5 mg) with EtOAc–*n*-hexane (6:4) afforded a partially separated fraction PSF2/6/1 (9.8 mg), which was subjected to semi-preparative reverse phase HPLC (Waters Xbridge®BEH C18 Prep Column, 5 μm, 10 X 100 mm) under isocratic elution [MeCN–MeOH–H_2O (0.1% TFA), 25:25:50, 2.5 mL/min for 15 min, 30°C] to yield **15** (5.0 mg) and **16** (2.4 mg). The fourth major fraction PSF4 (1.45 g) was also re-chromatographed with column chromatography, affording four subfractions (PSF4/1 – PSF4/4). CTLC of PSF4/1 (47 mg) under isocratic elution (DCM–MeOH–NH_3, 9:1:0.1) gave a partially separated subfraction, PSF4/1/2 (16.8 mg), which was purified by semi-preparative reverse phase HPLC (Waters Xbridge®BEH C18 Prep Column, 5 μm, 10 X 100 mm) under gradient elution [MeCN–H_2O (0.1% TFA), 10:90 → 30:70, 2.5 mL/min for 15 min, 27°C] to give **13** (12.0 mg). Last but not least, fraction PSF5 (2.58 g) was re-chromatographed with vacuum column chromatography to give five subfractions (PSF5/1 – PSF5/5). CTLC of PSF5/4 (1.1 g) under isocratic elution (DCM–MeOH–

NH_3, 9:1:0.1) afforded a partially separated subfraction PSF5/4/3 (800 mg), which contained a mixture of **11**, **13** and **14**. Re-CTLC of PSF5/4/3 under isocratic elution by DCM–MeOH–HCO_2H (8.5:1.5:0.1) resolved compounds **11** (221.2 mg), **13** (181.8 mg) and **14** (57.9 mg).

Chiral-phase HPLC analyses of compound **13** – **18** were performed on a DAICEL CHIRALPAK® IA Column (5 μm, 15 X 46 mm) under gradient elution [*n*-hexane (0.1% DEA)–EtOH 95:5 → 60:40, 1.0 mL/min for 30 min, 27°C]. All analytes were dissolved in EtOH prior to injection. The analyte loading volume and concentration per injection were 10.0 μm and 1.5 mg/mL, respectively.

6.6 Isolation of Compounds 8 – 10 from the Bark of *P. saccardianus*

10.0 g of the bark crude alkaloid extract of *P. saccardianus* was initially fractionated by vacuum column chromatography under gradient elution ($CHCl_3$–MeOH, 1:0 → 7:3) to afford five major fractions, i.e., PSBF1 – PSBF5. Fraction PSBF2 (728 mg) was subjected to CTLC under isocratic elution (Et_2O–cyclohexane–MeOH, 5:5:0.02), giving three subfractions (PSBF2/1 – PSBF2/3). Compounds **8** (8.8 mg) and **9** (12.1 mg) were isolated by CTLC of PSBF2/1 (134 mg) under isocratic elution (Et_2O–MeOH, 10:0.02). The third major fraction PSBF3 (187.4 mg) was subjected to re-CTLC under gradient elution (DCM–MeOH–*n*-hexane, 5:0:5 → 8:1:1), giving three subfractions (PSBF3/1 – PSBF3/3). Compound **10** (4.6 mg) was isolated from PSBF3/1 (15 mg) via CTLC under isocratic elution (DCM–MeOH–*n*-hexane, 5:0.2:5).

6.7 Extraction and Isolation of Saccardianoside (21) from the Leaves of *P. saccardianus*

10.0 g of the dried grounded leaves of *P. saccardianus* were percolated for 2 h with 95% EtOH at 60°C. The ethanolic extract was concentrated via rotary-evaporation to yield 850 mg of crude EtOH extract, which was partitioned with $CHCl_3$ and a mixture of MeOH–H_2O (4:1) in a separatory funnel. The MeOH–H_2O layer was concentrated *in vacuo* to afford a highly polar fraction, PSLT1 (401.9 mg). CTLC of PSLT1 under isocratic elution ($CHCl_3$–MeOH, 8:2) yielded compound **21** (14.1 mg).

6.8 Determination of Absolute Configuration of Sugar Moieties in Saccardianoside (21)

2.5 mg of compound **21** was dissolved in MeOH (20 μL) and hydrolised with 1M HCl solution (5.0 mL) at 70°C for two h. The hydrolysate was partitioned with EtOAc (2 X 5 mL) to remove the aglycone, while the aqueous fraction was concentrated *in vacuo* to obtain the liberated sugars (0.8 mg). The absolute configurations of the sugars were determined by reverse phase HPLC analysis following arylthiocarbomyl-thiazolidine derivatisation.[103] Briefly, the hydrolysate was dissolved in pyridine (1.0 mL) and heated with L-cysteine methyl ester hydrochloride (0.5 mg) at 60°C for 1 h before addition of *o*-tolylisothiocyanate (0.5 mL) and continued heating for another hour. The reaction mixture was analysed directly with reverse phase HPLC [Waters CORTECS® C18 column, 2.7 μm, 4.6 X 50 mm] under gradient elution [MeCN–H_2O (0.1% TFA), 10:90 → 35:65, 2.5 mL/min for 50 min, 30°C]. Similarly, authentic

D-glucose, L-glucose, and L-rhamnose were also derivatised and analysed. Due to the unavailability of D-rhamnose, a standard of L-rhamnose and D-cysteine methyl ester hydrochloride was prepared for HPLC analysis instead. The retention times of the hydrolysates and sugar derivatives were as follows: D-glucose derivative (R_t 6.4 min), L-glucose derivative (R_t 5.9 min), L-rhamnose L-cysteine methyl ester hydrochloride derivative (R_t 10.2 min), L-rhamnose D-cysteine methyl ester hydrochloride derivative (R_t 8.4 min) (Appendix 82).

6.9 Extraction and Isolation of Compounds 12, 20, 22 and 23 from the Leaves of *P. saccardianus*

200 g of the dried grounded leaves of *P. saccardianus* were extracted with 95% EtOH for three times at 60°C. The ethanolic extract was concentrated via rotary-evaporation to yield ca. 2 g of crude EtOH extract, which was basified with NaOH (1%, m/v) in saturated NaCl solution. The basified mixture was extracted with $CHCl_3$ to remove non-acidic components, while the aqueous layer was acidified to pH 1.0 with addition of HCl (5%, v/v) in saturated NaCl solution. The acidified mixture was extracted with $CHCl_3$–MeOH (9:1), which was concentrated *in vacuo* to afford a crude extract, PSLT2 (965 mg). PSLT2 was subjected to CTLC, yielding 10 subfractions (PSLT2/1 – PSLT2/10). Re-CTLC of PSLT2/3 (33 mg) under isocratic elution (DCM–MeOH, 9.5:0.5) yielded **20** (18.4 mg). Re-CTLC of PSLT2/4 (80 mg) and PSLT2/6 (140.4 mg) under gradient elution (EtOAc–*n*-hexane, 6:2 → 8:2) gave **22** (200 mg) and **23** (18 mg). Lastly, **12** (12.0 mg) was isolated from PSLT2/7 (95 mg) via CTLC under isocratic elution ($CHCl_3$–MeOH, 9:1).

6.10 Semi-synthesis of Pellaspirone (20) from Platyphyllenone (22)

Epoxidation of platyphyllenone (**22**) was achieved by oxidation with H_2O_2 under basic dihydrotalcite catalysis.[98] Briefly, **22** (100 mg) was dissolved in MeOH (0.85 mL) and added to a mixture of dihydrotalcite (25 mg), H_2O_2 (30%, v/v, 0.16 mL), *n*-dodecyltrimethylammonium bromide (5.0 mg) and H_2O (50 μL). The reaction mixture was heated at 40°C and stirred gently for 6 h. Subsequently, MnO_2 (10 mg) was added to quench excess H_2O_2, prior to filtration through celite to remove the dihydrotalcite/MnO_2 particulates. CTLC of the concentrated reaction mixture with isocratic elution (Et_2O–MeOH, 9.5:0.5) afforded the epoxide derivative **J** (95.4 mg). 15.0 mg of **J** was treated with similar extraction and isolation procedure as **20** (*vide supra*), affording **20** (13.5 mg) at 95.5% yield.

6.11 Attempted Semi-synthesis of Bissaccardine (13) and Trissaccardine (14) from 3α-Cinnamoyloxynortropane (11)

In a typical procedure, to a solution of **11** was added an appropriate amount of acid or base catalyst. The reaction mixture was stirred at room temperature under inert (nitrogen) atmosphere for 6 – 24 h. TLC and 2D TLC were conducted to monitor the reaction progress, viz., presence of **13** and **14**, every 1 – 2 h, using DCM–MeOH–HCO_2H (8.5:1.5:0.1). The reaction details of the individual experiments are shown in Table 6.2.

Table 6.2: Reaction conditions for aza-Michael reaction of **11**.

Catalyst (Amount), **type**	Solvent	Total reaction time, condition	Reference
Ammonia 25% v/v (10 mol%, 27.24 uL), **base**	MeOH	Monitored for 8 h, rtp, open-air	
Tartaric acid 3% v/v (10 mL), **acid**	H_2O	Similar to acid base extraction (section 6.3.1)	
CAN[a] (6 mol%, 0.64 mg), **Lewis acid**	MeOH	Monitored for 8 h, rtp, N_2 atmosphere, ultrasonication	[98]
CAN[a] (10 mol%,1.07 mg), **Lewis acid**	THF	24 h, rtp, N_2 atmosphere	[98]
Samarium (III) triflate 10 mol% (1.16 mg), **Lewis acid**	DCM	Monitored for 6 h, ended at 24 h, rtp, N_2 atmosphere	[99]
DBU[b] (0.5 mol%,1.48 mg), **base**	MeCN (dried)	Monitored for 6 h, ended at 24 h, rtp, N_2 atmosphere	[97]

[a]Ammonium Cerium (IV) Nitrate, $(NH_4)_2Ce(NO_3)_6$
[b]1,8-Diazabicyclo[5.4.0]undec-7-ene

6.12 Compound Data

*Hippofoline A (**1**)*: light yellowish oil; $[\alpha]^{25}_D$ −41 (*c* 0.18, $CHCl_3$); ECD (MeCN), λ_{max} ($\Delta\varepsilon$): 210 (−5.92), 229 (0.15), 263 (0.12) nm; IR ν_{max} 1733cm^{-1}; ^{1}H NMR ($CDCl_3$, 600 MHz) and ^{13}C NMR data ($CDCl_3$, 150 MHz), see Table 2.1; HRDARTMS *m/z* 424.2468 $[M+H]^+$ (calcd for $C_{26}H_{33}NO_4$ + H, 424.2488).

*Hippofoline B (**2**):* light yellowish oil; $[\alpha]^{25}_{D}$ −61 (*c* 0.17, $CHCl_3$); ECD (MeCN), λ_{max} ($\Delta\varepsilon$): 216 (−4.02), 256 (0.09), 278 (−0.05) nm; IR ν_{max} 1732, 3264cm^{-1}(OH); ^{1}H NMR ($CDCl_3$, 600 MHz) and ^{13}C NMR data ($CDCl_3$, 150 MHz), see Table 2.2; HRDARTMS *m/z* 382.2397 $[M+H]^+$ (calcd for $C_{24}H_{31}NO_3$ + H, 382.2382).

*(2R,6S,2′′S)-Lobeline (**3**):* yellowish block crystals (DCM); mp 111–113°C; $[\alpha]^{25}_{D}$ −34 (*c* 0.76, $CHCl_3$); ECD (MeCN), λ_{max} ($\Delta\varepsilon$): 205 (−4.81), 236 (1.07), 275 (−0.22), 295 (0.16) nm; IR ν_{max} 1683, 3357cm^{-1}; ^{1}H NMR ($CDCl_3$, 600 MHz) and ^{13}C NMR data ($CDCl_3$, 150 MHz), see Table 2.3; HRDARTMS *m/z* 338.2124 $[M+H]^+$ (calcd for $C_{22}H_{27}NO_2$ + H, 338.2120).

*(2R,6S,2′S,2′′S)-Diphenyllobelidiol (**4**):* colorless block crystals (DCM); mp 110–112 °C; $[\alpha]^{25}_{D}$ −56 (*c* 0.34, $CHCl_3$); ECD (MeCN), λ_{max} ($\Delta\varepsilon$): 215 (−1.42), 233 (0.03), 261 (0.17) nm; IR (dry film) ν_{max} 3390 cm^{-1}; ^{1}H NMR ($CDCl_3$, 600 MHz) and ^{13}C NMR data ($CDCl_3$, 150 MHz), see Table 2.4; HRDARTMS *m/z* 340.2262 $[M+H]^+$ (calcd for $C_{22}H_{29}NO_2$ + H, 340.2277).

*(2R,6S,2′S,2′′S)-Diphenyllobelidiol N-oxide (**5**):* white amorphous solid; $[\alpha]_D$ −56 (*c* 0.13, $CHCl_3$); ^{1}H NMR ($CDCl_3$, 600 MHz) and ^{13}C NMR data ($CDCl_3$, 150 MHz), see Table 2.5; HRDARTMS *m/z* 356.2224 $[M+H]^+$ (calcd for $C_{22}H_{29}NO_3$ + H, 356.2226).

*3α-Cinnamoyloxy-N-phloretoylnortropane (**6**):* colourless oil; UV (MeOH) λ_{max} (log ε) 216 (4.30), 223 (4.25), 278 (4.26) nm; IR ν_{max} 3225, 3061, 2953, 2922, 1706, 1632, 1605, 1590, 1515, 1449, 1163, 1079, 1033, 984, 830, 768 cm^{-1}; ^{1}H NMR ($CDCl_3$, 600 MHz) and ^{13}C NMR ($CDCl_3$, 150 MHz) data, see Table 3.1; HRDARTMS *m/z* 406.20153 $[M + H]^+$ (calcd for $C_{25}H_{27}NO_4$ + H, 406.20128).

*3α-Cinnamoyloxy-N-formylnortropane (**7**):* colourless oil; UV (MeOH) λ_{max} (log ε) 216 (4.29), 223 (4.19), 277 (4.35) nm; IR ν_{max} 3061, 2955, 2922, 2882, 1708, 1660, 1639, 1449, 1311, 1176, 1163, 1038 cm^{-1}; ^{1}H NMR ($CDCl_3$, 600 MHz) and ^{13}C NMR ($CDCl_3$, 150 MHz) data, see Table 3.2; HRESIMS *m/z* 308.12576 $[M + Na]^+$ (calcd for $C_{17}H_{19}NO_3$ + Na, 308.12571).

*3α-Phenylacetoxy-N-formylnortropane (**8**):* colourless oil; UV (MeOH) λ_{max} (log ε) 273 (4.40) nm; IR ν_{max} 3027, 2953, 2922, 1727, 1663, 1497, 1367, 1235, 1156, 1032, 947, 704 cm^{-1}; ^{1}H NMR ($CDCl_3$, 600 MHz) and ^{13}C NMR ($CDCl_3$, 150 MHz) data, see Table 3.3; HRESIMS *m/z* 274.1440 $[M + H]^+$ (calcd for $C_{16}H_{19}NO_3$ + H, 274.14377).

*3α-Benzoyloxy-N-formylnortropane (**9**):* colourless oil; UV (MeOH) λ_{max} (log ε) 228 (3.96), 274 (4.18) nm; IR ν_{max} 2956, 2918, 1712, 1662, 1498, 1272, 1108, 1033, 946, 712 cm^{-1}; ^{1}H NMR ($CDCl_3$, 600 MHz) and ^{13}C NMR ($CDCl_3$, 150 MHz) data, see Table 3.4; HRESIMS *m/z* 260.1287 $[M + H]^+$ (calcd for $C_{15}H_{17}NO_3$ + H, 260.12812).

*3α-Acetoxy-N-formylnortropane (**10**):* colourless oil; UV (MeOH) λ_{max} (log ε) 273 (4.28) nm; IR ν_{max} 2956, 2923, 1730, 1659, 1501, 1370, 1236, 1036, 952, 812 cm^{-1}; ^{1}H NMR ($CDCl_3$, 600 MHz) and ^{13}C NMR ($CDCl_3$, 150 MHz) data, see Table 3.5; HRESIMS *m/z* 198.1129 $[M + H]^+$ (calcd for $C_{10}H_{15}NO_3$ + H, 198.11247).

*3α-Cinnamoyloxynortropane (**11**)*: colourless oil; UV (MeOH) λ_{max} (log ε) 216 (3.91), 222 (3.84) and 276 (4.00) nm; IR ν_{max} 3406, 2954, 1710, 1642, 1311, 1171, 977, 766 cm^{-1}; ^{1}H NMR ($CDCl_3$, 600 MHz) and ^{13}C NMR ($CDCl_3$, 150 MHz) data, see Table 3.6; HRESIMS *m/z* 258.14818 $[M + H]^+$ (calcd for $C_{16}H_{19}NO_2$ + H, 258.14940).

*3α-Benzoyloxynortropane (**12**):* colourless oil; UV (MeOH) λ_{max} (log ε) 229 (2.36) nm; IR ν_{max} 3395, 2959, 2927, 1712, 1587, 1268, 1109, 1026, 712 cm^{-1}; ^{1}H NMR (CD_3OD, 600 MHz) and ^{13}C NMR (CD_3OD, 150 MHz) data, see Table 3.7; HRESIMS *m/z* 232.1343 $[M + H]^+$ (calcd for $C_{16}H_{19}NO_2$ + H, 232.13375).

*(±)-Bissaccardine (**13**):* colourless oil; $[\alpha]^{25}_D$ ± 0 (*c* 0.05, MeOH); UV (MeOH) λ_{max} (log ε) 216 (4.44), 223 (4.31), 277 (4.46) nm; IR ν_{max} 2954, 2875, 1707, 1636, 1450, 1305, 1278, 1167, 1029, 842, 765, 701cm^{-1}; ^{1}H NMR ($CDCl_3$, 600 MHz) and ^{13}C NMR ($CDCl_3$, 150 MHz) data, see Table 3.8; HRESIMS *m/z* 515.2927 $[M + H]^+$ (calcd for $C_{32}H_{39}NO_4$, 515.29043).

*(±)-Trissaccardine (**14**):* colourless oil; $[\alpha]^{25}_D$ ± 0 (*c* 0.02, MeOH); IR ν_{max} 3373, 2956, 2926, 2855, 1733, 1636, 1597, 1515, 1460, 1378, 1269, 1164, 1032, 768 cm^{-1}; ^{1}H NMR ($CDCl_3$, 600 MHz) and ^{13}C NMR ($CDCl_3$, 150 MHz) data, see Table 3.9a and Table 3.9b; HRESIMS *m/z* 772.4341 $[M + H]^+$ (calcd for $C_{48}H_{57}N_3O_6$ + H, 772.43201).

*(±)-Saccardianone A (**15**):* colourless block crystals (Et_2O); mp 215–216 °C; $[\alpha]^{25}_D$ ±0 (*c* 0.05, MeOH); UV (MeOH) λ_{max} (log ε) 225 (4.10), 278 (3.45) nm; IR ν_{max} 3362, 3021, 2923, 1652, 1614, 1514, 1446, 1231, 1206, 831 cm^{-1}; ^{1}H NMR (CD_3OD, 600 MHz) and ^{13}C NMR (CD_3OD, 150 MHz) data, see Table 4.1;

HRESIMS *m/z* 427.1905 $[M - H]^-$ (calcd for $C_{28}H_{28}O_4$ – H, 427.19148).

*(±)-Saccardianone B (**16**):* colourless oil; $[\alpha]^{25}_D$ ±0 (*c* 0.025, MeOH); UV (MeOH) λ_{max} (log ε) 225 (4.04), 278 (3.36) nm; IR ν_{max} 3357, 3022, 2924, 1650, 1614, 1514, 1445, 1209, 833 cm^{-1}; ^1H NMR (CD_3OD, 600 MHz) and ^{13}C NMR (CD_3OD, 150 MHz) data, see Table 4.1; HRESIMS *m/z* 427.1918 $[M - H]^-$ (calcd for $C_{28}H_{28}O_4$ – H, 427.19148).

*(±)-Saccardianine A (**17**):* yellowish oil; $[\alpha]^{25}_D$ ±0 (*c* 0.03, MeOH); UV (MeOH) λ_{max} (log ε) 225 (4.21), 279 (3.59) nm; IR ν_{max} 3301, 3022, 2927, 1699, 1612, 1514, 1447, 1234, 827 cm^{-1}; ^1H NMR (CD_3OD, 600 MHz) and ^{13}C NMR (CD_3OD, 150 MHz) data, see Table 4.2; HRESIMS *m/z* 446.2338 $[M + H]^+$ (calcd for $C_{28}H_{31}NO_4$ + H, 446.23258).

*(±)-Saccardianine B (**18**):* yellowish oil; $[\alpha]^{25}_D$ ±0 (*c* 0.04, MeOH); UV (MeOH) λ_{max} (log ε) 225 (4.25), 278 (3.63) nm; IR ν_{max} 3361, 3025, 2931, 1615, 1513, 1456, 1241, 828 cm^{-1}; ^1H NMR (CD_3OD, 600 MHz) and ^{13}C NMR (CD_3OD, 150 MHz) data, see Table 4.3; HRESIMS *m/z* 576.3111 $[M + H]^+$ (calcd for $C_{38}H_{41}NO_4$ + H, 576.31084).

*Saccardianine C (**19**):* light yellowish oil; IR ν_{max} 3061, 3015, 2928, 1612, 1595, 1514, 1478, 1435, 1171, 812, 780, 751 cm^{-1}; ^1H NMR ($CDCl_3$, 600 MHz) and ^{13}C NMR ($CDCl_3$, 150 MHz) data, see Table 4.4; HRDARTMS *m/z* 200.1076 $[M + H]^+$ (calcd for $C_{13}H_{14}NO$, 200.10699).

*Pellaspirone (**20**):* colourless prism (CH_2Cl_2); mp 139–140 °C; UV (MeOH) λ_{max} (log ε) 224 (4.29) nm; IR ν_{max} 3246, 3039, 2929, 1657, 1607, 1514, 1224, 860, 732cm^{-1}; ^1H NMR ($CDCl_3$, 600 MHz) and ^{13}C NMR ($CDCl_3$, 150 MHz) data, see

Table 4.5; HRESIMS *m/z* 293.1193 $[M - H]^-$ (calcd for $C_{19}H_{18}O_3$ – H, 293.11832).

*Saccardianoside (**21**):* colourless oil; $[\alpha]^{25}_D$ –48.5 (*c* 0.071, MeOH); UV (MeOH) λ_{max} (log ε) 224 (4.28), 278 (3.76) nm; IR ν_{max} 3397, 3014, 2926, 1703, 1515, 1425, 1362, 1227, 1047, 829, 532 cm^{-1}; ^1H NMR (CD_3OD, 600 MHz) and ^{13}C NMR (CD_3OD, 150 MHz) data, see Table 4.6; HRESIMS *m/z* 621.2547 $[M - H]^-$ (calcd for $C_{31}H_{42}O_{13}$ – H, 621.25526).

*Platyphyllenone (**22**):* yellowish oil; UV (MeOH) λ_{max} (log ε) 225 (4.31), 278 (3.51) nm; IR ν_{max} 3326, 3021, 2926, 1670, 1614, 1513, 1221, 823 ^1H NMR ($CDCl_3$, 600 MHz) and ^{13}C NMR ($CDCl_3$, 150 MHz) data, see Table 4.7; HRESIMS *m/z* 295.1336 $[M - H]^-$ (calcd for $C_{19}H_{20}O_3$ – H, 295.13397).

*(±)-5-Hydroxy-1,7-bis-(4-hydroxyphenyl)-3-heptanone (**23**):* colourless oil; $[\alpha]^{25}_D$ ±0 (*c* 0.068, MeOH); UV (MeOH) λ_{max} (log ε) 224 (4.09), 279 (3.46) nm; IR ν_{max} 3318, 2926, 1695, 1509, 1225, 821 cm^{-1};^1H NMR (CD_3COCD_3, 600 MHz) and ^{13}C NMR (CD_3COCD_3, 150 MHz) data, Table 4.8; HRESIMS *m/z* 313.1454 $[M - H]^-$ (calcd for $C_{19}H_{22}O_4$ – H, 313.14453).

6.13 X-ray Crystallography Data of Compounds 3, 4, (±)-15 and 20

X-ray diffraction analysis was carried out on a Rigaku Oxford (formerly Agilent Technologies) SuperNova Dual diffractometer with Cu Kα radiation (λ = 1.54184 Å) at room temperature (Chemistry Department, University of Malaya). The structure was solved with SHELXT-2018/2 structure solution program using Intrinsic Phasing and refined with SHELXL-2018/3 refinement package using Least Square minimization. All non-hydrogen atoms were refined anisotropically, and all hydrogen atoms were placed in idealised positions and

refined as riding atoms with the relative isotropic parameters. Crystallographic data for **3**, **4**, (±)-**15** and **20** were deposited at the Cambridge Crystallographic Data Centre (CCDC). Copies of the data can be obtained, free of charge, on application to the Director, CCDC, 12 Union Road, Cambridge CB2 1EZ, UK (fax: +44 (0)1223-336033, or e-mail: deposit@ccdc.cam.ac.uk).

Crystallographic data of **3**: Light orange block crystals from CH_2Cl_2 (slow evaporation), $C_{22}H_{27}NO_2$, *M*r = 337.44, monoclinic, space group $P2_1$, a = 7.8270(8) Å, b = 7.0153(7) Å, c = 17.0351(18) Å, γ=99.237(11), V = 923.25(17) Å^3, Z = 2, D_{calcd} = 1.214 gcm^{-3}, crystal size 0.5 × 0.4 × 0.4 mm^3, F(000) = 364, Cu Kα radiation (λ = 1.54178 Å), T=185(3) K. A total of 3677 reflections were measured with 2491 independent reflections (R_{int} = 0.0243, R_{sigma} = 0.0273). The final R_1 value was 0.0334 [$I > 2\sigma(I)$] and wR_2 value was 0.0890 (all data). The absolute configuration of **3** was determined on the basis of Flack parameter [x = 0.0(0.2)] and corroborated by use of the Hooft parameter [y = 0.05(0.19)]. CCDC number: 1861617.

Crystallographic data of **4**: Colorless block crystals from CH_2Cl_2 (slow evaporation), $C_{22}H_{29}NO_2$, *M*r=339.46, orthorhombic, space group $P2_12_12_1$, a = 7.1416(4) Å, b = 11.6532(4) Å, c = 23.7471(7) Å, V = 1976.31(13) Å^3, Z = 4, D_{calcd} = 1.141 gcm^{-3}, crystal size 0.40 × 0.20 × 0.05 mm^3, F(000) = 736, Cu Kα radiation (λ = 1.54178 Å), T = 298(2) K. A total of 42207 reflections were measured with 3988 independent reflections (R_{int} = 0.0711, R_{sigma} = 0.0200). The final R_1 value was 0.0396 [$I > 2\sigma(I)$] and wR_2 value was 0.1124 (all data). The absolute configuration of **4** was determined on the basis of Flack parameter [x = 0.00(0.13)] and corroborated by use of the Hooft parameter [y = 0.04(0.12)].

CCDC number: 1861618.

Crystallographic data of **15**: colorless block crystals from Et_2O (slow evaoration), $C_{18}H_{28}N_4$, *M*r = 428.50, orthorhombic, space group *Pbca*, *a* = 17.1064(11) Å, *b* = 14.6802(8) Å, *c* = 18.3619(8) Å, *V* = 4611.1(4) Å^3, *Z* = 8, D_{calcd} = 1.234 gcm^{-3}, crystal size 0.5 x 0.41 x 0.28 mm^3, *F*(000) = 1824, Cu K*α* radiation (λ = 1.54178 Å), *T* = 293(2) K, 8956 reflections measured (9.286° ≤ 2θ ≤ 147.456°), 4472 unique (R_{int} = 0.0248, R_{sigma} = 0.0296) which were used in all calculations. The final R_1 value was 0.0643 [*I>2σ(I)*] and wR_2 was 0.1936. CCDC number: 2005485.

Crystallographic data of **20**: Colorless prisms from $CHCl_3$ (slow evaporation), $C_{19}H_{18}O_3$ ($CHCl_3$), *M*r = 294.33, orthorhombic, space group $P2_12_12_1$, *a* = 9.0832(7) Å, *b* = 12.7957(9) Å, *c* = 13.8859(10) Å, *V* = 1613.9(2) Å^3, *Z* = 4, D_{calcd} = 1.211 gcm^{-3}, crystal size 0.5 x 0.38 x 0.09 mm^3, *F*(000) = 1824, Cu Kα radiation (λ = 1.54178 Å), *T* = 293(2) K, 5948 reflections measured (9.398° ≤ 2θ ≤ 148.076°), 4152 unique (R_{int} = 0.0224, R_{sigma} = 0.0239) which were used in all calculations. The final R_1 value was 0.0499 [*I>2σ(I)*] and wR_2 was 0.1376.

6.14 Computational Method for ECD Calculations of Compounds 1 and 2

The conformations of compounds **1** (2*R*,6*S*,2′*S*,2′′*S*) and **2** (2*R*,6*S*,2′*S*,2′′*S* and 2*S*,6*R*,2′*S*,2′′*S*) were obtained by Spartan'14 software (Wavefunction, Inc., Irvine, CA, USA) using the MMFF94 forcefield. Conformers occurring within a 10kcal mol^{-1} energy window from the global minimum were then imported into the Gaussian 09 software (Gaussian 09, Revision C.01, Gaussian, Inc.,Wallingford, CT, USA) for Density Functional Theory (DFT)-level geometry optimization and

frequency calculation using the B3LYP functional with a basis set of 6–31 G(d). Time-dependent Density Functional Theory (TDDFT) ECD calculations were performed at the B3LYP/6-311++G(d,p) level with the optimised conformers using a Polarisable Continuum Model (PCM) solvation model for MeCN. The ECD curve for each optimised conformer was weighted by Boltzmann distribution after UV correction, and the overall ECD curves were produced by SpecDis, version 1.64, software.[142] Optical rotation calculations at the wavelength of 589.3 nm were performed with the optimised conformers at the B3LYP/6-311++G(d,p) computational level using a PCM solvation model for $CHCl_3$.

Chapter 7: Research Limitations, Future Studies and Conclusion

7.1 Research Limitations and Future Studies

In line with the aim and objectives, the research had successfully isolated and elucidated novel alkaloids and diarylheptanoids, with some showing marked biological activities, from two understudied plant species, i.e., *Hippobroma longiflora* and *Pellacalyx saccardianus*. However, several limitations were encountered during the research, which warrant future attention and continued investigation:

1. The anti-muscarinic activity of (–)-lobeline (**3**) and its derivatives (**2** and **4**) was largely inferred based on their relaxation activity on carbachol induced contraction of rat-isolated trachea smooth muscles. It should be noted that the murine trachea smooth muscles are mainly mediated by M_3 mAChR subtype,[143] whereas other mAChRs are expressed in different tissues such as the aorta and ileum. Further organ bath experiments using tissues with different mAChR subtypes will be conducted to ascertain the anti-muscarinic selectivity of **3**.

2. Chiral-phase HPLC isolation of the tropane alkaloid oligomers (±)-bissaccardine (**13**) and (±)-trissaccardine (**14**) were unsuccessful due to rapid chemical degradation into **11** via retro aza-Michael reaction (Appendices 45 and 46). The degradation reaction was particularly prominent in the presence of diethylamine (DEA), which was used as 0.1% mobile phase additive. However, chromatographic resolutions of **13** and **14** were unsatisfactory without using DEA. Different solvent systems or different chiral-phase HPLC columns will be employed to effectively resolve **13** and **14** for the establishment of their absolute

configurations. If the individual enantiomers could be isolated and characterised, their cytotoxic activity will be compared to the racemates. It was also recently discovered that alkaloid **13** tend to degrade in chloroform solution. Prolonged storage of **13** and **14** in chloroform (including $CDCl_3$) should be avoided.

3. Due to paucity of material, chiral-phase HPLC separation of the racemic diarylheptanoids **15** – **18** did not afford appreciable yield of individual enantiomers to ascertain their optical rotation values. As a result, the absolute configurations of **15** – **18** could not be established. Besides, **17** and **18** were not obtained in sufficient quantities for the testing of their biological activity. Hence, large scale re-collection of *P. saccardianus*, followed by re-extraction and re-isolation of **15** – **18** in larger quantities are planned in the future. It should be noted that different *P. saccardianus* specimens collected at different timing and locations tend to exhibit different phytochemical profiles. This phenomenon is well-expected in natural product research. Care must be taken to collect specimens in a similar region and timing to increase the consistency and likelihood of re-isolating compounds **15** – **18**.

4. The relative stereochemistry of saccardianine A (**17**) remained unresolved. This was mainly caused by shortage of material (< 3.0 mg) in addition to chemical degradation during chiral-phase HPLC analysis (Appendix 65). At the time of writing, extra attempts to crystallise the remaining samples of **17** (< 1.5 mg) are in progress, aiming to obtain crystals suitable for X-ray diffraction analysis.

5. Pellaspirone (**20**) and saccardianoside (**21**) were isolated from two independent small-scale experiments (Sections 6.7 and 6.9), which were aimed

to extract highly polar and/or acidic diarylheptanoids from the leaves of *P. saccardianus*. Although the same batch of plant material was used, the absence of **20** and **21** from the large-scale extraction procedure (Section 6.5) implied that acid-base chemical separation had excluded and/or degraded certain compounds of interest. Indeed, **13** and **14** were unstable in ammonical solvents, while **20** was most likely an acid-base induced artifact. Thus, considering the presence acid-base labile natural products in *P. saccardianus*, acid-base chemical separation should be performed with extra precautions in the future. Prolonged standing of the crude extract in acidic or alkali solutions should be avoided. The basification step could be attempted with bicarbonate instead of ammonia. Furthermore, acid-base separation might have inadvertently excluded some non-alkaloidal diarylheptanoids like **15** and **16**, as well as glycoside **21**, resulting in very low to negligible isolation yields. Hence, the extraction procedure in Section 6.7 could be scaled up to target non-alkaloidal diarylheptanoids in the left-over aqueous layer following acid-base separation.

6. Due to constraints in time and resources, this research only investigated the cytotoxic activity of diarylheptanoids **15**, **16**, **20** and **22**. However, given that diarylheptanoids generally exhibit pleiotropic biological activities (Section 1.4.5), other *in vitro* bioassays could be explored for compounds **15** – **23** in the future, with emphasis on their antibacterial, antiviral and anti-inflammation properties.

7.2 Conclusion

In conclusion, the present research had successfully isolated and elucidated novel alkaloids and diarylheptanoids with valuable biological activities from two understudied plant species, i.e., *Hippobroma longiflora* and *Pellacalyx saccardianus*. The aim of the research had been achieved.

Three new diphenethylpiperidine alkaloids (**1**, **2** and **5**) were isolated and characterised from the whole plant of *H. longiflora*. Hippofolines A and B (**1** and **2**) are asymmetrical acetate derivatives of (−)-*cis*-2′,2′′-diphenyllobelidiol (**4**), while **5** is the *N*-oxide derivative of **4**. The absolute configurations of **1** and **2** were deduced based on experimental and calculated ECD spectra. The absolute configurations of (−)-lobeline (**3**) and **4** in their free base form were confirmed for the first time by X-ray diffraction analysis. Compounds **2** and **3** exhibited potent relaxation effects on rat-isolated tracheal rings with EC_{50} values of 26.0 and 1.2 nM, respectively. This was possibly due to their antagonism of muscarinic acetylcholine receptors present in the tracheal smooth muscles. While the novel antimuscarinic activity of the diphenethylpiperidine alkaloids demands further investigation, alkaloids **2** – **4** are identified as valuable antispasmodic drug leads.

3α-Cinnamoyloxy-*N*-phloretoylnortropane (**6**) and four *N*-formylnotropane esters (**7** – **10**), together with two oligomeric nortropane alkaloids, (±)-bissaccardine (**13**) and (±)-trissaccardine (**14**), were characterised from the leaves and bark of *P. saccardianus*. Two known nortropane alkaloids (**11** and **12**) were co-isolated in high yield. The relative configuration of **13** was determined on the basis of chiral-phase HPLC analysis. The biogenetic origin of

compounds **13** and **14** were proposed to arise from aza-Michael addition of monomer **11**. The possibility of them being artifacts arising from the extraction/isolation procedure was ruled out by our attempted semi-synthesis experiments. Compounds **13** and **14** exhibited potent cytotoxicity towards a panel of pancreatic cancer cell lines (AsPC-1, SW1990, BxPC-3 and PanC-1), with **13** being especially selective (IC_{50} 1.13 – 10.85 μM). Even though the cytotoxic mechanism of **13** and **14** has yet to be elucidated, the discovery of novel cytotoxic alkaloids bearing the tropane skeleton is noteworthy. Additionally, alkaloids **6**, **9**, **11** – **13** demonstrated weak relaxation effects on rat isolated trachea rings that were pre-contracted with carbachol. Analyses of their structure activity relationships with regards to antimuscarinic activity suggested plausible weak receptor-binding interactions that may lead to poor antispasmodic activity.

Investigation into the diarylheptanoid contents of the leaves of *Pellacalyx saccardianus* had afforded four compounds with novel alicyclic core structures. They are two pairs of enantiomeric diarylheptanoid-phenylpropanoid adducts incorporating a cyclohexenone core, (±)-saccardianones A and B (**15** and **16**), an alkaloidal diarylheptanoid-phenylpropanoid adduct incorporating a 4-piperidone core, (±)-saccardianine A (**17**), and a pair of enantiomeric dimeric diarylheptanoid alkaloids incorporating a tetrahydropyridine core, (±)-saccardianine B (**18**). Besides, a suspected degradation product, saccardianine C (**19**), a diarylheptanoid derived spirocompound, pellaspirone (**20**), and a diarylheptanoid-rutinoside, saccardianoside (**21**) were obtained along with two known diarylheptanoids (**22** and **23**). The relative configuration of **15** was elucidated by X-ray data analysis, while that of **18** was determined based on the

NOESY data. The absolute configuration of **21** was established by HPLC analyses following chemical derivatisation. Through semi-synthesis, **20** was deduced to be an artifact arising from the acid-base separation. The biogenetic pathways of **15** – **18** were postulated with **23** as their common precursor. Compounds **16** and **20** showed moderate but selective cytotoxicity towards pancreatic AsPC-1 (IC_{50} 15.47 μM) and breast MDA-MB-231 (IC_{50} 13.32 μM) cancer cell lines, respectively.

Lastly, the present research has demonstrated that continuous efforts in phytochemistry research would be rewarded with natural products with useful bioactivity and/or novel structures. It is therefore imperative to conserve Earth's ecosystems along with the various understudied species in order to preserve the immense chemical diversity nature has to offer. Natural products with known structures and/or bioactivity also demand continual research because while new drug targets are being discovered, old drugs can be repurposed.

References

(1) Zhou, Y.; Hou, Y.; Shen, J.; Huang, Y.; Martin, W.; Cheng, F. *Cell Discov.* **2020**, *6*, 1–18.

(2) Schlesinger, N.; Firestein, B. L.; Brunetti, L. *Curr. Pharmacol. Rep.* **2020**, *6*, 137–145.

(3) Sharun, K.; Dhama, K.; Patel, S. K.; Pathak, M.; Tiwari, R.; Singh, B. R.; Sah, R.; Bonilla-Aldana, D. K.; Rodriguez-Morales, A. J.; Leblebicioglu, H. *Ann. Clin. Microbiol. Antimicrob.* **2020**, *19*, 1–5.

(4) Evans. W. C. *Trease and Evans' Pharmacognosy*; Saunders: New York, 2009; pp 353–415.

(5) Dewick, P. M. *Medicinal Natural Products. A Biosynthetic Approach*; John Wiley & Sons: United Kingdom, 2009; pp 291–398.

(6) Schardl, C. L.; Grossman, R. B.; Nagabhyru, P.; Faulkner, J. R.; Mallik, U. P. *Phytochemistry* **2007**, *68*, 980–996.

(7) Larson, R. A.; Marley, K. A. *Phytochemistry* **1984**, *23*, 2351–2354.

(8) McKenna, D. J. *Pharmacol Therapeut* **2004**, *102*, 111–129.

(9) Belser-Ehrlich, S.; Harper, A.; Hussey, J.; Hallock, R. *Toxicol. Ind. Health* **2013**, *29*, 307–316.

(10) Cannon, J. S.; Overman, L. E. *Angew. Chemie* **2012**, *51*, 4288–4311.

(11) Mueller, K. L.; Hoon, M. A.; Erlenbach, I.; Chandrashekar, J.; Zuker, C. S.; Ryba, N. J. P. *Nature* **2005**, *434*, 225–229.

(12) Gomberg, M. *J. Am. Chem. Soc.* **1896**, *18*, 331–342.

(13) Rubia, L. B.; Gomez, R. *J. Pharm. Sci.* **1977**, 66, 1656–1657.

(14) Anderson, L. A.; Dogget, N. S.; Ross, M. S. F. *Planta Med.* **1977**, *32*, 125–129.

(15) Warren, W. H.; Weiss R. S. *J. Biol. Chem.* **1907**, *3*, 327–338.

(16) Ziegler, J.; Facchini, P. J. *Annu. Rev. Plant Biol.* **2008**, *59*, 735–769.

(17) Herbert, R. B. *Nat. Prod. Rep.* **2003**, *20*, 494–508.

(18) Patrick, G. L. *An Introduction to Medicinal Chemistry*; Oxford University Press: New York, 2009; pp 579–630.

(19) Rang, H. P.; Ritter, J. M.; Flower, R. J.; Henderson, G. *Rang & Dales's Pharmacology*; Elsevier: Edinburgh, 2012; pp 151–172.

(20) Kesting, J. R.; Tolderlund, I. L.; Pedersen, A. F.; Witt, M.; Jaroszewski, J. W.; Staerk, D. *J. Nat. Prod.* **2009**, *72*, 312–315.

(21) Felpin, F.-X.; Lebreton, J. *Tetrahedron* **2004**, *60*, 10127–10153.

(22) A. Crooks, P.; Zheng, G.; P. Vartak, A.; P. Culver, J.; Zheng, F.; B. Horton, D.; P. Dwoskin, L. *Curr. Top. Med. Chem.* **2011**, *11*, 1103–1127.

(23) Dwoskin, L. P.; Crooks, P. A. *Biochem. Pharmacol*. **2002**, *63,* 89–98.

(24) Grynkiewicz, G.; Gadzikowska, M. *Pharmacol. Reports* **2008**, *60*, 439–463.

(25) De Simone, R.; Margarucci, L.; De Feo, V. *Pharmacologyonline* **2008**, *1*, 70–89.

(26) Kohnen-Johannsen, K. L.; Kayser, O. *Molecules* **2019**, *24*, 796.

(27) Macht, D. I. *J. Am. Chem. Soc.* **1922**, *11*, 882–897.

(28) Humam, M.; Shoul, T.; Jeannerat, D.; Muñoz, O.; Christen, P. *Molecules* **2011**, *16*, 7199–7209.

(29) Griffin, W. J.; Lin, G. D. *Phytochemistry.* **2000**, *53*, 623–637.

(30) Christen, P.; Cretton, S.; Humam, M.; Bieri, S.; Muñoz, O.; Joseph-Nathan, P. *Phytochem. Rev.* **2019**, 1–27.

(31) Cretton, S.; Bartholomeusz, T. A.; Humam, M.; Marcourt, L.; Allenbach, Y.; Jeannerat, D.; Muñoz, O.; Christen, P. *J. Nat. Prod.* **2011**, *74*, 2388–2394.

(32) Molyneux, R. J.; Nash, R. J.; Asano, N. In *Alkaloids: Chemical and Biological Perspectives*; Pelletier S. W., Ed.; Pergamon: New York, 1996; Vol. 11, Chapter 4, pp 303–343.

(33) Bick, I. R. C.; Gillard, J. W.; Leow, H. M. *Aust. J. Chem.* **1979**, *32*, 2537–2543.

(34) Geng, C. A.; Ma, Y. B.; Chen, J. J. *Chinese Chem. Lett.* **2013**, *24*, 236–238.

(35) Oliveira, S. L.; Da Silva, M. S.; Tavares, J. F.; Sena-Filho, J. G.; Lucena, H. F. S.; Romero, M. A. V.; Barbosa-Filho, J. M. *Chem. Biodivers.* **2010**, *7*, 302–326.

(36) Aripova, S. F.; Sharova, E. G.; Yunusov, S. Y. *Chem. Nat. Compd.* **1982**, *18*, 606–607.

(37) Jenett-Siems, K.; Mann, P.; Kaloga, M.; Siems, K.; Jakupovic, J.; Witte, L.; Eich, E. *Phytochemistry* **1998**, *49*, 1449–1451.

(38) Taha, A. M.; Rücker, G. *J. Pharm. Sci.* **1978**, *67*, 775–779.

(39) Bishop, R. J.; Fodor, G.; Katritzky, A. R.; Soti, F.; Sutton, L. E.; Swinbourne, F. J. J. Chem. Soc. **1966**, 74, 74–77.

(40) Villar, H. O.; Loew, G. H. *J. Comput. Chem.* **1990**, *11*, 1111–1118.

(41) Chua, W. H.; Balakrishnan, V.; Chan, Y. H.; Tong, L.; Ling, Y.; Quah, B. L.; Tan, D. *Ophthalmology* **2006**, *113*, 2285–2291.

(42) Sofuoglu, M.; Kosten, T. R. *Expert Opin. Emerg. Drugs* **2006**, *11*, 91–98.

(43) Lv, H.; She, G. *Nat. Prod. Commun.* **2010**, *5*, 1687–1708.

(44) Keserü, G. M.; Nógrádi, M. *Stud. Nat. Prod. Chem.* **1995**, *17*, 357–394.

(45) Alberti, Á.; Riethmüller, E.; Béni, S. *J. Pharm. Biomed. Anal.* **2018**, *147*, 13–34.

(46) Ganapathy, G.; Preethi, R.; Moses, J. A.; Anandharamakrishnan, C. *Biocatal. Agric. Biotechnol.* **2019**, *19*.

(47) Srinivasan, K. R. *J. Pharm. Pharmacol.* **1953**, *5*, 448–457.

(48) Priyadarsini, K. I. *Molecules* **2014**, *19*, 20091–20112.

(49) Vidaković, V.; Novaković, M.; Popović, Z.; Janković, M.; Matić, R.; Tešević, V.; Bojovicć, S. *Holzforschung* **2017**, *72*, 9–16.

(50) An, N.; Zhang, H. W.; Xu, L. Z., Yang, S. L.; Zou, Z. M. *Food Chem.* **2010**, *119*, 513–517.

(51) Zhao, L.; Liang, J. Y.; Qu, W. *Chem. Nat. Compd.* **2012**, *48*, 836–838.

(52) Liu, H.; Wu, Z. L.; Huang, X. J.; Peng, Y.; Huang, X.; Shi, L.; Wang, Y.; Ye, W. C. *J. Nat. Prod.* **2018**, *81*, 162–170.

(53) Jahng, Y.; Park, J. G. *Molecules* **2018**, *23*, 3107.

(54) Gupta, S. C.; Patchva, S.; Aggarwal, B. B. *AAPS J.* **2013**, *15*, 195–218.

(55) Nelson, K. M.; Dahlin, J. L.; Bisson, J.; Graham, J.; Pauli, G. F.; Walters, M. A. *J. Med. Chem.* **2017**, *60*, 1620–1637.

(56) Choi, J. G.; Lee, M. W.; Choi, S. E.; Kim, M. H.; Kang, O. H.; Lee, Y. S.; Chae, H. S.; Obiang-Obounou, B.; Oh, Y. C.; Kim, M. R.; Shin, D. W.; Lee, J. H. *Eur. Rev. Med. Pharmacol. Sci.* **2012**, *16*, 853–859.

(57) Tung, N. H.; Kwon, H. J.; Kim, J. H.; Ra, J. C.; Ding, Y.; Kim, J. A.; Kim, Y. H. *Bioorganic Med. Chem. Lett.* **2010**, *20*, 1000–1003.

(58) Morikawa, T.; Tao, Jing.; Toguchida, I.; Matsuda, H.; Yoshikawa, M. *J. Nat. Prod.* **2003**, *66*, 86–91.

(59) Jones, J. R.; Lebar, M. D.; Jinwal, U. K.; Abisambra, J. F.; Koren III, J.; Blair, L.; O'Leary, J.C.; Davey, Z., Trotter, J.; Johnson, A.G.; Weeber, E., Eckman, C. B.; Baker, B. J., Dickey, C. A. *J. Nat. Prod.* **2011**, *74*, 38-44.

(60) Yang, Y.; Kinoshita, K.; Koyama, K.; Takahashi, K.; Tai, T.; Nunoura, Y.; Watanabe, K. *J. Nat. Prod.* **1999**, *62*, 1672–1674.

(61) Crespo, M. B.; Serral, L.; Turland, N. *Taxon* **2010**, *45*, 117–120.

(62) Nicolson, D. H. *Taxon* **1994**, *43*, 97–107.

(63) Antonelli, A. *Mol. Phylogenet. Evol.* **2008**, *46*, 1–18.

(64) Chen, L. Y.; Wang, Q. F.; Renner, S. S. *Taxon* **2016**, *65*, 293–304.

(65) Wiart, C. Medicinal Plants of the Asia-pacific: Drugs for the Future?; World Scientific: New Jersey, 2006; pp. 573.

(66) Arthur, H. R.; Chan, R. P. K. *J. Chem. Soc.* **1963**, 750–751.

(67) Sukari, M. A.; Rahmani, M.; Manas, A. R.; Takahashi, S. *Pertanika J. Trop. Agric. Sci.* **1992**, *14*, 41–44.

(68) Abdul Rasyid, Z.; Farida, A.; Daud, S. H.; Wiwin, S.; Wijaya, K.I.; Tangke, A. E. *GSC Biol. Pharm. Sci.* **2020**, *11*, 091–098.

(69) Arifin, H.; Alwi, T. I.; Aisyahharma, O.; Juwita, D. A. *J. Sains Farm. Klin.* **2018**, *5*, 112–118.

(70) Hou, D. *Flora Malesiana - Ser. 1, Spermatophyta* **1957**, *5*, 429–493.

(71) Juncosa, A. M.; Tomlinson, P. B. *Ann. Missouri Bot. Gard.* **1988**, *75*, 1278–1295.

(72) Sheue, C. R.; Chesson, P.; Chen, Y. J.; Wu, S. Y.; Wu, Y. H.; Yong, J. W. H.; Guu, T. Y.; Lim, C. L.; Randrianasolo, R. M. A.; Razanajatovo, M. H.; Yang, Y. P. *Bot. J. Linn. Soc.* **2013**, *172*, 449–464.

(73) Setoguchi, H.; Kosuge, K.; Tobe, H. *J. Plant Res.* **1999**, *112*, 443–455.

(74) Matthews, M. L.; Endress, P. K. *Bot. J. Linn. Soc.* **2011**, *166*, 331–416.

(75) Ong, H. C.; Lina, E.; Milow, P. *Stud. Ethno-Medicine* **2012**, *6*, 207–211.

(76) Abed, S. A.; Sirat, H. M.; Zulkifli, R. M. *Phytochem. Lett.* **2015**, *13*, 20–29.

(77) Abed, S. A.; Sirat, H. M. *J. Teknol.* **2016**, *78*, 15–18.

(78) Abed, S.A.; Structural Elucidation and Bioactivity Evaluation of Phytochemicals from *Pellacalyx Saccardianus* Scortech and *Gynotroches Axillaris* Blume. PhD Thesis, University Teknologi Malaysia: Johor, Malaysia, 2015.

(79) Arbain, D.; Wiryani, R. D.; Sargent, M. V. *Aust. J. Chem.* **1991**, *44*, 1013–1015.

(80) Kuthi, N. A.; Sirat, H. M. *eProceed. Chem.* **2017**, *2*, 18–26.

(81) Ahmad Kuthi, N.; Basar, N. *Mal. J. Fund. Appl. Sci.* **2019**, *15*, 394–397.

(82) Glaser, R.; Hug, P.; Drouin, M.; Michelc, A. *J. Chem. Soc. Perkin Trans.* **1992**, *2*, 1071–1079.

(83) Siddiqui, S.; Sultana, N.; Ahmed, S. S.; Haider, S. I. *J. Nat. Prod.* **1986**, *49*, 511–513.

(84) Naqvi, A. A.; Mandal, S.; Verma, R. K. *Phytochem. Anal.* **1998**, *9*, 168–170.

(85) Zanolari, B.; Guilet, D.; Marston, A.; Queiroz, E. F.; De Queiroz Paulo, M.; Hostettmann, K. *J. Nat. Prod.* **2005**, *68*, 1153–1158.

(86) Paulsen, H.; Todt, K. *Angew. Chem. Int. Ed.* **1966**, *5*, 899–900.

(87) Tantisewie, B., Pharadai, T., Pandhuganont, M., Guinaudeau, H., Freyer, A. J.; Shamma, M. *J. Nat. Prod.* **1989**, *52*, 652–654.

(88) Büchi, G.; Gould, S. J.; Näf, F. *J. Am. Chem. Soc.* **1971**, *93*, 2492–2501.

(89) Yang, B. Y.; Xia, Y. G.; Wang, Q. H.; Dou, D. Q.; Kuang, H. X. *Fitoterapia* **2010**, *81*, 1003–1005.

(90) Moradi-Afrapoli, F.; Yassa, N.; Zimmermann, S.; Saeidnia, S.; Hadjiakhoondi, A.; Ebrahimi, S. N.; Hamburger, M. *Nat. Prod. Commun.* **2012**, *7*, 753–755.

(91) Razzakov, N. A.; Aripova, S. F. *Chem. Nat. Compd.* **2004**, *40*, 54–55.

(92) Gilbert, B.; Duarte, A. P.; Nakagawa, Y.; Joule, J. A.; Flores, S. E.; Aguayo Brissolese, J.; Campello, J.; Carrazzoni, E. P.; Owellen, R. J.; Blossey, E. C.; Brown Jr., K. S.; Djerassi, C. *Tetrahedron* **1965**, *21*, 1141–1166.

(93) Bastida, J.; Viladomat, F.; Llabres, J. M.; Codina, C.; Feliz, M.; Rubiralta, M. *Phytochemistry* **1987**, *26*, 1519–1524.

(94) El Sayed, K. A.; Hamann, M. T.; Abd El-Rahman, H. A.; Zaghloul, A. M. *J. Nat. Prod.* **1998**, *61*, 848–850.

(95) Fisch, M. H.; Gramain, J. C.; Oleson, J. A. *Chem. Commun.* **1970**, *1*, 13–14.

(96) Al-said, M. S.; Evans, W. C.; Grout, R. J. *Phytochemistry* **1986**, *25*, 851–853.

(97) Yeom, C. E.; Kim, M. J.; Kim, B. M. *Tetrahedron* **2007**, *63*, 904–909.

(98) Duan, Z.; Xuan, X.; Li, T.; Yang, C.; Wu, Y. *Tetrahedron Lett.* **2006**, *47*, 5433–5436.

(99) Yadav, J. S.; Ramesh Reddy, A.; Gopal Rao, Y.; Narsaiah, A. V.; Subba Reddy, B. V. *Synthesis.* **2007**, (22), 3447–3450.

(100) Ali, M. S.; Tezuka, Y.; Awale, S.; Banskota, A. H.; Kadota, S. *J. Nat. Prod.* **2001**, *64*, 289–293.

(101) Liu, H.; Wang, X.; Shi, Q.; Li, L.; Zhang, Q.; Wu, Z. L.; Huang, X. J.; Zhang, Q. W.; Ye, W. C.; Wang, Y.; Shi, L. *ACS Omega* **2020**, *5*, 10167–10175.

(102) Kuo, Y. H.; Ou, J. C.; Lee, K. H.; Chen, C. F. *J. Nat. Prod.* **1995**, *58*, 1103–1108.

(103) Liu, J.; Nakamura, S.; Matsuda, H.; Yoshikawa, M. *Tetrahedron Lett.* **2013**, *54*, 32–34.

(104) Fajardo, V.; Araya, M.; Cuadra, P.; Oyarzun, A.; Gallardo, A.; Cueto, M.; Diaz-Marrero, A. R.; Darias, J.; Villarroel, L.; Álvarez, C.; Mora-Pérez, Y.; Joseph-Nathan, P. *J. Nat. Prod.* **2009**, *72*, 1355–1356.

(105) Schuster, D. I.; Curran, W. V. *J. Org. Chem*. **1970**, *35*, 4192–4201.

(106) Yamaguchi, K.; Mori, K.; Mizugaki, T.; Ebitani, K.; Kaneda, K. *J. Org. Chem.* **2000**, *65*, 6897–6903.

(107) Hoye, T. R.; Ayyad, S. N.; Beckord, H. J.; Brown, S. G. *Nat. Prod. Commun.* **2013**, *8*, 351–358.

(108) Kang, K. Bin; Park, E. J.; Kim, J.; Sung, S. H. *J. Nat. Prod.* **2017**, *80*, 2778–2786.

(109) Kamiya, S.; Esaki, S.; Konishi, F. *Agr. Biol. Chem.* **1972**, *36*, 1461–1466.

(110) Backinowsky, L. V.; Balan, N. F.; Shashkov, A. S.; Kochetkov, N. K. *Carbohydr. Res.* **1980**, *84*, 225–235.

(111) Tanaka, T.; Nakashima, T.; Ueda, T.; Tomii, K.; Kouno, I. *Chem. Pharm. Bull.* **2007**, *55*, 899–901.

(112) Bubb, W. A. *Concepts Magn. Reson. Part A Bridg. Educ. Res.* **2003**, *19*, 1–19.

(113) Chandler, B. V.; Harper, K. A. *Aust. J. Chem.* **1961**, *14*, 586–595.

(114) Seo, S.; Tomita, Y.; Tori, K.; Yoshimura, Y. *J. Am. Chem. Soc.* **1978**, *100*, 3331–3339.

(115) Giang, P. M.; Son, P. T.; Matsunami, K.; Otsuka, H. *Nat. Prod. Res.* **2012**, *26*, 1195–1200.

(116) Jiang, H.; Shen, Y.; Yasuda, E.; Chiba, M.; Terazawa, M. *Eurasian J. For. Res.* **2001**, *3*, 49–54.

(117) Gilli, C.; Orlowska, E.; Kaiser, D.; Steyrer, J.; Rathgeb, A.; Lorbeer, E.; Brecker, L.; Schinnerl, J. *Biochem. Syst. Ecol.* **2014**, *56*, 178–184.

(118) Park, D.; Kim, H. J.; Jung, S. Y.; Yook, C. S.; Jin, C.; Lee, Y. S. *Chem. Pharm. Bull.* **2010**, *58*, 238–241.

(119) Loong, B. J.; Tan, J. H.; Lim, K. H.; Mbaki, Y.; Ting, K. N. *Naunyn-Schmiedebergs. Arch. Pharmacol.* **2015**, *388*, 1061–1067.

(120) Janssen, L. J.; Wattie, J.; Lu-Chao, H.; Tazzeo, T. *J. Appl. Physiol.* **2001**, *91*, 1142–1151.

(121) Baker, K. E.; Bonvini, S. J.; Donovan, C.; Foong, R. E.; Han, B.; Jha, A.; Shaifta, Y.; Smit, M.; Johnson, J. R.; Moir, L. M. *Pulm. Pharmacol. Ther.* **2014**, *29*, 181–198.

(122) Barlow, R. B.; Franks, F. Specificity of Some Ganglion Stimulants. *Br. J. Pharmacol.* **1971**, *42*, 137–142.

(123) Terry, A. V.; Williamson, R.; Gattu, M.; Beach, J. W.; McCurdy, C. R.; Sparks, J. A.; Pauly, J. R. *Neuropharmacology* **1998**, *37*, 93–102.

(124) Cherkez, S.; Yellin, H.; Kashman, Y.; Yaavetz, B.; Sokolovsky, M. *Mol. Pharmacol.* **1978**, *14*, 781–786.

(125) Cherkez, S.; Yellin, H.; Kashman, Y.; Yaavetz, B.; Sokolovsky, M. *J. Med. Chem.* **1979**, *22*, 18–21.

(126) Mi, Q.; Cui, B.; Silva, G. L.; Lantvit, D.; Lim, E.; Chai, H.; You, M.; Hollingshead, M. G.; Mayo, J. G.; Kinghorn, A. D.; Pezzuto, J. M. *Cancer Res.* **2001**, *61*, 4030–4037.

(127) Chávez, D.; Cui, B.; Chai, H. B.; García, R.; Mejía, M.; Farnsworth, N. R.; Cordell, G. A.; Pezzuto, J. M.; Kinghorn, A. D. *J. Nat. Prod.* **2002**, *65*, 606–610.

(128) Dong, G. Z.; Jeong, J. H.; Lee, Y. I.; Lee, S. Y.; Zhao, H. Y.; Jeon, R.; Lee, H. J.; Ryu, J. H. *Arch. Pharm. Res.* **2017**, *40*, 509–517.

(129) Er, J. L.; Goh, P. N.; Lee, C. Y.; Tan, Y. J.; Hii, L. W.; Mai, C. W.; Chung, F. F. L.; Leong, C. O. *Apoptosis* **2018**, *23*, 343–355.

(130) Bailey, P.; Chang, D. K.; Nones, K.; Johns, A. L.; Patch, A. M.; Gingras, M. C.; Miller, D. K.; Christ, A. N.; Bruxner, T. J. C.; Quinn, M. C.; Nourse, C.; Murtaugh, L.C.; Harliwong, I.; Idrisoglu, S.; Manning, S.; Nourbakhsh, E.; Wani, S.; Fink, L.; Holmes, O.; Chin, V.; Anderson, M. J.; Kazakoff, S.; Leonard, C.; Newell, F.; Waddell, N.; Wood, S.; Xu, Q.; Wilson, P. J.; Cloonan, N.; Kassahn, K. S.; Taylor, D.; Quek, K.; Robertson, A.; Pantano, L.; Mincarelli, L.; Sanchez, L. N.; Evers, L.; Wu, J.; Pinese, M.; Cowley, M. J.; Jones, M. D.; Colvin, E. K.; Nagrial, A. M.; Humphrey, E. S.; Chantrill, L. A.; Mawson, A.; Humphris, J.; Chou, A.; Pajic, M.; Scarlett, C. J.; Pinho, A. V.; Giry-Laterriere, M.; Rooman, I.; Samra, J. S.; Kench, J. G.; Lovell, J. A.; Merrett, N. D.; Toon, C. W.; Epari, K.; Nguyen, N. Q.; Barbour, A.; Zeps, N.; Moran-Jones, K.; Jamieson, N. B.; Graham, J. S.; Duthie, F.; Oien, K.; Hair, J.; Grützmann, R.; Maitra, A.; Iacobuzio-Donahue, C. A.; Wolfgang, C. L.; Morgan, R. A.; Lawlor, R. T.; Corbo, V.; Bassi, C.; Rusev, B.; Capelli, P.; Salvia, R.; Tortora, G.; Mukhopadhyay, D.; Petersen, G. M.; Australian Pancreatic Cancer Genome Initiative; Munzy, D. M.; Fisher, W. E.; Karim, S. A.; Eshleman, J. R.; Hruban, R. H.; Pilarsky, C.; Morton, J.P.; Sansom, O. J.; Scarpa, A.; Musgrove, E. A.; Bailey, U. H.; Hofmann, O.; Sutherland, R. L.; Wheeler, D.A.; Gill, A. J.; Gibbs, R. A.; Pearson, J.V.; Waddell, N.; Biankin, A.V.; Grimmond, S.M. *Nature* **2016**, *531*, 47–52.

(131) Oberstein, P. E.; Olive, K. P. *Therap Adv Gastroenterol.* **2013**, *6*, 321–337.

(132) Zeng, S.; Pöttler, M.; Lan, B.; Grützmann, R.; Pilarsky, C.; Yang, H. *Int. J. Mol. Sci.* **2019**, *20*, 4504.

(133) Mota, A. D. L.; Evangelista, A. F.; Macedo, T.; Oliveira, R.; Scapulatempo-Neto, C.; Vieira, R. A. D. C.; Marques, M. M. C. *Oncol. Lett.* **2017**, *13*, 4708–4712.

(134) Chavez, K. J.; Garimella, S. V.; Lipkowitz, S. *Breast Dis* **2012**, *32*, 35–48.

(135) Xu, L.; Yin, S.; Reddy, K. B. *Mol Cancer Ther.* **2011**, *10*, 550–557.

(136) Heller, L.; Schwarz, S.; Perl, V.; Köwitsch, A.; Siewert, B.; Csuk, R. *Eur. J. Med. Chem.* **2015**, *101*, 391–399.

(137) Gersch, M.; Kreuzer, J.; Sieber, S. A. *Nat. Prod. Rep.* **2012**, *29*, 659–682.

(138) Gan, F. F.; Kaminska, K. K.; Yang, H.; Liew, C. Y.; Leow, P. C.; So, C. L.; Tu, L. N. L.; Roy, A.; Yap, C. W.; Kang, T. S.; Chui, W. K.; Chew, E. H. *Antioxid. Redox. Signal.* **2013**, *19*, 1149–1165.

(139) Sherma, J.; Fried, B. *Handbook of Thin-Layer Chromatography*; Marcel Dekker: New York, 2003; pp 73–74.

(140) Gottlieb, H. E.; Kotlyar, V.; Nudelman, A. *J. Org. Chem.* **1997**, *62*, 7512–7515.

(141) Fulmer, G. R.; Miller, A. J. M.; Sherden, N. H.; Gottlieb, H. E.; Nudelman, A.; Stoltz, B. M.; Bercaw, J. E.; Goldberg, K. I. *Organometallics* **2010**, *29*, 2176–2179.

(142) Bruhn, T., Schaumlö el, A., Hemberger, Y. **2015**. SpecDis, Version 1.64. University of Wuerzburg, Germany.

(143) Preuss, J. M. H.; Goldie, R. G. *Eur. J. Pharmacol.* **1999**, *372*, 269–277.

Appendices

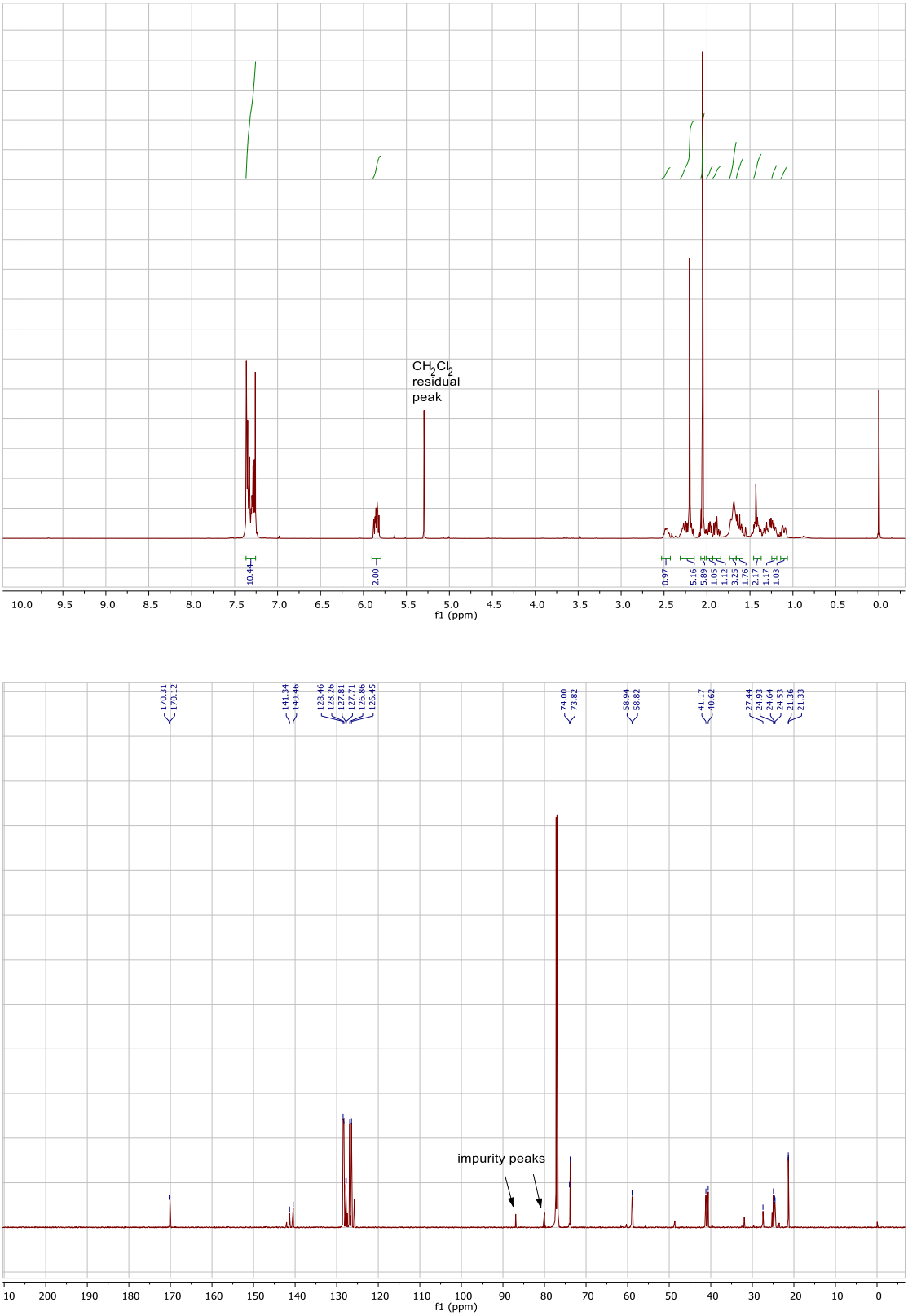

Appendix 1: ^{1}H and ^{13}C NMR Spectra of Hippofoline A (**1**).

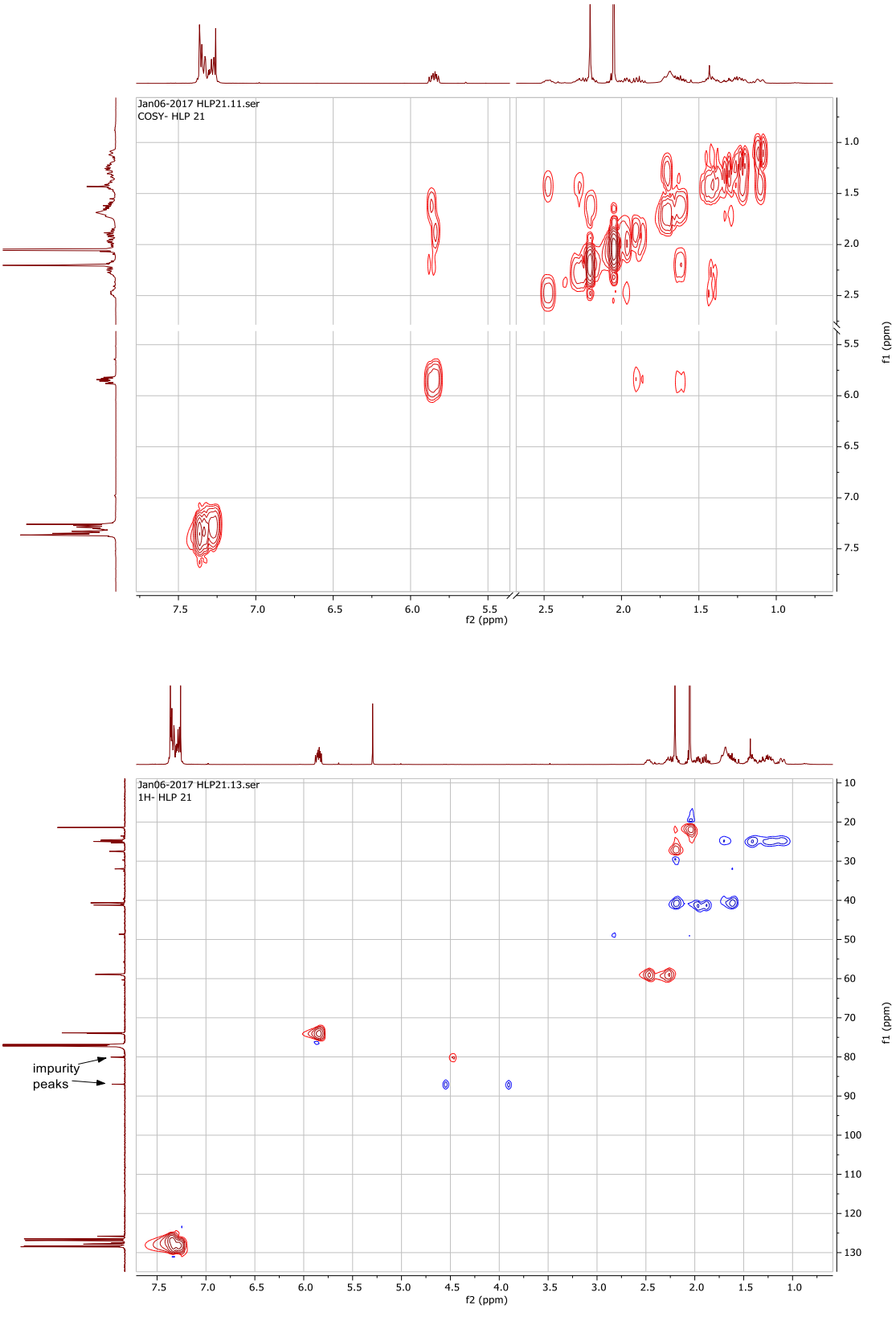

Appendix 2: COSY and HSQC Spectra of Hippofoline A (**1**).

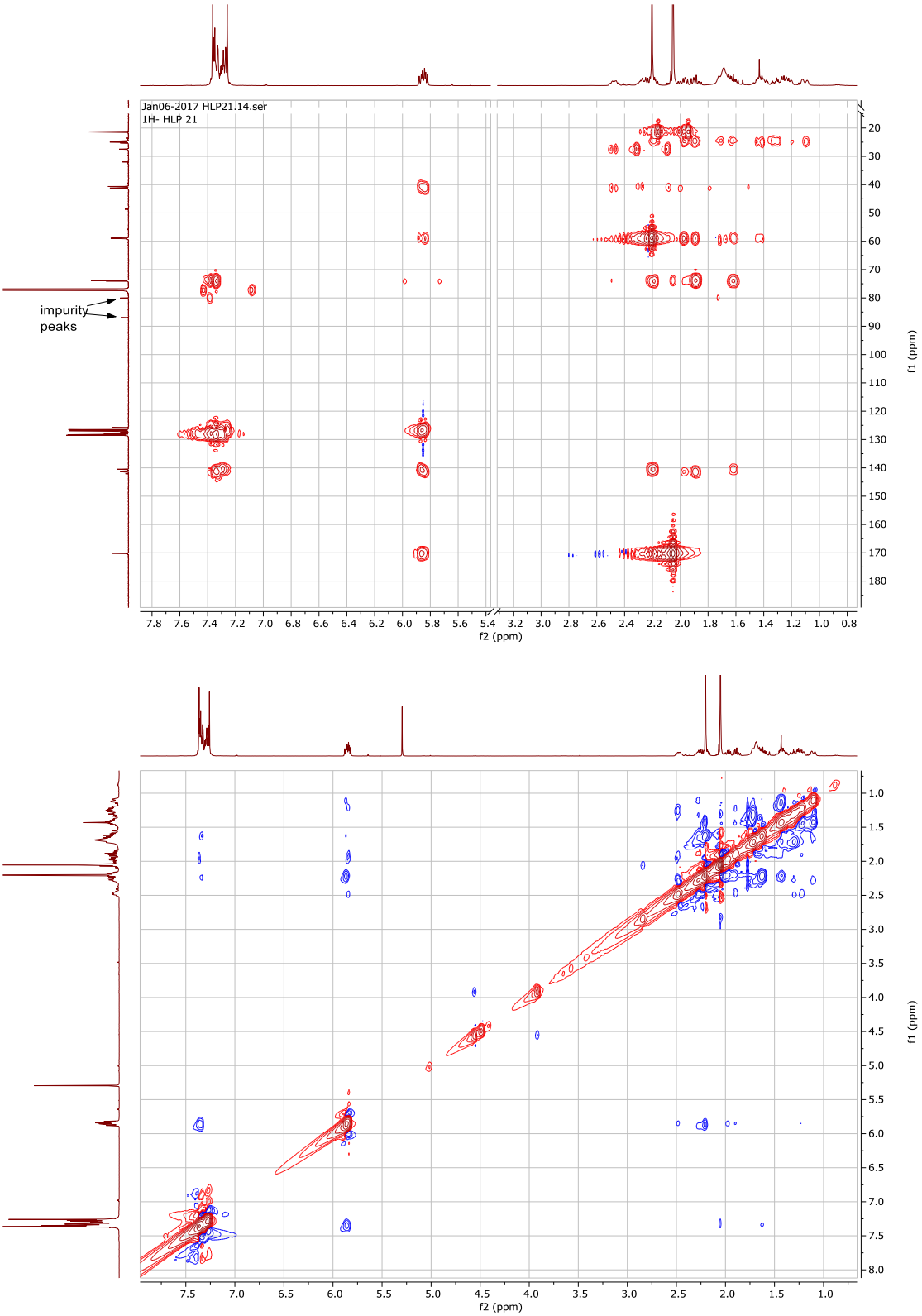

Appendix 3: HMBC and NOESY Spectra of Hippofoline A (**1**).

Data:HLP3
Sample Name:
Description:
Ionization Mode:ESI+
History:Determine m/z[Peak Detect[Centroid,30,Area];Correct Base[0.5%]];Correct Ba...

Acquired:2/24/2016 6:47:03 PM
Operator:AccuTOF
Mass Calibration data:Calibration2
Created:3/2/2016 3:46:20 PM
Created by:AccuTOF

Charge number:1 Tolerance:30.00(ppm), 5.00 .. 15.00(mmu) Unsaturation Number:0.0 .. 25.0 (Fractio...
Element:^{12}C:0 .. 50, ^{1}H:0 .. 50, ^{14}N:1 .. 10, ^{16}O:0 .. 20

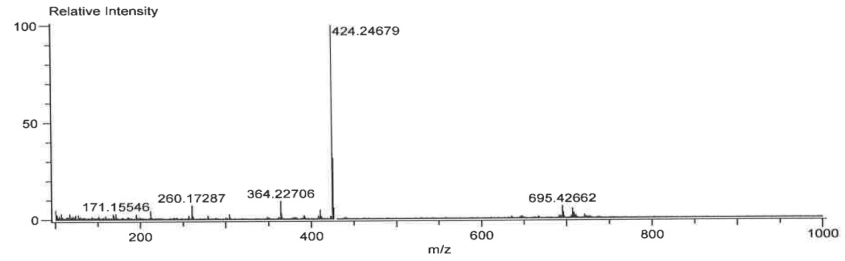

Mass	Intensity	Calc. Mass	Mass Difference (mmu)	Mass Difference (ppm)	Possible Formula
424.24679	150386.78	424.24744	-0.65	-1.54	$^{12}C_{24}{}^{1}H_{32}{}^{14}N_{4}{}^{16}O_{3}$
		424.24610	0.69	1.62	$^{12}C_{22}{}^{1}H_{30}{}^{14}N_{7}{}^{16}O_{2}$
		424.24878	-2.00	-4.71	$^{12}C_{26}{}^{1}H_{34}{}^{14}N_{1}{}^{16}O_{4}$
		424.24476	2.03	4.77	$^{12}C_{21}{}^{1}H_{34}{}^{14}N_{3}{}^{16}O_{6}$
		424.24475	2.03	4.79	$^{12}C_{20}{}^{1}H_{28}{}^{14}N_{10}{}^{16}O_{1}$
		424.25012	-3.33	-7.86	$^{12}C_{27}{}^{1}H_{30}{}^{14}N_{5}$
		424.24342	3.37	7.94	$^{12}C_{19}{}^{1}H_{32}{}^{14}N_{6}{}^{16}O_{5}$
		424.25063	-3.84	-9.06	$^{12}C_{13}{}^{1}H_{32}{}^{14}N_{10}{}^{16}O_{6}$
		424.25146	-4.68	-11.03	$^{12}C_{29}{}^{1}H_{32}{}^{14}N_{2}{}^{16}O_{1}$
		424.24208	4.71	11.09	$^{12}C_{18}{}^{1}H_{36}{}^{14}N_{2}{}^{16}O_{9}$
		424.24207	4.71	11.10	$^{12}C_{17}{}^{1}H_{30}{}^{14}N_{9}{}^{16}O_{4}$
		424.25197	-5.19	-12.22	$^{12}C_{15}{}^{1}H_{34}{}^{14}N_{7}{}^{16}O_{7}$
		424.24074	6.05	14.26	$^{12}C_{16}{}^{1}H_{34}{}^{14}N_{5}{}^{16}O_{8}$
		424.25331	-6.53	-15.39	$^{12}C_{17}{}^{1}H_{36}{}^{14}N_{4}{}^{16}O_{8}$
		424.23939	7.39	17.42	$^{12}C_{14}{}^{1}H_{32}{}^{14}N_{8}{}^{16}O_{7}$
		424.25465	-7.87	-18.54	$^{12}C_{18}{}^{1}H_{32}{}^{14}N_{8}{}^{16}O_{4}$
		424.25466	-7.87	-18.55	$^{12}C_{19}{}^{1}H_{38}{}^{14}N_{1}{}^{16}O_{9}$
		424.23889	7.90	18.62	$^{12}C_{28}{}^{1}H_{30}{}^{14}N_{3}{}^{16}O_{1}$
		424.25599	-9.21	-21.70	$^{12}C_{20}{}^{1}H_{34}{}^{14}N_{5}{}^{16}O_{5}$
		424.23754	9.24	21.78	$^{12}C_{26}{}^{1}H_{28}{}^{14}N_{6}$
		424.25733	-10.55	-24.86	$^{12}C_{21}{}^{1}H_{30}{}^{14}N_{9}{}^{16}O_{1}$
		424.25734	-10.55	-24.87	$^{12}C_{22}{}^{1}H_{36}{}^{14}N_{2}{}^{16}O_{9}$
		424.23621	10.58	24.94	$^{12}C_{25}{}^{1}H_{32}{}^{14}N_{2}{}^{16}O_{4}$
		424.25867	-11.89	-28.02	$^{12}C_{23}{}^{1}H_{32}{}^{14}N_{8}{}^{16}O_{2}$
		424.23486	11.92	28.10	$^{12}C_{23}{}^{1}H_{30}{}^{14}N_{5}{}^{16}O_{3}$

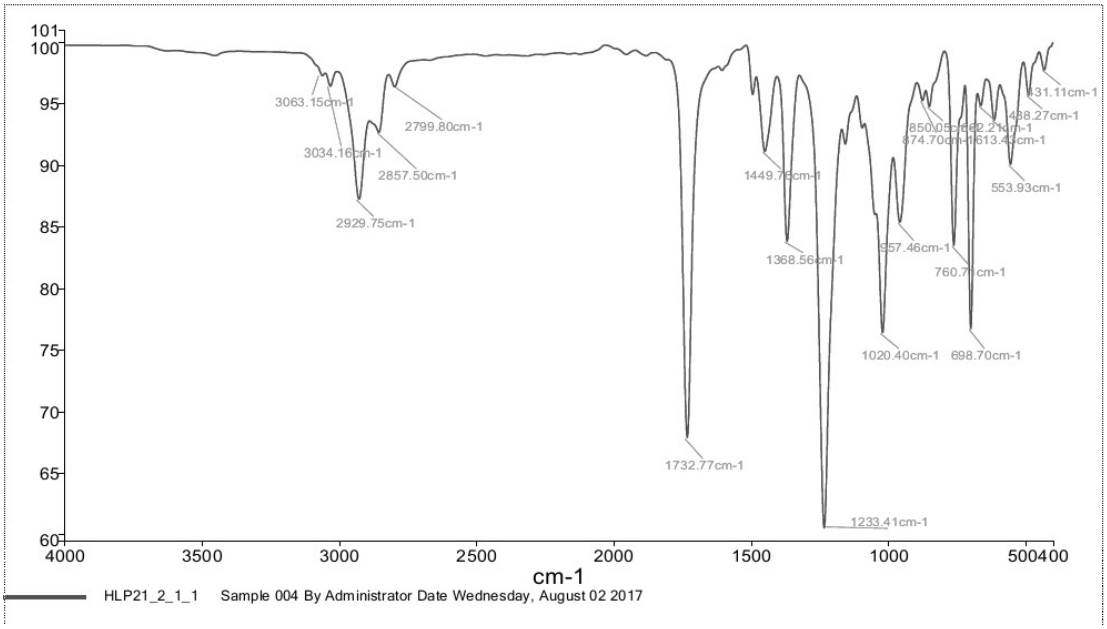

Appendix 4: HRDARTMS and IR Spectra of Hippofoline A (**1**).

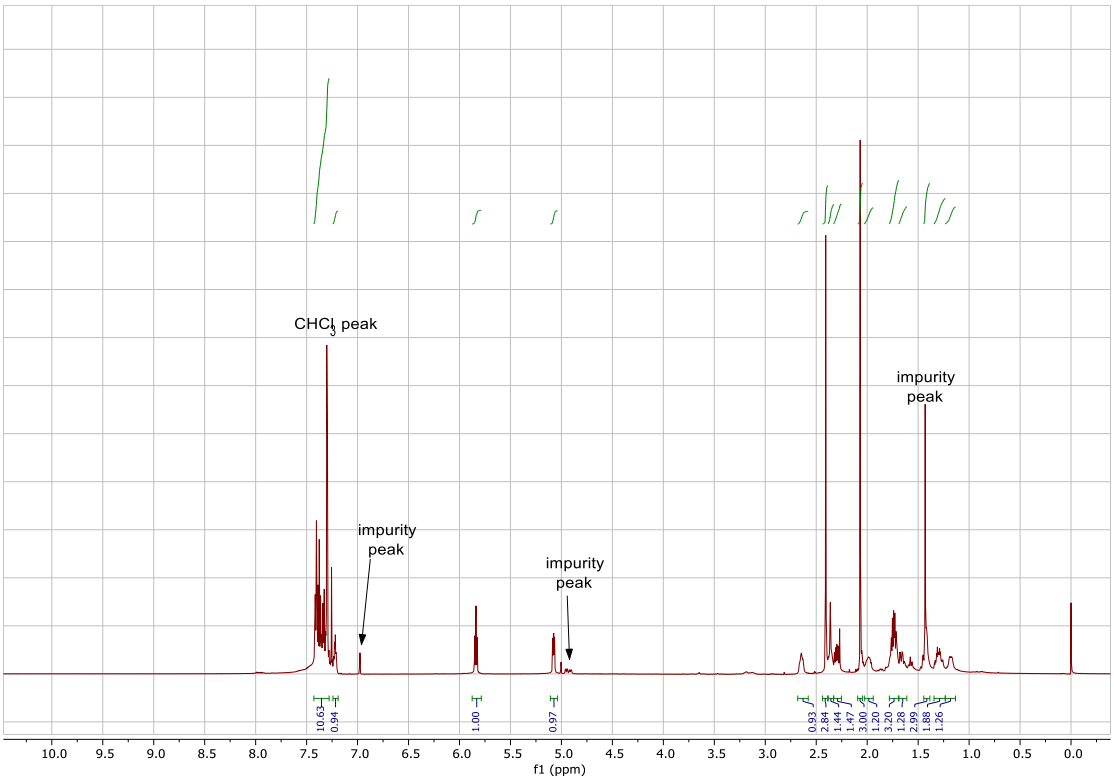

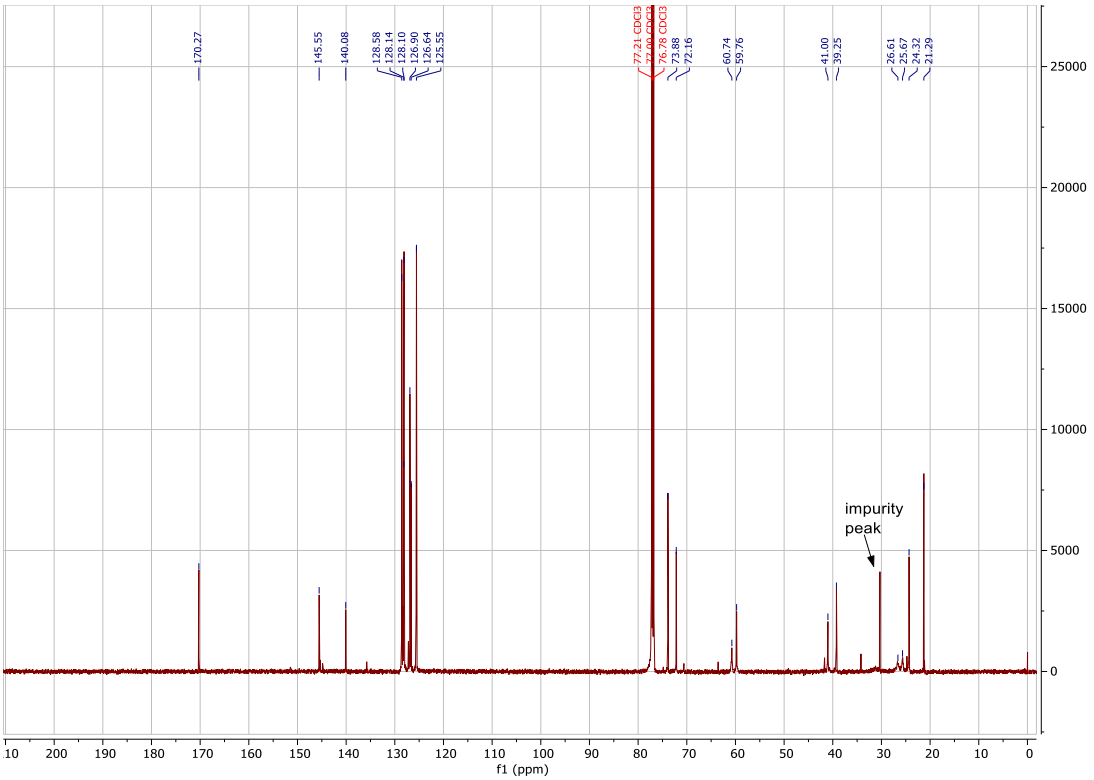

Appendix 5: ^{1}H and ^{13}C NMR Spectra of Hippofoline B (**2**).

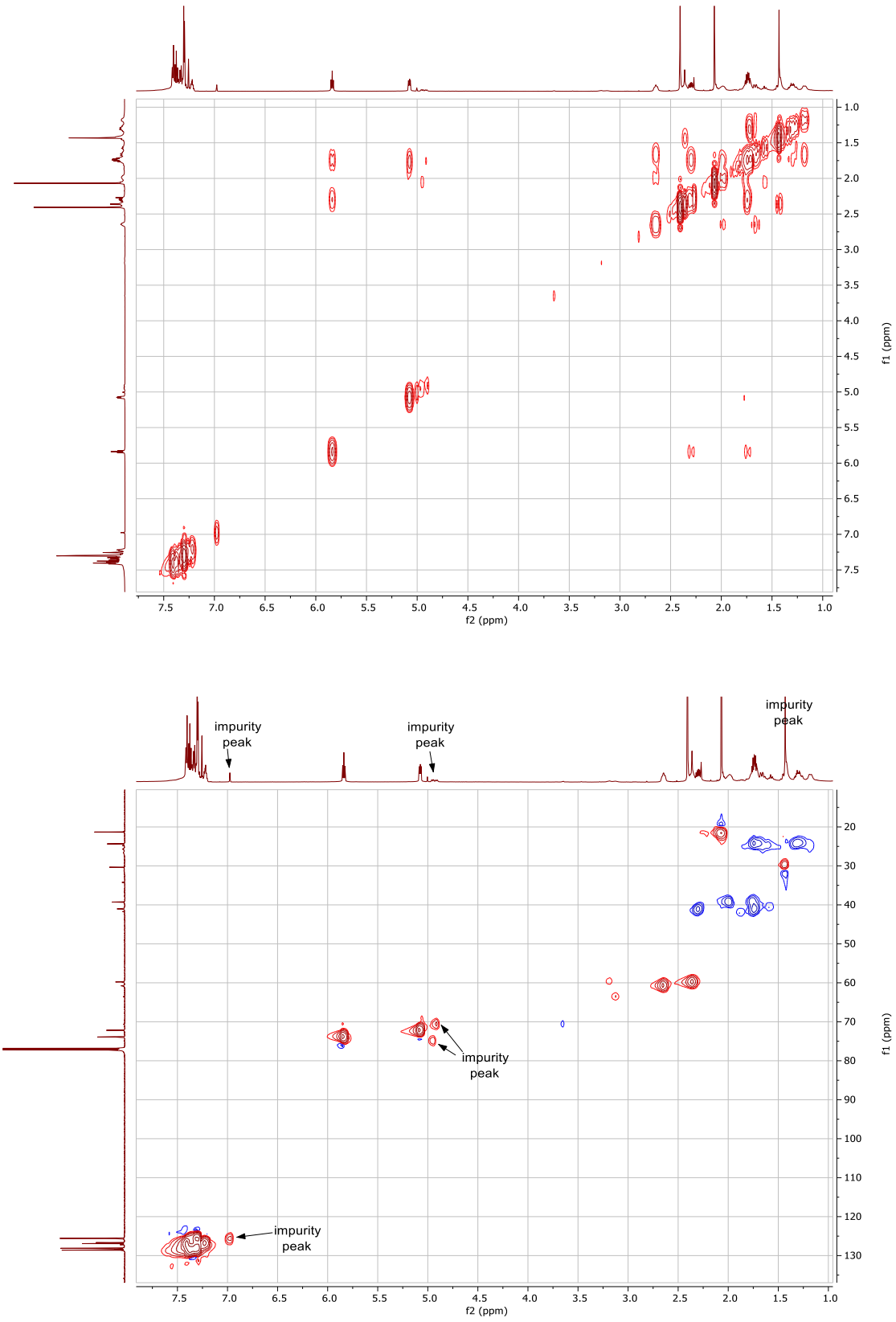

Appendix 6: COSY and HSQC NMR Spectra of Hippofoline B (**2**).

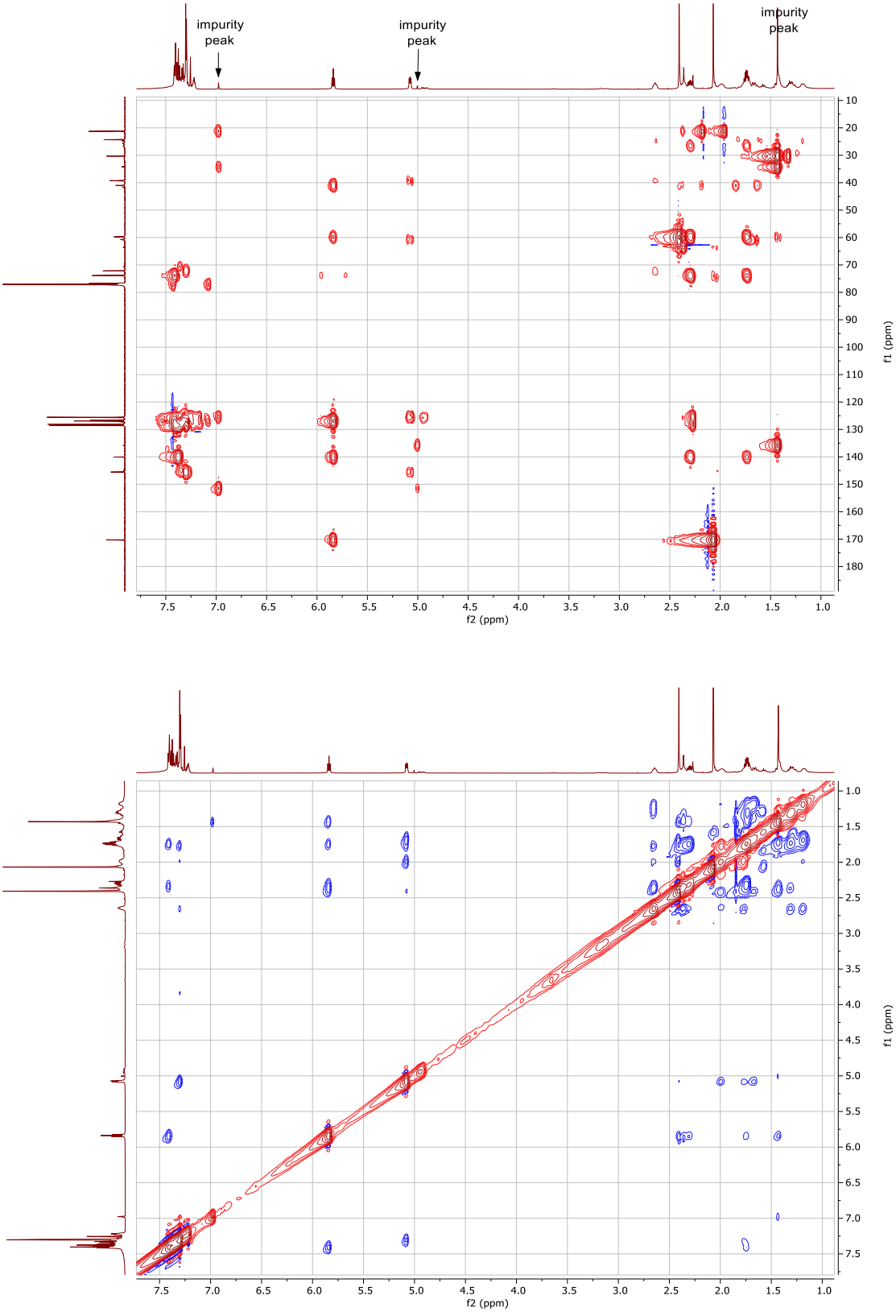

Appendix 7: HMBC and NOESY NMR Spectra of Hippofoline B (**2**).

Data:HLP5
Sample Name:
Description:
Ionization Mode:ESI+
History:Determine m/z[Peak Detect[Centroid,30,Area];Correct Base[0.5%]];Correct Ba...

Acquired:5/9/2016 12:00:46 PM
Operator:AccuTOF
Mass Calibration data:Calibration3
Created:5/9/2016 2:32:03 PM
Created by:AccuTOF

Charge number:1 Tolerance:30.00(ppm), 5.00 .. 15.00(mmu) Unsaturation Number:0.0 .. 25.0 (Fractio...
Element:^{12}C:0 .. 50, ^{1}H:0 .. 100, ^{14}N:0 .. 5, ^{16}O:0 .. 10

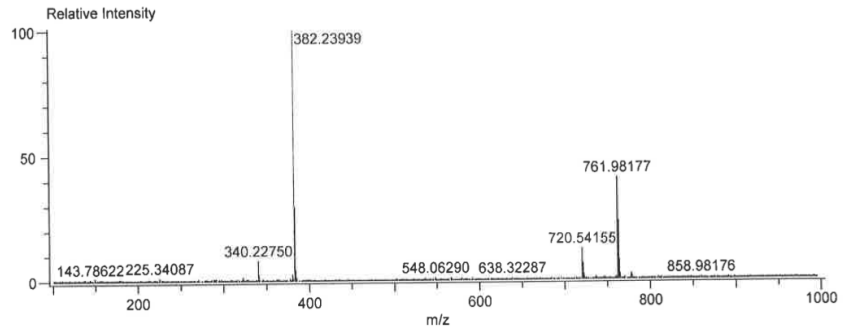

Mass	Intensity	Calc. Mass	Mass Difference (mmu)	Mass Difference (ppm)	Possible Formula
382.23939	123792.11	382.23822	1.17	3.06	$^{12}C_{24}{}^{1}H_{32}{}^{14}N_{1}{}^{16}O_{3}$
		382.24090	-1.51	-3.95	$^{12}C_{27}{}^{1}H_{30}{}^{14}N_{2}$
		382.23688	2.51	6.57	$^{12}C_{22}{}^{1}H_{30}{}^{14}N_{4}{}^{16}O_{2}$
		382.24275	-3.36	-8.80	$^{12}C_{15}{}^{1}H_{34}{}^{14}N_{4}{}^{16}O_{7}$
		382.23554	3.85	10.07	$^{12}C_{21}{}^{1}H_{34}{}^{16}O_{6}$
		382.24409	-4.70	-12.31	$^{12}C_{17}{}^{1}H_{36}{}^{14}N_{1}{}^{16}O_{8}$
		382.23420	5.19	13.58	$^{12}C_{19}{}^{1}H_{32}{}^{14}N_{3}{}^{16}O_{5}$
		382.24543	-6.04	-15.81	$^{12}C_{18}{}^{1}H_{32}{}^{14}N_{5}{}^{16}O_{4}$
		382.24677	-7.38	-19.32	$^{12}C_{20}{}^{1}H_{34}{}^{14}N_{2}{}^{16}O_{5}$
		382.23151	7.87	20.59	$^{12}C_{16}{}^{1}H_{34}{}^{14}N_{2}{}^{16}O_{8}$
		382.23017	9.21	24.11	$^{12}C_{14}{}^{1}H_{32}{}^{14}N_{5}{}^{16}O_{7}$
		382.22966	9.72	25.43	$^{12}C_{28}{}^{1}H_{30}{}^{16}O_{1}$
		382.24945	-10.06	-26.33	$^{12}C_{23}{}^{1}H_{32}{}^{14}N_{3}{}^{16}O_{2}$
		382.22832	11.06	28.95	$^{12}C_{26}{}^{1}H_{28}{}^{14}N_{3}$
		382.25079	-11.41	-29.84	$^{12}C_{25}{}^{1}H_{34}{}^{16}O_{3}$

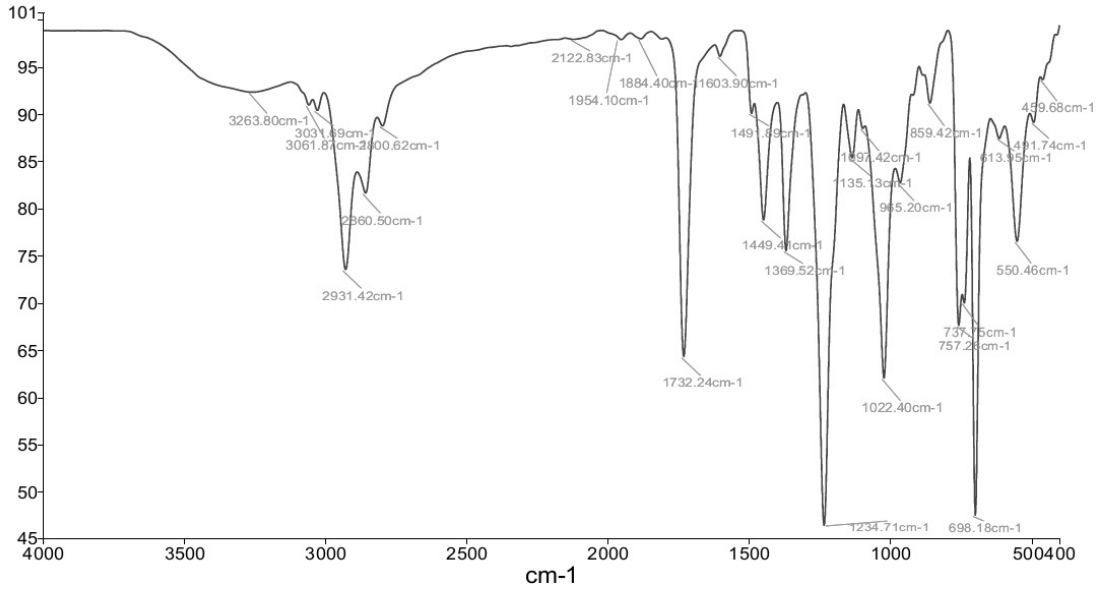

Appendix 8: HRDARTMS and IR Spectra of Hippofoline B (**2**).

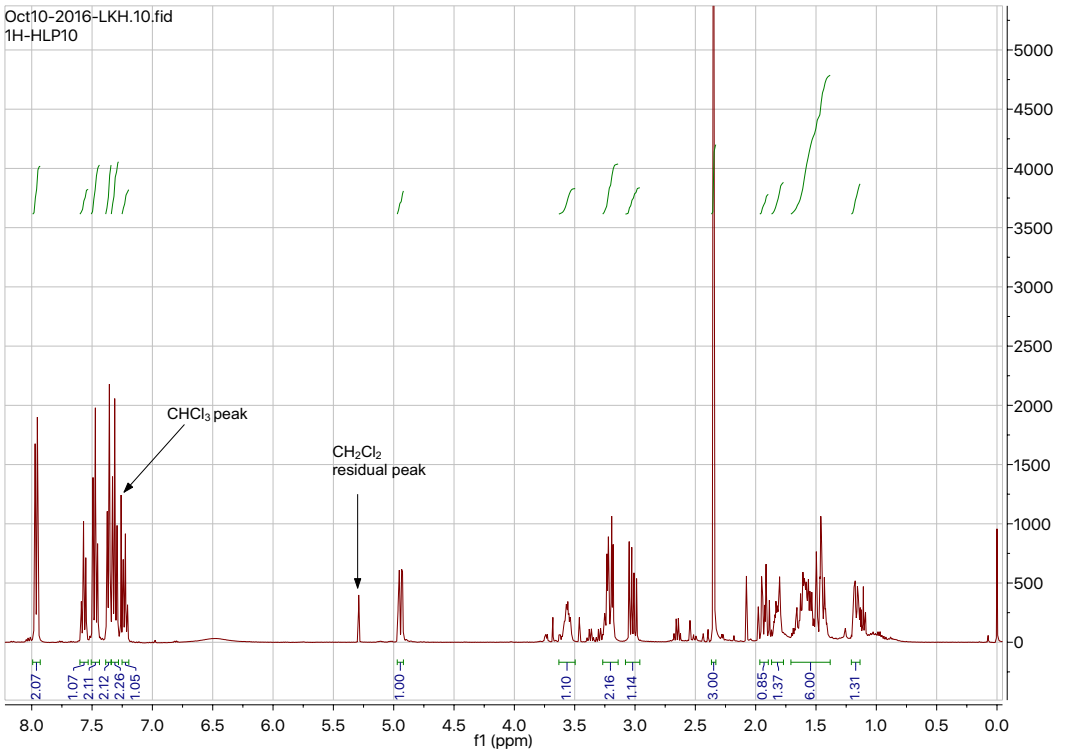

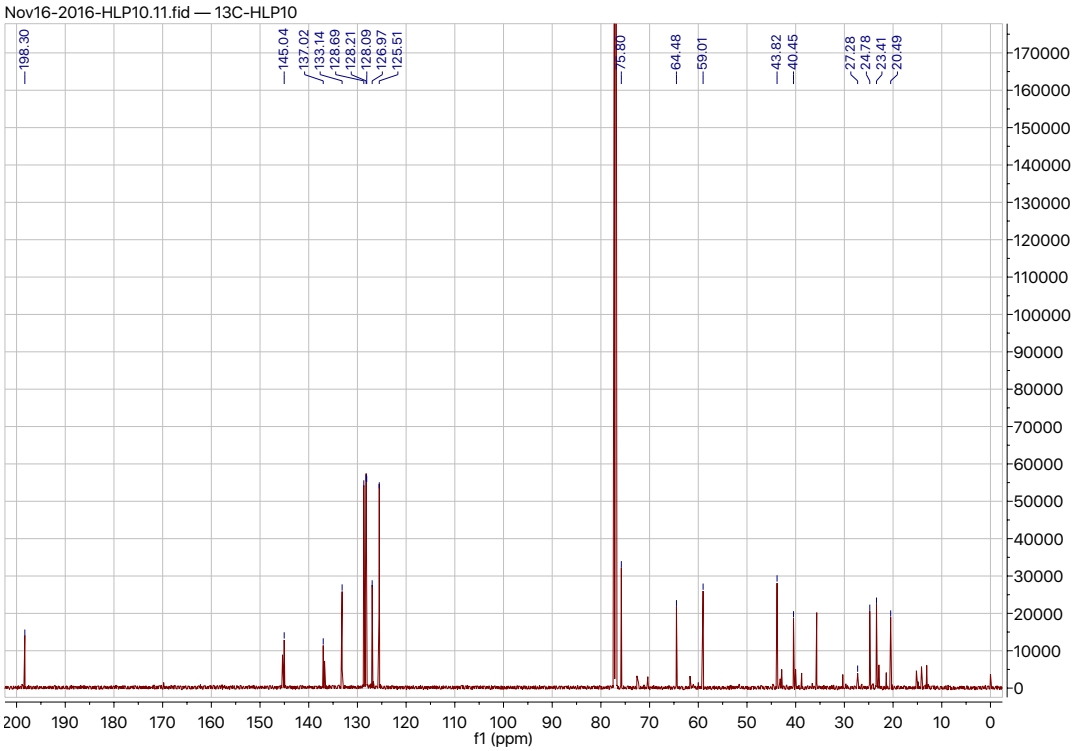

Appendix 9: ^{1}H and ^{13}C NMR Spectra of (–)-Lobeline (**3**).

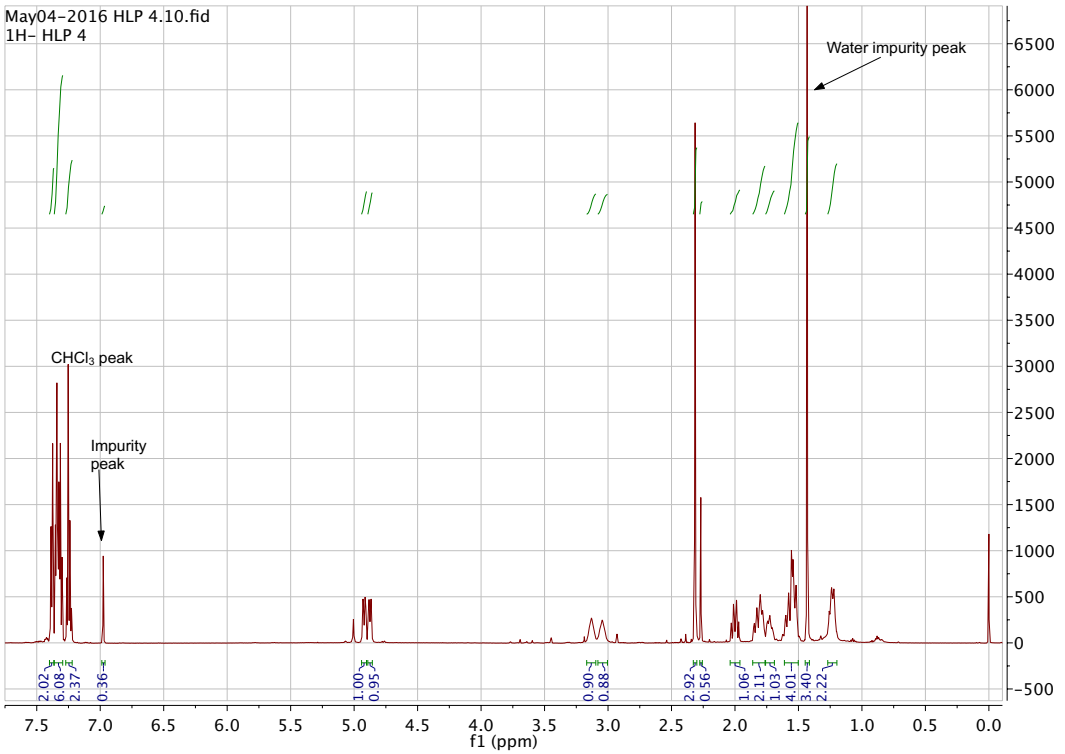

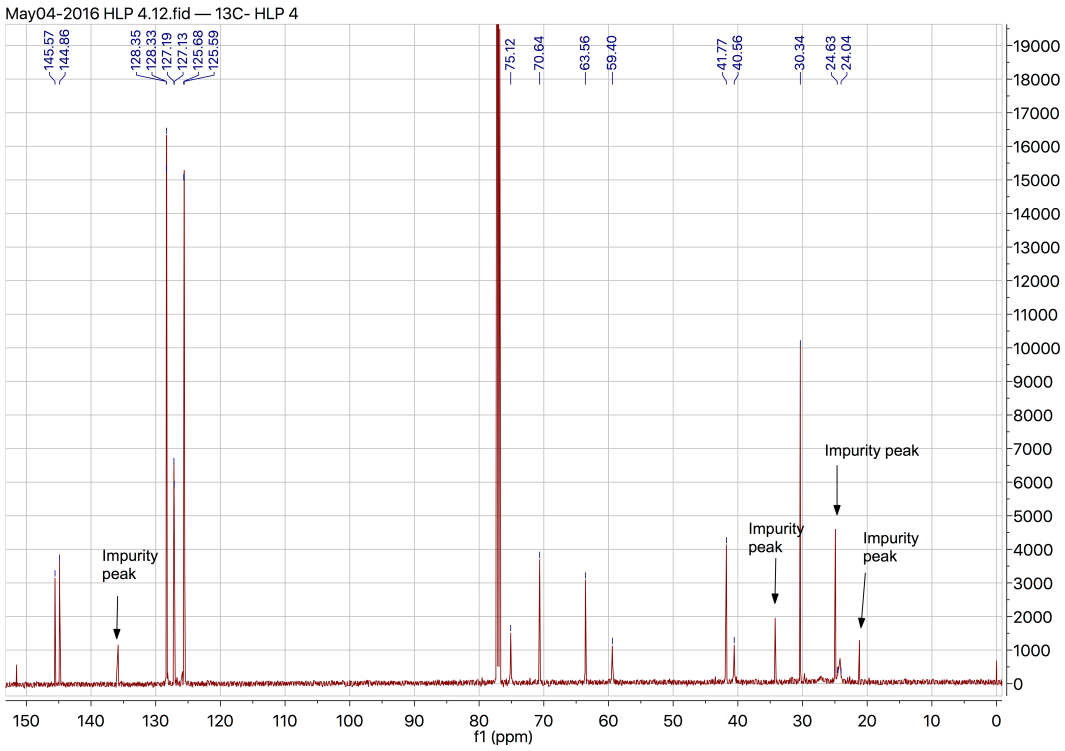

Appendix 10: ^{1}H and ^{13}C NMR Spectra of (–)-*Cis*-2′,2′′-Diphenyllobelidiol (**4**).

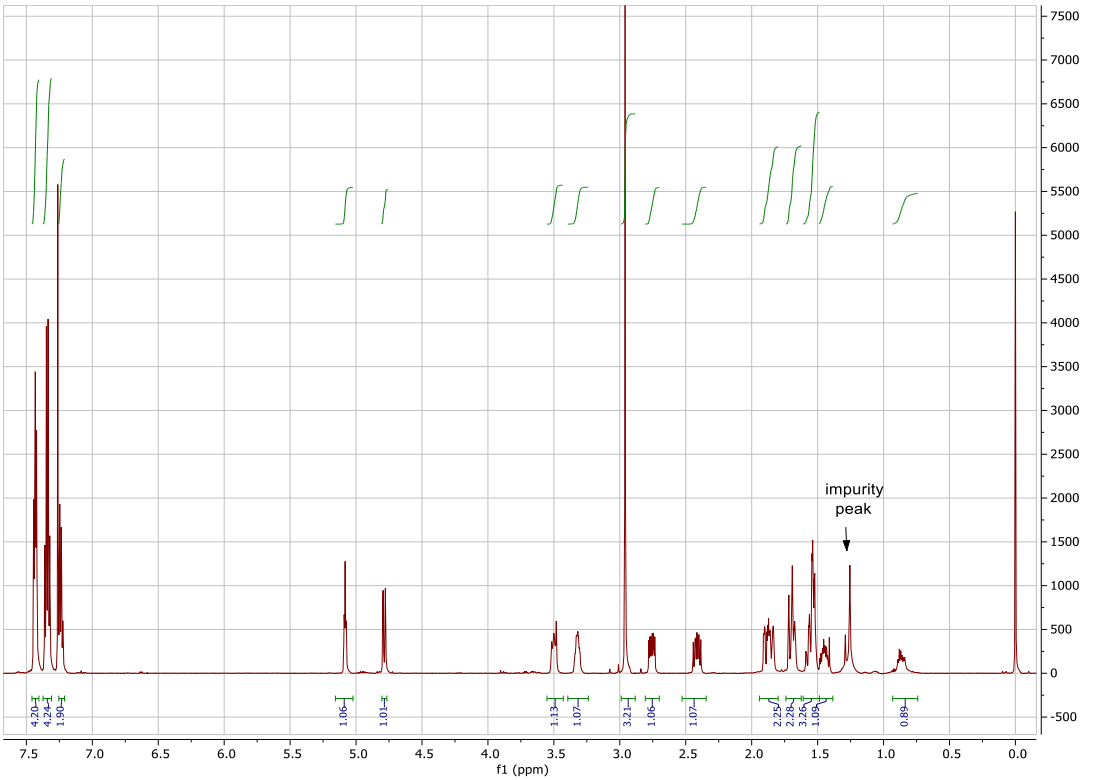

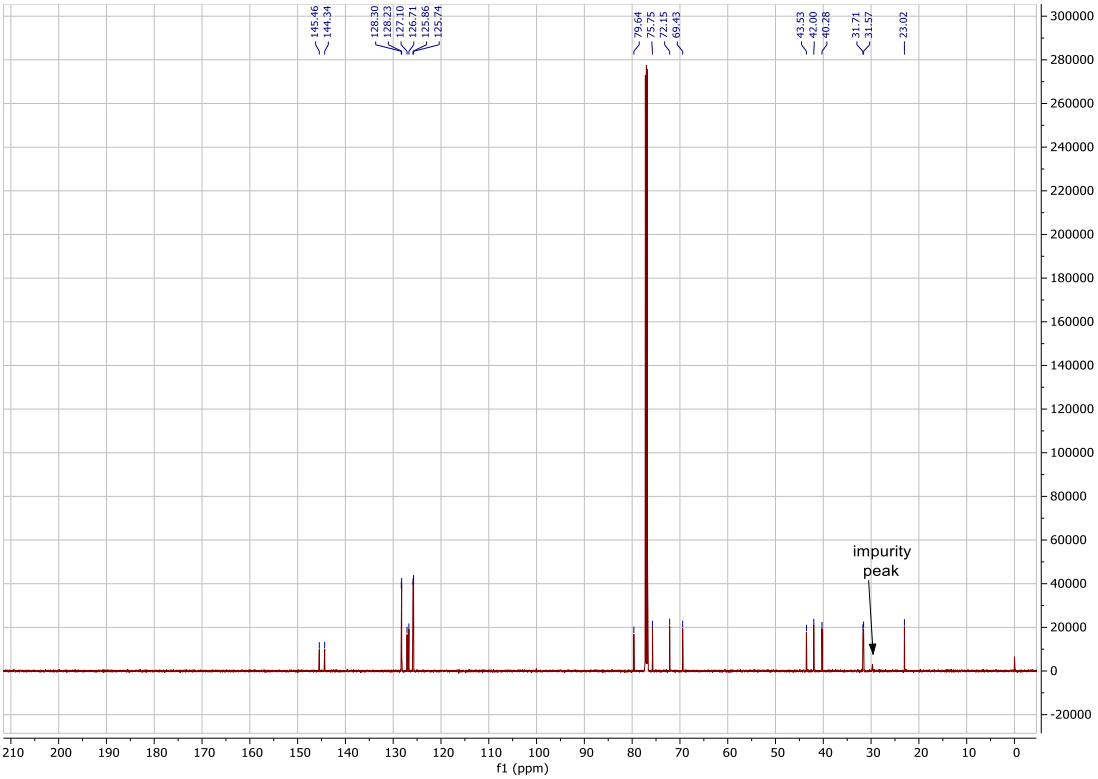

Appendix 11: ^{1}H and ^{13}C NMR Spectra of (–)-*Cis*-2′,2′′-Diphenyllobelidiol *N*-oxide (**5**).

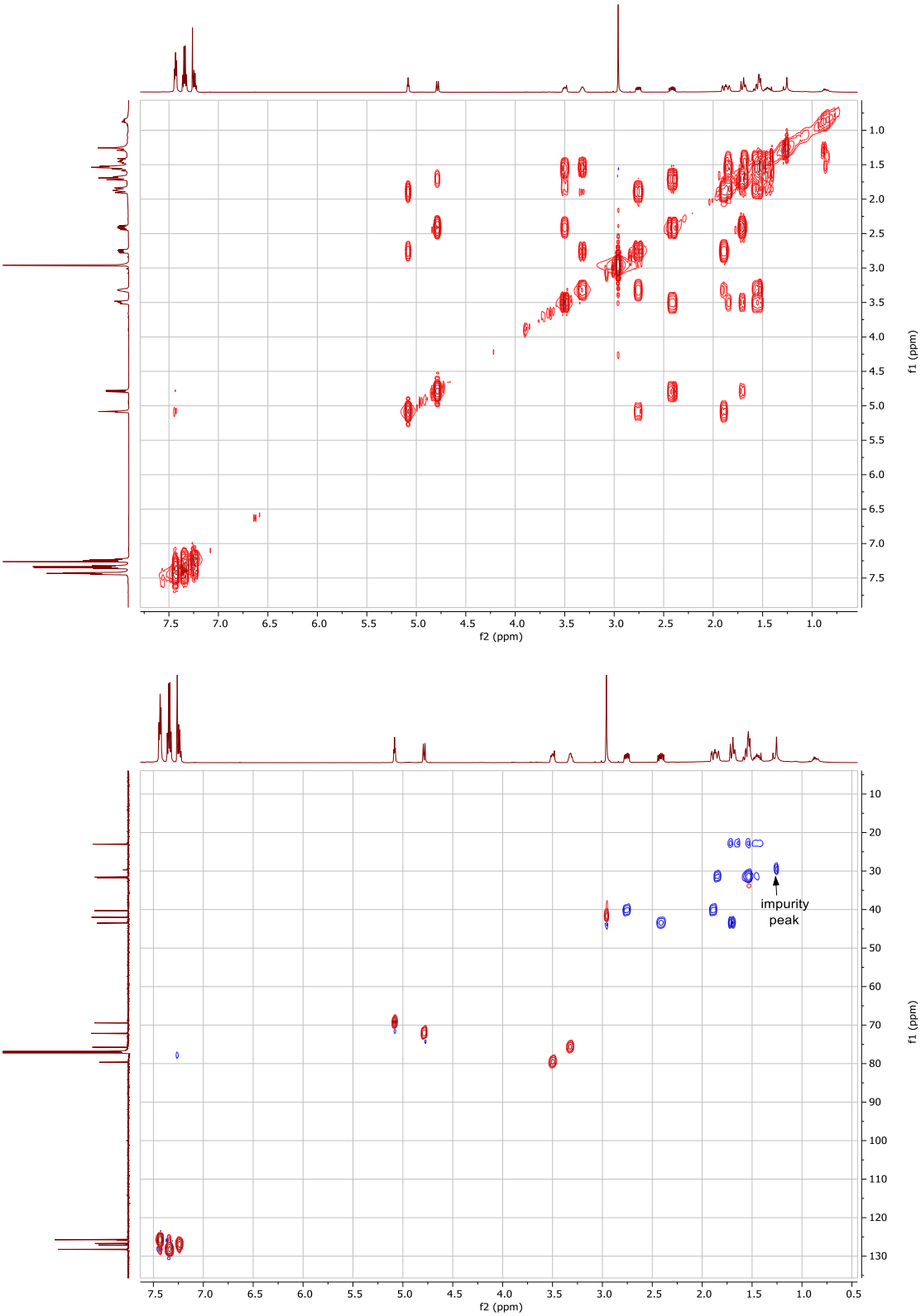

Appendix 12: COSY and HSQC Spectra of (–)-*Cis*-2′,2′′-Diphenyllobelidiol *N*-oxide (**5**).

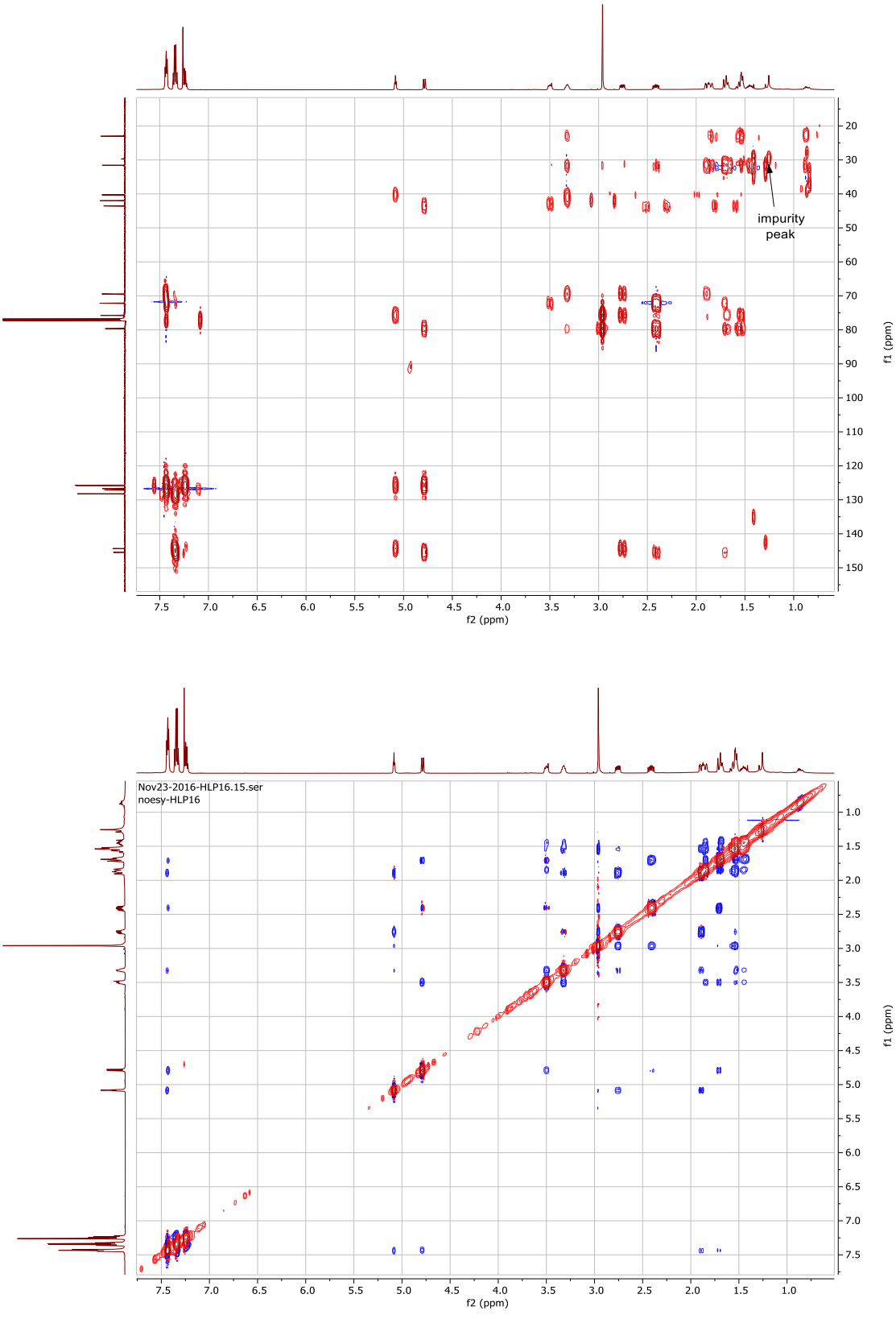

Appendix 13: HMBC and NOESY Spectra of (–)-*Cis*-2′,2′′-Diphenyllobelidiol *N*-oxide (**5**).

Data:HLP16_291116
Sample Name:
Description:
Ionization Mode:ESI+
History:Determine m/z[Peak Detect[Centroid,30,Area];Correct Base[0.5%]];Correct Ba...

Acquired:11/29/2016 12:24:05 PM
Operator:AccuTOF
Mass Calibration data:Int Calib 291116
Created:12/1/2016 3:34:46 PM
Created by:AccuTOF

Charge number:1 Tolerance:30.00(ppm), 5.00 .. 15.00(mmu) Unsaturation Number:0.0 .. 25.0 (Fractio...
Element:^{12}C:0 .. 40, ^{1}H:0 .. 40, ^{14}N:0 .. 5, ^{16}O:0 .. 5

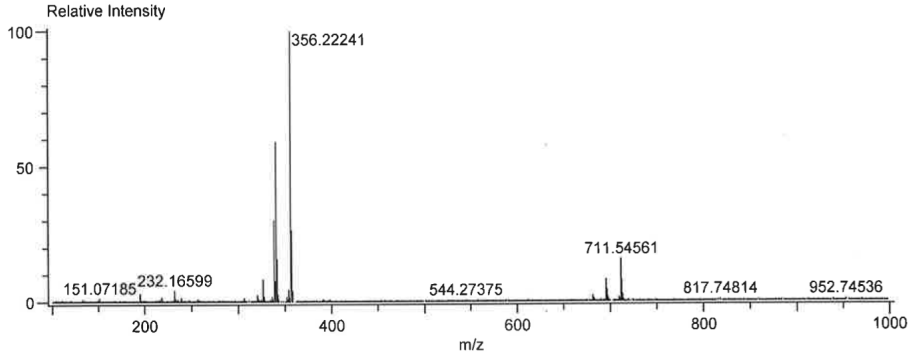

Mass	Intensity	Calc. Mass	Mass Difference (mmu)	Mass Difference (ppm)	Possible Formula
338.21161	51562.44	338.21200	-0.39	-1.15	$^{12}C_{22}{}^{1}H_{28}{}^{14}N_{1}{}^{16}O_{2}$
		338.21066	0.95	2.82	$^{12}C_{20}{}^{1}H_{26}{}^{14}N_{4}{}^{16}O_{1}$
		338.20932	2.29	6.78	$^{12}C_{19}{}^{1}H_{30}{}^{16}O_{5}$
		338.20798	3.63	10.75	$^{12}C_{17}{}^{1}H_{28}{}^{14}N_{3}{}^{16}O_{4}$
		338.21921	-7.60	-22.47	$^{12}C_{16}{}^{1}H_{28}{}^{14}N_{5}{}^{16}O_{3}$
		338.20345	8.16	24.14	$^{12}C_{26}{}^{1}H_{26}$
		338.22056	-8.94	-26.44	$^{12}C_{18}{}^{1}H_{30}{}^{14}N_{2}{}^{16}O_{4}$
340.22645	100896.31	340.22631	0.14	0.40	$^{12}C_{20}{}^{1}H_{28}{}^{14}N_{4}{}^{16}O_{1}$
		340.22765	-1.21	-3.55	$^{12}C_{22}{}^{1}H_{30}{}^{14}N_{1}{}^{16}O_{2}$
		340.22497	1.47	4.33	$^{12}C_{19}{}^{1}H_{32}{}^{16}O_{5}$
		340.22363	2.82	8.28	$^{12}C_{17}{}^{1}H_{30}{}^{14}N_{3}{}^{16}O_{4}$
		340.21910	7.35	21.59	$^{12}C_{26}{}^{1}H_{28}$
		340.23486	-8.42	-24.74	$^{12}C_{16}{}^{1}H_{30}{}^{14}N_{5}{}^{16}O_{3}$
		340.23621	-9.76	-28.69	$^{12}C_{18}{}^{1}H_{32}{}^{14}N_{2}{}^{16}O_{4}$
356.22241	171352.00	356.22257	-0.15	-0.43	$^{12}C_{22}{}^{1}H_{30}{}^{14}N_{1}{}^{16}O_{3}$
		356.22123	1.19	3.34	$^{12}C_{20}{}^{1}H_{28}{}^{14}N_{4}{}^{16}O_{2}$
		356.22525	-2.83	-7.96	$^{12}C_{25}{}^{1}H_{28}{}^{14}N_{2}$
		356.21855	3.87	10.86	$^{12}C_{17}{}^{1}H_{30}{}^{14}N_{3}{}^{16}O_{5}$
		356.22978	-7.36	-20.67	$^{12}C_{16}{}^{1}H_{30}{}^{14}N_{5}{}^{16}O_{4}$
		356.21401	8.40	23.58	$^{12}C_{26}{}^{1}H_{28}{}^{16}O_{1}$
		356.23112	-8.71	-24.44	$^{12}C_{18}{}^{1}H_{32}{}^{14}N_{2}{}^{16}O_{5}$
		356.21267	9.74	27.35	$^{12}C_{24}{}^{1}H_{26}{}^{14}N_{3}$
357.22614	45019.75	357.22637	-0.23	-0.65	$^{12}C_{17}{}^{1}H_{31}{}^{14}N_{3}{}^{16}O_{5}$
		357.22905	-2.91	-8.15	$^{12}C_{20}{}^{1}H_{29}{}^{14}N_{4}{}^{16}O_{2}$
		357.23039	-4.26	-11.91	$^{12}C_{22}{}^{1}H_{31}{}^{14}N_{1}{}^{16}O_{3}$
		357.22184	4.30	12.03	$^{12}C_{26}{}^{1}H_{29}{}^{16}O_{1}$
		357.22050	5.64	15.79	$^{12}C_{24}{}^{1}H_{27}{}^{14}N_{3}$
		357.23307	-6.94	-19.42	$^{12}C_{25}{}^{1}H_{29}{}^{14}N_{2}$
		357.21782	8.32	23.29	$^{12}C_{21}{}^{1}H_{29}{}^{14}N_{2}{}^{16}O_{3}$
		357.21647	9.66	27.05	$^{12}C_{19}{}^{1}H_{27}{}^{14}N_{5}{}^{16}O_{2}$

Appendix 14: HRDARTMS Spectrum of (–)-*Cis*-2′,2′′-Diphenyllobelidiol *N*-oxide (**5**).

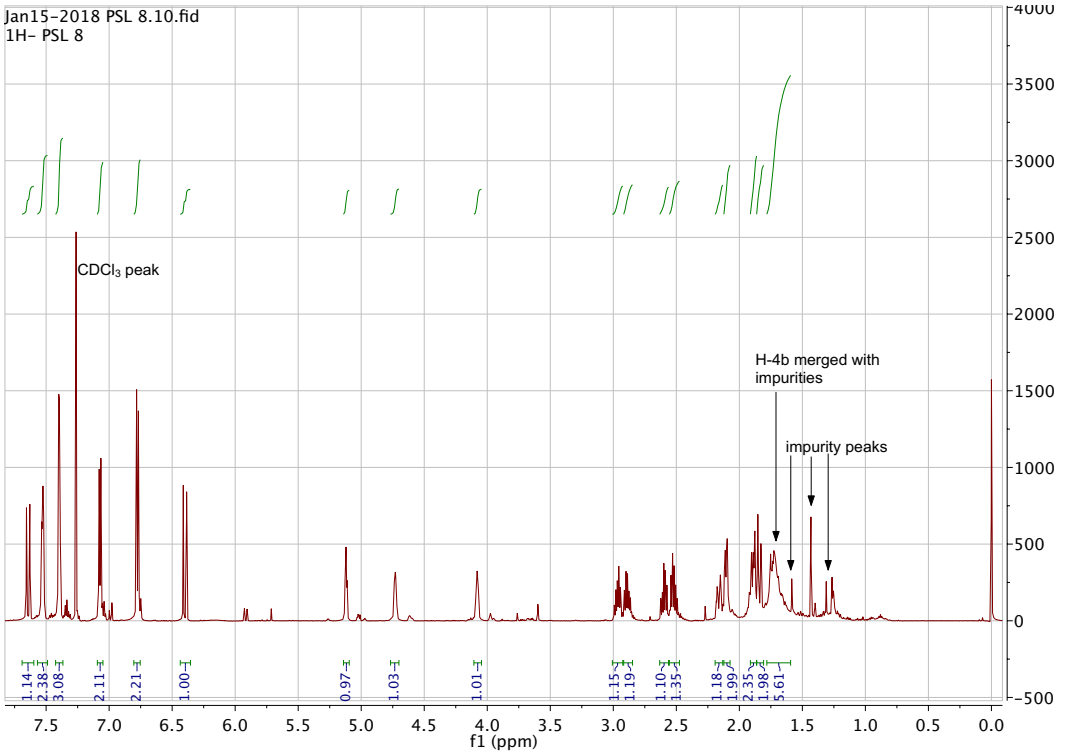

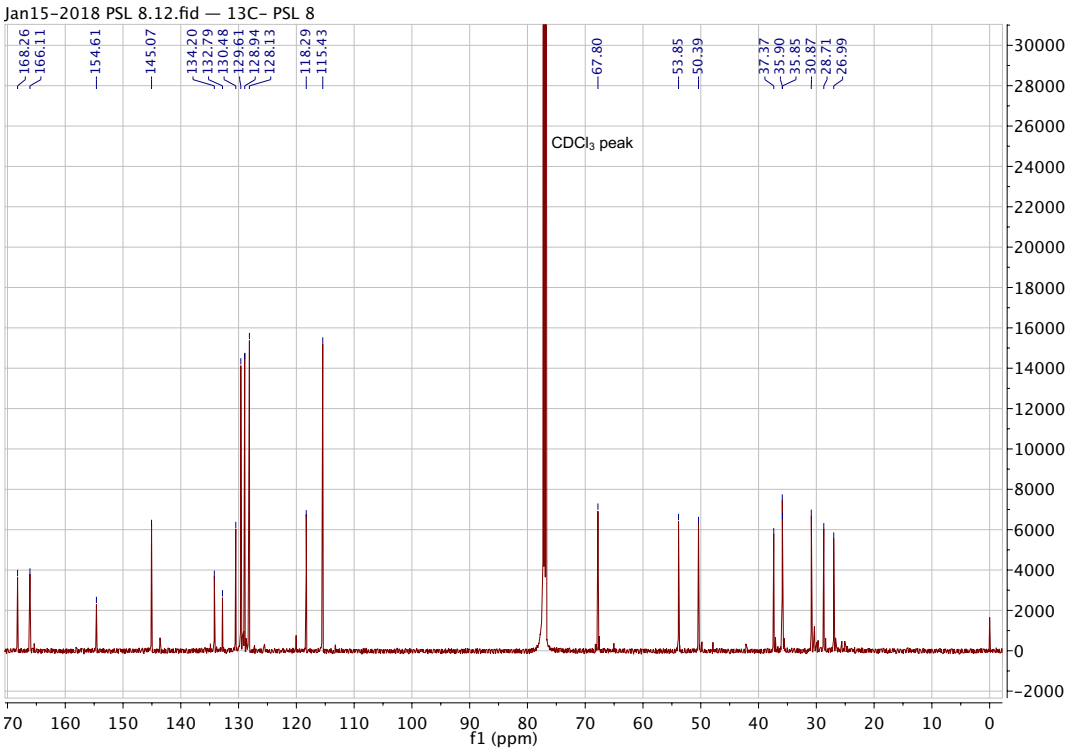

Appendix 15: ^{1}H and ^{13}C NMR Spectra of 3α-Cinnamoyloxy-*N*-phloretoylnortropane (**6**).

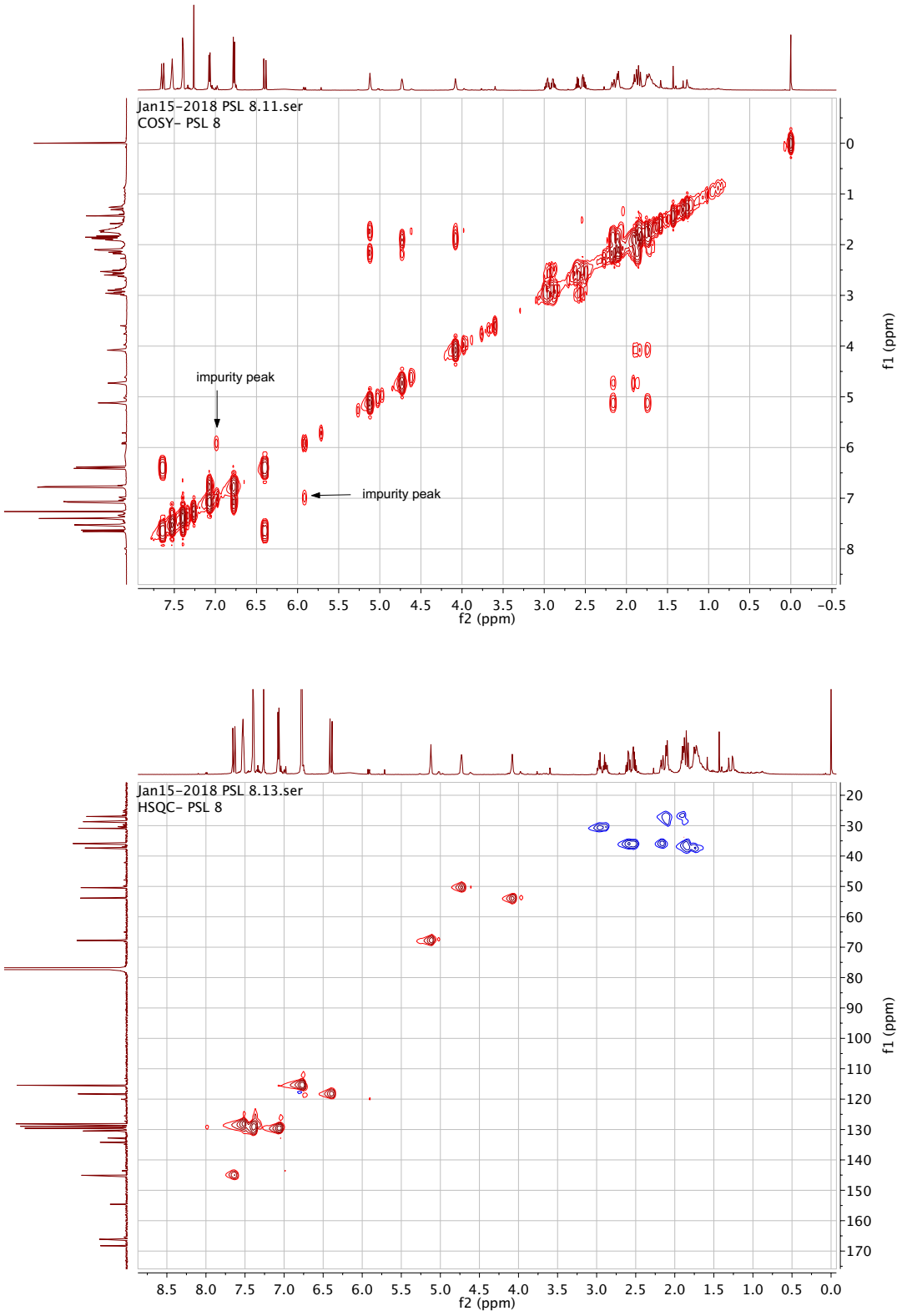

Appendix 16: COSY and HSQC Spectra of 3α-Cinnamoyloxy-*N*-phloretoylnortropane (**6**).

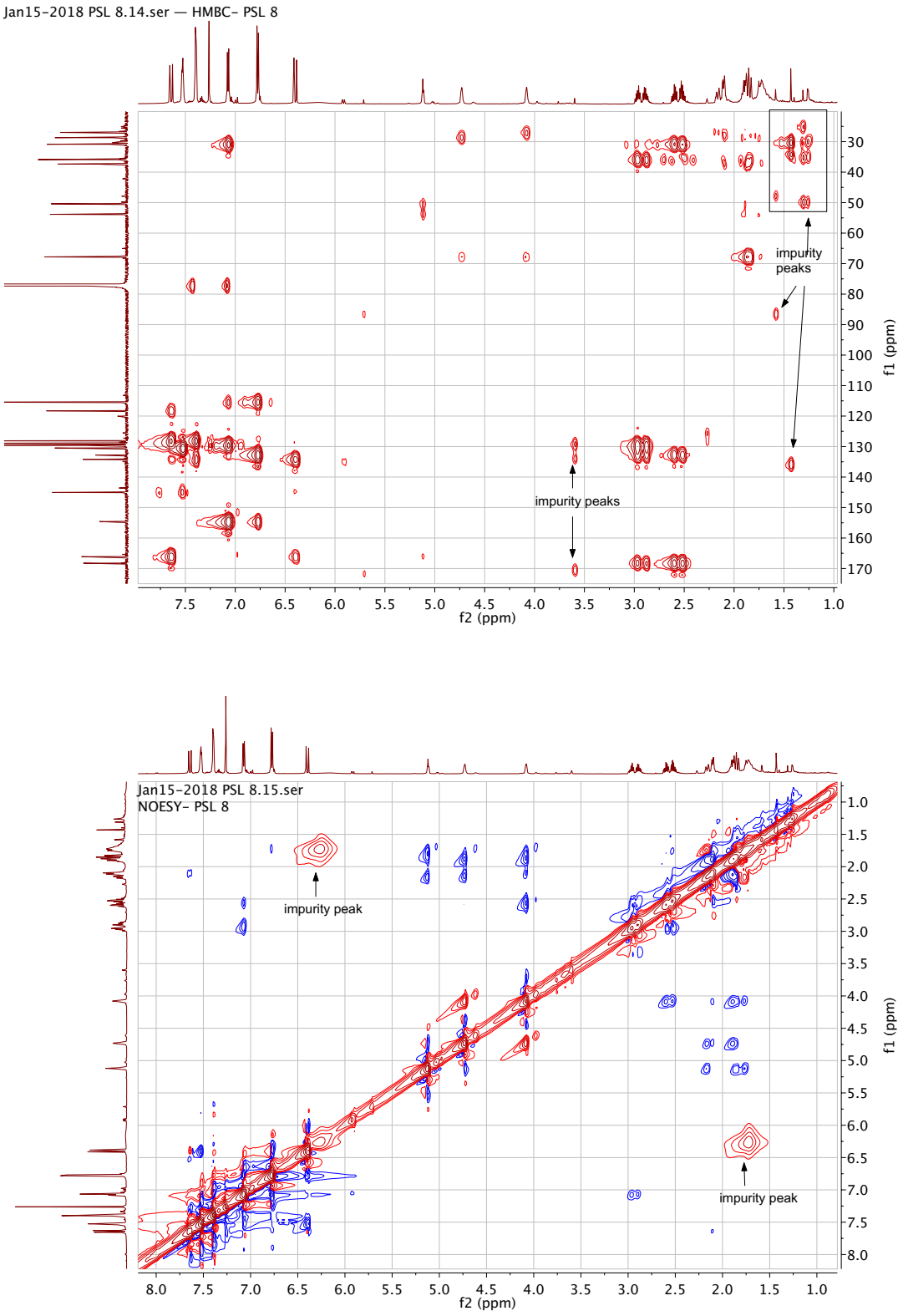

Appendix 17: HMBC and NOESY Spectra of 3α-Cinnamoyloxy-*N*-phloretoylnortropane (**6**).

Data:PSL8-3
Sample Name:
Description:
Ionization Mode:ESI+
History:Determine m/z[Peak Detect[Centroid,30,Area];Correct Base[0.5%]];Correct Ba...

Acquired:1/30/2018 11:16:30 AM
Operator:AccuTOF
Mass Calibration data:Calibration_300118
Created:1/30/2018 12:16:43 PM
Created by:AccuTOF

Charge number:1 Tolerance:20.00(ppm), 0.00 .. 30.00(mmu) Unsaturation Number:0.0 .. 25.0 (Fractio...
Element:^{12}C:0 .. 35, ^{1}H:0 .. 40, ^{14}N:0 .. 3, ^{16}O:0 .. 8

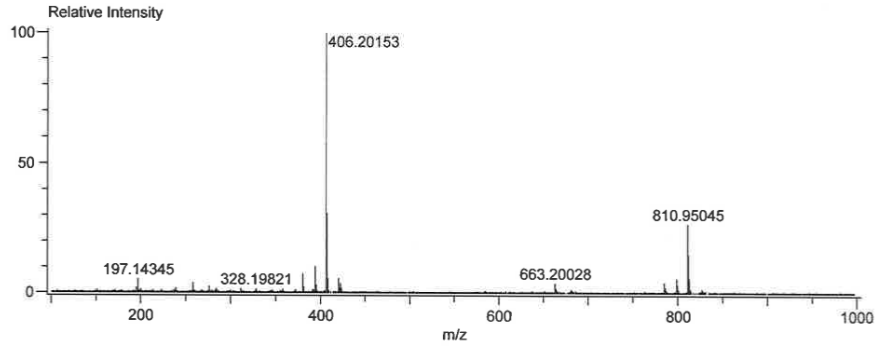

Mass	Intensity	Calc. Mass	Mass Difference (mmu)	Mass Difference (ppm)	Possible Formula
406.20153	141272.50	406.20183	-0.30	-0.75	$^{12}C_{25}{}^{1}H_{28}{}^{14}N_{1}{}^{16}O_{4}$ ✓
		406.19915	2.38	5.85	$^{12}C_{22}{}^{1}H_{30}{}^{16}O_{7}$
		406.20451	-2.98	-7.35	$^{12}C_{28}{}^{1}H_{26}{}^{14}N_{2}{}^{16}O_{1}$
		406.19781	3.72	9.16	$^{12}C_{20}{}^{1}H_{28}{}^{14}N_{3}{}^{16}O_{6}$

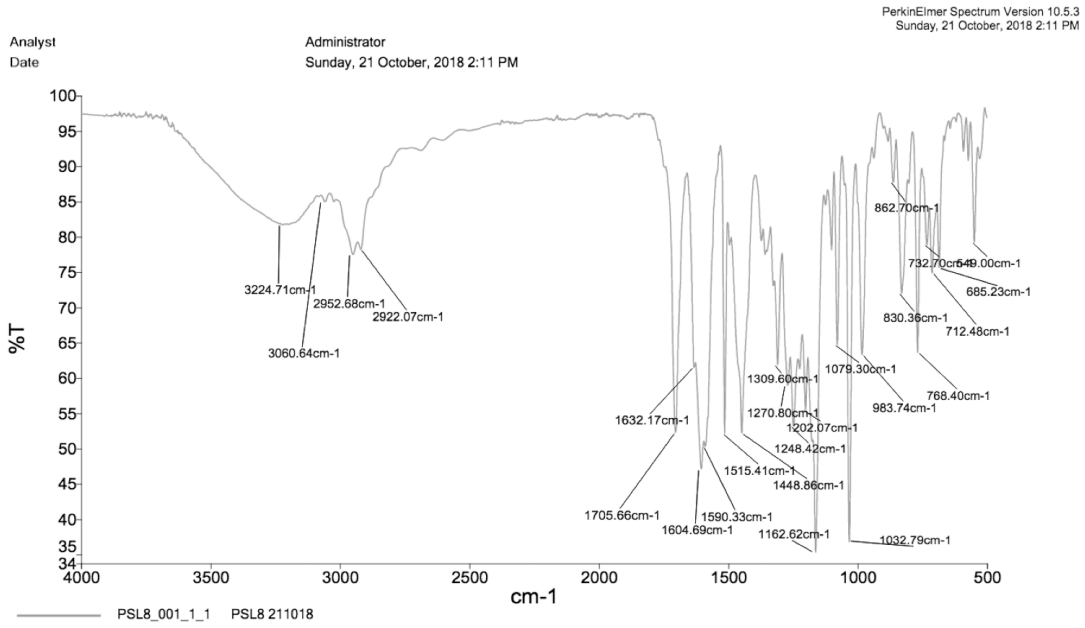

Appendix 18: HRDARTMS and IR Spectra of 3α-Cinnamoyloxy-*N*-phloretoylnortropane (**6**).

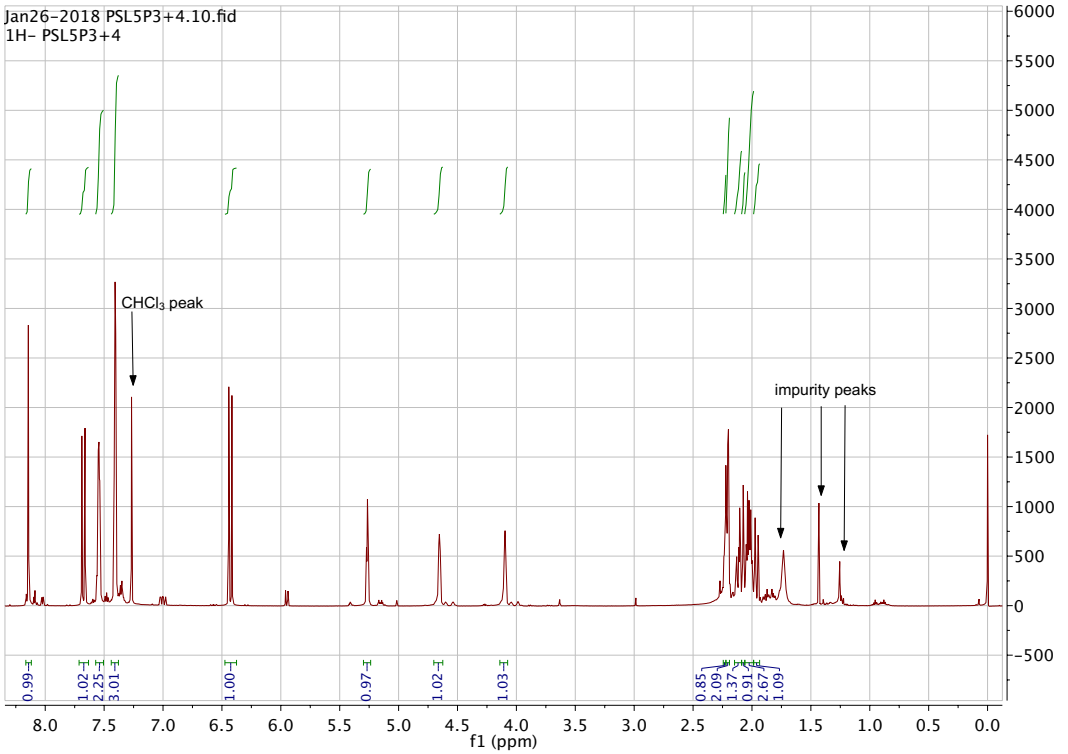

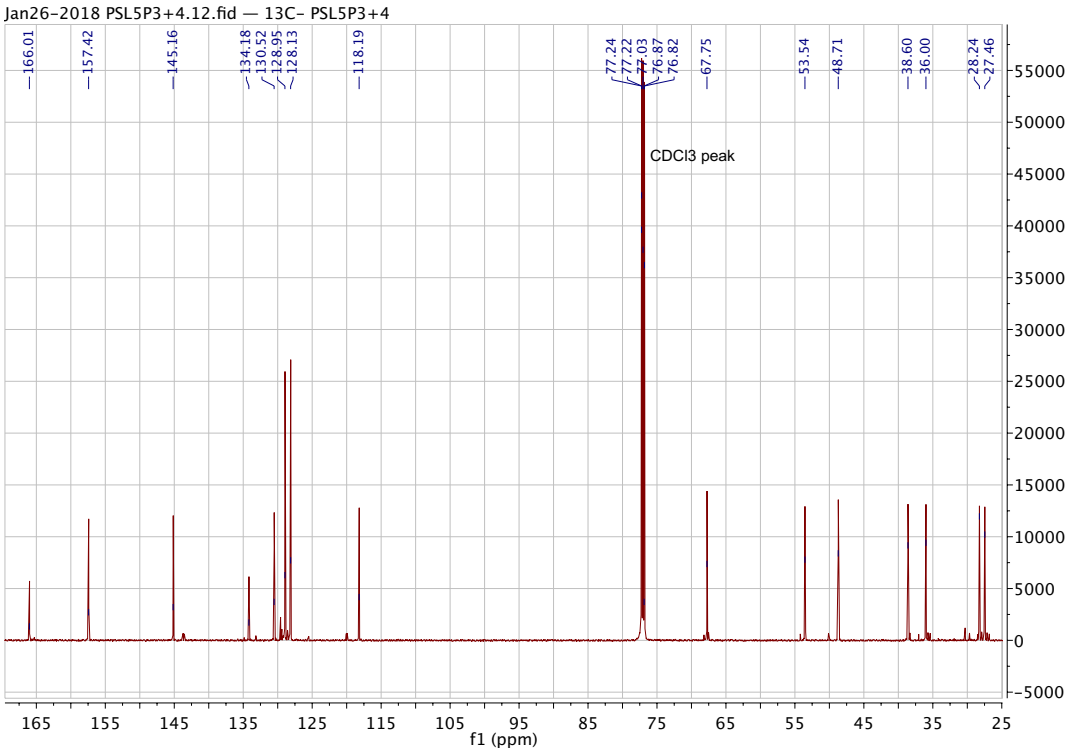

Appendix 19: ^{1}H and ^{13}C NMR Spectra of 3α-Cinnamoyloxy-*N*-formylnortropane (**7**).

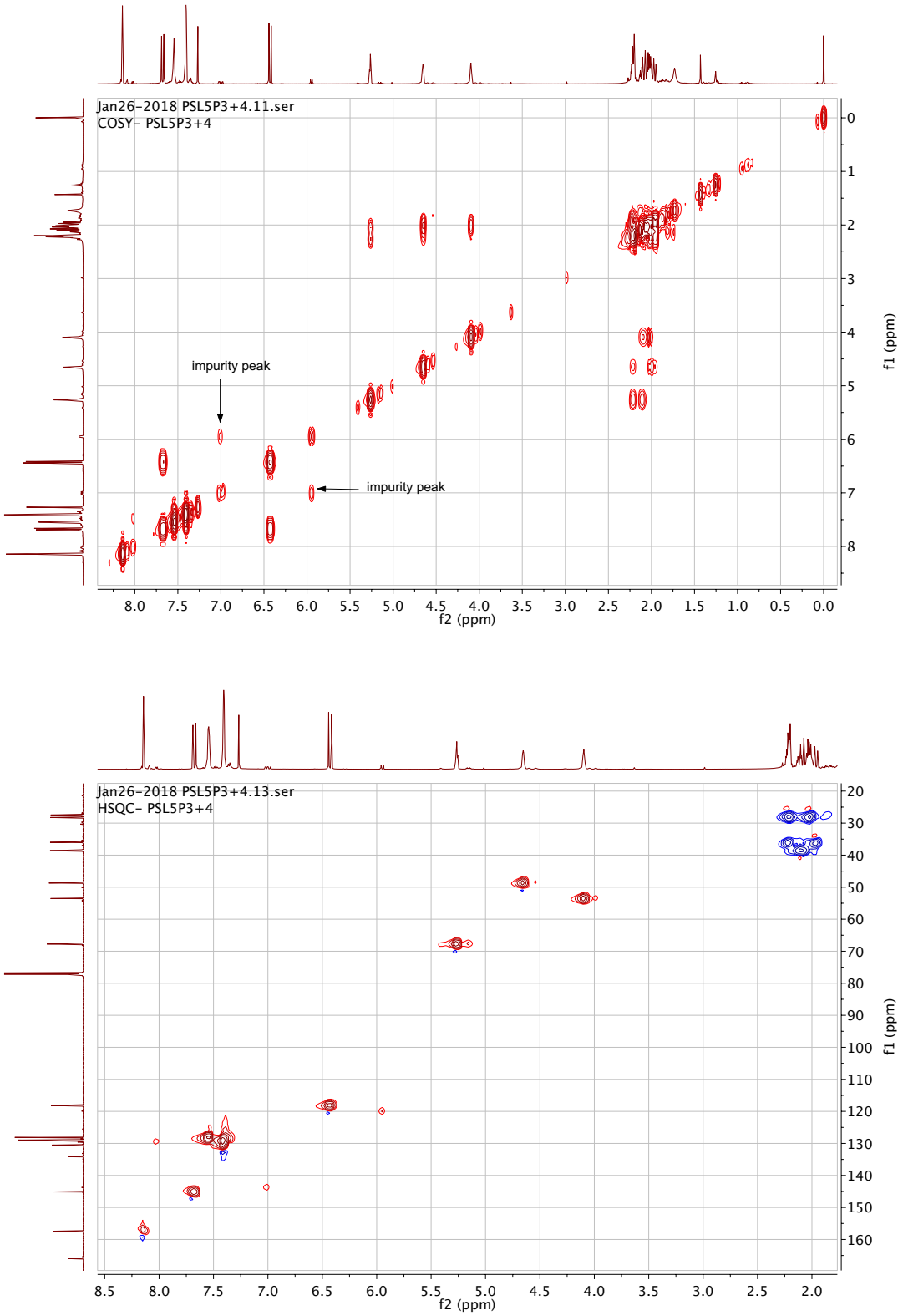

Appendix 20: COSY and HSQC Spectra of 3α-Cinnamoyloxy-*N*-formylnortropane (**7**).

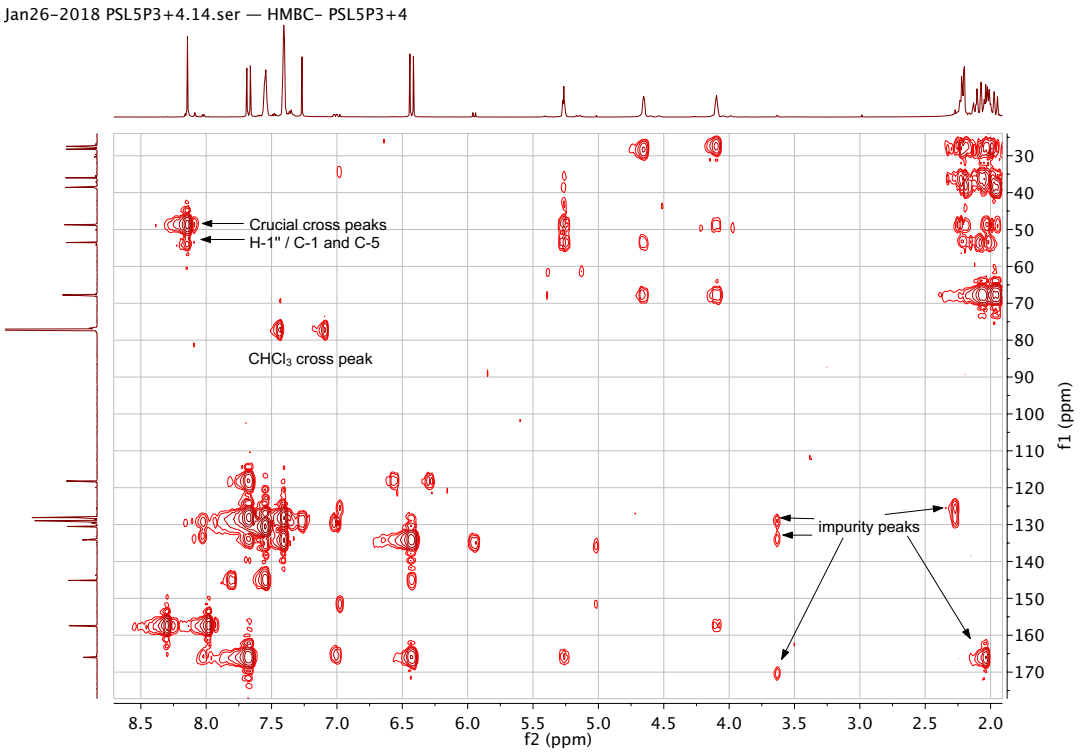

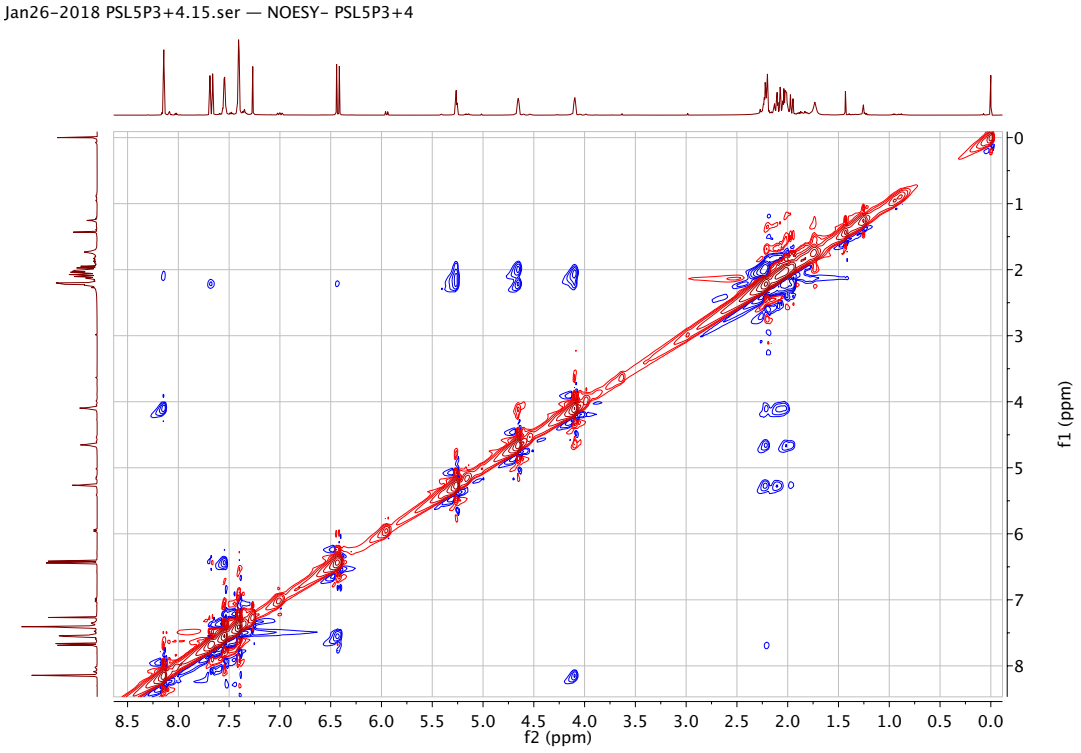

Appendix 21: HMBC and NOESY Spectra of 3α-Cinnamoyloxy-*N*-formylnortropane (**7**).

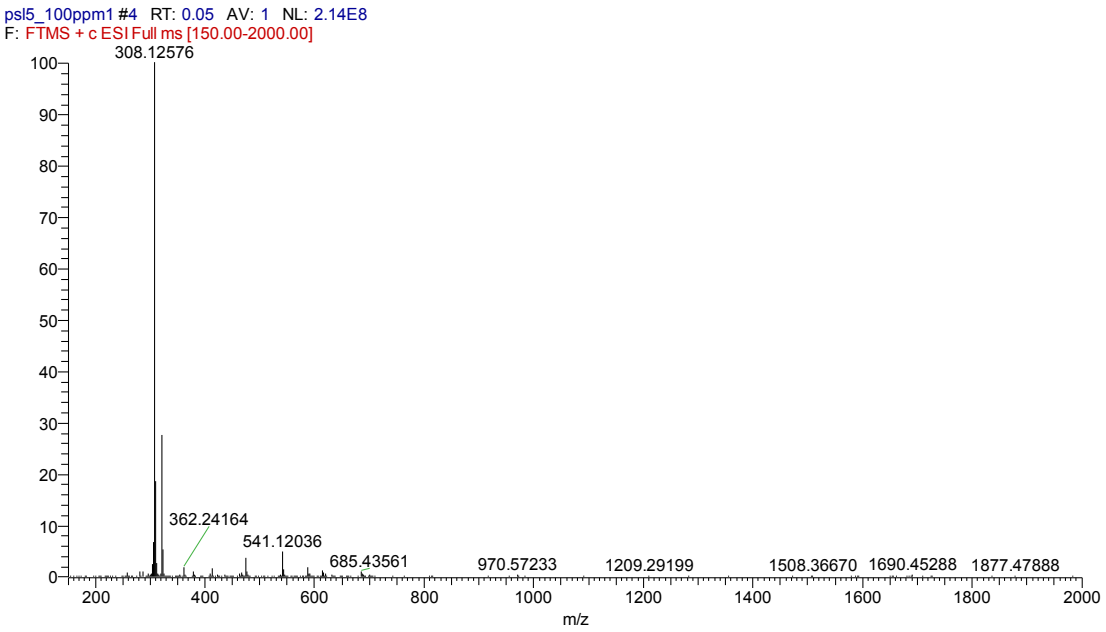

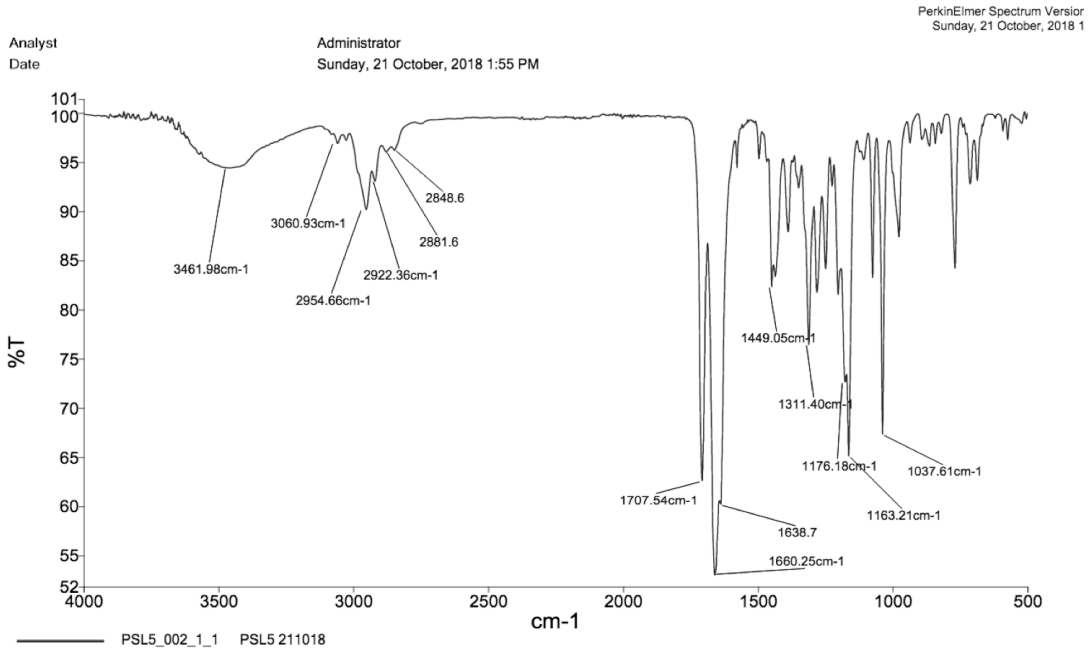

Appendix 22: HRESIMS (ESI+) and IR Spectra of 3α-Cinnamoyloxy-*N*-formylnortropane (**7**).

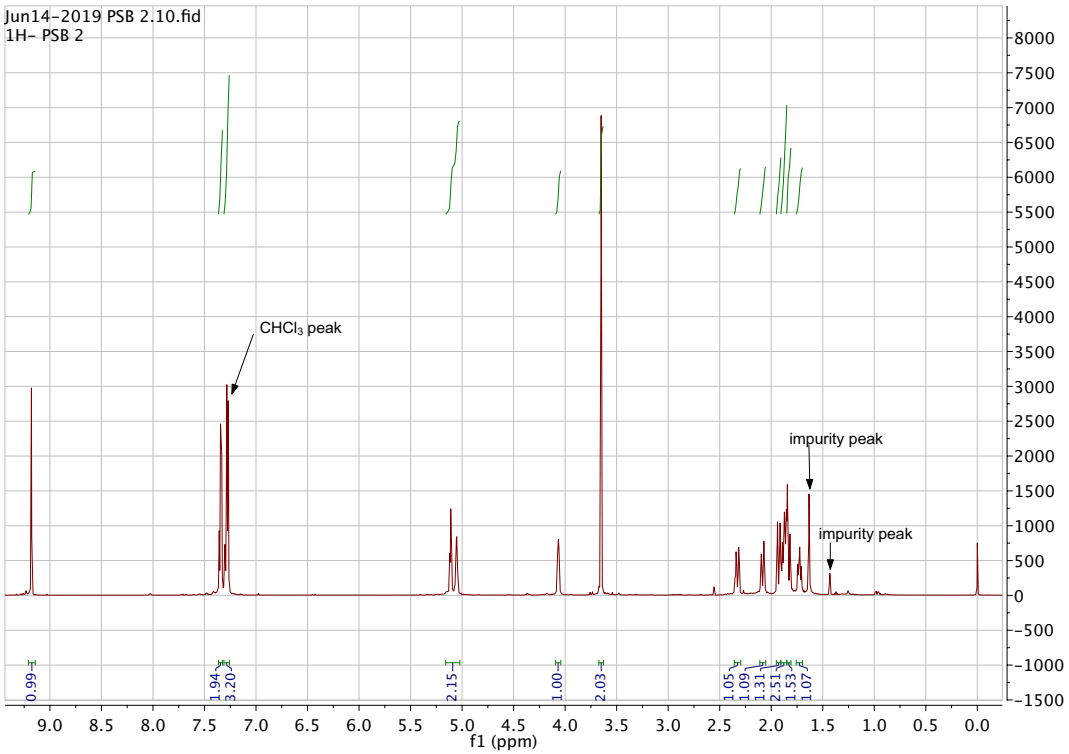

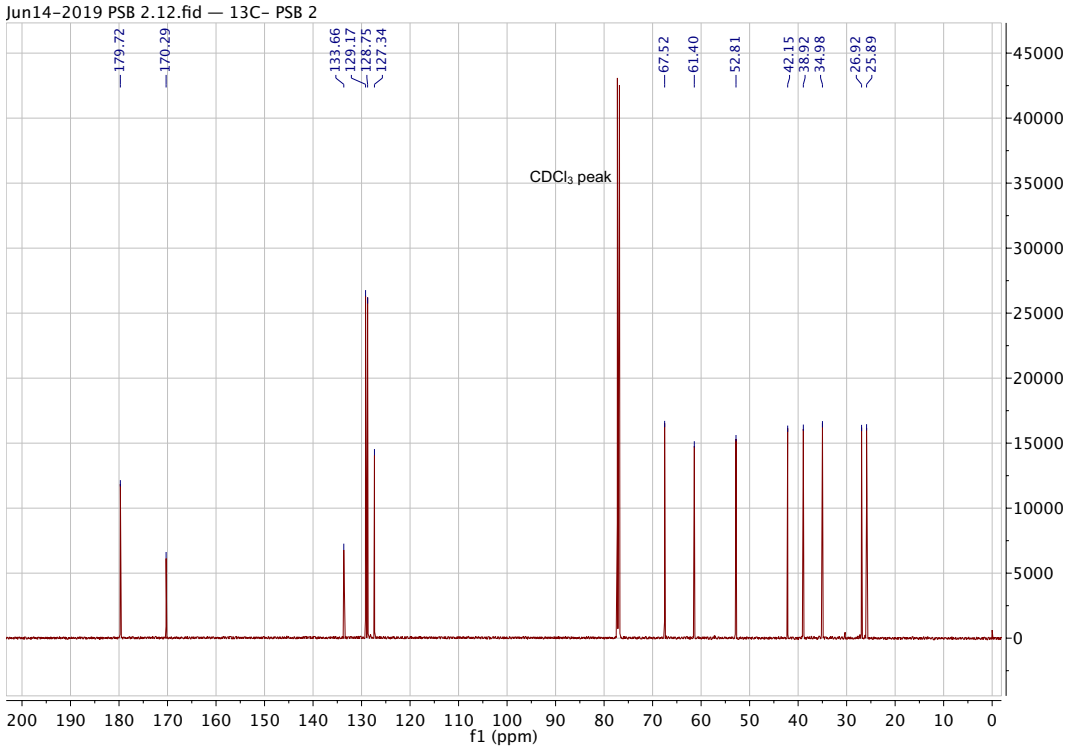

Appendix 23: ^{1}H and ^{13}C NMR Spectra of 3α-Phenylacetoxy-*N*-formylnortropane (**8**).

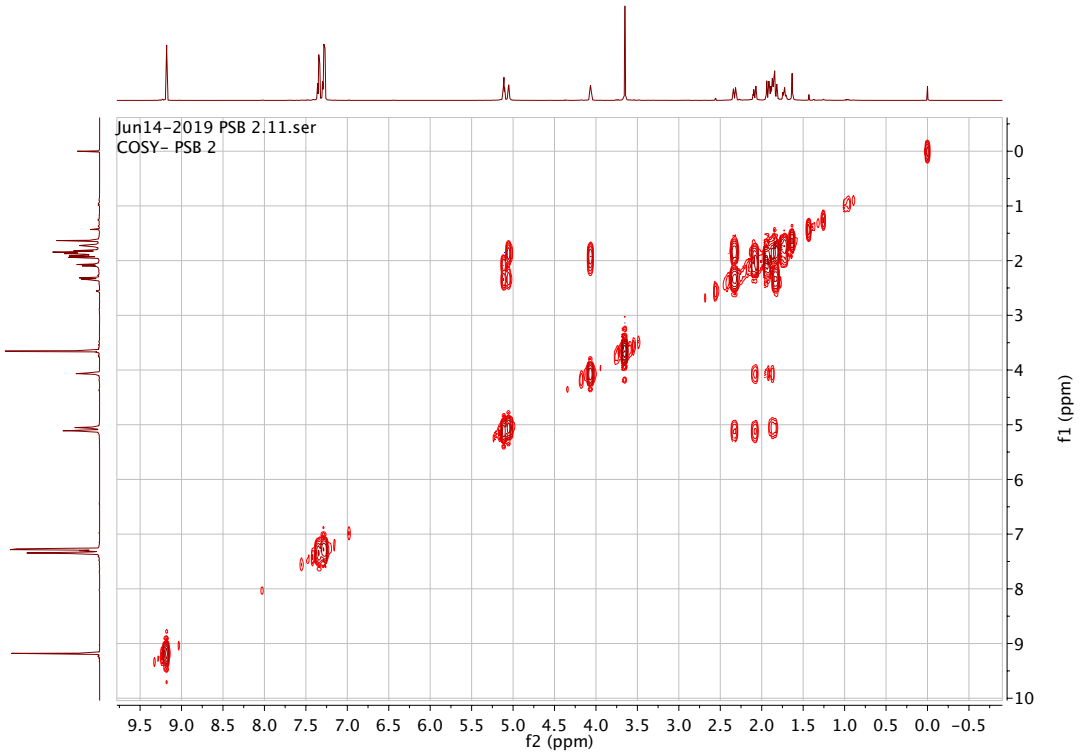

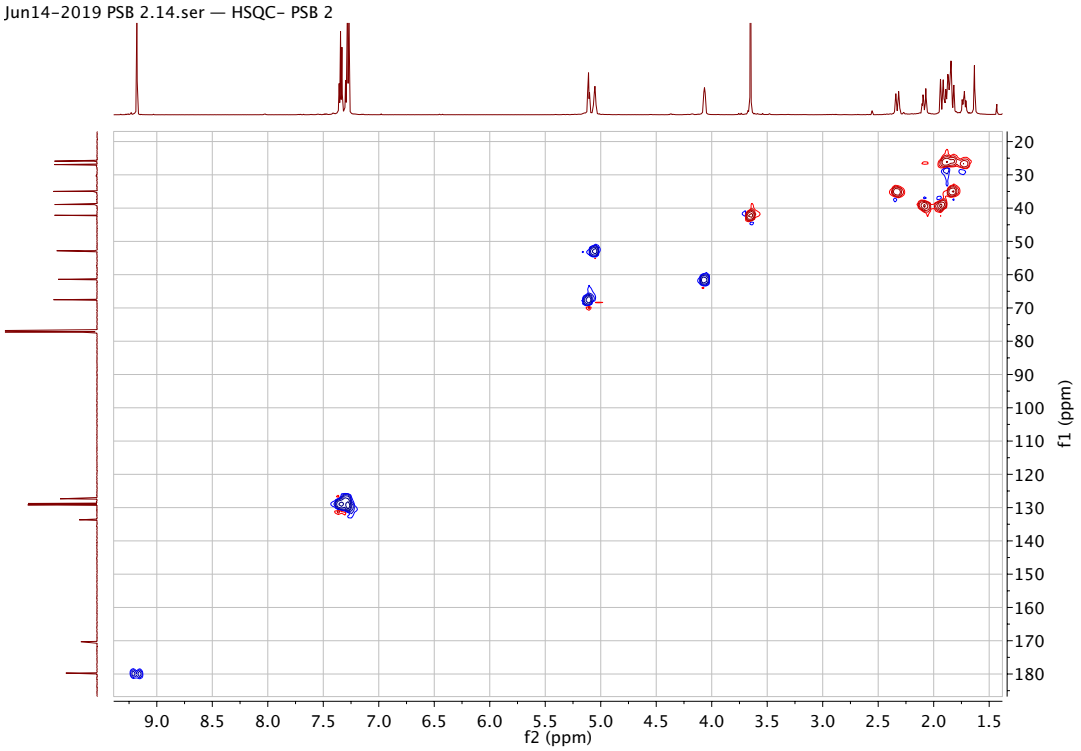

Appendix 24: COSY and HSQC Spectra of 3α-Phenylacetoxy-*N*-formylnortropane (**8**).

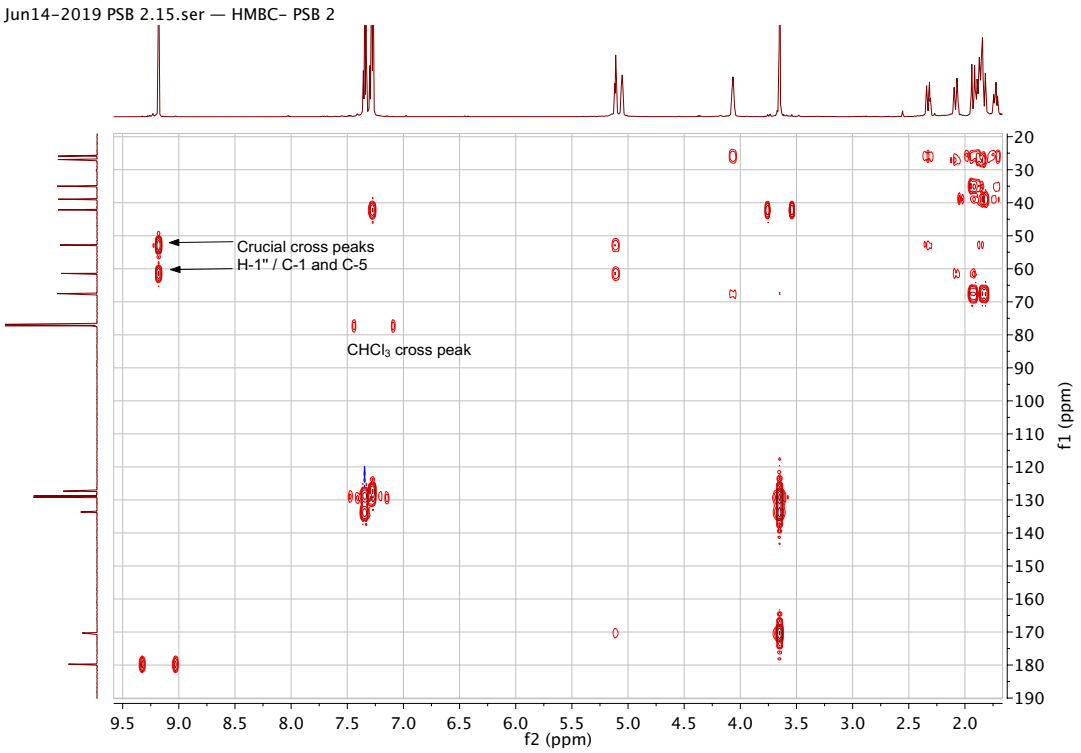

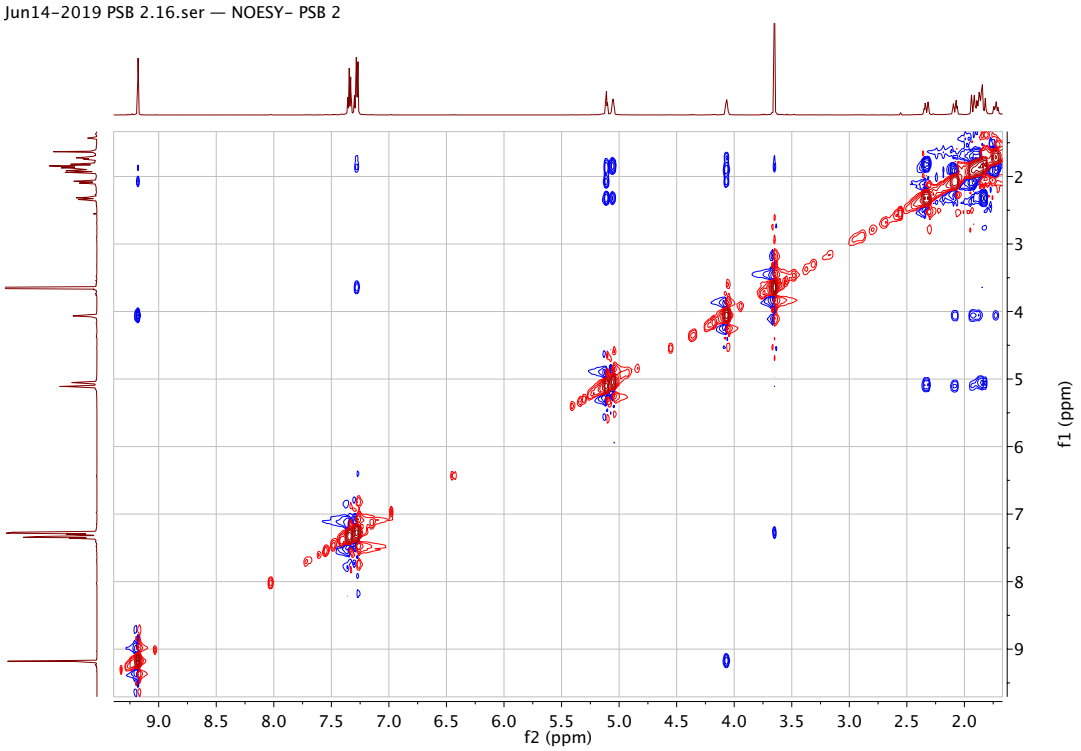

Appendix 25: HMBC and NOESY Spectra of 3α-Phenylacetoxy-*N*-formylnortropane (**8**).

User Spectra

Fragmentor Voltage	Collision Energy	Ionization Mode
80	0	ESI

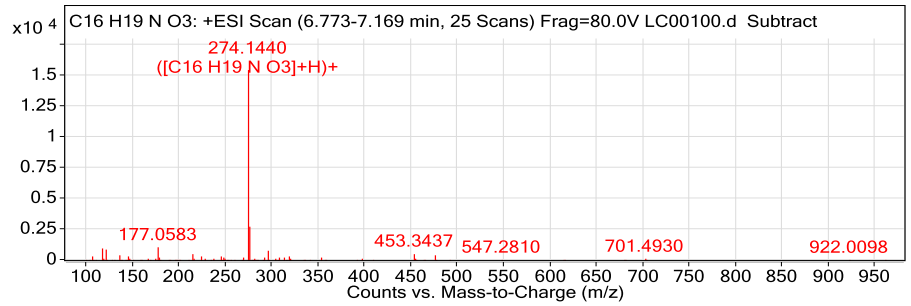

Peak List

m/z	z	Abund	Formula	Ion
117.0911	1	973.93		
121.0509	1	938.47		
136.0644	2	456.28		
177.0583	1	1112.18		
214.5908	2	592.91		
274.144	1	15459.02	C16 H19 N O3	(M+H)+
275.1474	1	2817.87	C16 H19 N O3	(M+H)+
296.1269	1	870.67		
453.3437	1	588.31		
475.326	1	434.54		

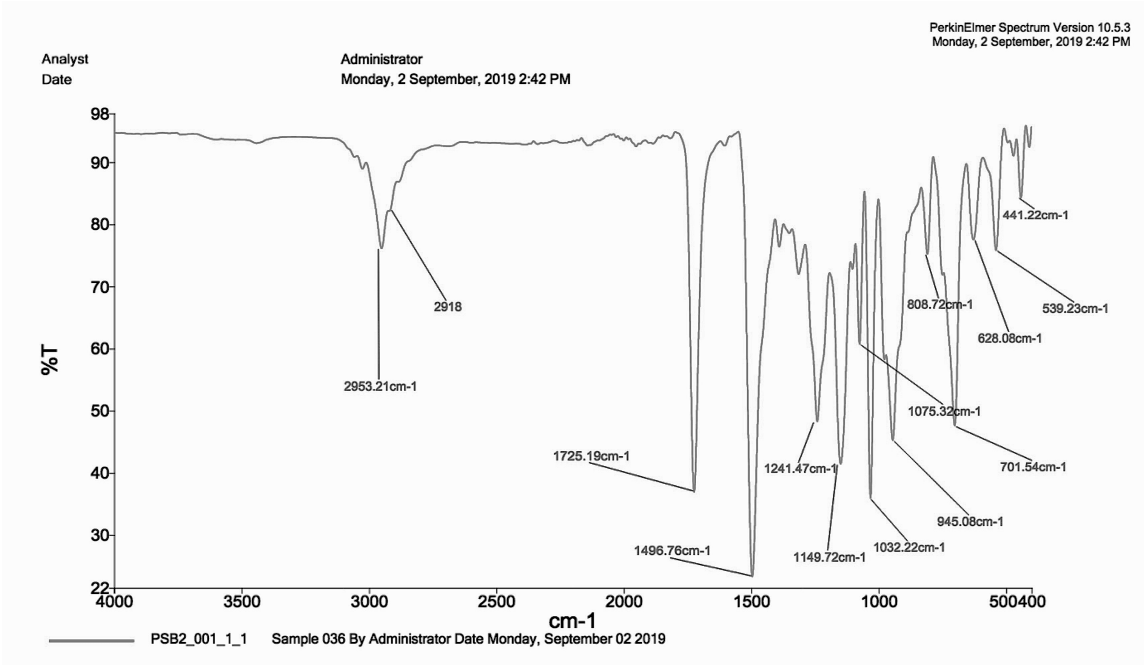

Appendix 26: HRESIMS (ESI+) and IR Spectra of 3α-Phenylacetoxy-*N*-formylnortropane (**8**).

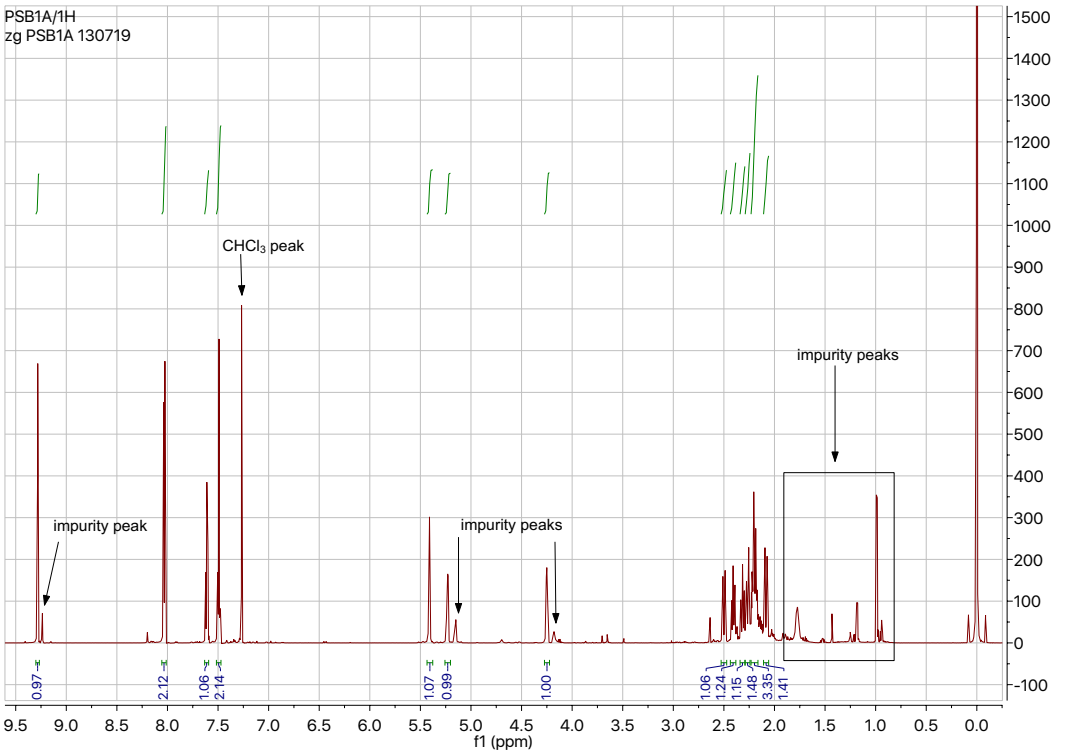

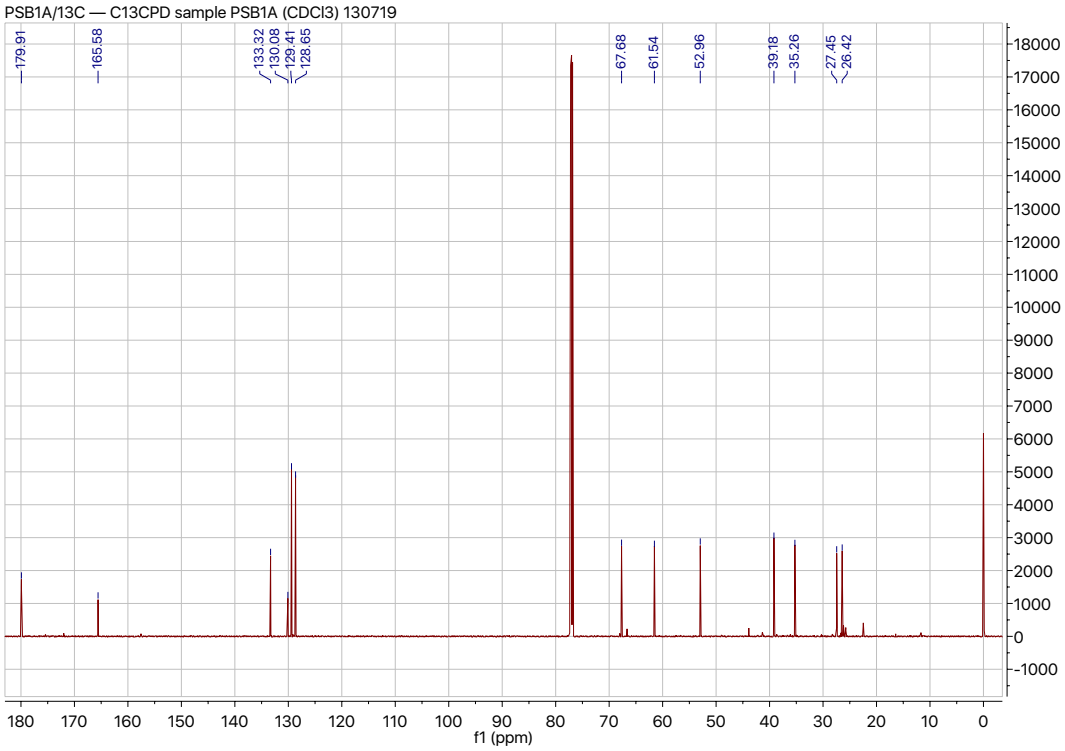

Appendix 27: ^{1}H and ^{13}C NMR Spectra of 3α-Benzoyloxy-*N*-formylnortropane (**9**).

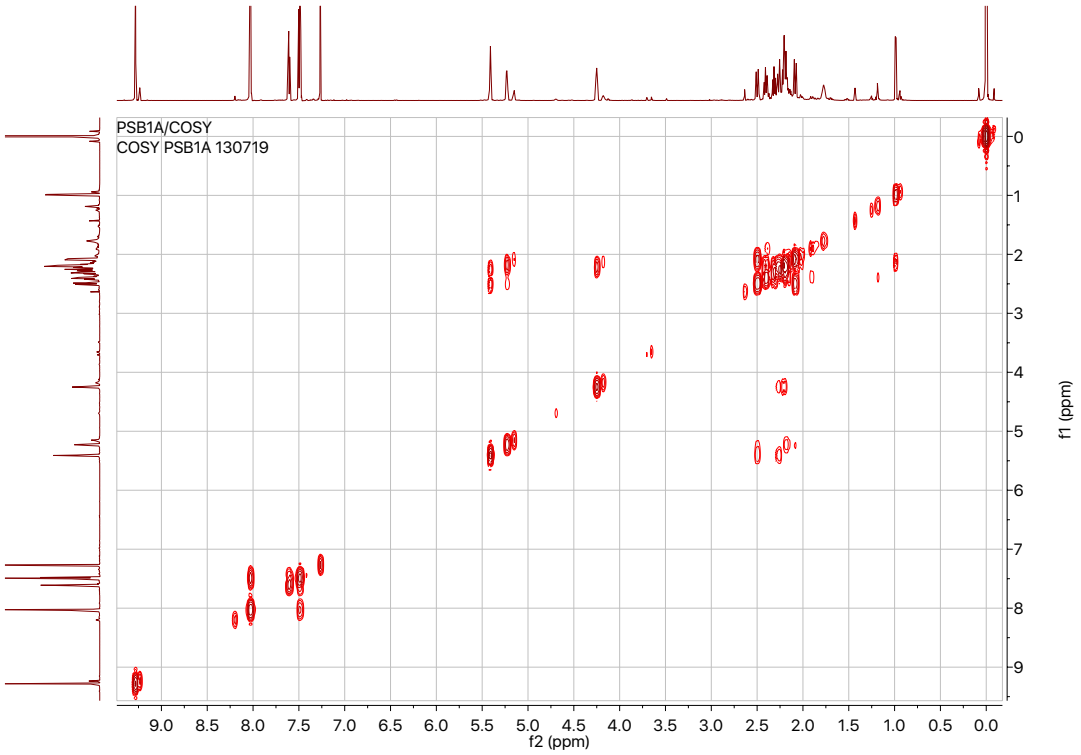

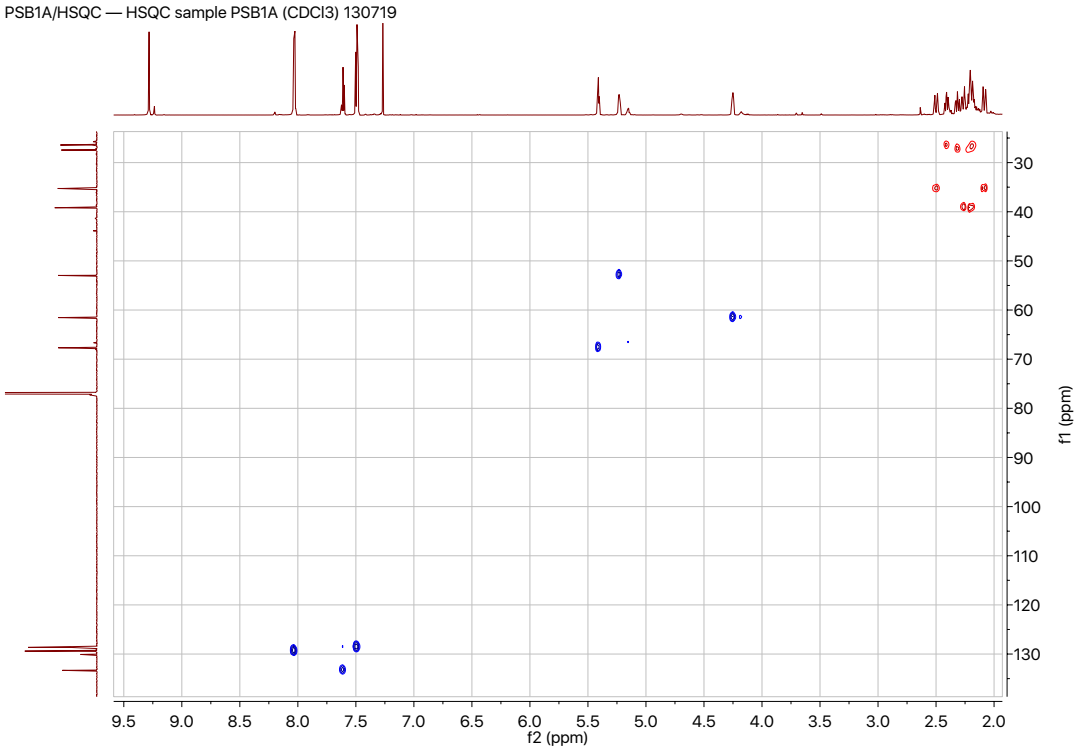

Appendix 28: COSY and HSQC Spectra of 3α-Benzoyloxy-*N*-formylnortropane (**9**).

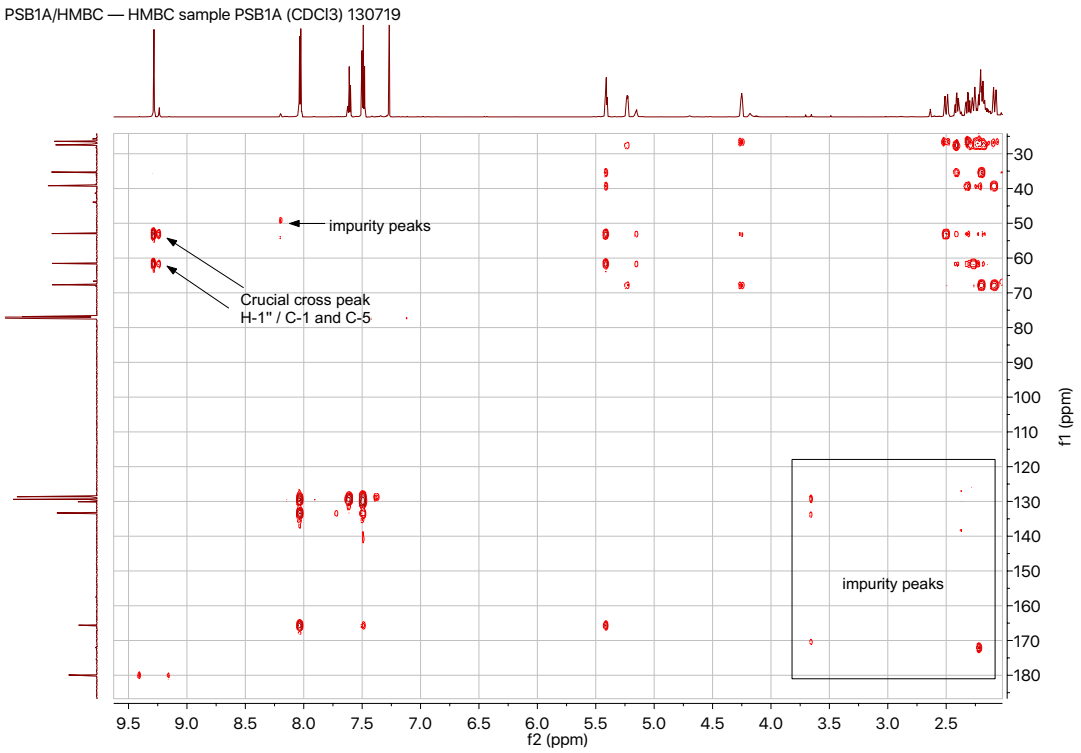

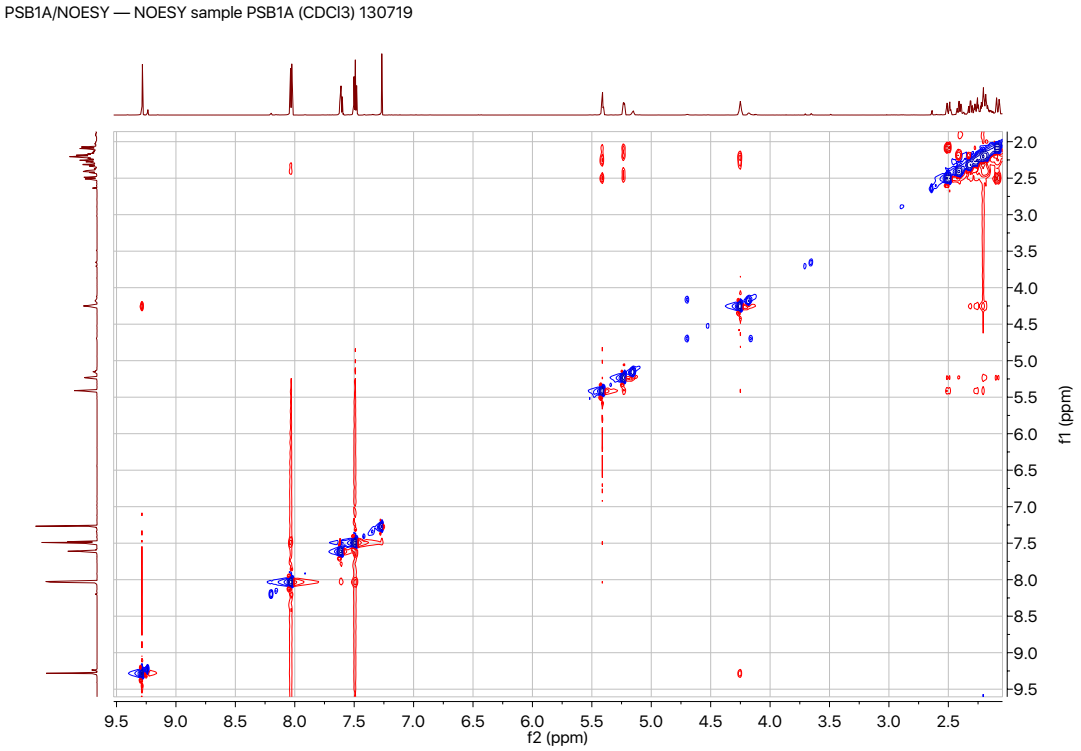

Appendix 29: HMBC and NOESY Spectra of 3α-Benzoyloxy-*N*-formylnortropane (**9**).

User Spectra

Fragmentor Voltage	Collision Energy	Ionization Mode
120	0	ESI

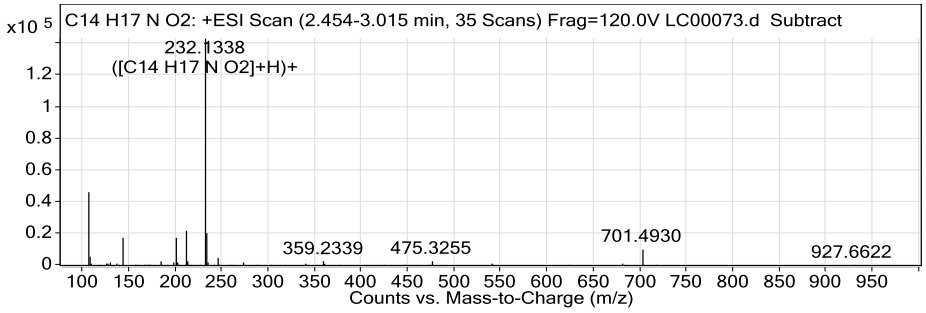

Peak List

m/z	z	Abund	Formula	Ion
107.044	2	46805.18		
107.5446	2	5894.71		
143.0021	2	17723.33		
201.0435	1	17457.47		
212.1647	1	22443.66		
232.1338	1	143224.83	C14 H17 N O2	(M+H)+
232.2696	1	4337.98		
233.1367	1	20461.07	C14 H17 N O2	(M+H)+
246.1492	1	4899.97		
701.493	1	10647.51		

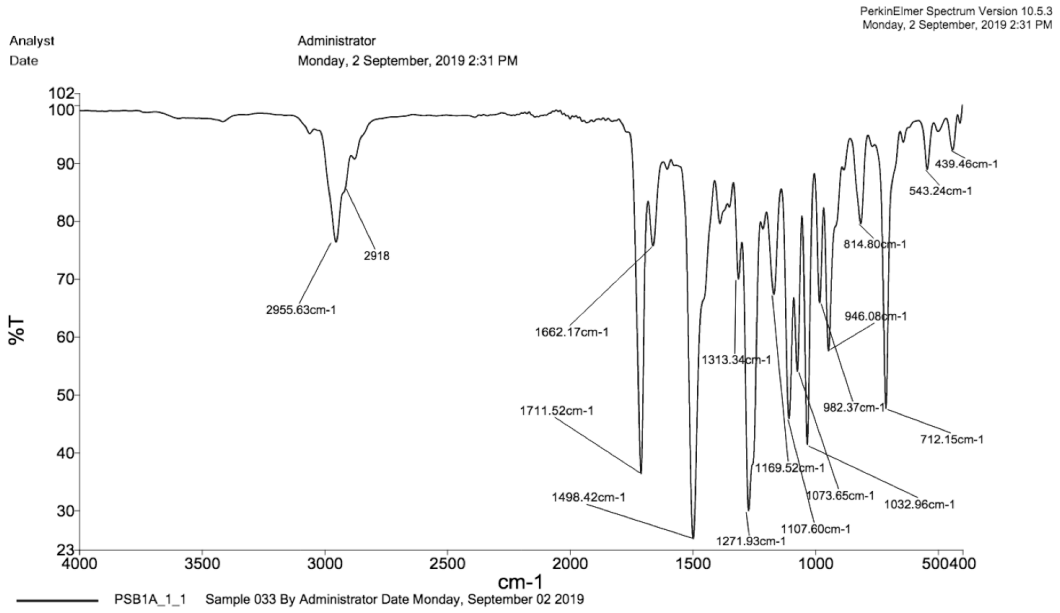

Appendix 30: HRESIMS and IR Spectra of 3α-Benzoyloxy-*N*-formylnortropane (**9**).

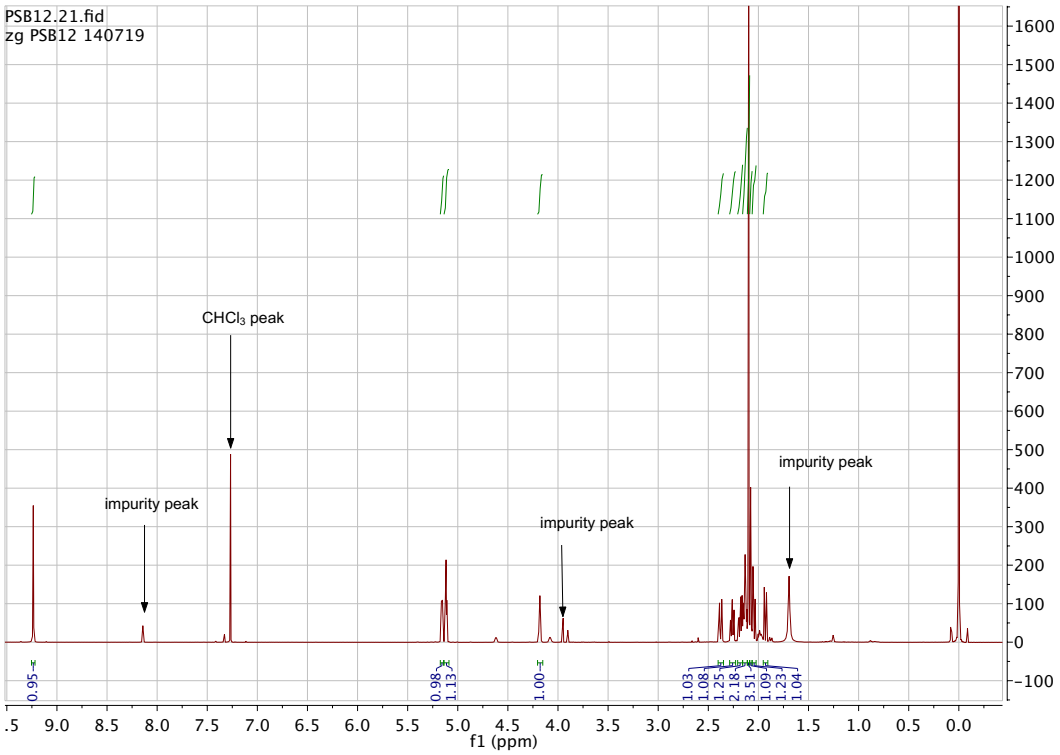

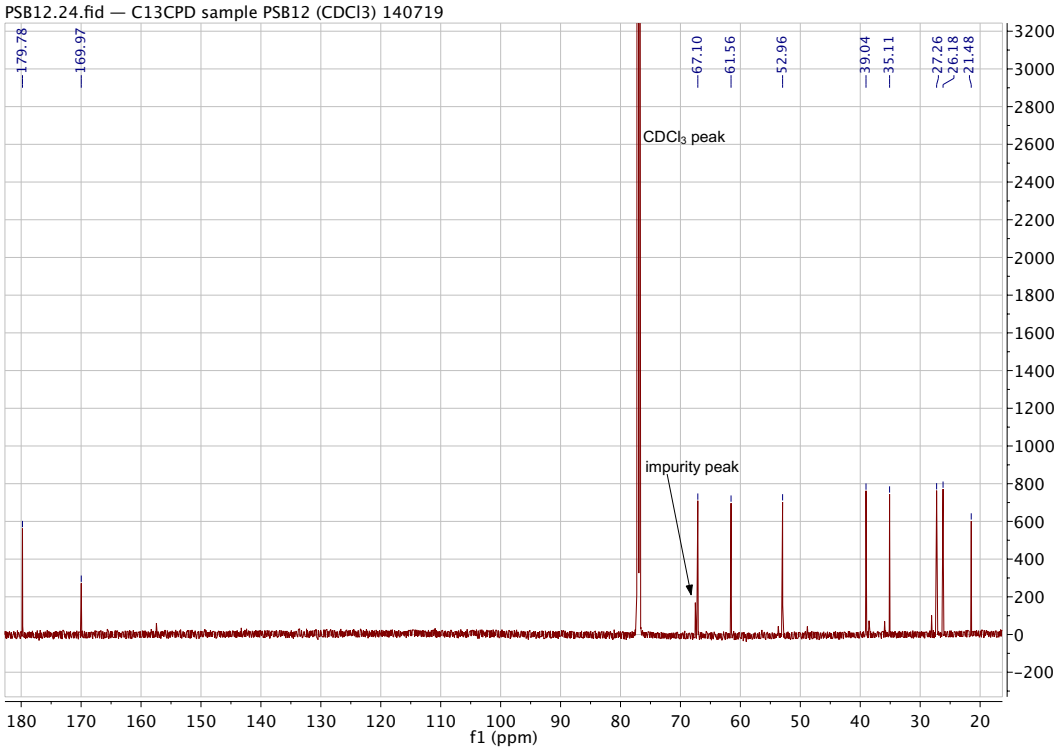

Appendix 31: ^{1}H and ^{13}C NMR Spectra of 3α-Acetoxy-*N*-formylnortropane (**10**).

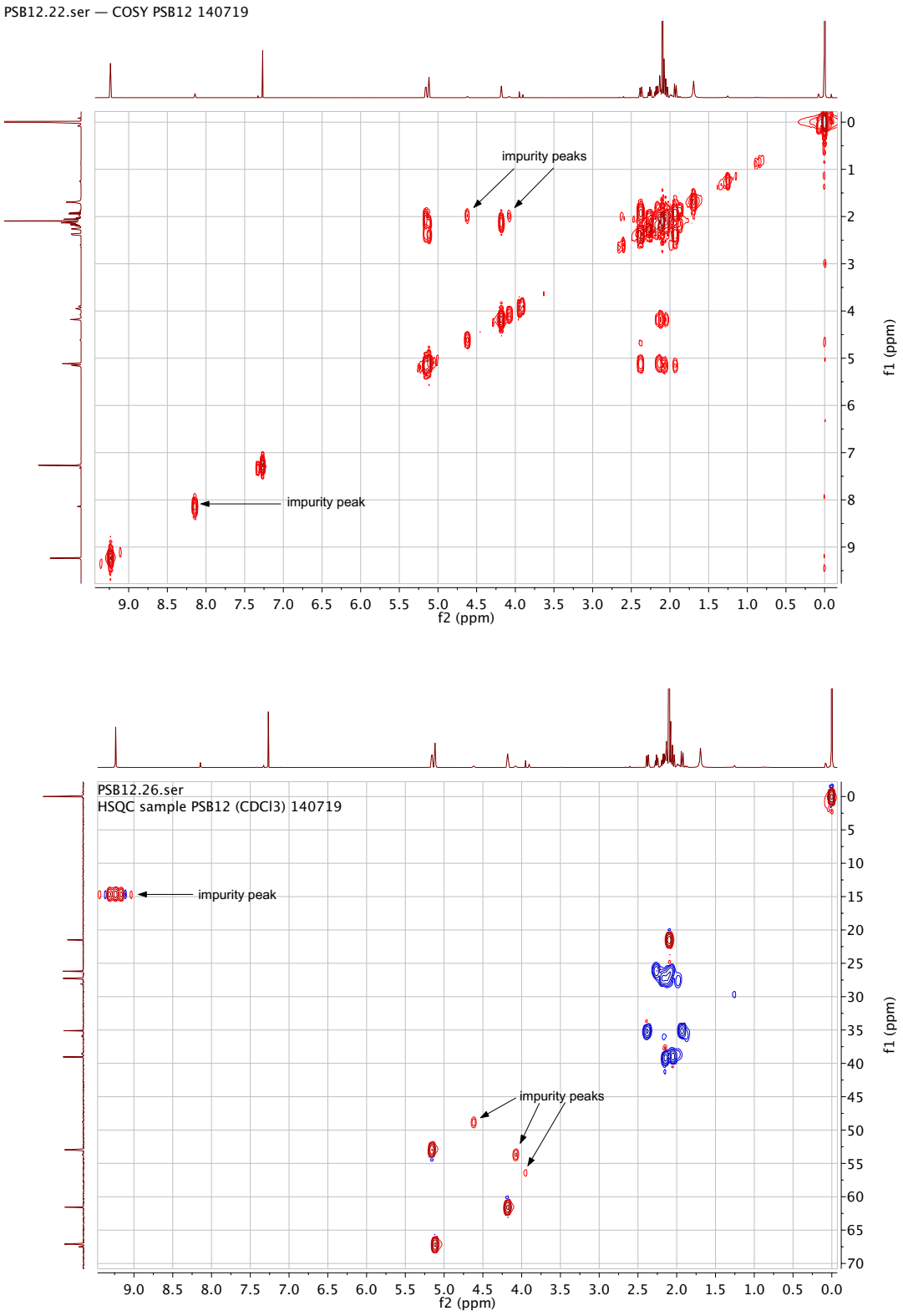

Appendix 32: COSY and HSQC Spectra of 3α-Acetoxy-*N*-formylnortropane (**10**).

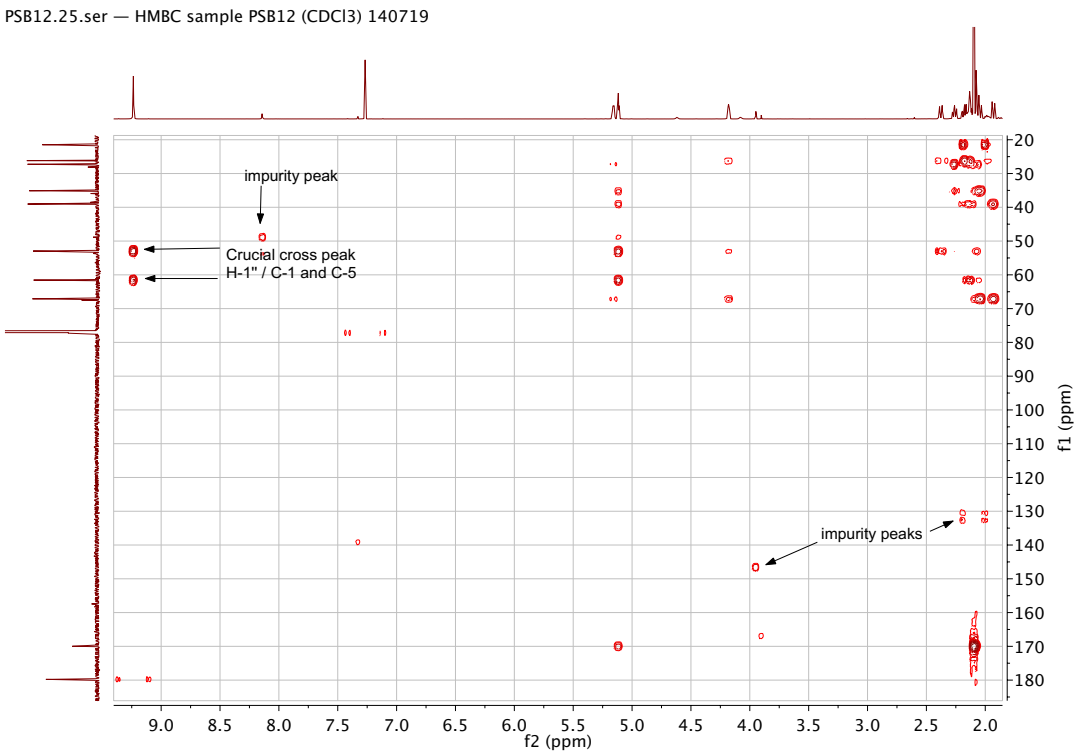

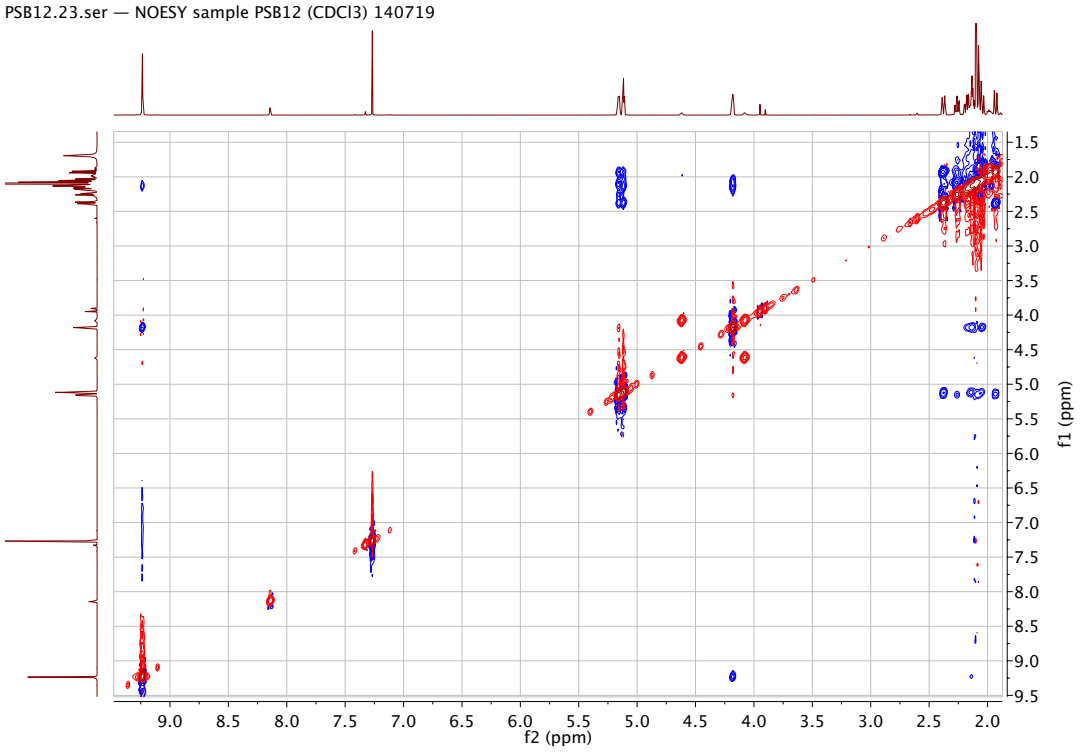

Appendix 33: HMBC and NOESY Spectra of 3α-Acetoxy-*N*-formylnortropane (**10**).

User Spectra

Fragmentor Voltage	Collision Energy	Ionization Mode
120	0	ESI

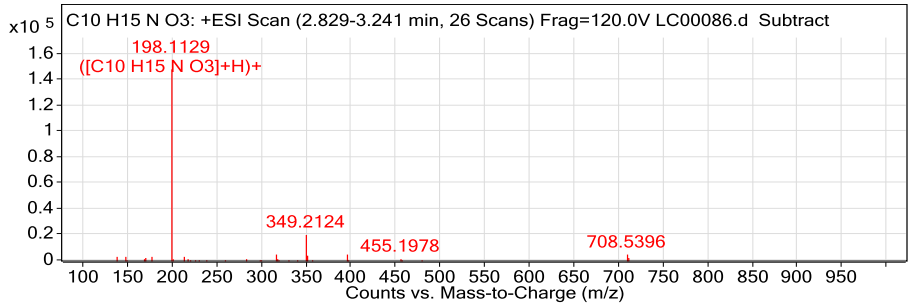

Peak List

m/z	z	Abund	Formula	Ion
138.0914	1	3469.5		
176.5753	1	3810.12		
198.1129	1	148438.06	C10 H15 N O3	(M+H)+
198.2386	2	4587.9		
199.1159	1	15477.26	C10 H15 N O3	(M+H)+
316.1339	1	5721.53		
349.2124	1	20707.74		
350.2177	1	4239.14		
395.217	1	5087.42		
708.5396	1	5210.56		

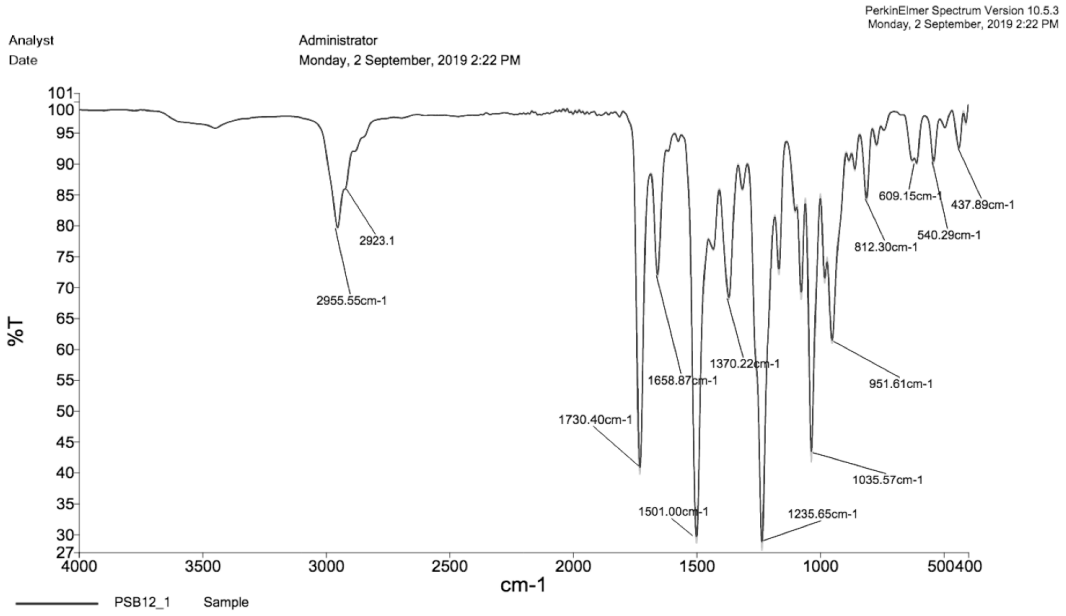

Appendix 34: HRESIMS (ESI+) and IR Spectra of 3α-Acetoxy-*N*-formylnortropane (**10**).

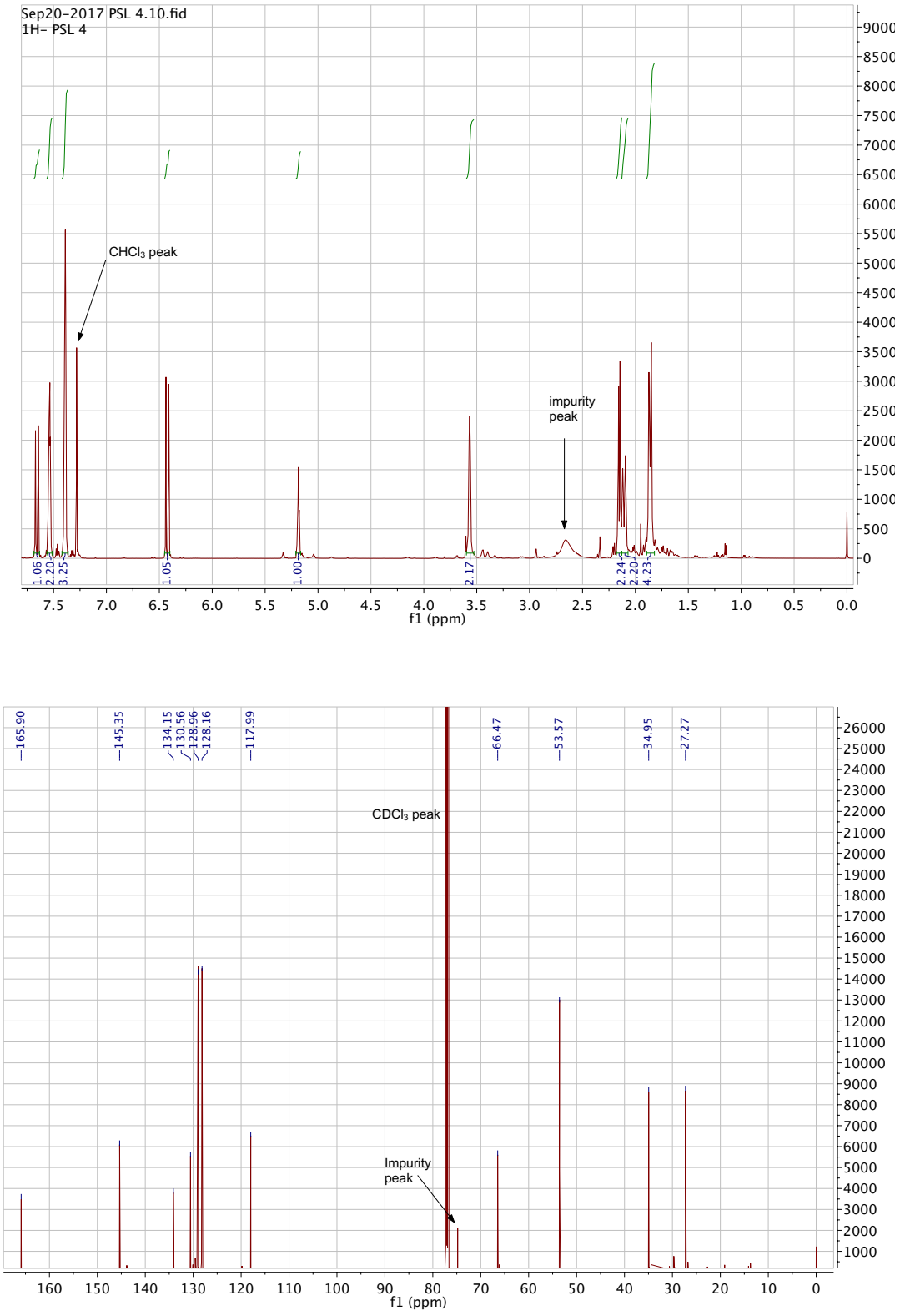

Appendix 35: ^{1}H and ^{13}C NMR Spectra of 3α-Cinnamoyloxynortropane (**11**).

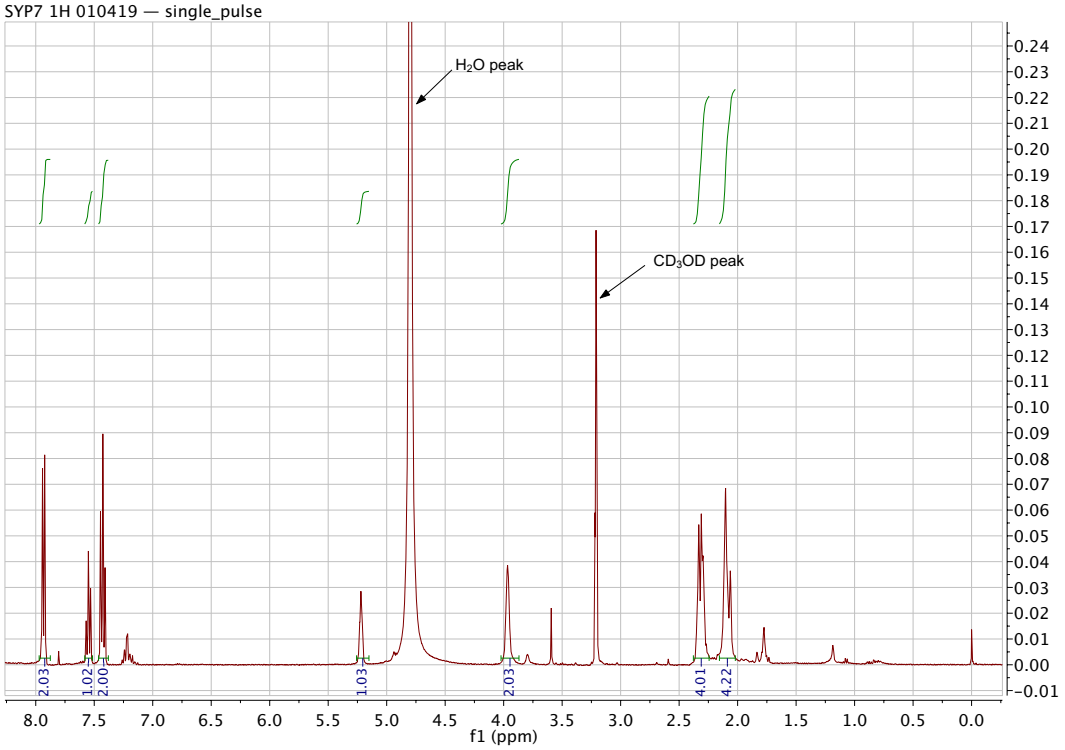

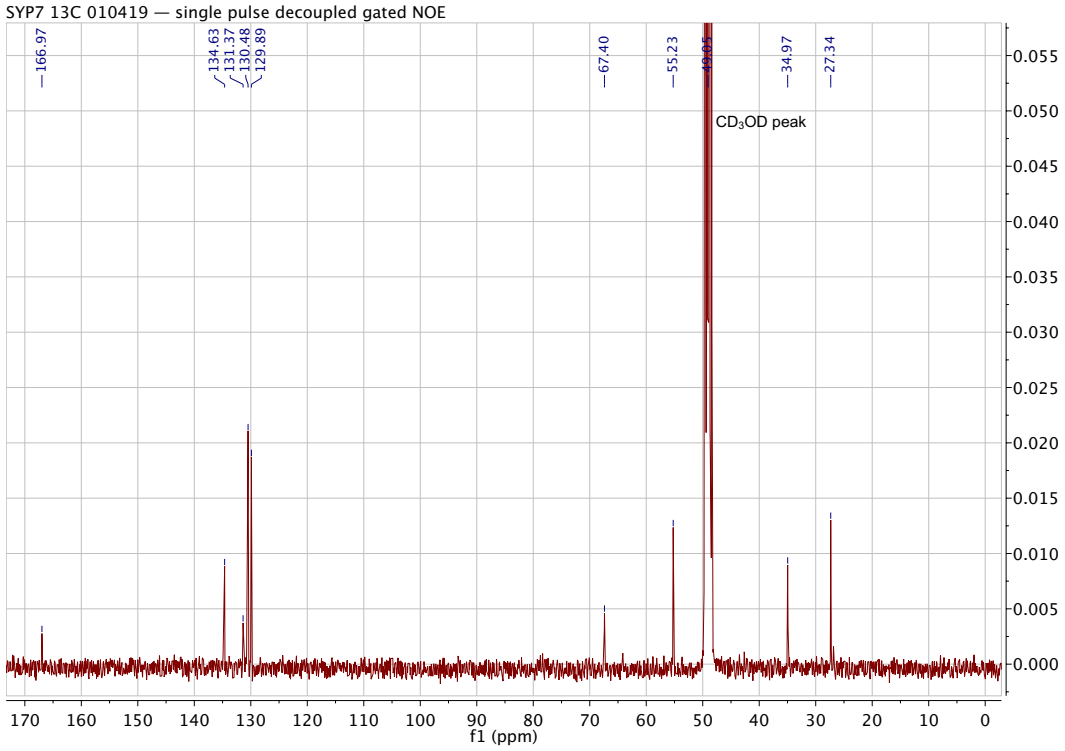

Appendix 36: ^{1}H and ^{13}C NMR Spectra of 3α-Benzoyloxynortropane (**12**).

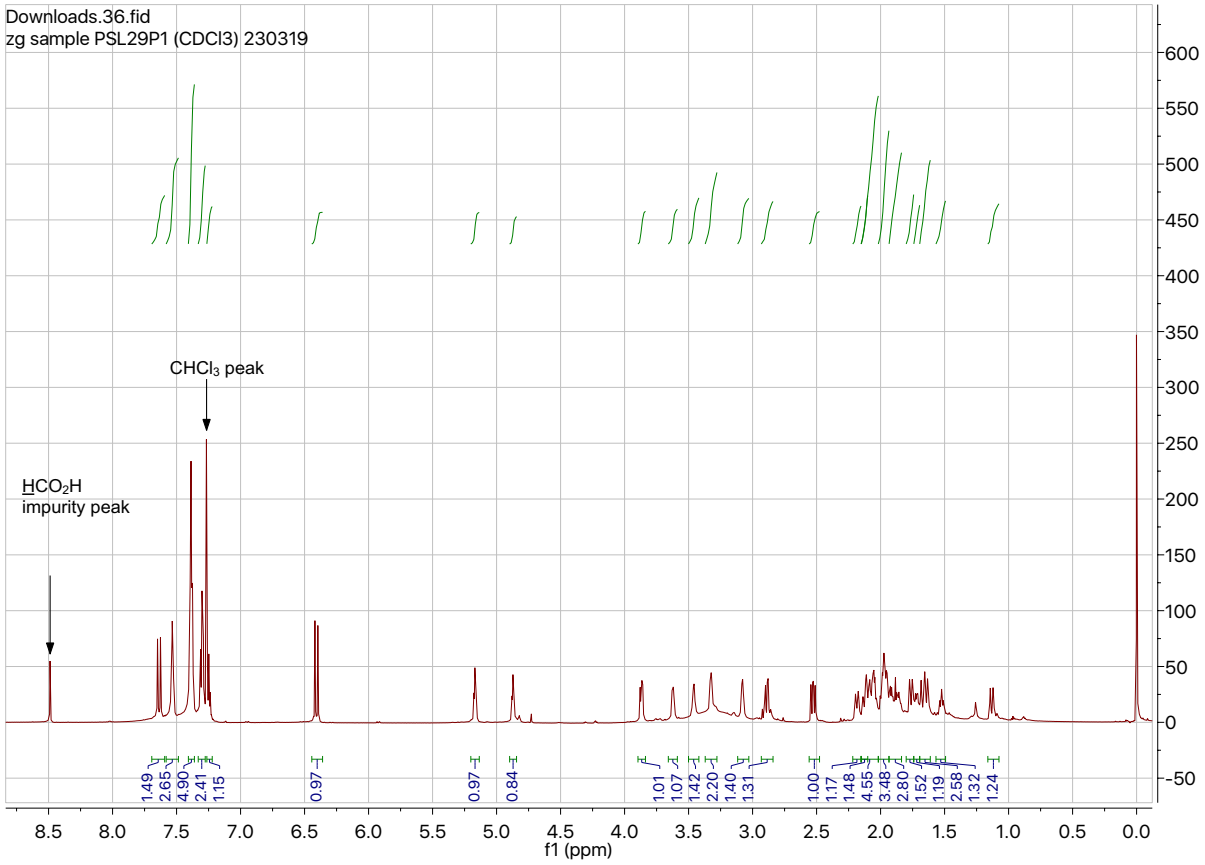

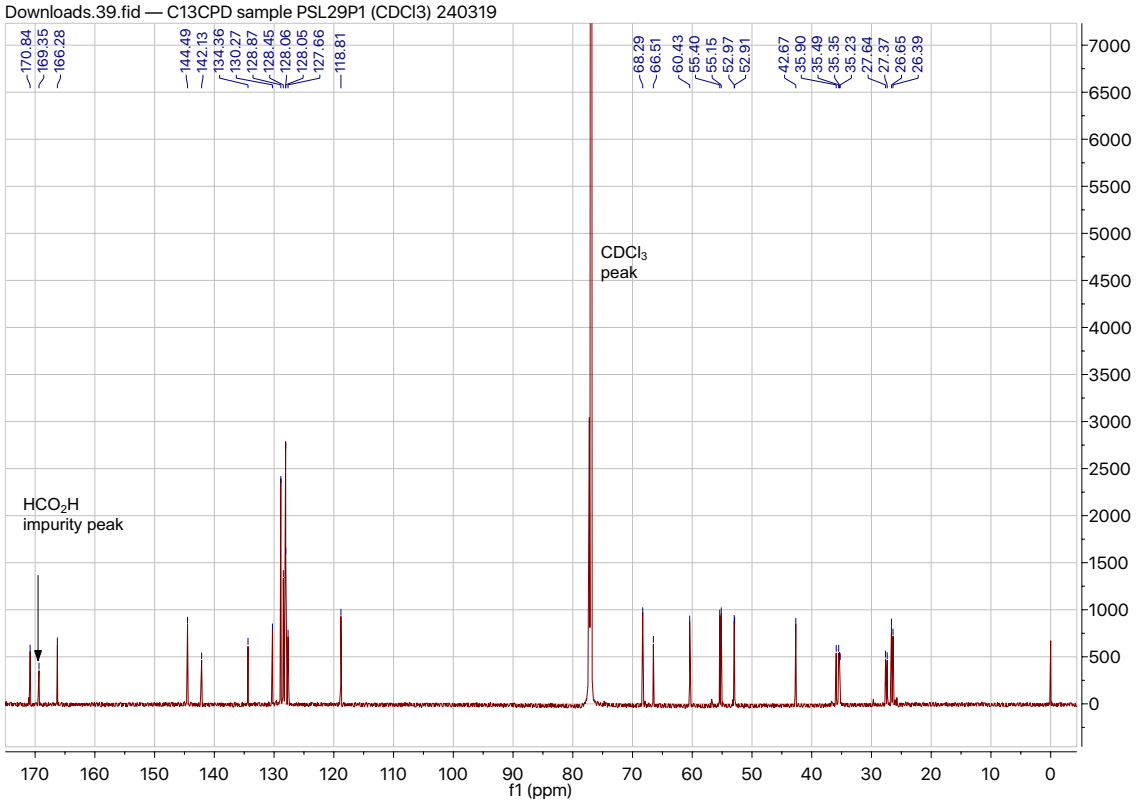

Appendix 37: ^{1}H and ^{13}C NMR Spectra of (±)-Bissaccardine (**13**).

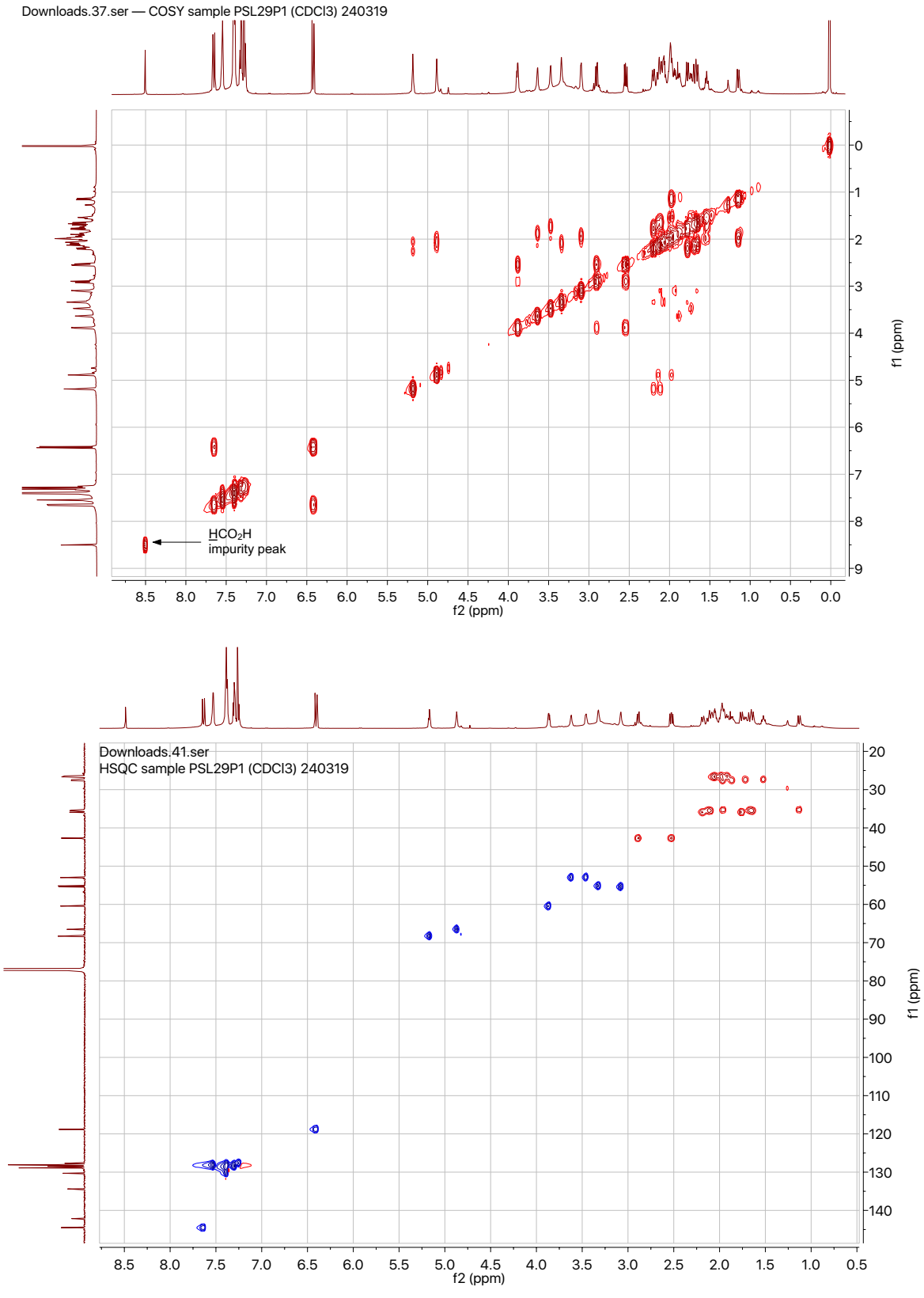

Appendix 38: COSY and HSQC Spectra of (±)-Bissaccardine (**13**).

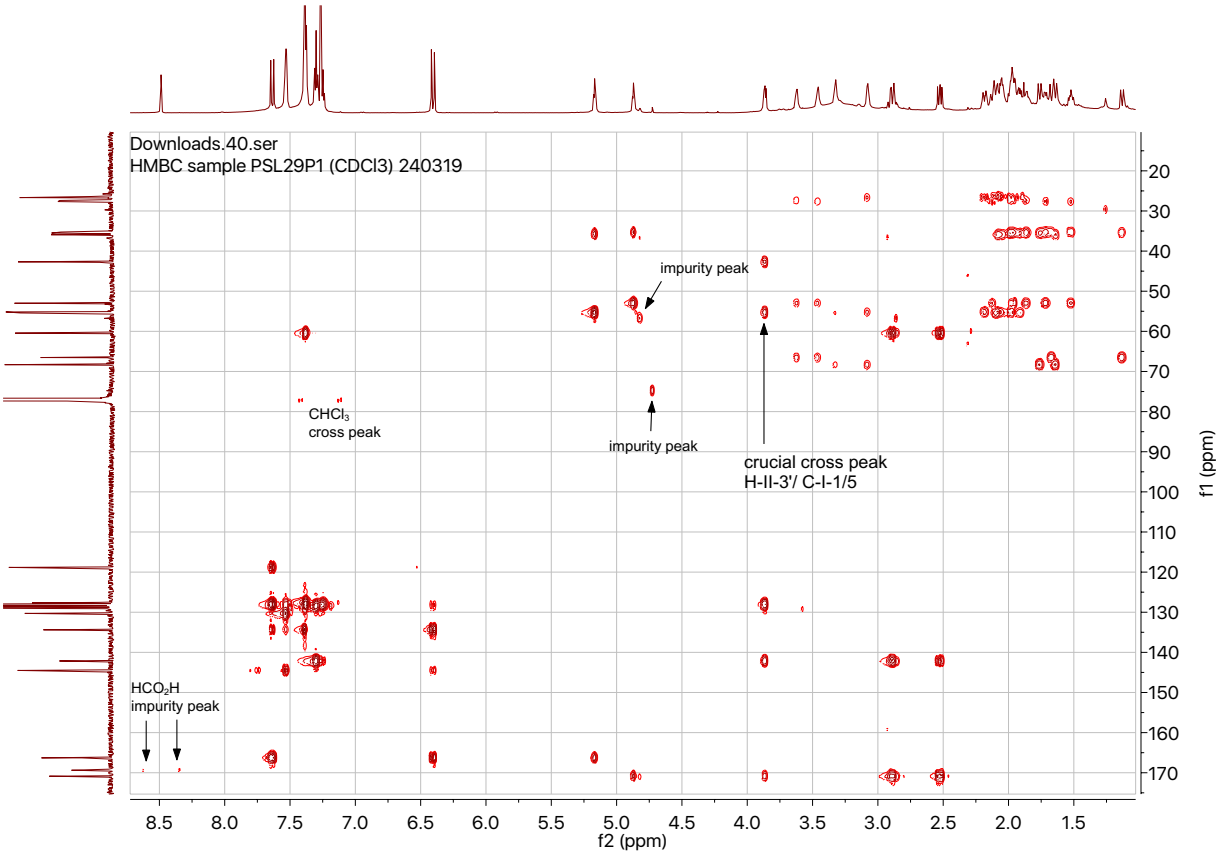

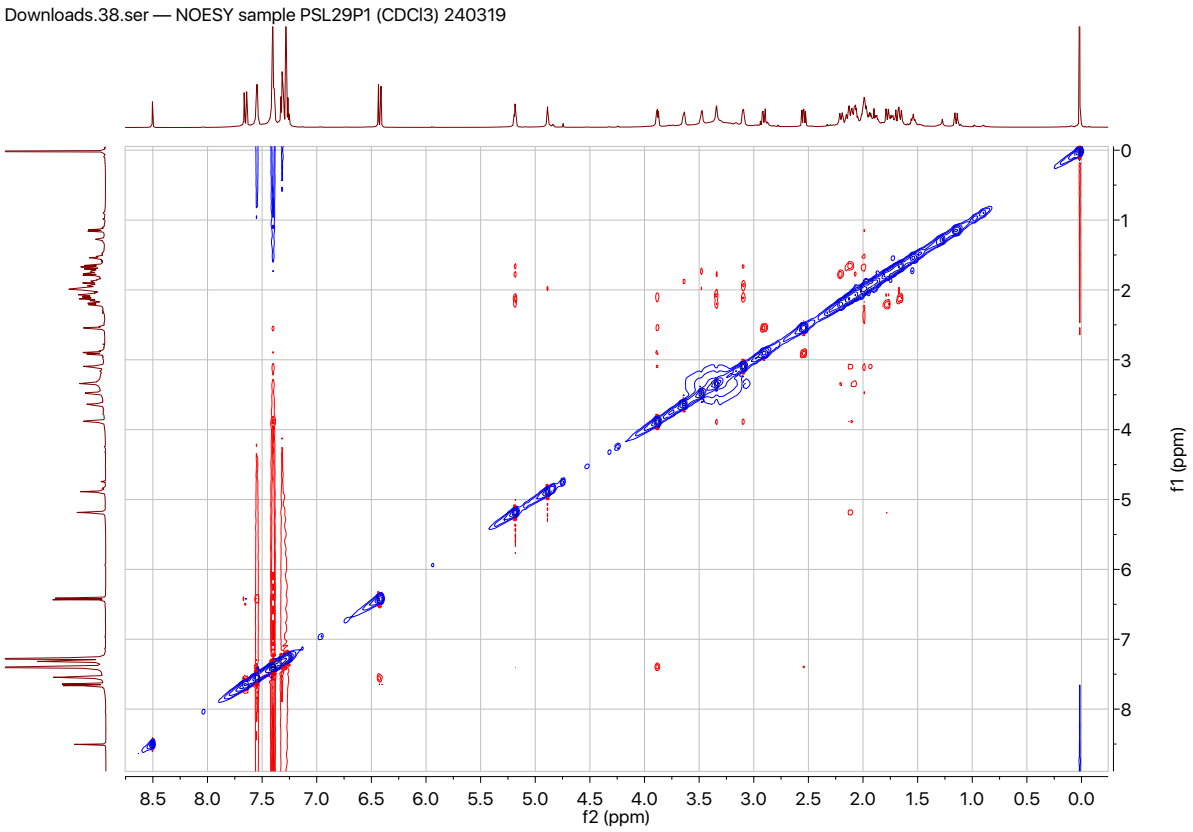

Appendix 39: HMBC and NOESY Spectra of (±)-Bissaccardine (**13**).

User Spectra

Fragmentor Voltage	Collision Energy	Ionization Mode
120	0	ESI

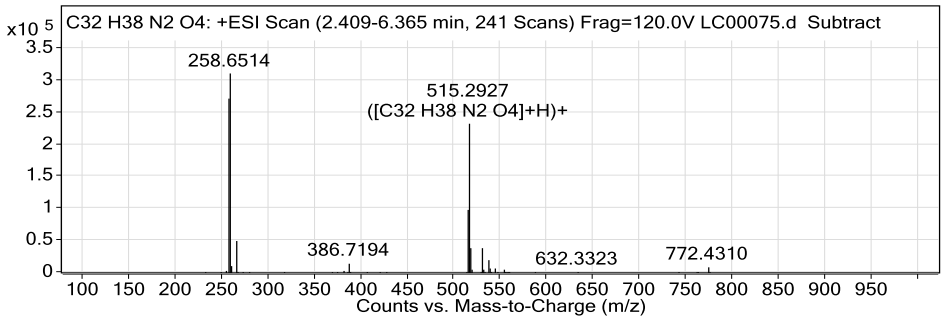

Peak List

m/z	z	Abund	Formula	Ion
258.1307		205772.95		
258.152		271310		
258.1784		237694.48		
258.6514	2	311376.31		
259.1526	2	71890.69		
265.1572	2	49881.65		
515.2635	2	98674.7		
515.2927		233100.47	C32 H38 N2 O4	(M+H)+
515.3295		136222.61	C22 H42 N8 O6	(M+H)+
516.2945	1	213965.78	C25 H37 N7 O5	(M+H)+

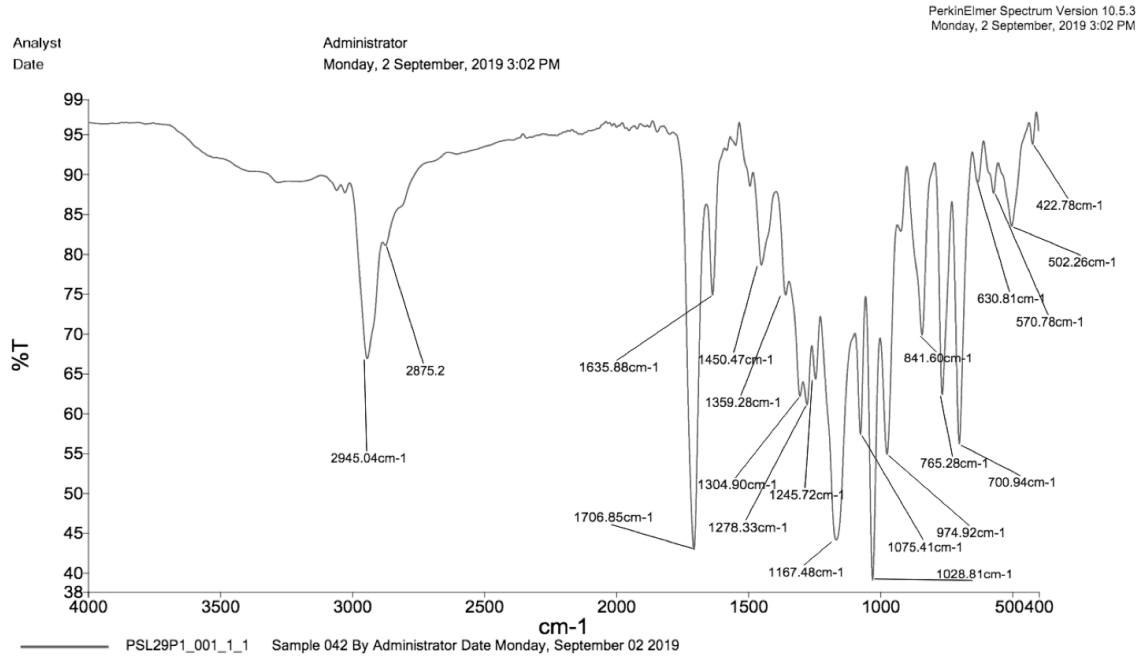

Appendix 40: HRESIMS (ESI+) and IR Spectra of (±)-Bissaccardine (**13**).

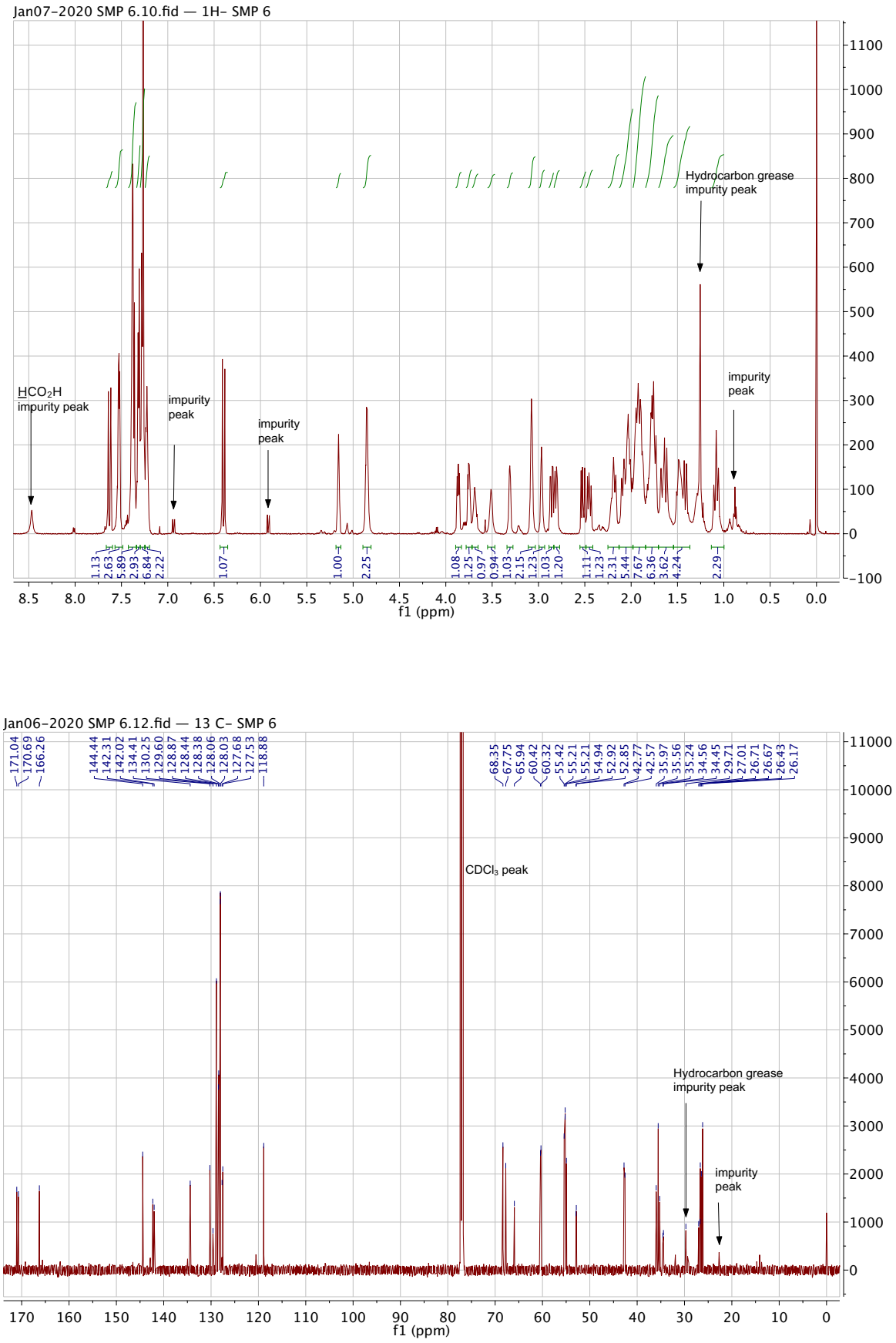

Appendix 41: ^{1}H and ^{13}C NMR Spectra of (±)-Trissaccardine (**14**).

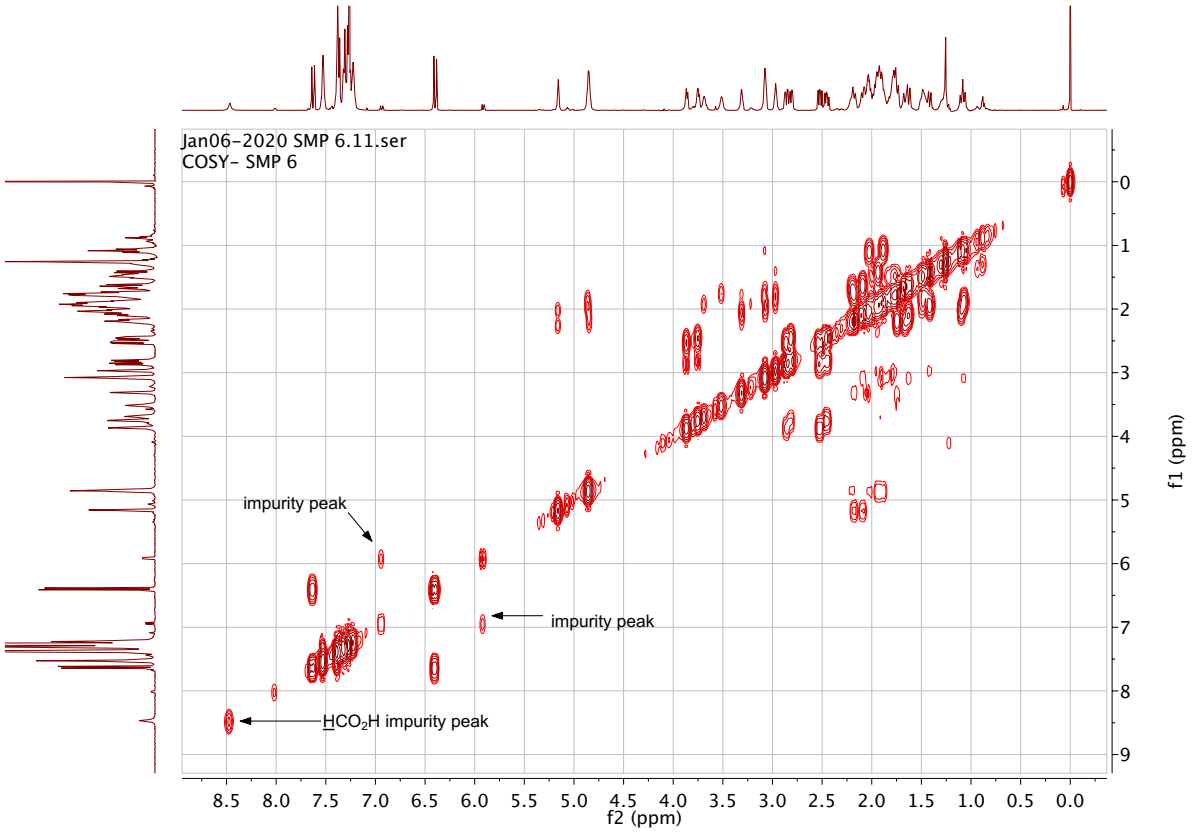

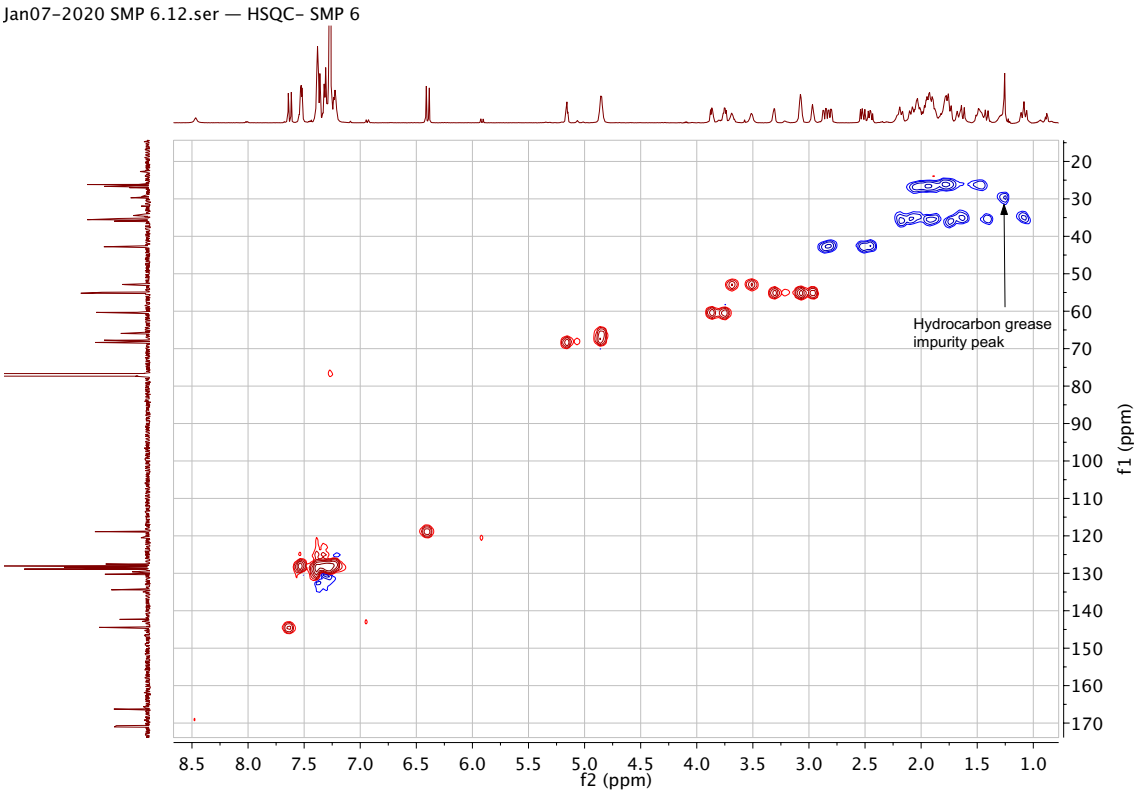

Appendix 42: COSY and HSQC Spectra of (±)-Trissaccardine (**14**).

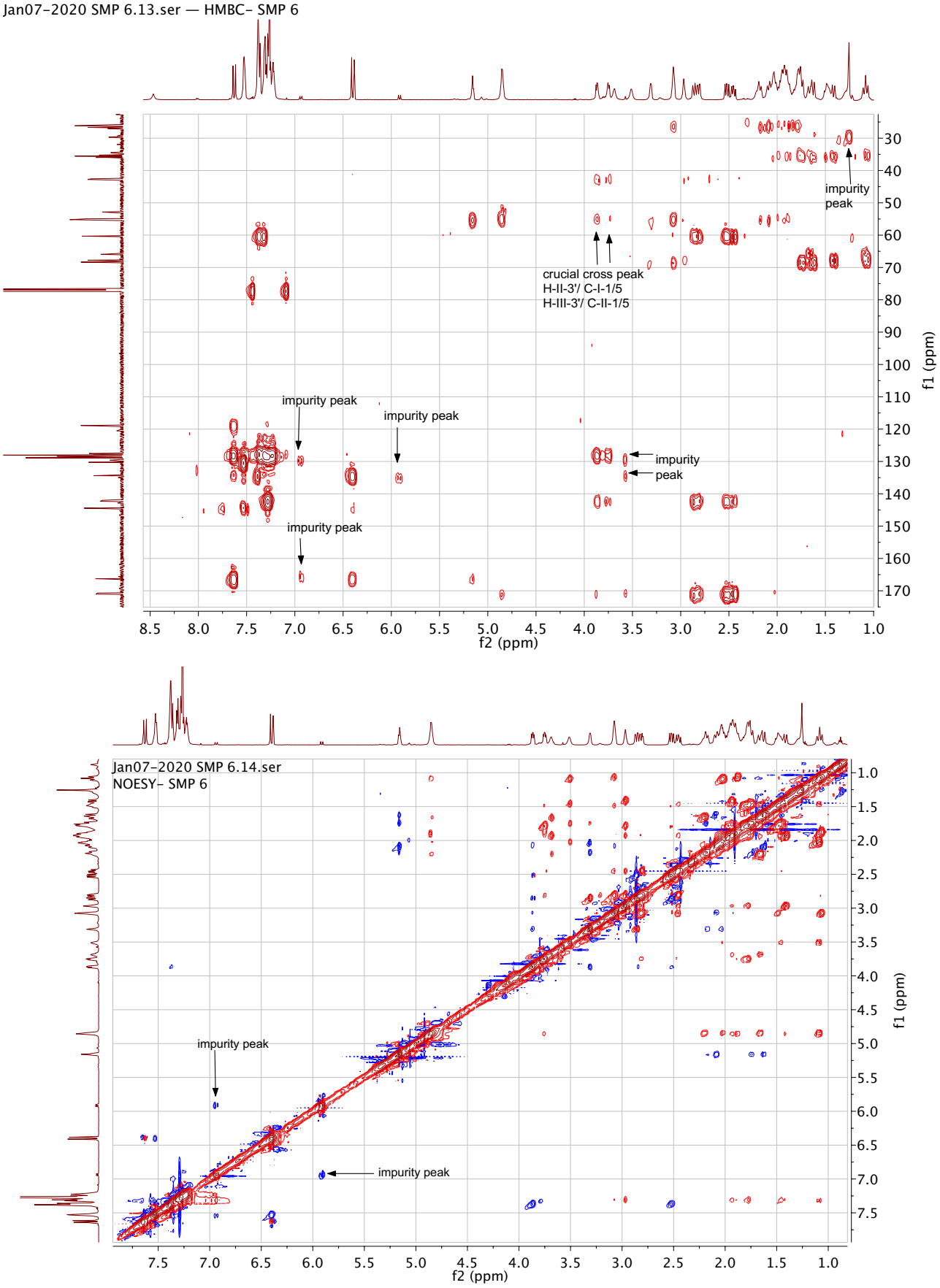

Appendix 43: HMBC and NOESY Spectra of (±)-Trissaccardine (**14**).

User Spectra

Fragmentor Voltage	Collision Energy	Ionization Mode
175	0	ESI

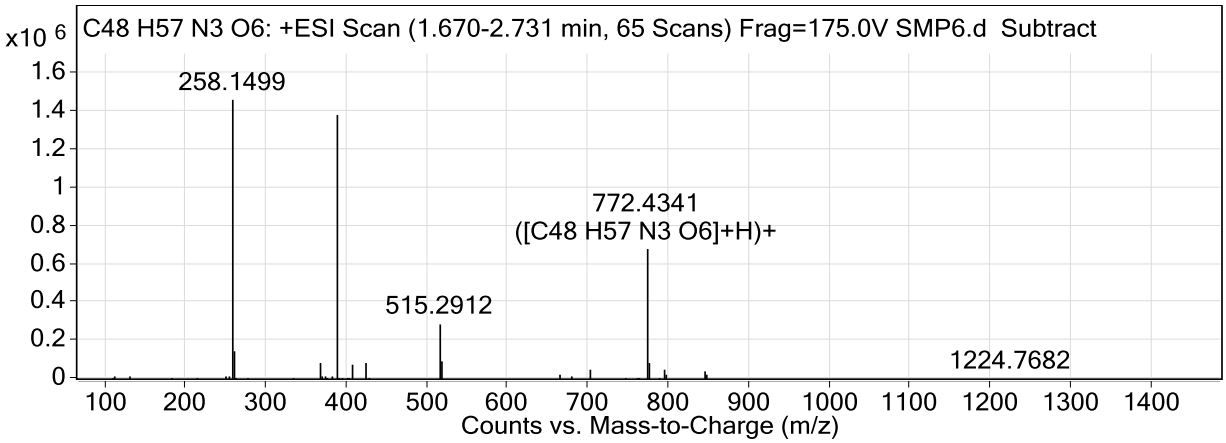

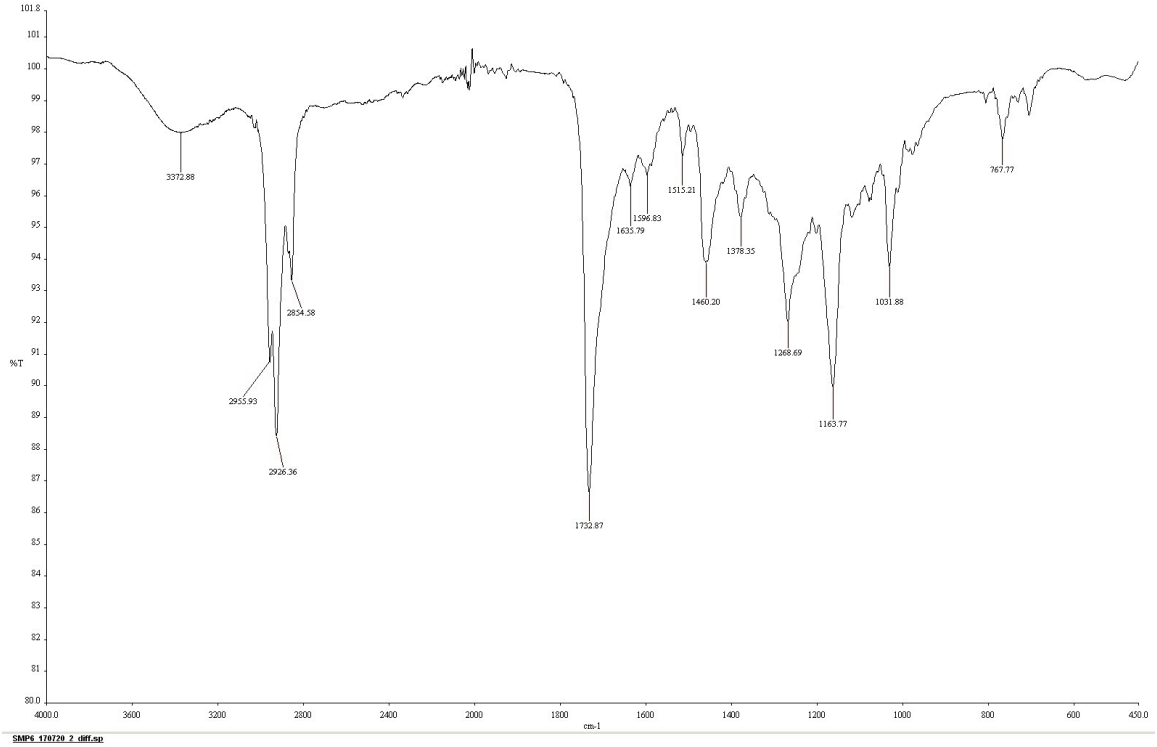

Appendix 44: HRESIMS (ESI+) and IR Spectra of (±)-Trissaccardine (**14**).

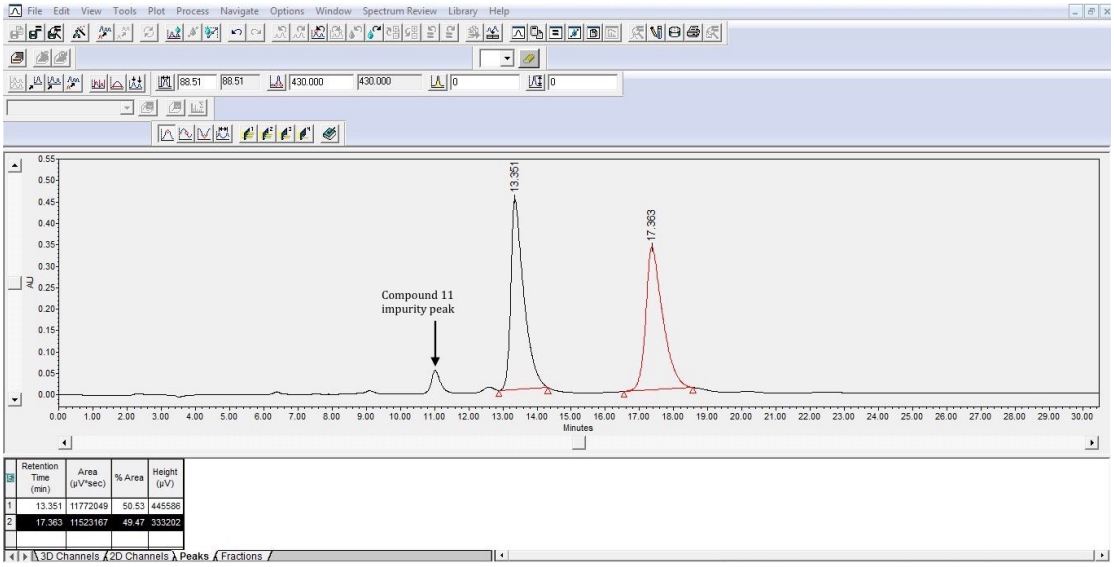

Appendix 45: Chiral-phase HPLC Chromatogram of (±)-Bissaccardine (**13**).
Note: Partial decomposition of **13** into **11** was observed.

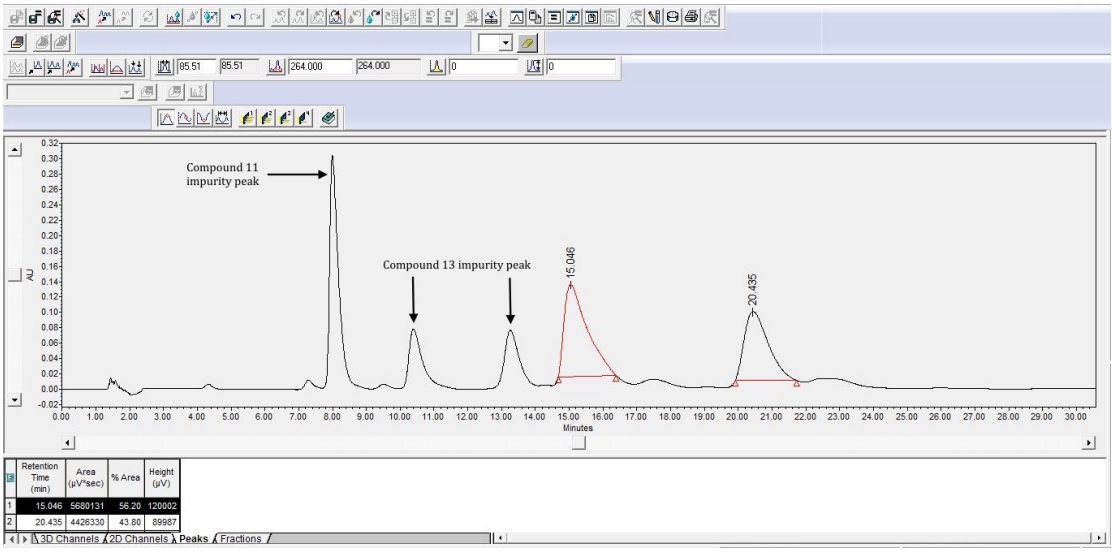

Appendix 46: Chiral-phase HPLC Chromatogram of (±)-Trissaccardine (**14**).
Note: Partial decomposition of **14** into **11** and **13** was observed.

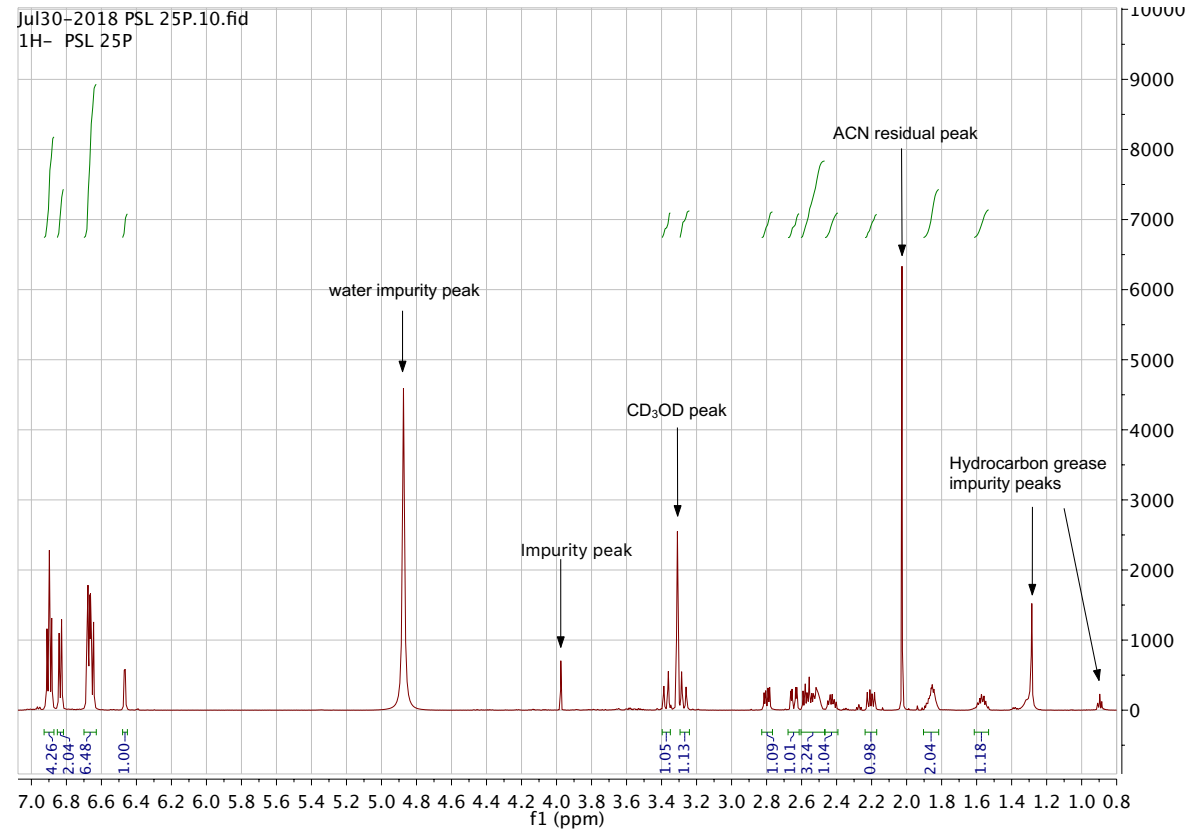

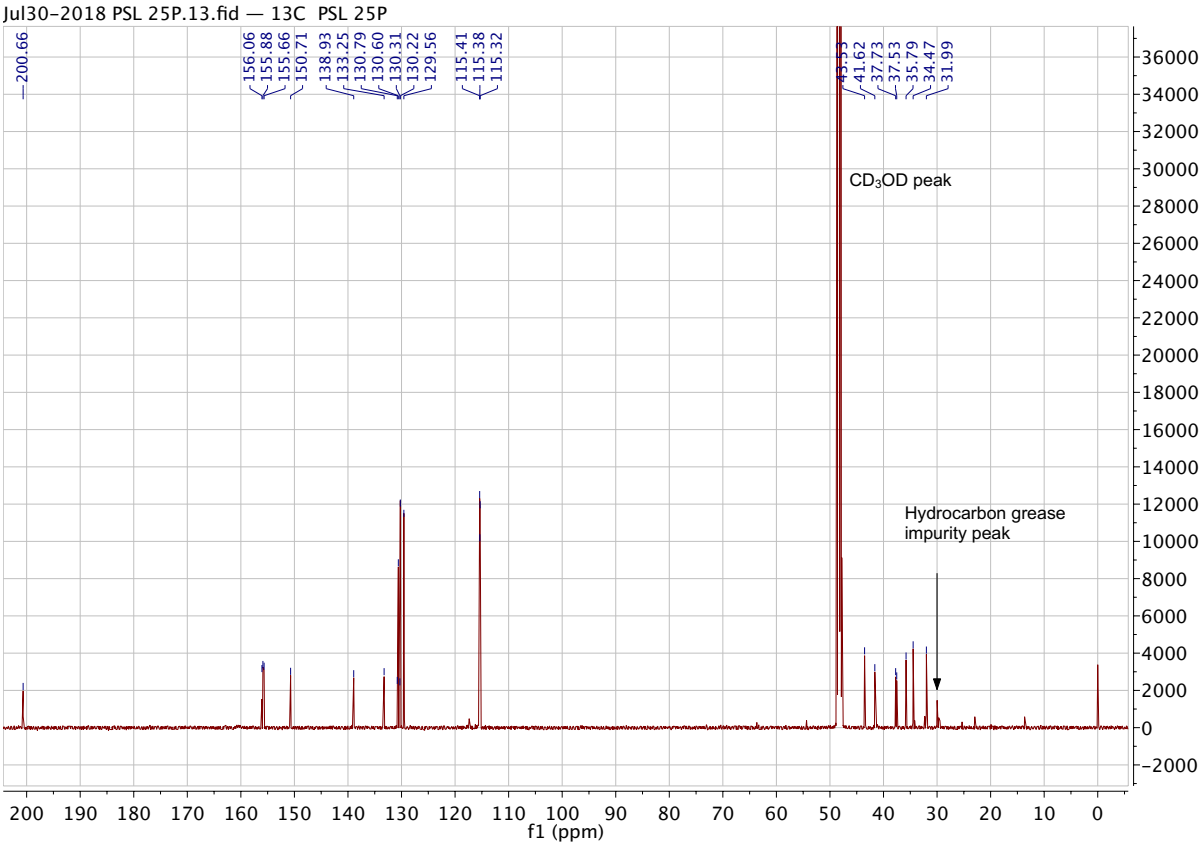

Appendix 47: ^{1}H and ^{13}C NMR Spectra of (±)-Saccardianone A (**15**).

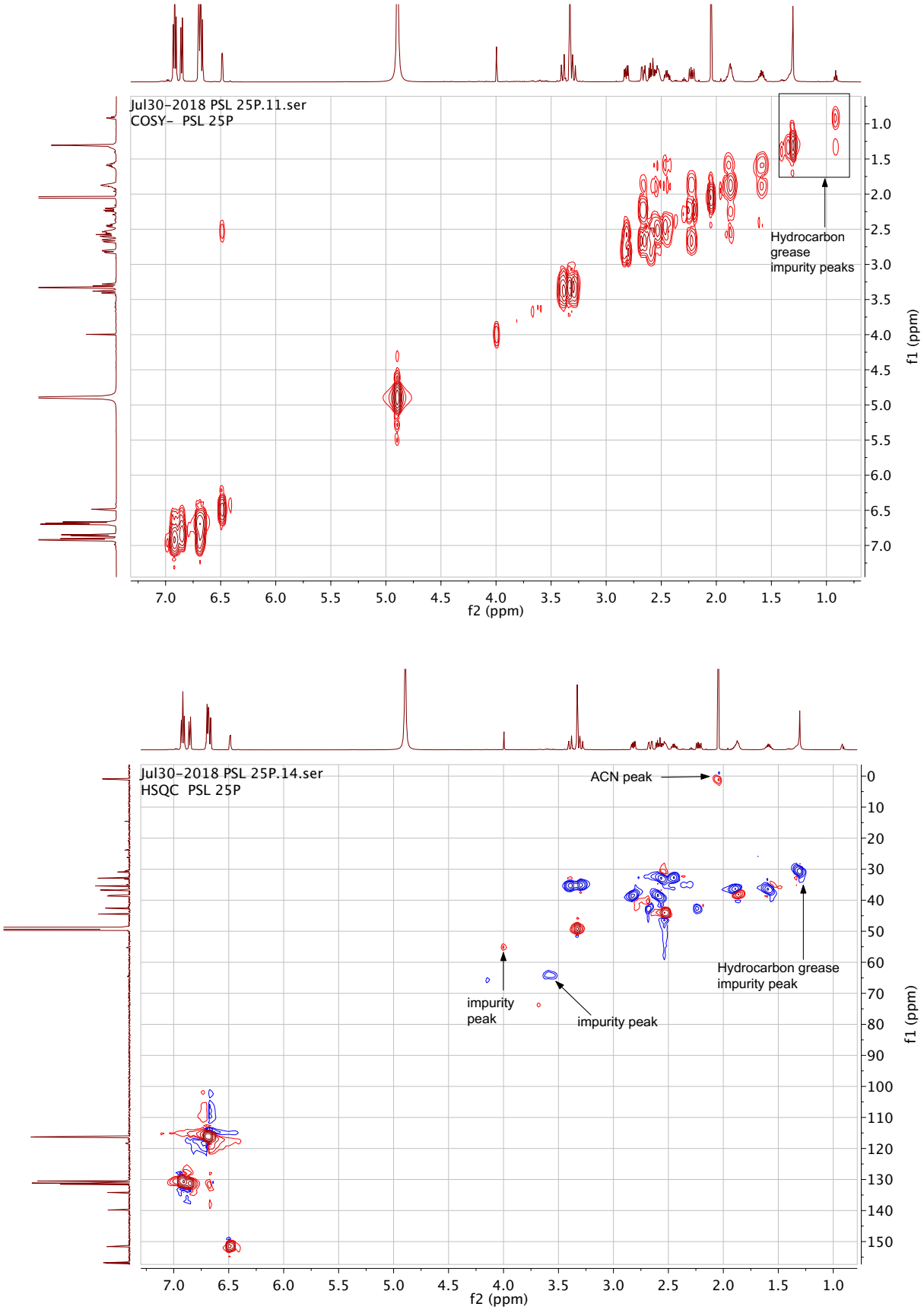

Appendix 48: COSY and HSQC Spectra of (±)-Saccardianone A (**15**).

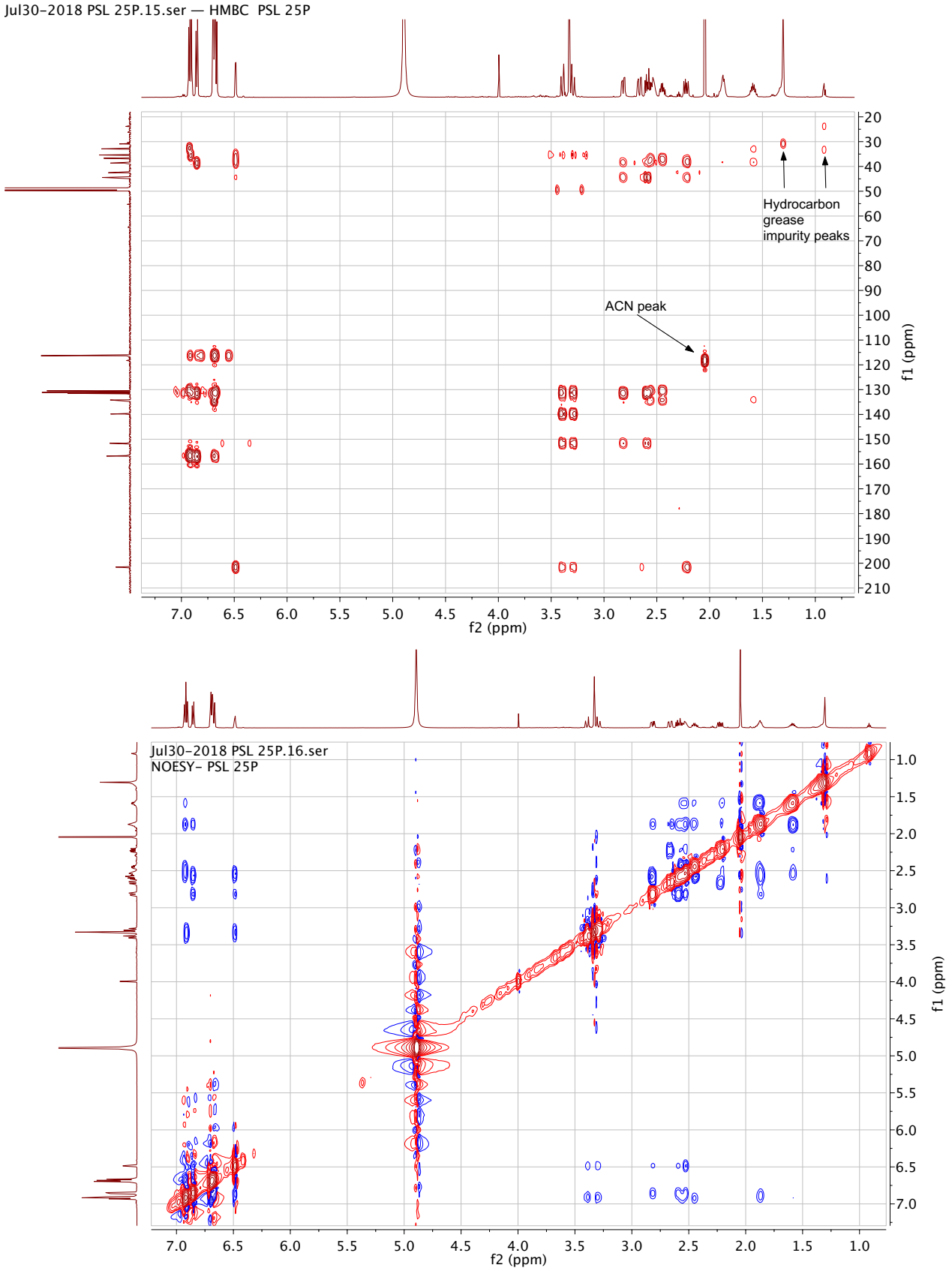

Appendix 49: HMBC and NOESY Spectra of (±)-Saccardianone A (**15**).

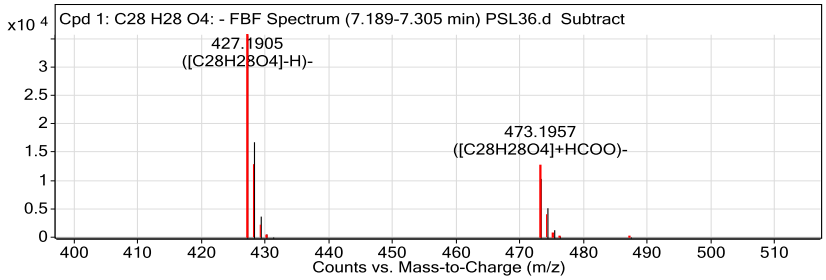

MS Spectrum Peak List

m/z	z	Abund	Formula	Ion
427.1905	1	35691.42	C28H28O4	(M-H)-
428.195	1	16926.09	C28H28O4	(M-H)-
429.199	1	3808.62	C28H28O4	(M-H)-
430.2026	1	726.09	C28H28O4	(M-H)-
431.2016	1	154.29	C28H28O4	(M-H)-
473.1957	1	10557.34	C28H28O4	(M+HCOO)-
474.2	1	5365.83	C28H28O4	(M+HCOO)-
475.2046	1	1472.26	C28H28O4	(M+HCOO)-
476.2082	1	308.7	C28H28O4	(M+HCOO)-
487.2088	1	117.18	C28H28O4	(M+CH3COO)-

--- End Of Report ---

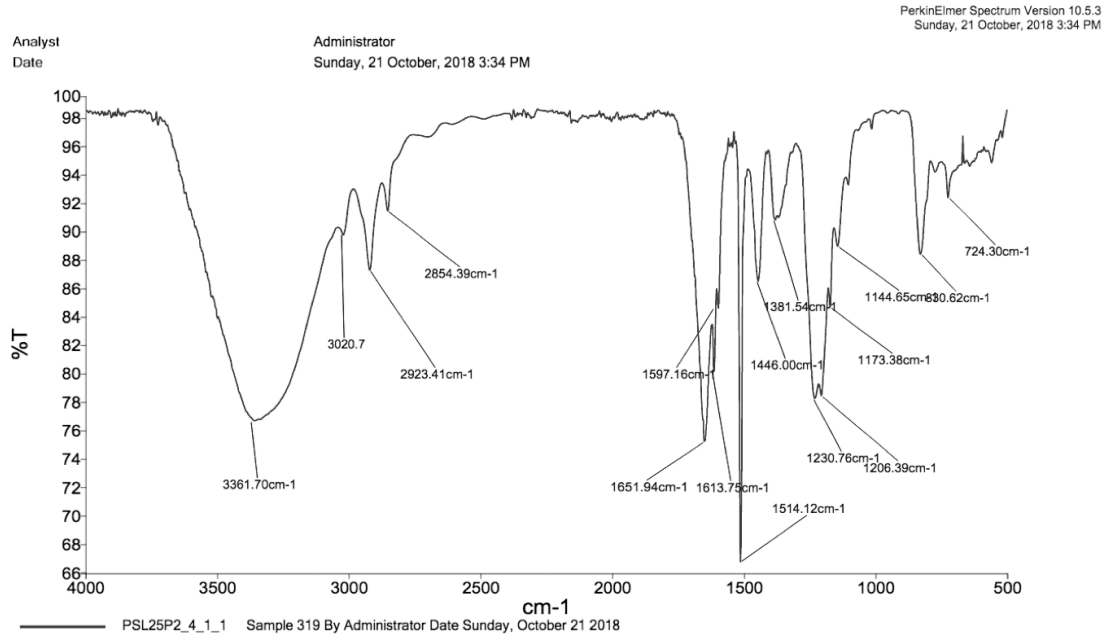

Appendix 50: HRESIMS (ESI-) and IR Spectra of (±)-Saccardianone A (**15**).

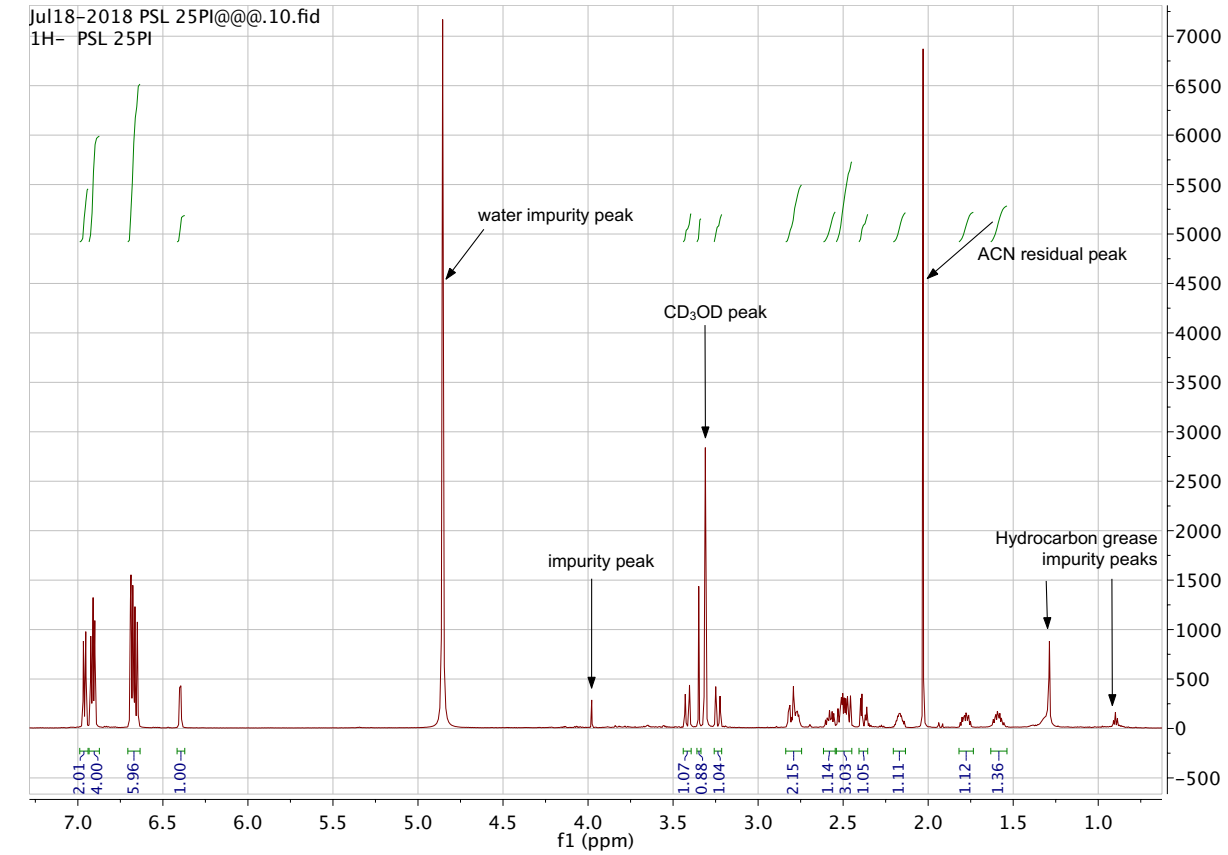

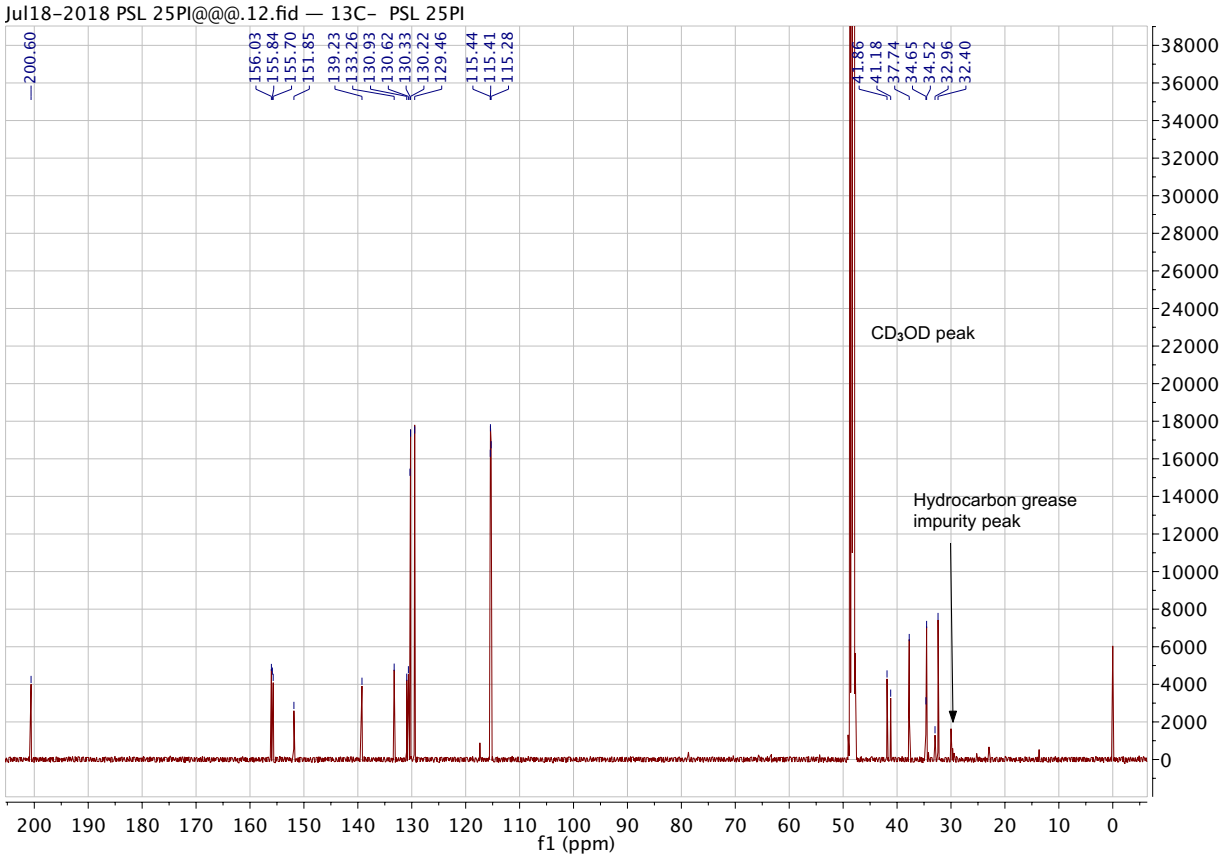

Appendix 51: ^{1}H and ^{13}C NMR Spectra of (±)-Saccardianone B (**16**).

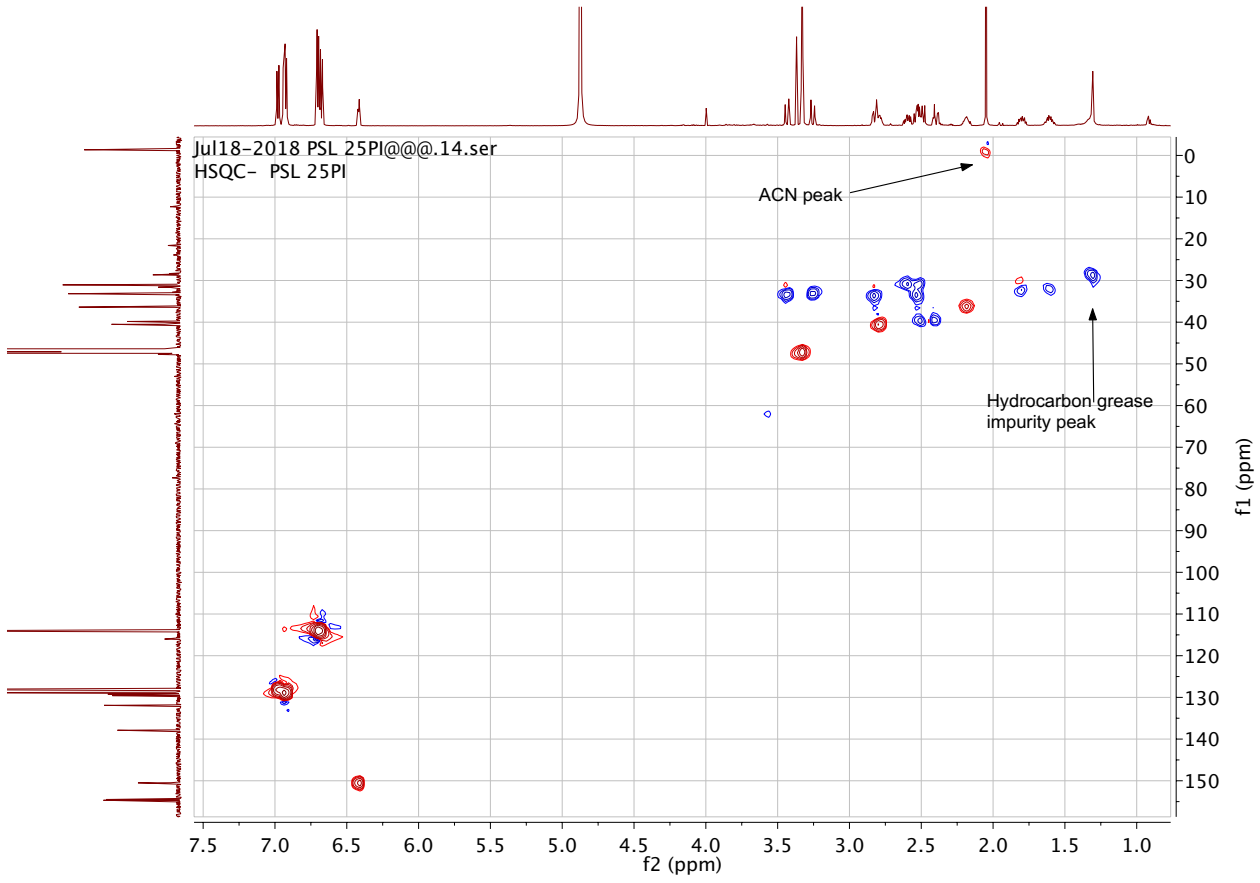

Appendix 52: COSY and HSQC Spectra of (±)-Saccardianone B (**16**).

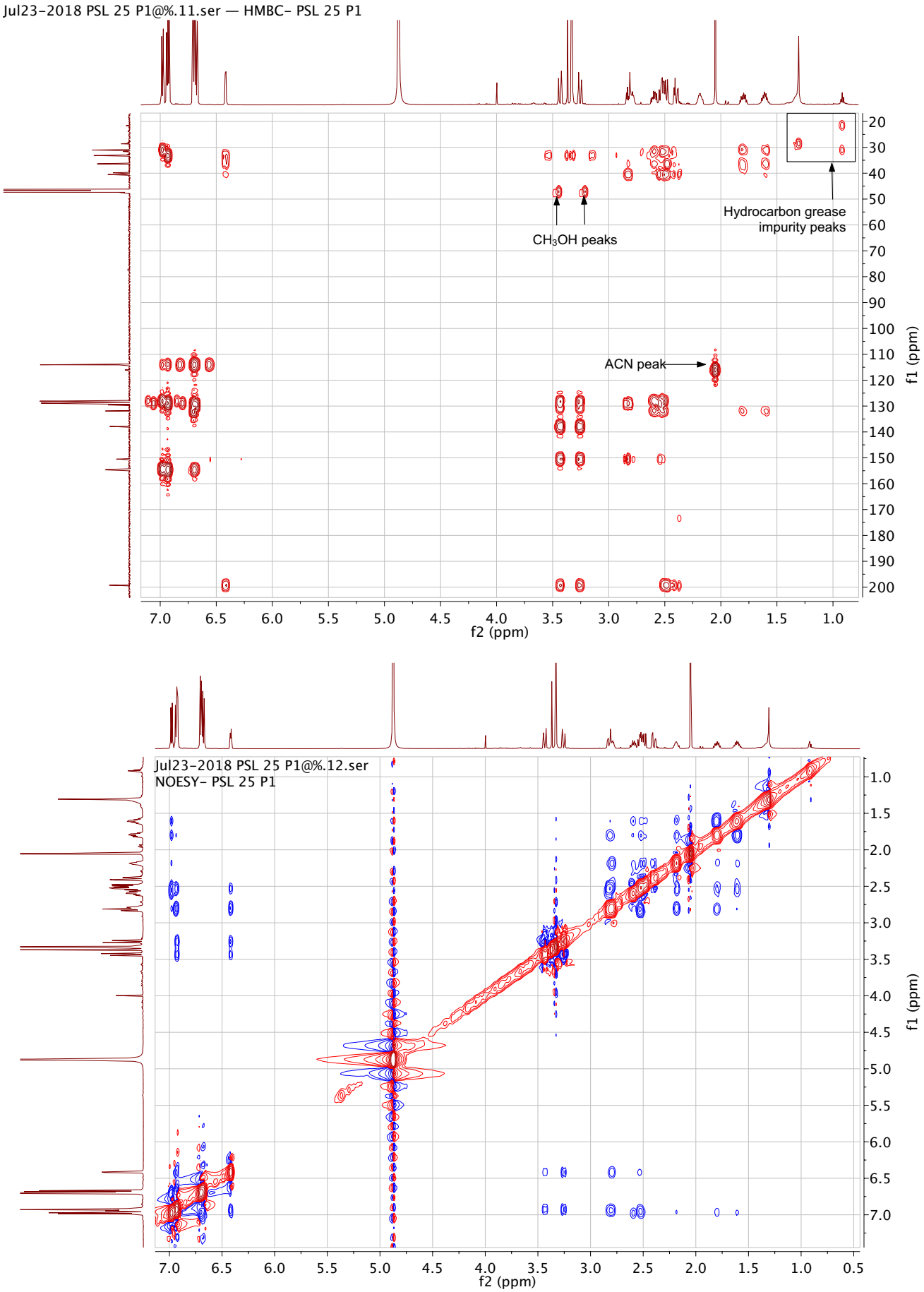

Appendix 53: HMBC and NOESY Spectra of (±)-Saccardianone B (**16**).

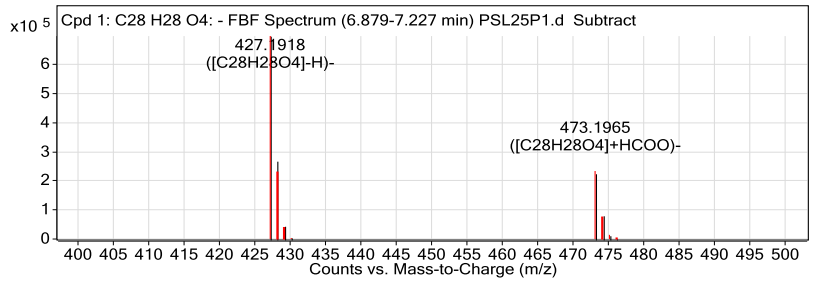

MS Spectrum Peak List

m/z	z	Abund	Formula	Ion
427.1918	1	698272.56	C28H28O4	(M-H)-
428.1956	1	270736.63	C28H28O4	(M-H)-
429.1989	1	47592.61	C28H28O4	(M-H)-
430.2017	1	5807.72	C28H28O4	(M-H)-
431.2042	1	762.58	C28H28O4	(M-H)-
473.1965	1	226685	C28H28O4	(M+HCOO)-
474.2005	1	82321.99	C28H28O4	(M+HCOO)-
475.2039	1	15568.39	C28H28O4	(M+HCOO)-
476.207	1	2324.81	C28H28O4	(M+HCOO)-
477.2087	1	339.67	C28H28O4	(M+HCOO)-

--- End Of Report ---

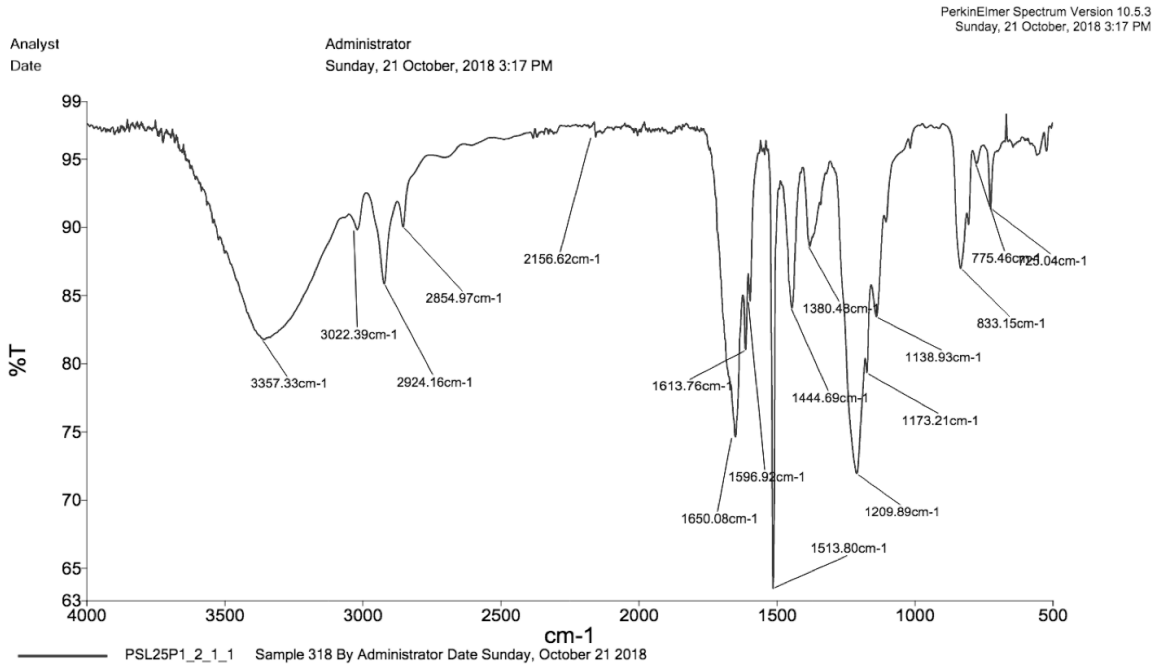

Appendix 54: HRESIMS (ESI-) and IR Spectra of (±)-Saccardianone B (**16**).

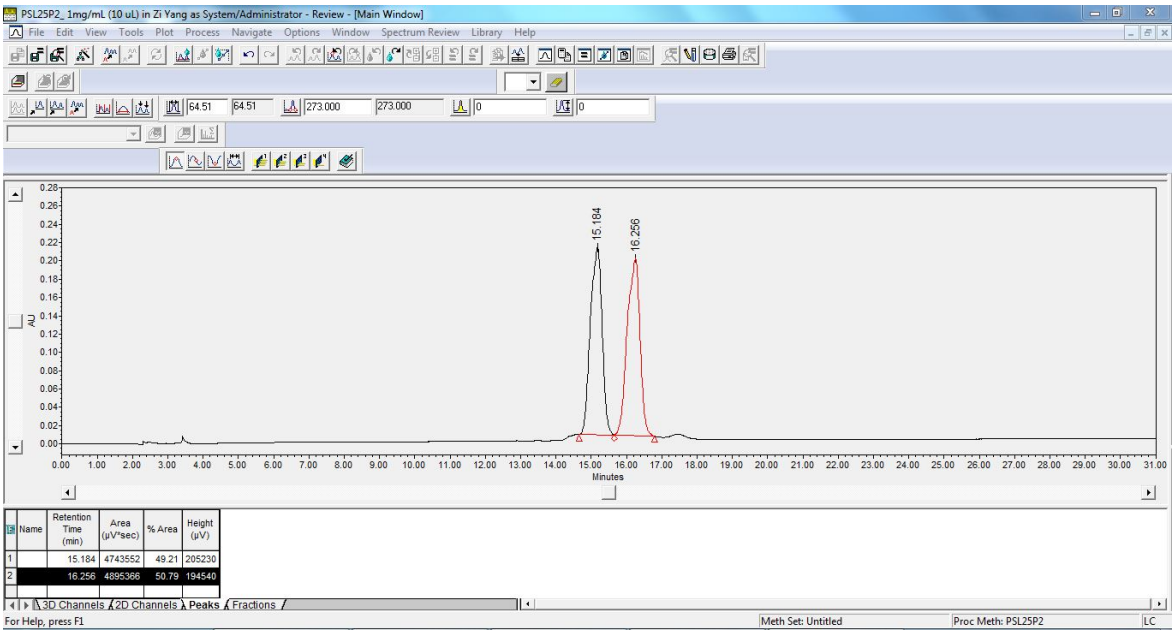

Appendix 55: Chiral-phase HPLC Chromatogram of (±)-Saccardianone A (**15**).

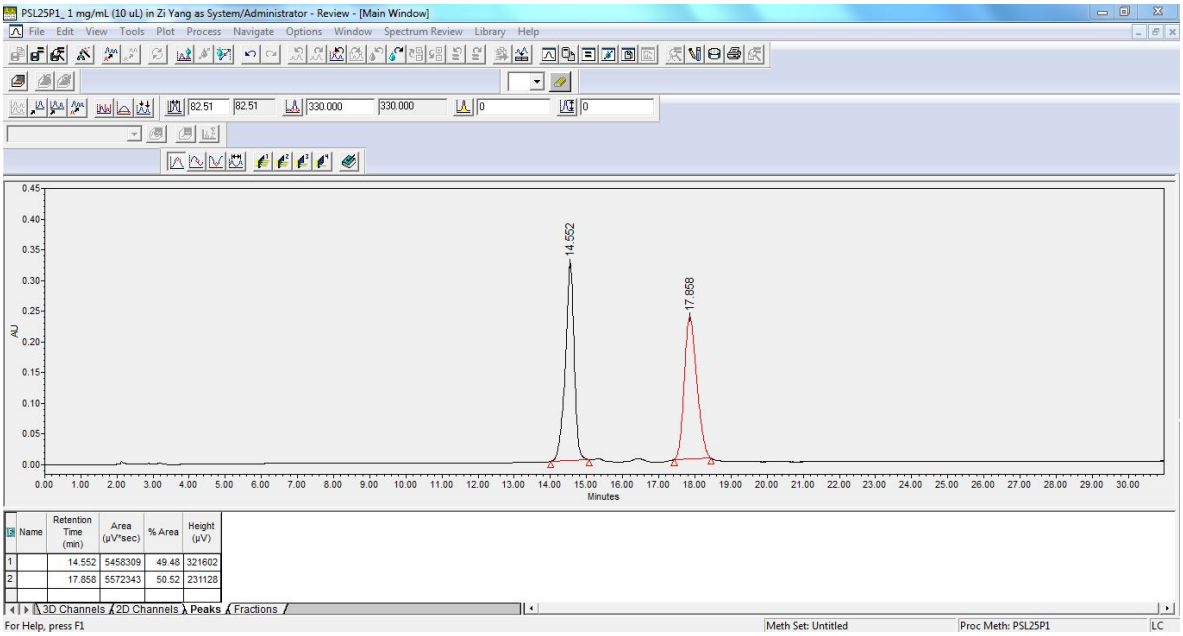

Appendix 56: Chiral-phase HPLC Chromatogram of (±)-Saccardianone B (**16**).

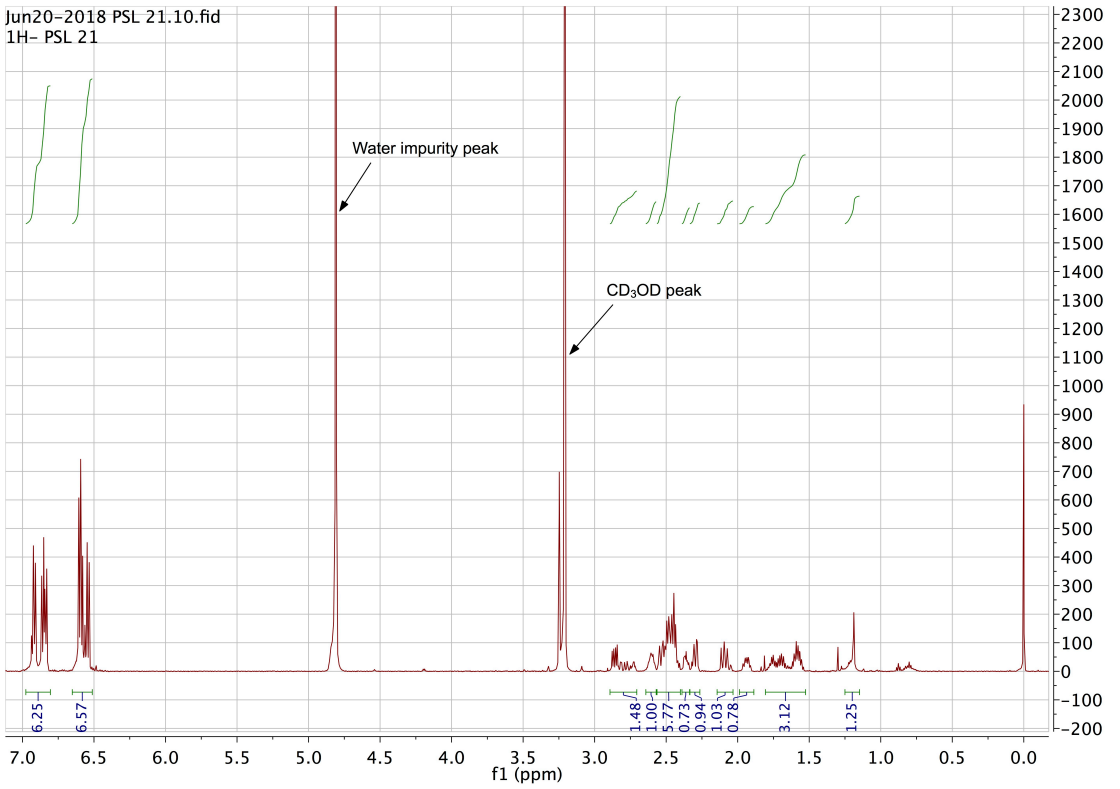

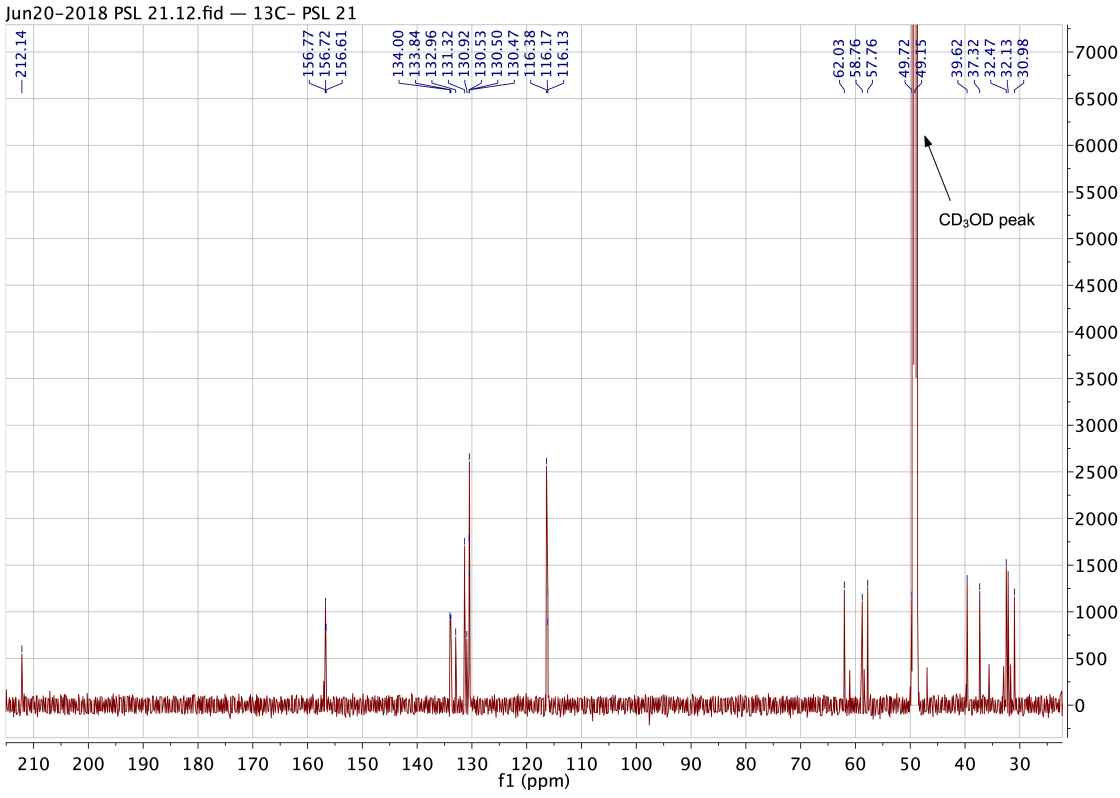

Appendix 57: ^{1}H and ^{13}C NMR Spectra of (±)-Saccardianine A (**17**).

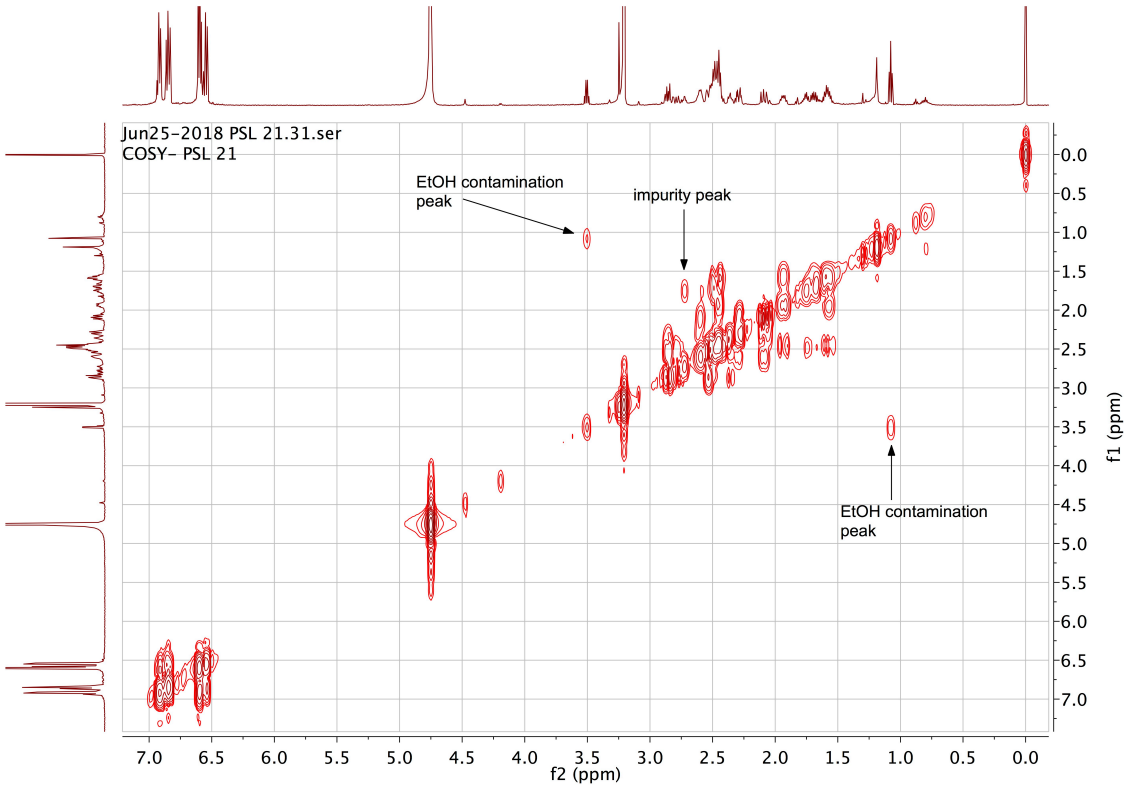

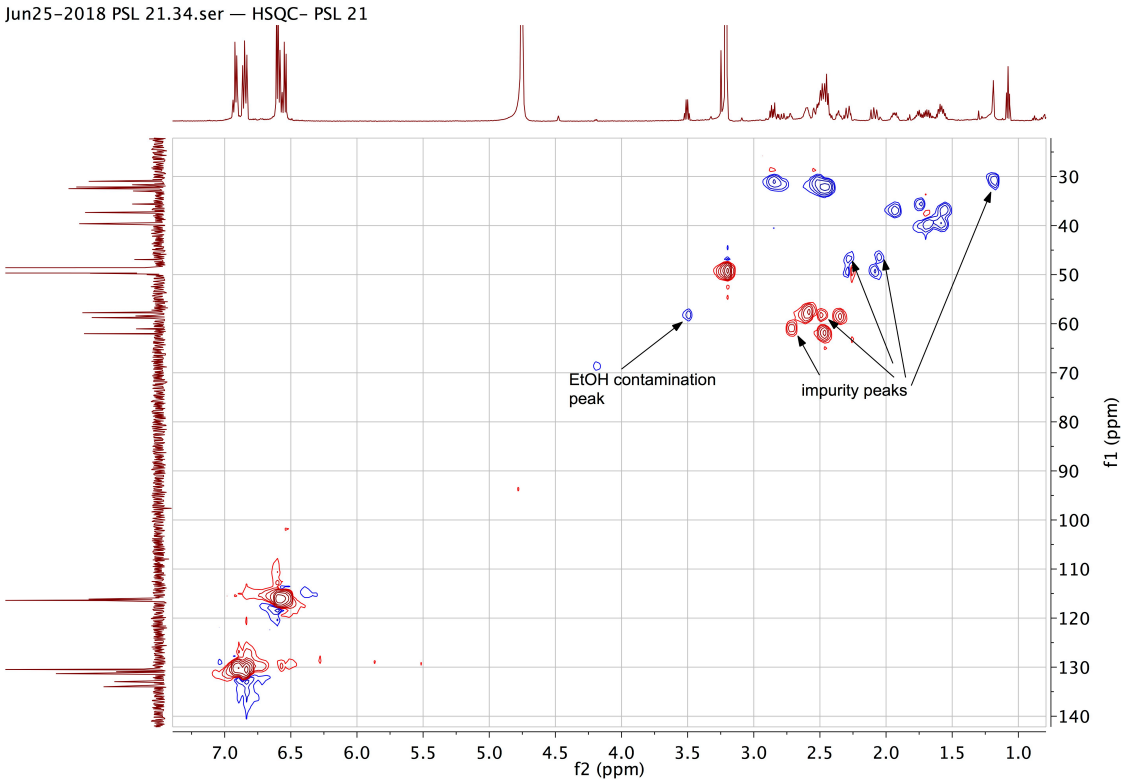

Appendix 58: COSY and HSQC Spectra of (±)-Saccardianine A (**17**).

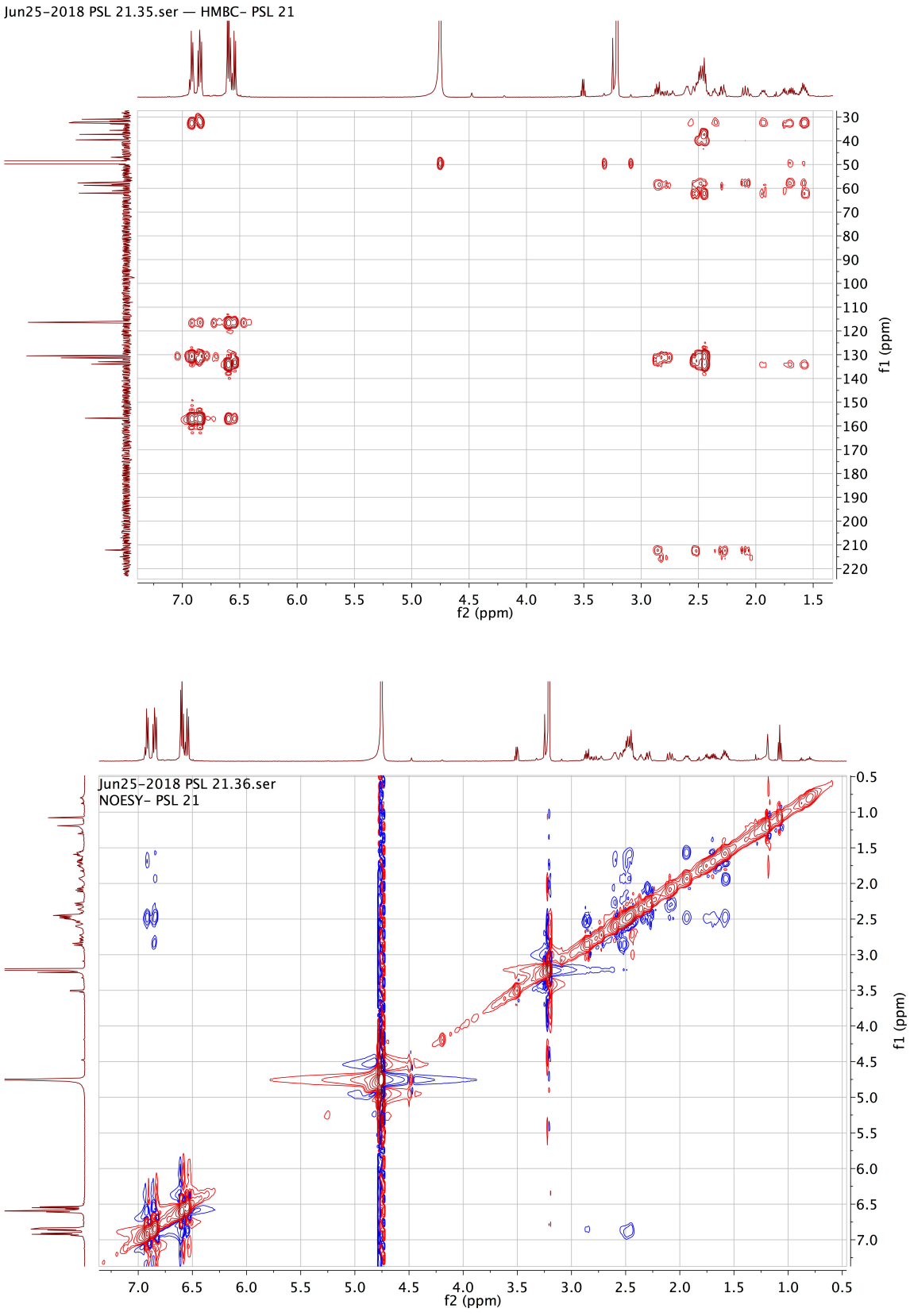

Appendix 59: HMBC and NOESY Spectra of (±)-Saccardianine A (**17**).

Compound Spectrum List Report

Cmpd 9, Dissect, 8.4 min

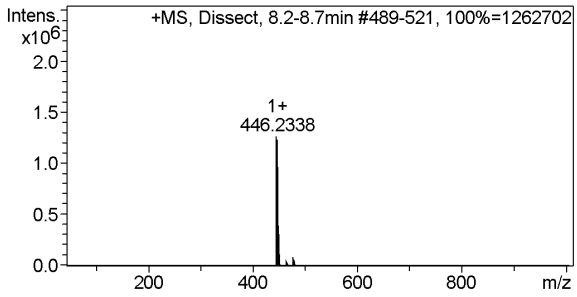

#	m/z	z	I	FWHM	S/N
1	446.2338	1+	1262702	0.0827	144.2
2	446.7372		26217	0.0990	3.0
3	447.2391	1+	1230852	0.0821	140.6
4	448.2459	1+	1012600	0.0719	115.6
5	449.2489	1+	397643	0.0582	45.4
6	450.2517	1+	77928	0.0551	8.9
7	464.2432		34259	0.0557	3.9
8	465.2481	1+	40497	0.0552	4.6
9	478.2586	1+	84686	0.0564	9.7
10	479.2630	1+	56020	0.0562	6.4

C28H32NO4 [M+H]
D: -2.73 ppm

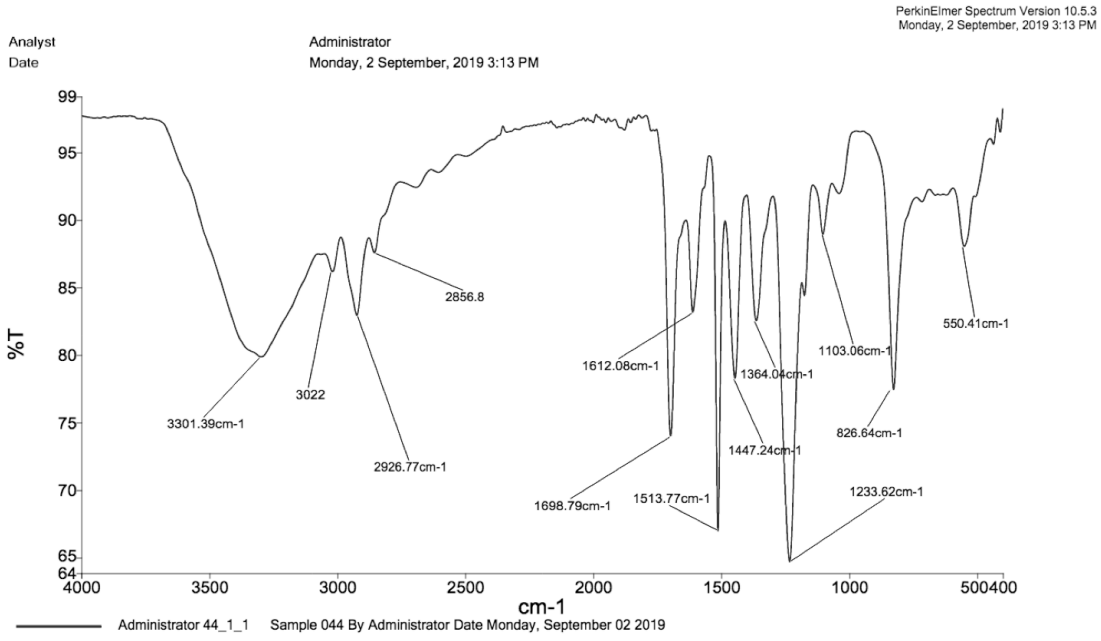

Appendix 60: HRESIMS (ESI+) and IR Spectra of (±)-Saccardianine A (**17**).

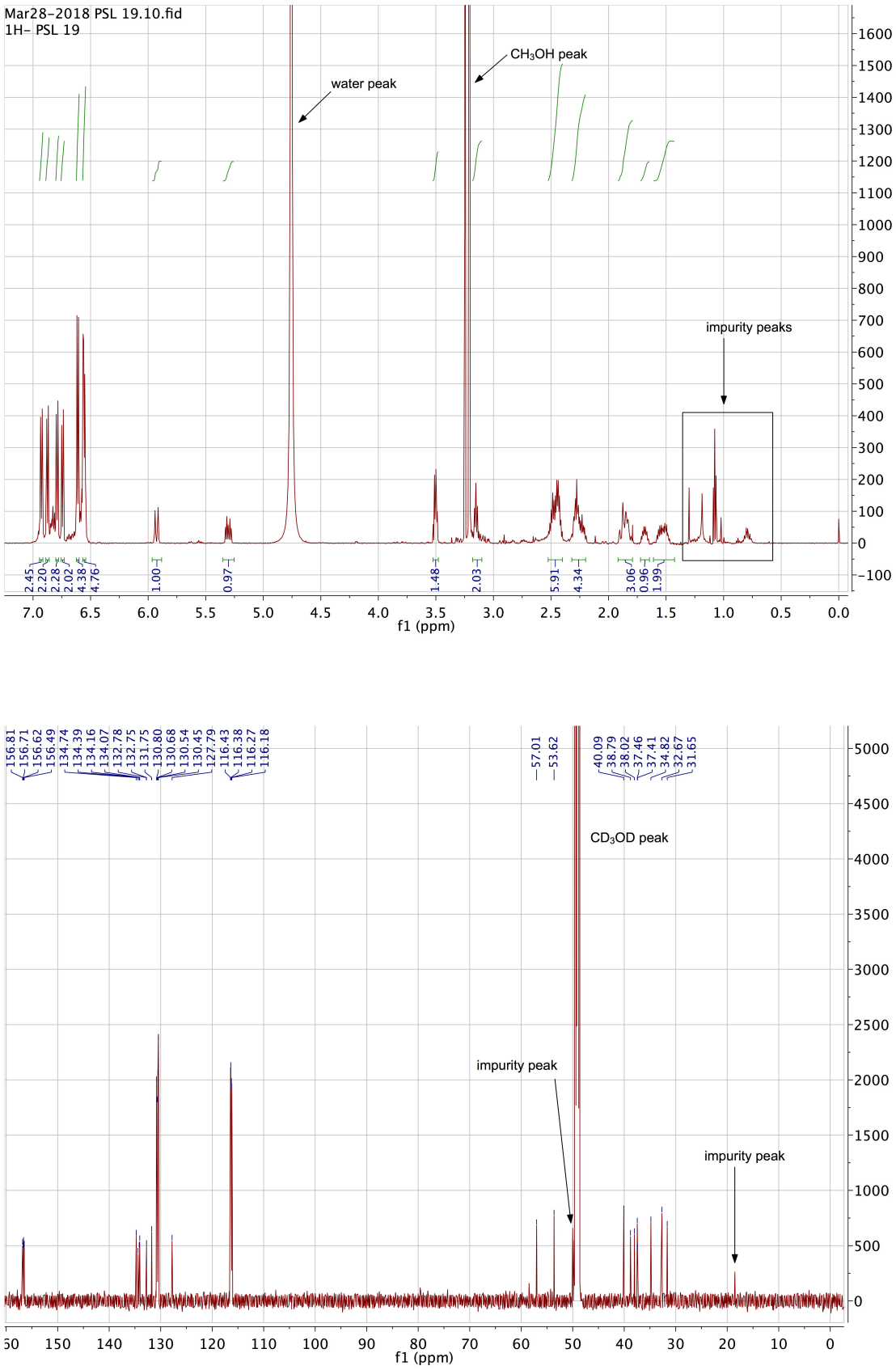

Appendix 61: ^{1}H and ^{13}C NMR Spectra of (±)-Saccardianine B (**18**).

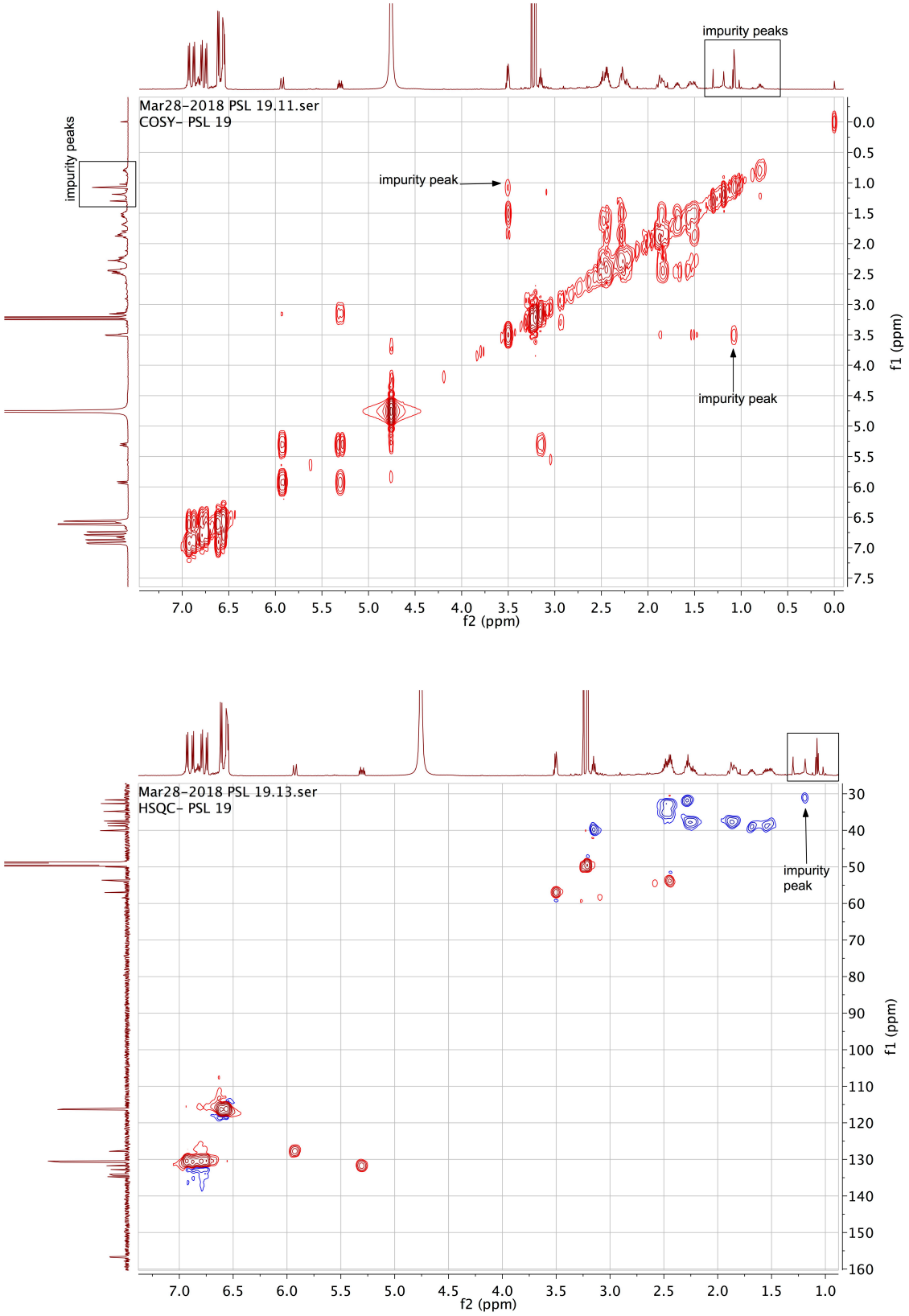

Appendix 62: COSY and HSQC Spectra of (±)-Saccardianine B (**18**).

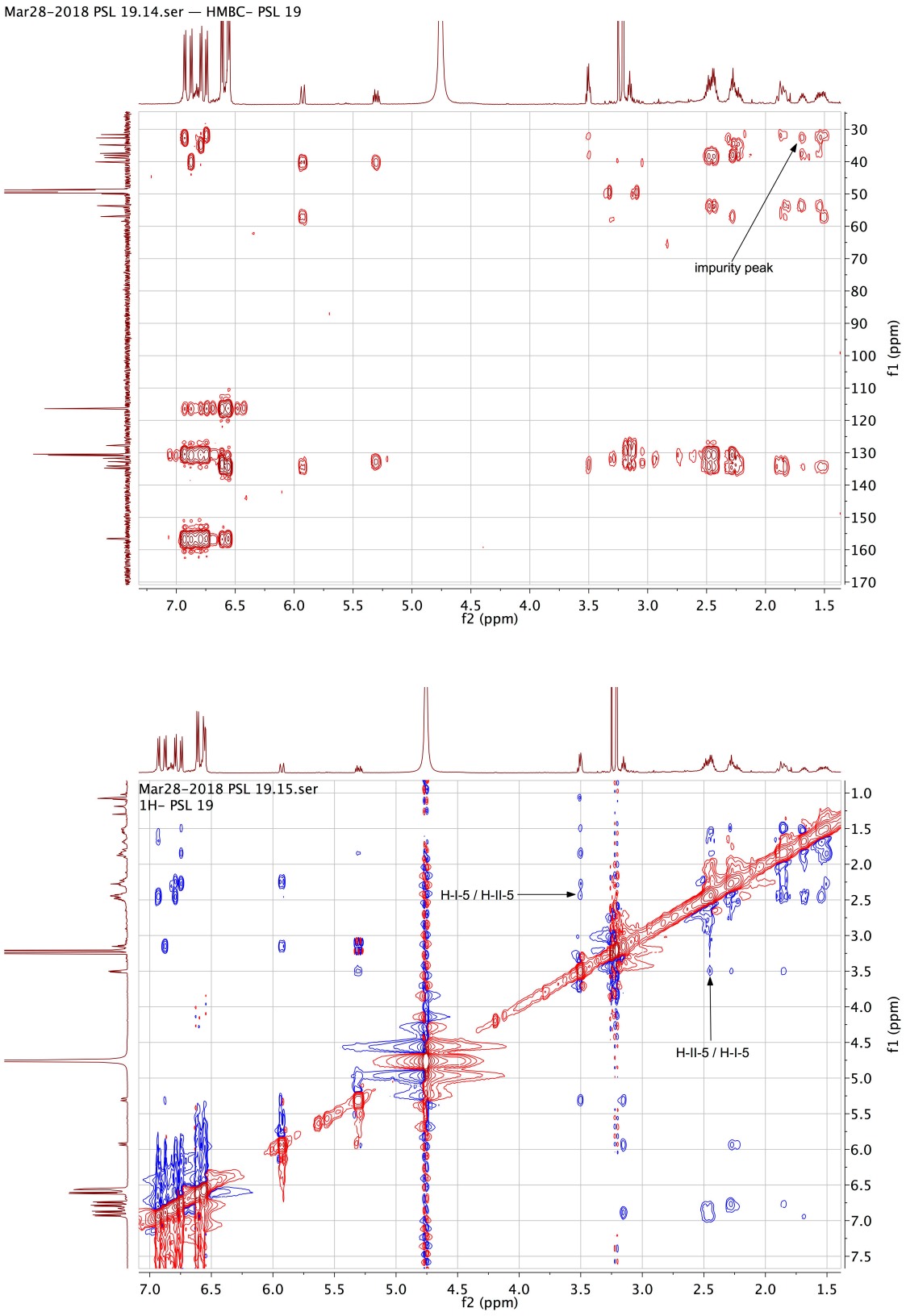

Appendix 63: HMBC and NOESY Spectra of (±)-Saccardianine B (**18**).

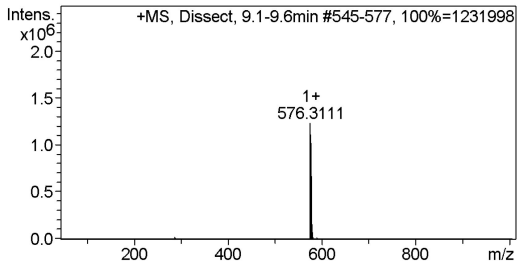

#	m/z	z	I	FWHM	S/N
1	288.2865		8878	0.0418	3946.2
2	575.8573		12095	0.3679	5376.2
3	576.3111	1+	1231998	0.1006	547628.3
4	576.8779		27945	0.1060	12421.6
5	577.3185	1+	1020642	0.0862	453679.8
6	577.8774		9592	0.1276	4263.5
7	578.3220	1+	446339	0.0686	198399.3
8	579.3266	1+	104316	0.0686	46368.7
9	580.3305	1+	19196	0.0654	8532.6
10	590.3243		10188	0.0643	4528.6

C38H42NO4 [M+H]
D: -0.46 ppm

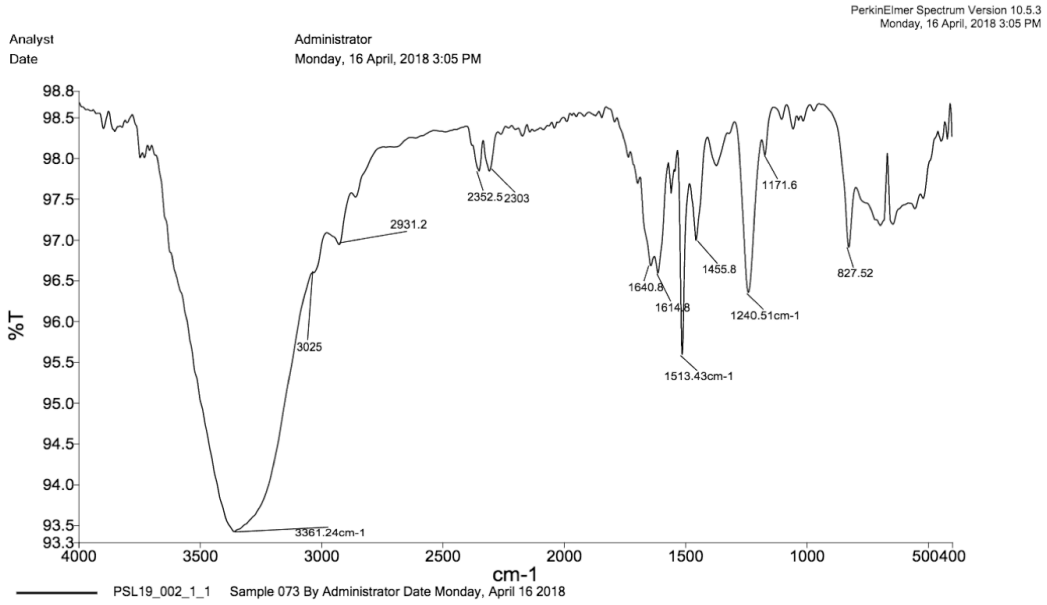

Appendix 64: HRESIMS (ESI+) and IR Spectra of (±)-Saccardianine B (**18**).

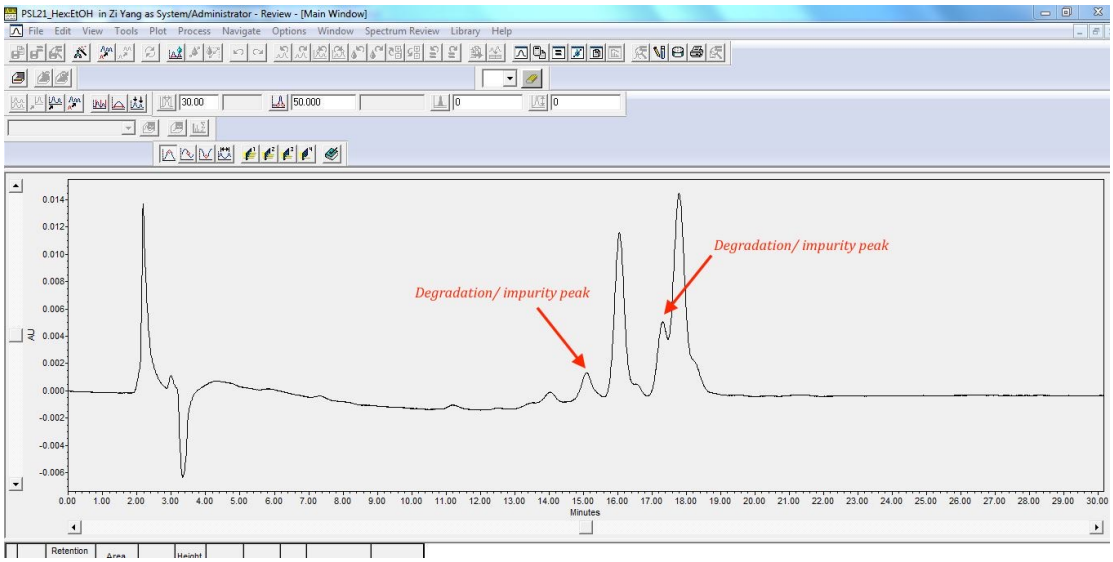

Appendix 65: Chiral-phase HPLC Chromatogram of (±)-Saccardianine A (**17**). Note: Co-elution of degradation and/or impurity peaks.

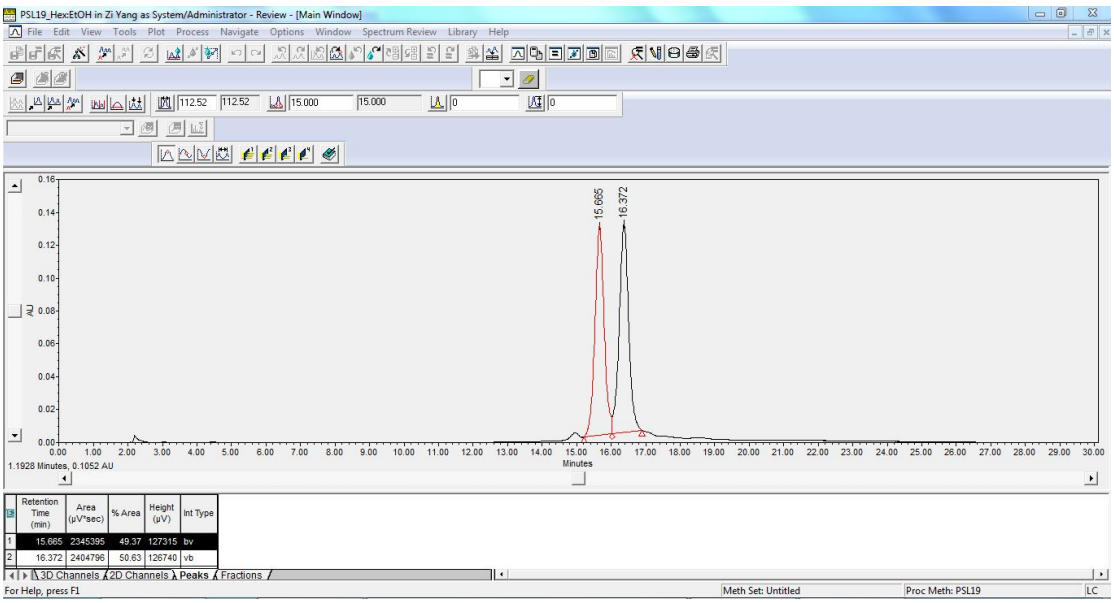

Appendix 66: Chiral-phase HPLC Chromatogram of (±)-Saccardianine B (**18**).

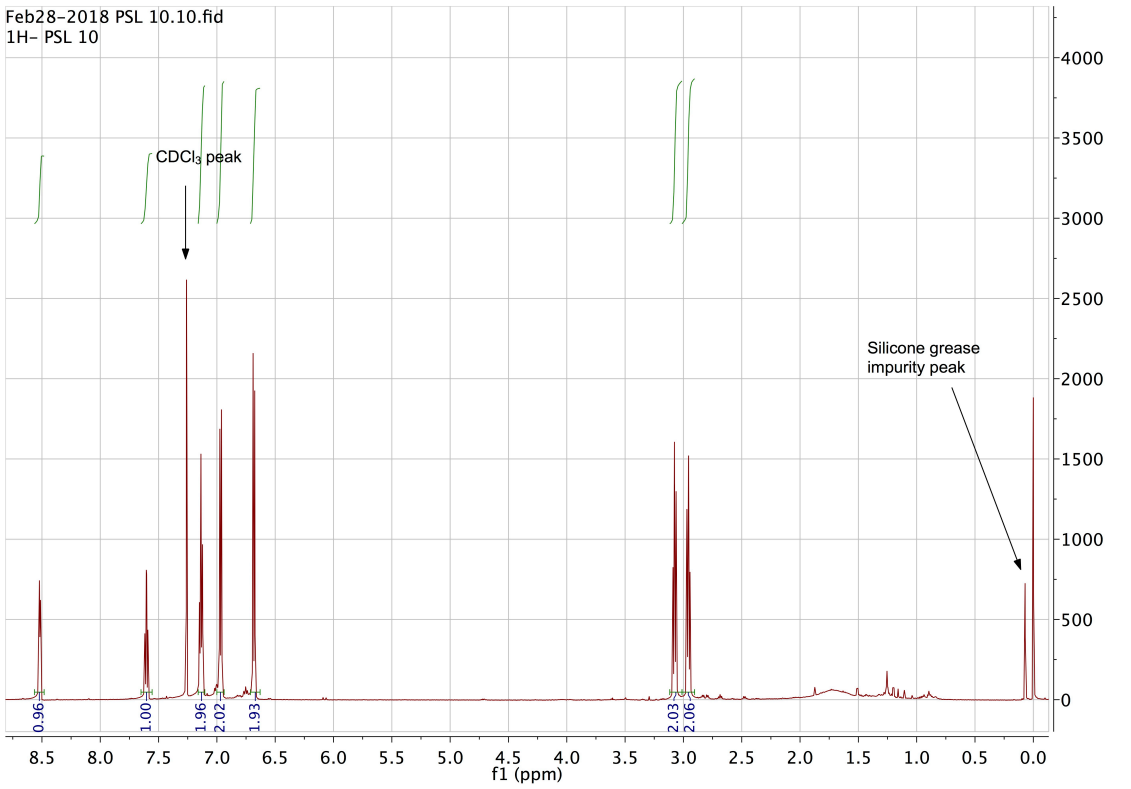

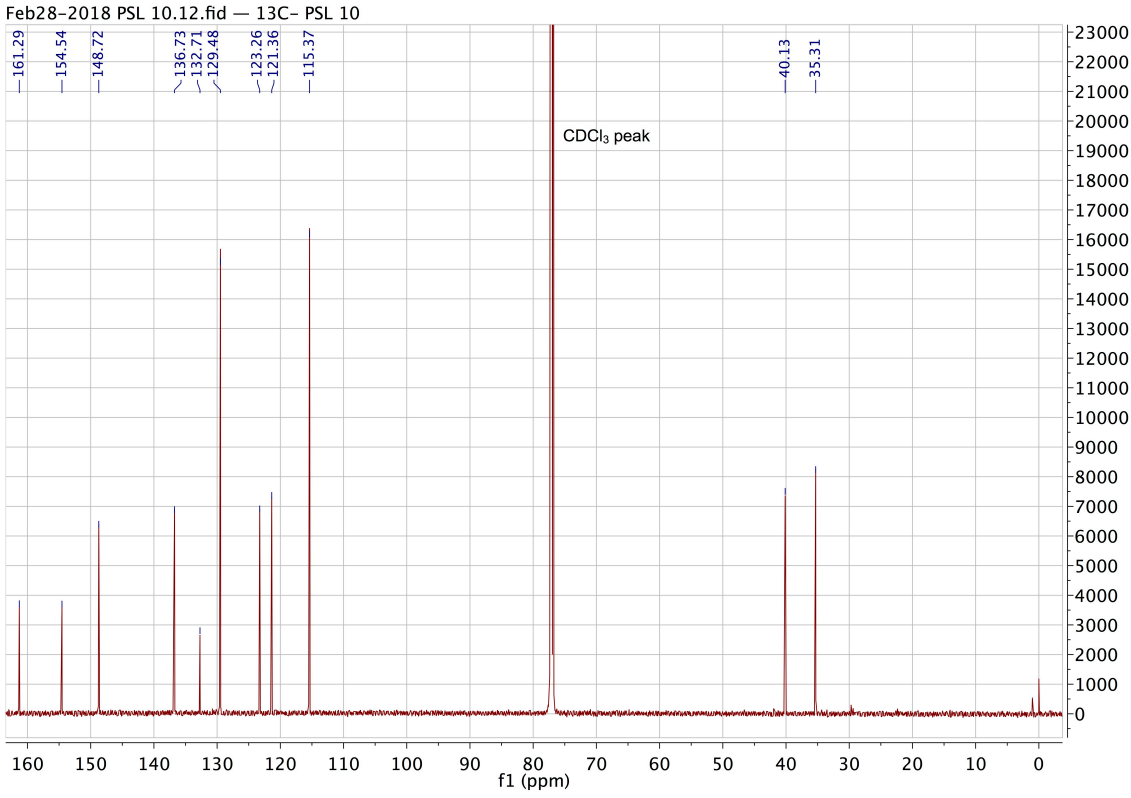

Appendix 67: ^{1}H and ^{13}C NMR Spectra of Saccardianine C (**19**).

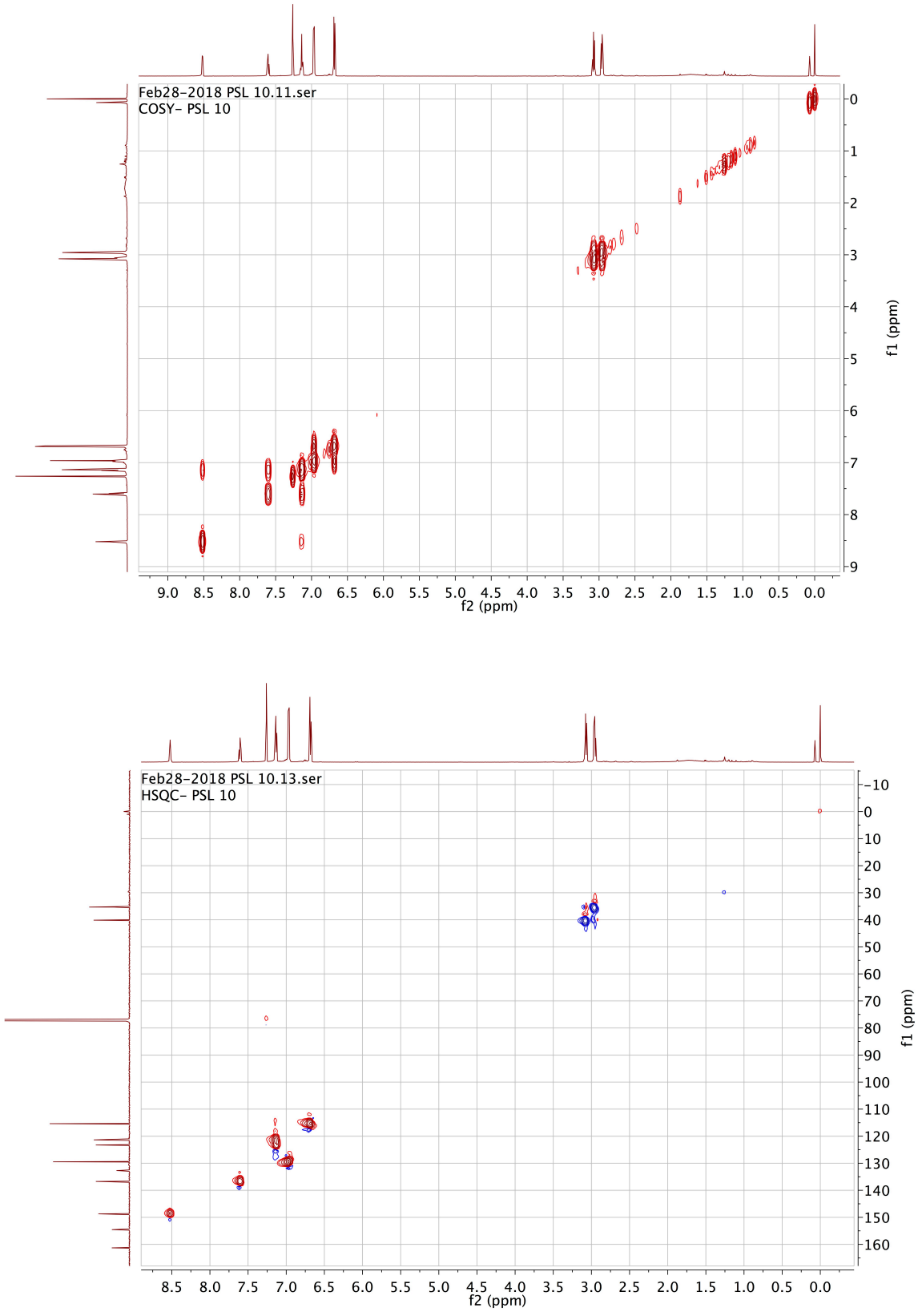

Appendix 68: COSY and HSQC Spectra of Saccardianine C (**19**).

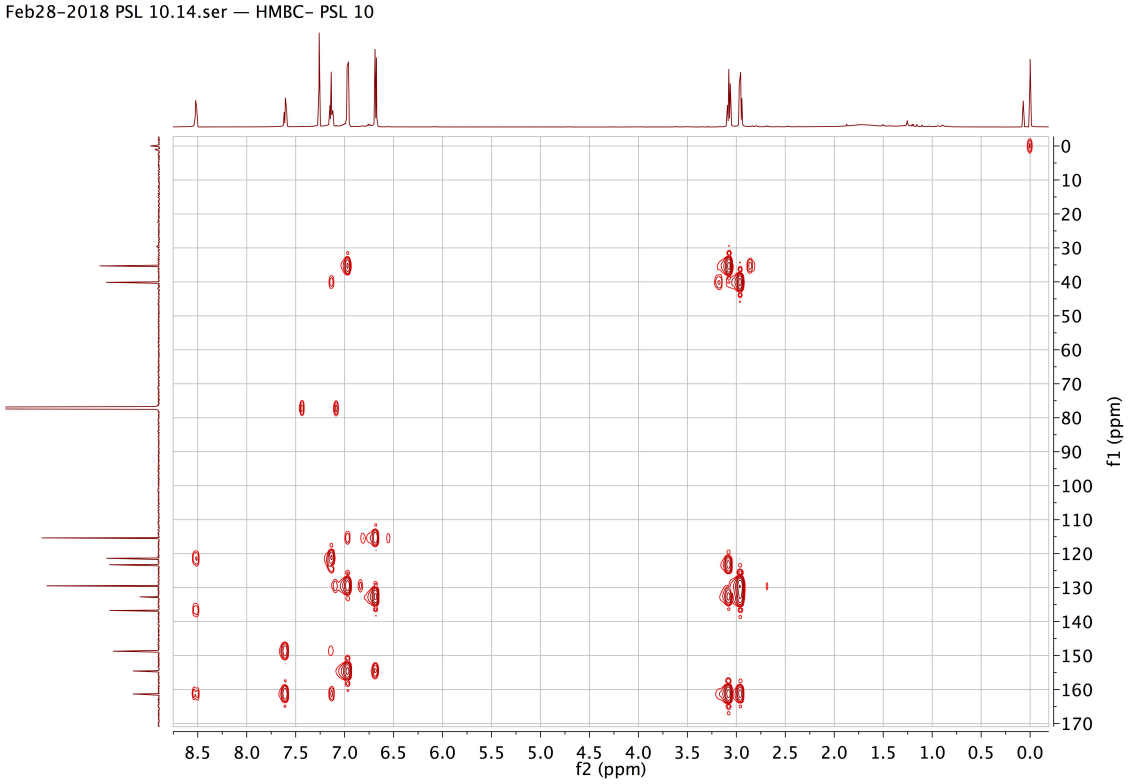

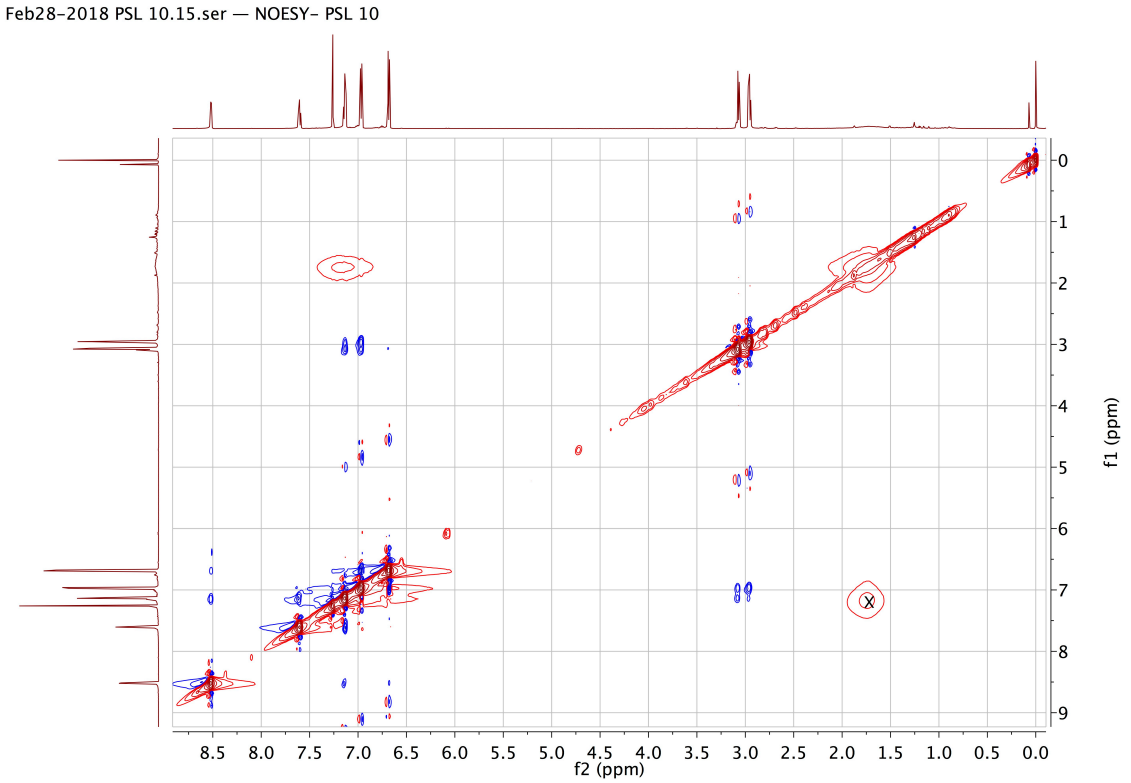

Appendix 69: HMBC and NOESY Spectra of Saccardianine C (**19**).

Data:PSL10
Sample Name:
Description:
Ionization Mode:ESI+
History:Determine m/z[Peak Detect[Centroid,30,Area];Correct Base[0.5%]];Correct Ba...

Acquired:1/30/2018 11:11:21 AM
Operator:AccuTOF
Mass Calibration data:Calibration_300118
Created:1/30/2018 1:15:39 PM
Created by:AccuTOF

Charge number:1 Tolerance:20.00(ppm), 0.00 .. 30.00(mmu) Unsaturation Number:0.0 .. 25.0 (Fractio...
Element:^{12}C:0 .. 25, ^{1}H:0 .. 30, ^{14}N:0 .. 2, ^{16}O:0 .. 6

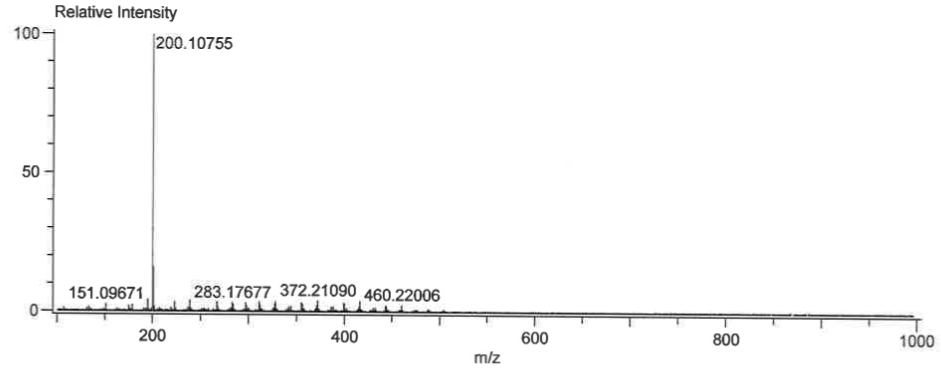

Mass	Intensity	Calc. Mass	Mass Difference (mmu)	Mass Difference (ppm)	Possible Formula
200.10755	195623.25	200.10754	0.01	0.07	$^{12}C_{13}{}^{1}H_{14}{}^{14}N_{1}{}^{16}O_{1}$
		200.10486	2.69	13.46	$^{12}C_{10}{}^{1}H_{16}{}^{16}O_{4}$

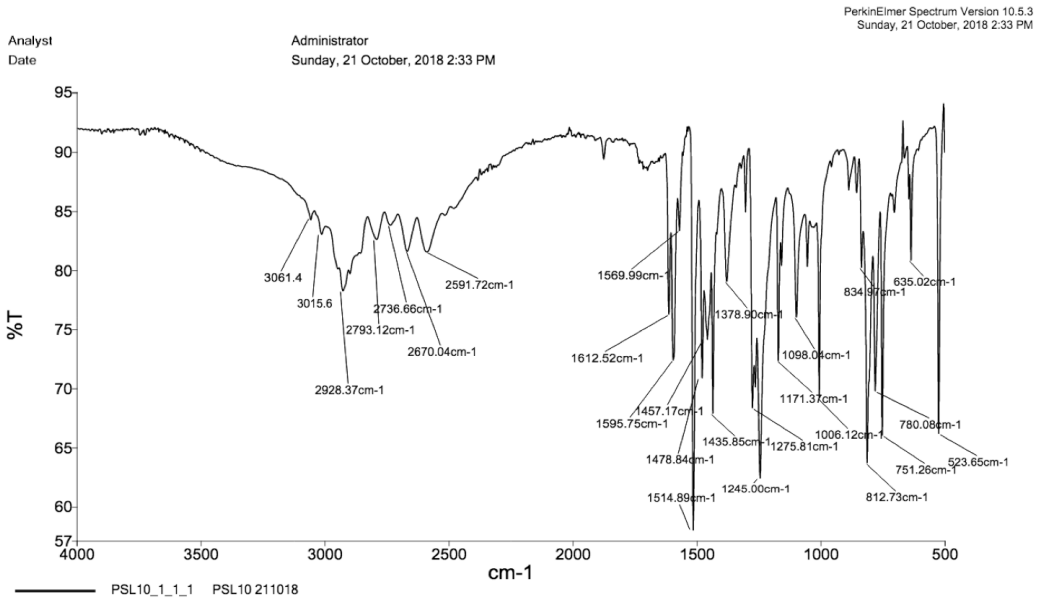

Appendix 70: HRDARTMS and IR Spectra of Saccardianine C (**19**).

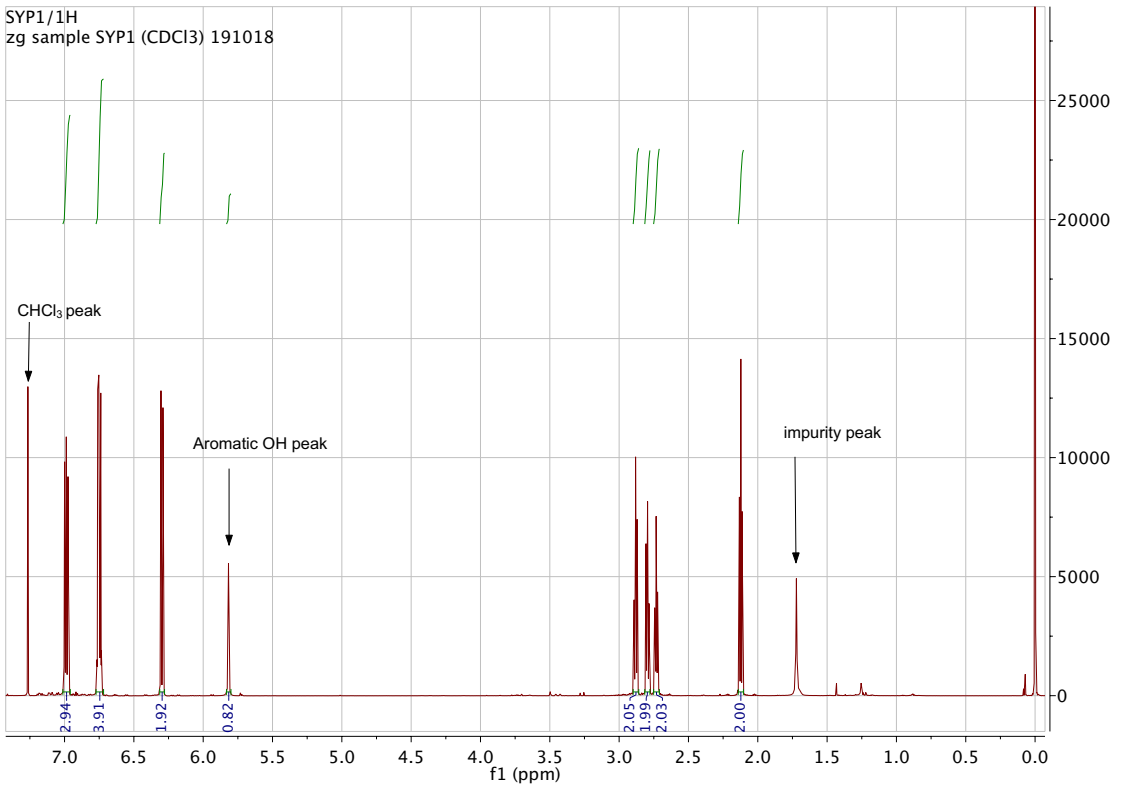

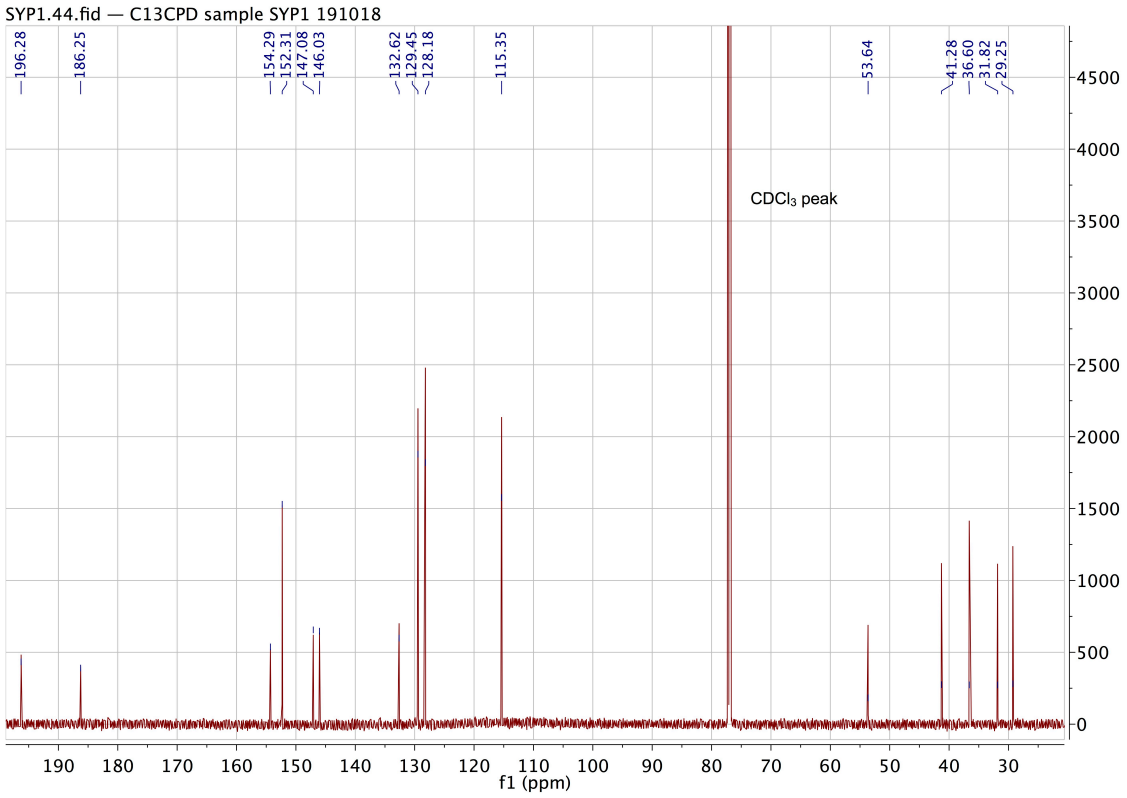

Appendix 71: ^{1}H and ^{13}C NMR Spectra of Pellaspirone (**20**).

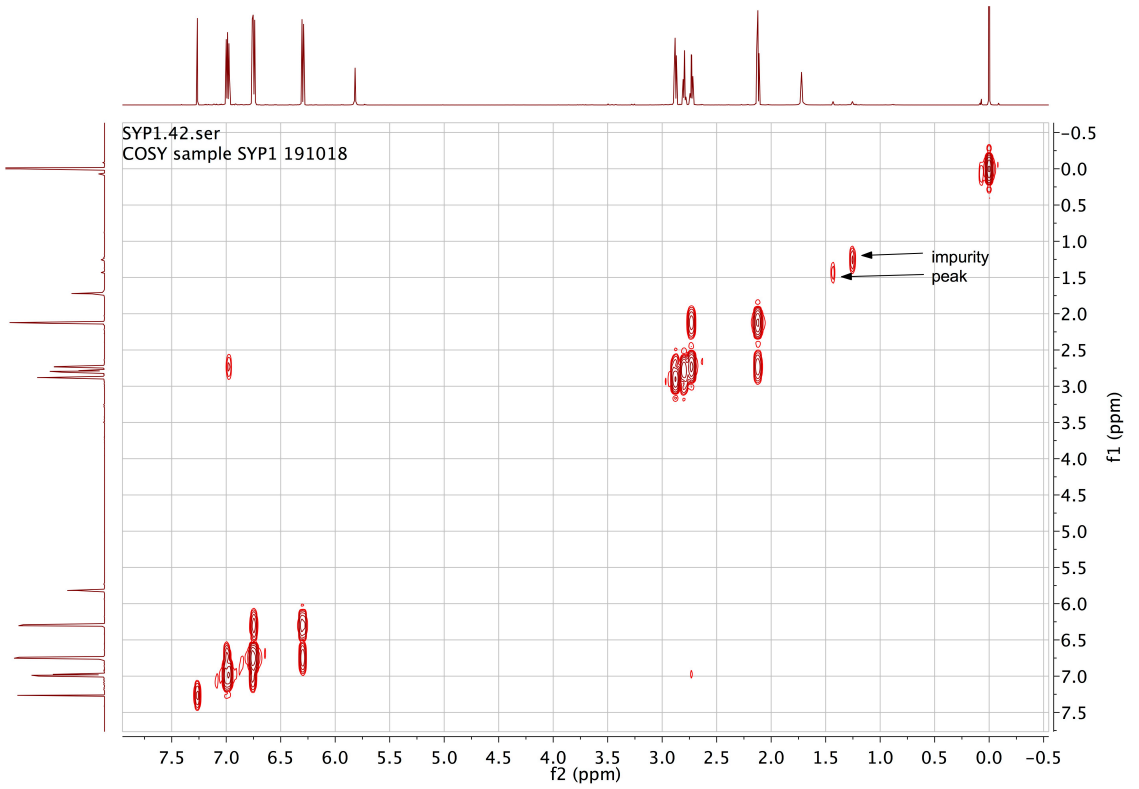

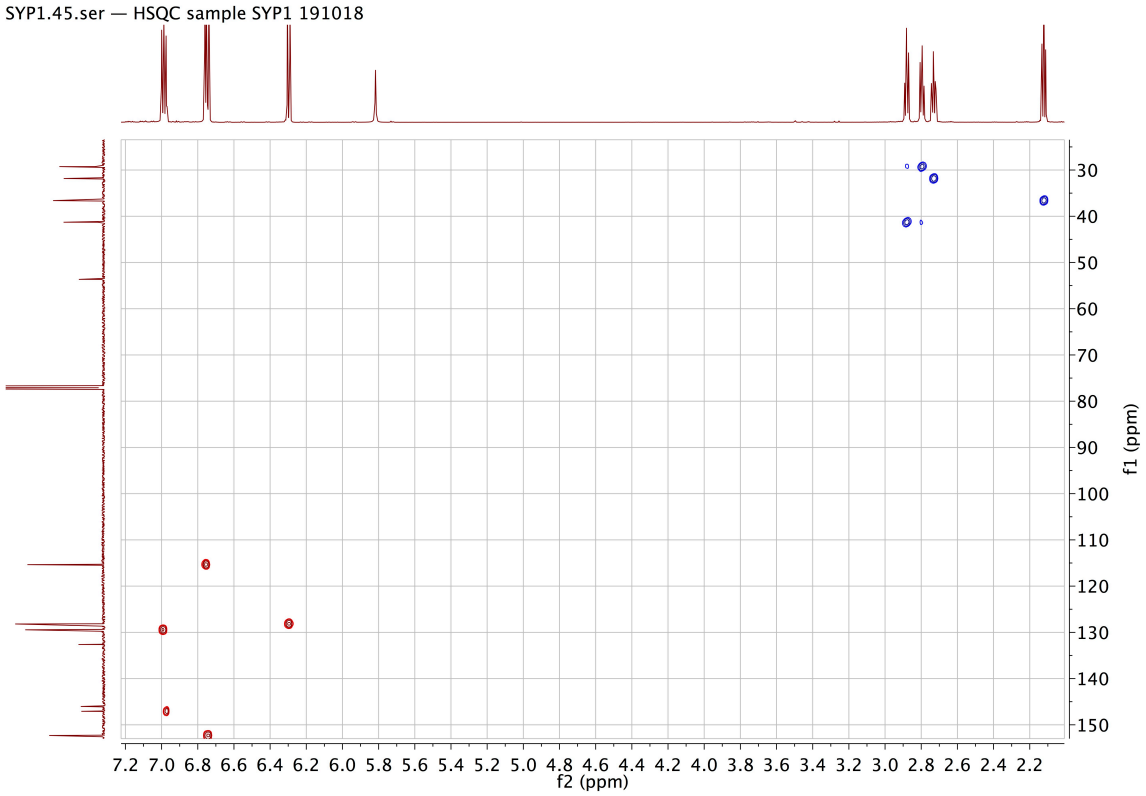

Appendix 72: COSY and HSQC Spectra of Pellaspirone (**20**).

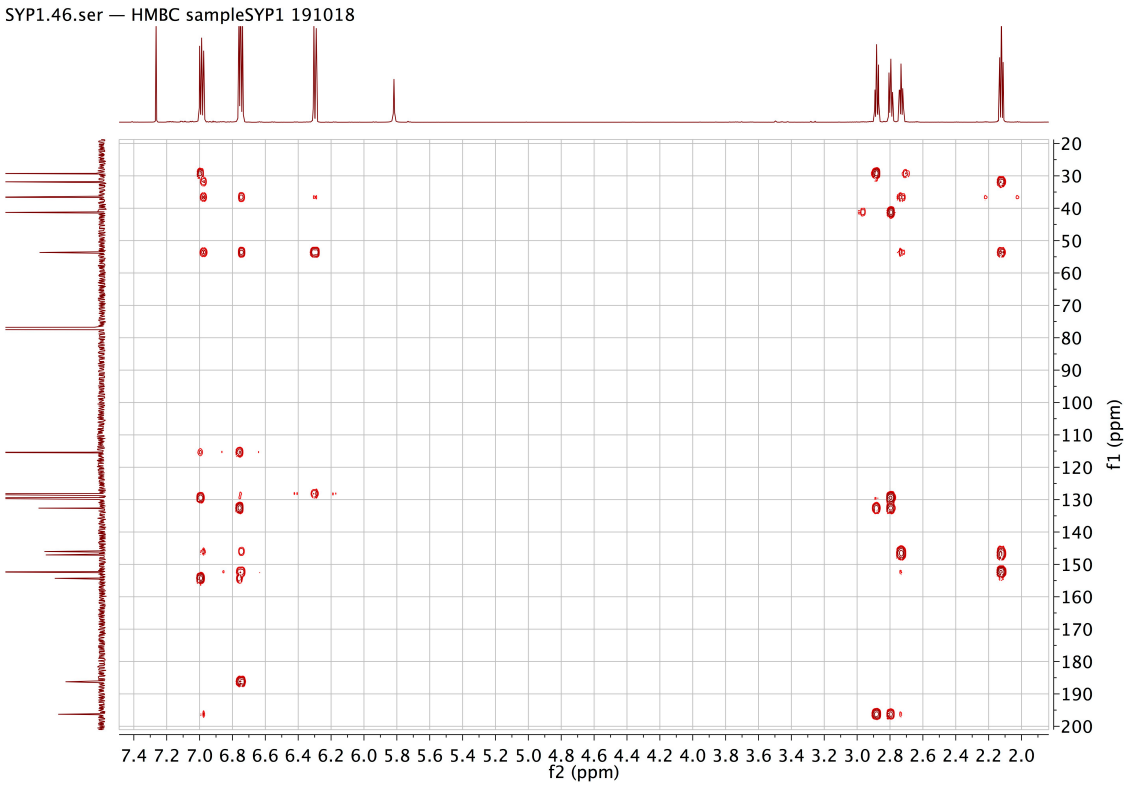

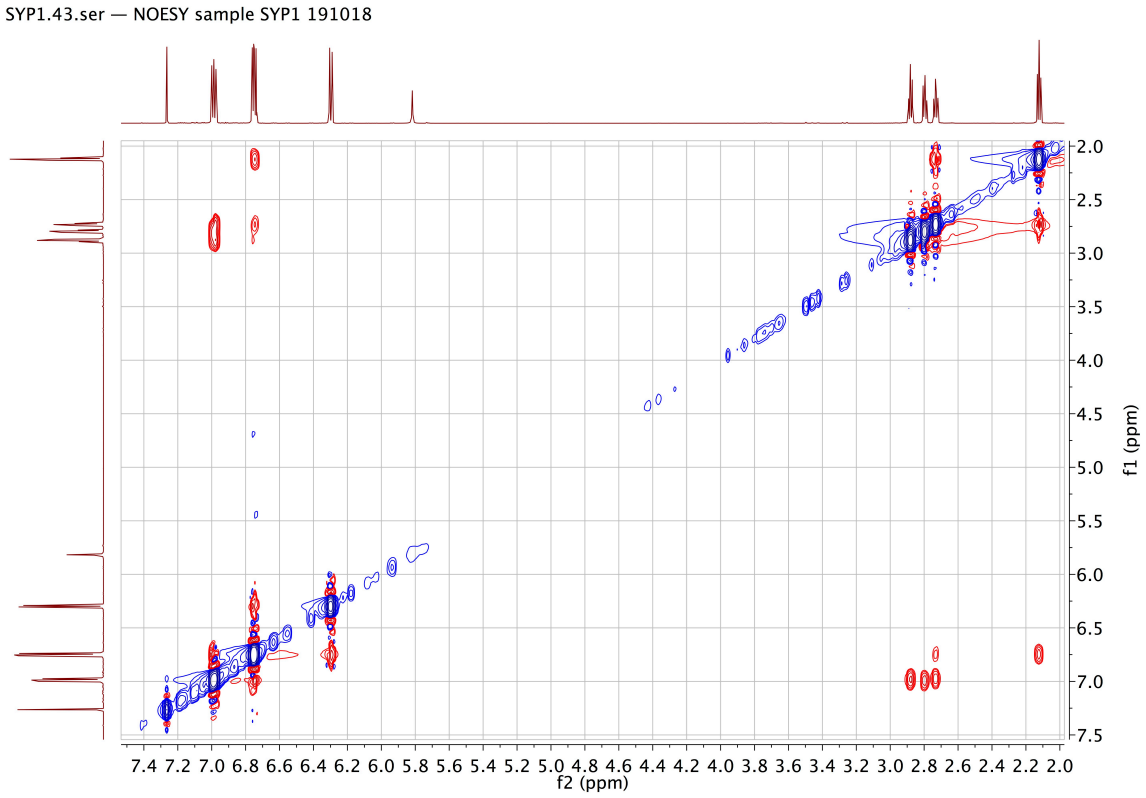

Appendix 73: HMBC and NOESY Spectra of Pellaspirone (**20**).

Cmpd 2, Dissect, 10.5 min

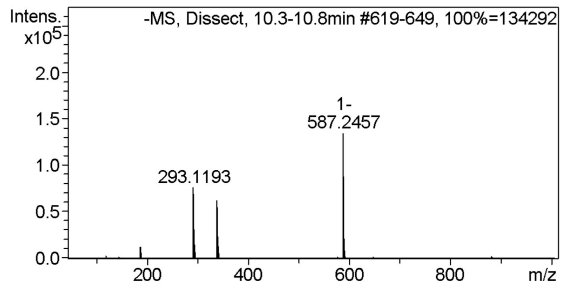

#	m/z	z	I	FWHM	S/N
1	119.0505		2463	0.0227	1308.9
2	187.0764		13298	0.0292	7066.7
3	293.1193		76396	0.0402	40598.1
4	294.1231		16027	0.0407	8517.1
5	339.1250		63015	0.0444	33487.5
6	340.1283		14906	0.0422	7921.6
7	341.1309		2219	0.0444	1179.3
8	587.2457	1-	134292	0.0607	71365.2
9	588.2491	1-	56193	0.0608	29862.0
10	589.2523	1-	13002	0.0610	6909.6

C19H17O3 [M-H]
D: -3.34 ppm

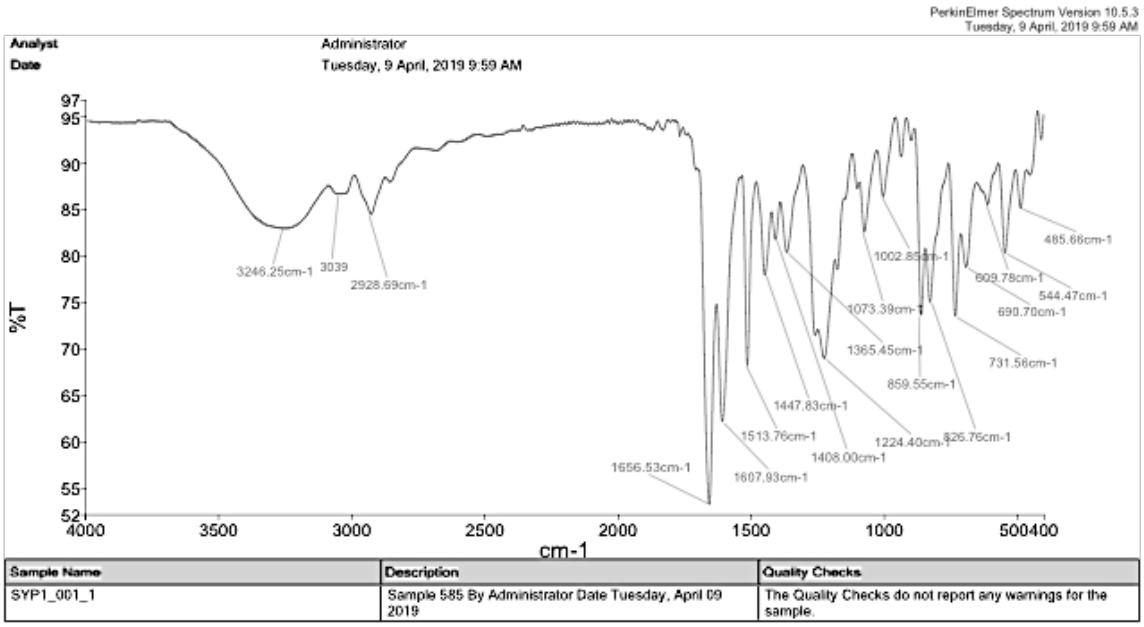

Sample Name	Description	Quality Checks
SYP1_001_1	Sample 585 By Administrator Date Tuesday, April 09 2019	The Quality Checks do not report any warnings for the sample.

Appendix 74: HRESIMS (ESI-) and IR Spectra of Pellaspirone (**20**).

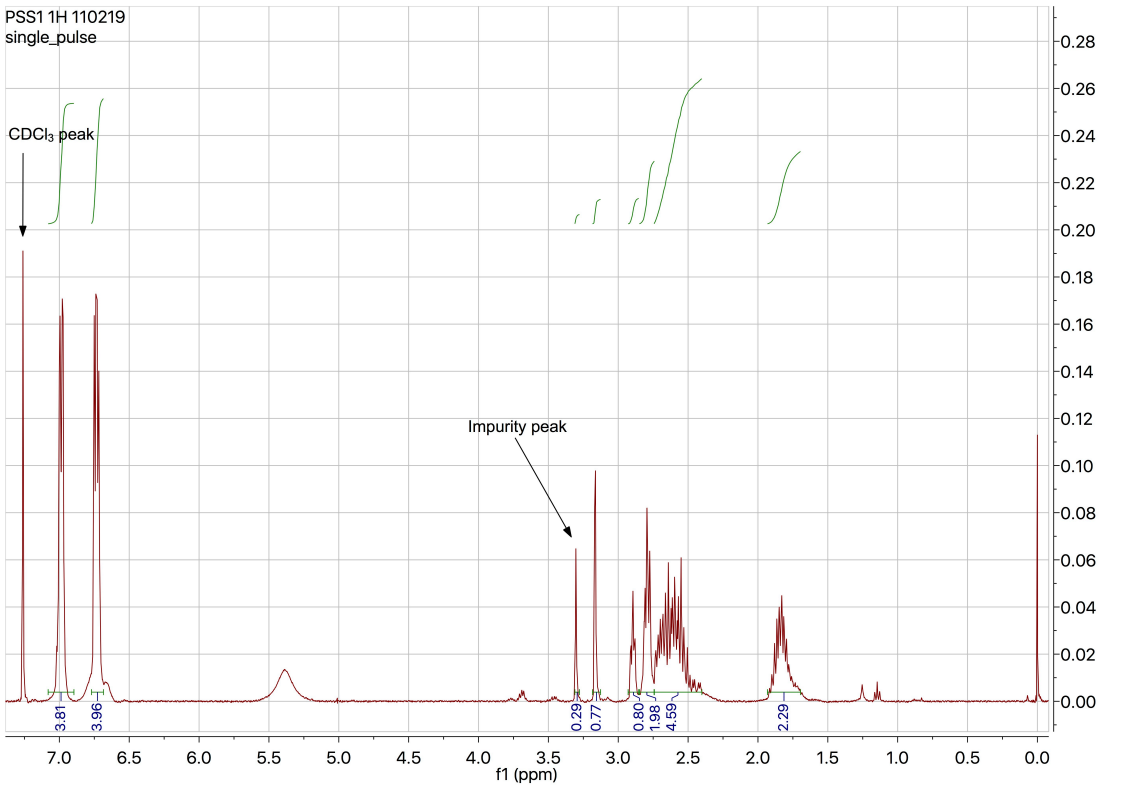

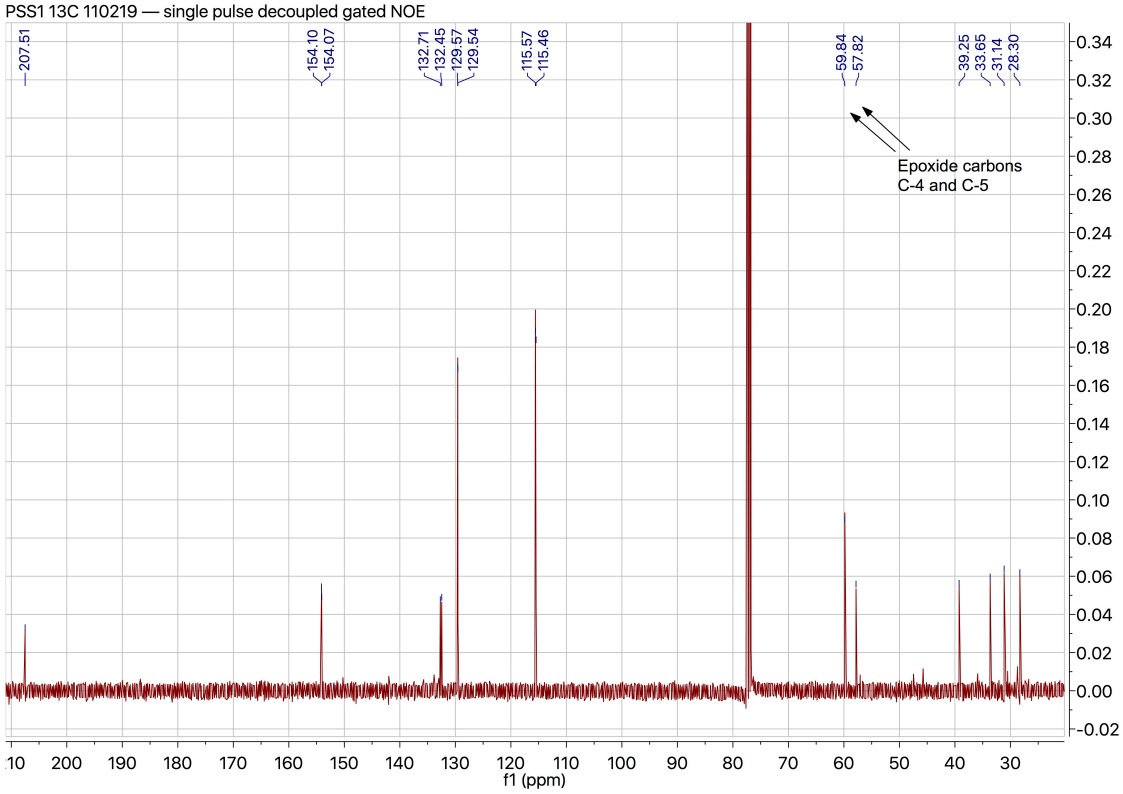

Appendix 75: ^{1}H and ^{13}C NMR Spectra of Epoxide **J** (semi-synthesised).

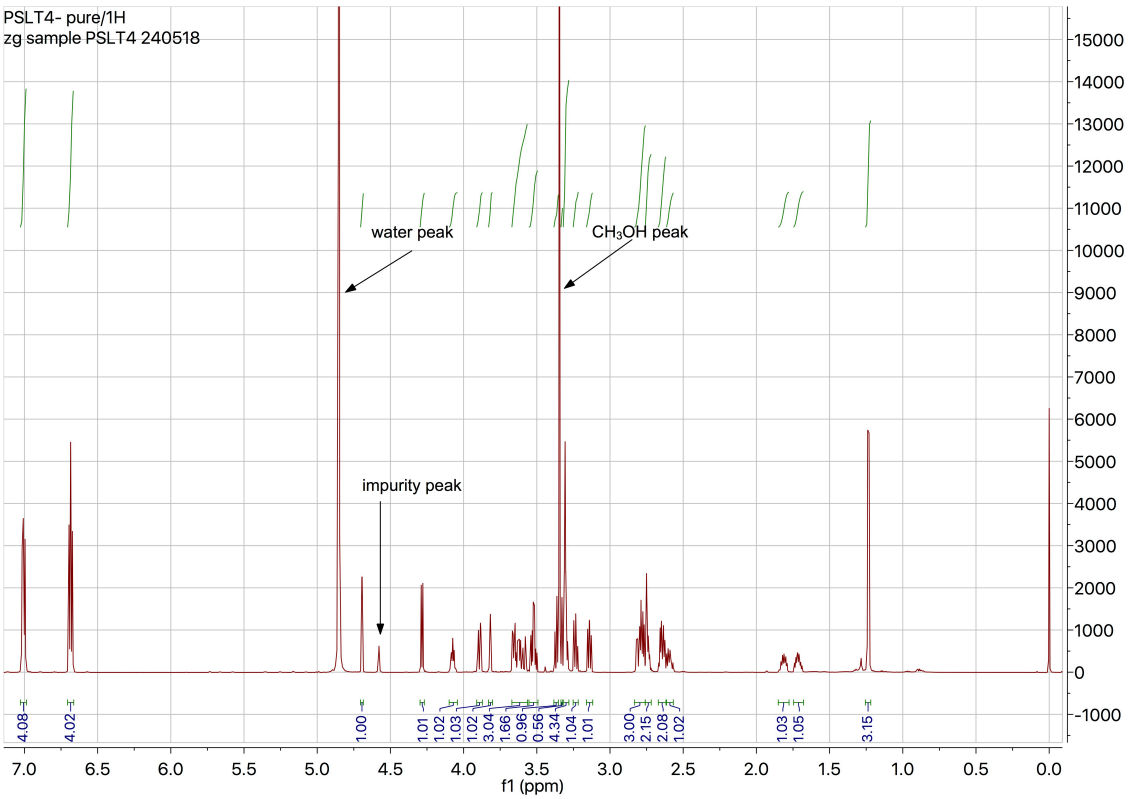

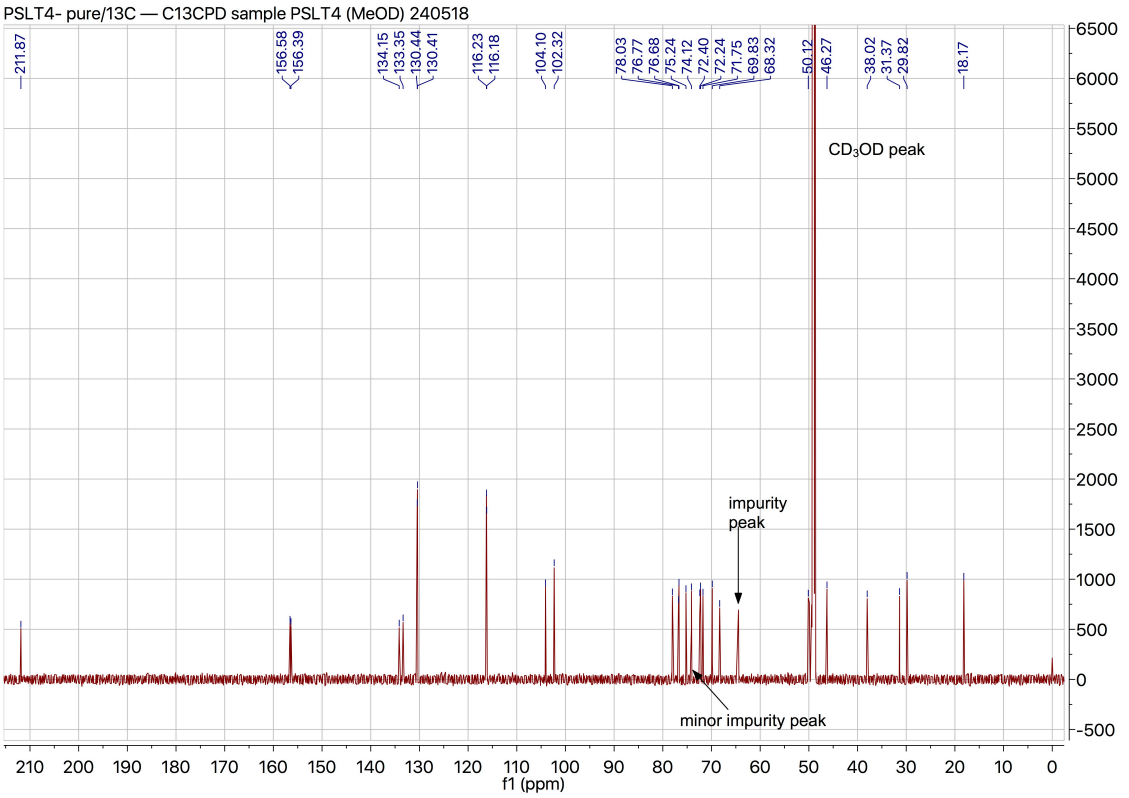

Appendix 76: ^{1}H and ^{13}C NMR Spectra of Saccardianoside (**21**).

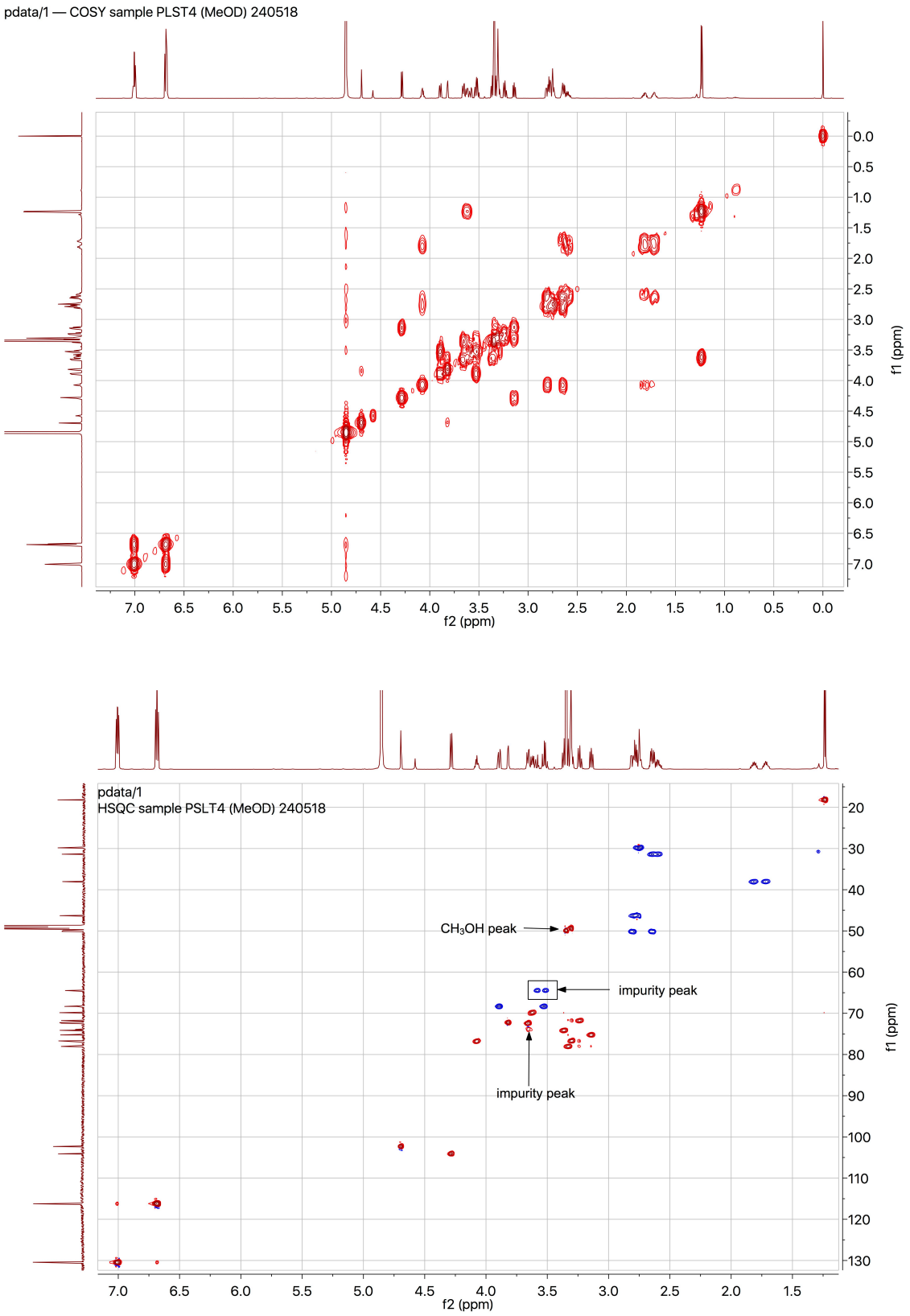

Appendix 77: COSY and HSQC Spectra of Saccardianoside (**21**).

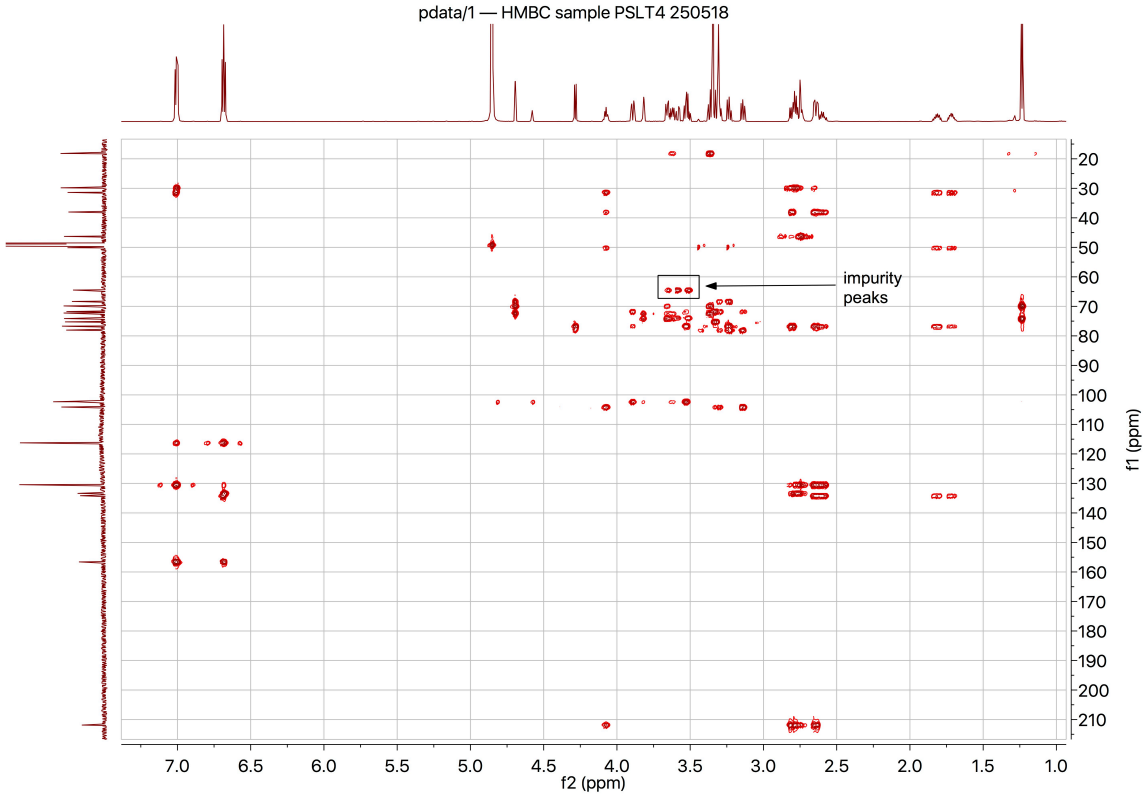

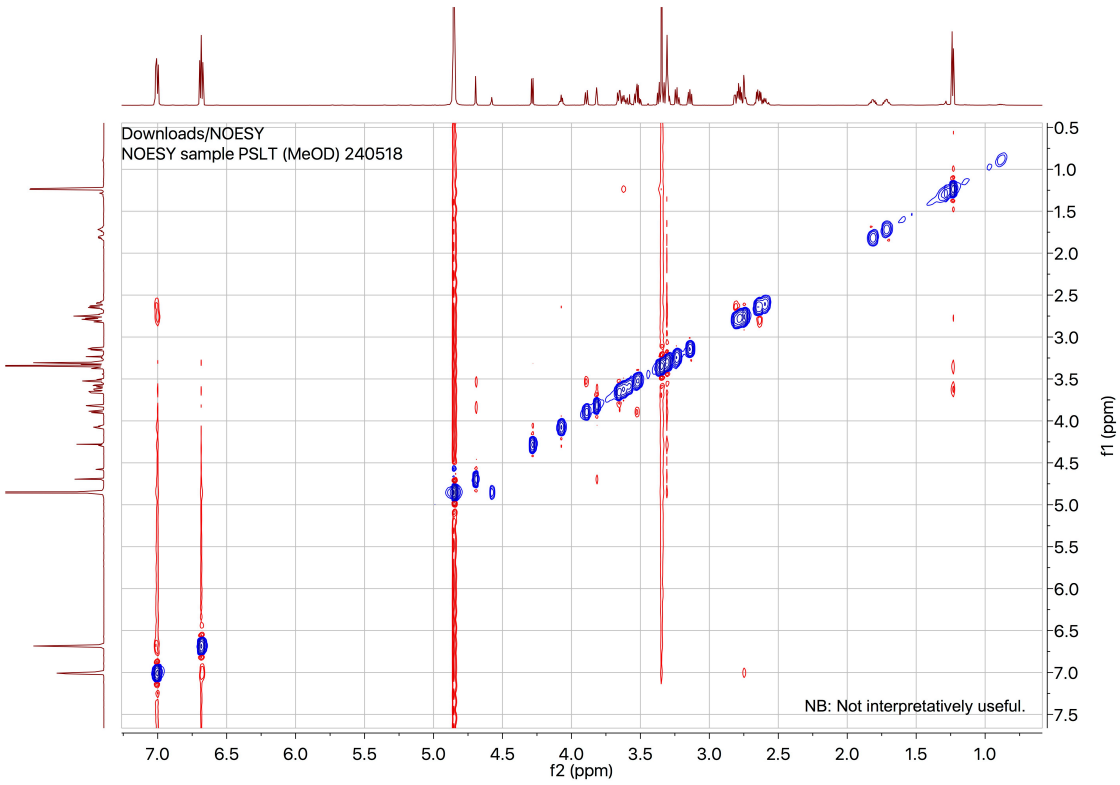

Appendix 78: HMBC and NOESY Spectra of Saccardianoside (**21**).

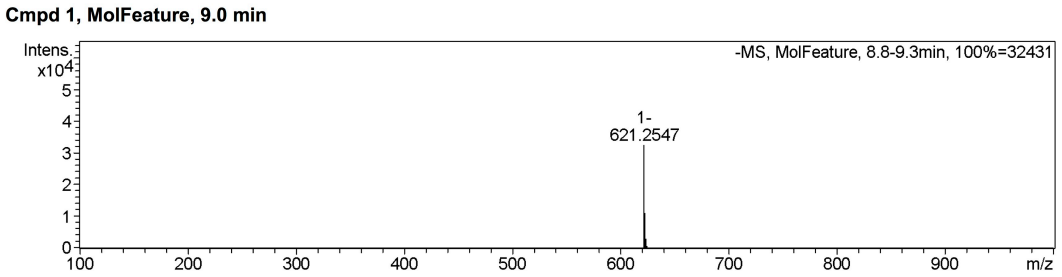

	Meas. m/z	#	Ion Formula	Score	m/z	err [mDa]	err [ppm]	mSigma	rdb	e⁻ Conf	N-Rule	Adduct
[M-H]- C31H42O13	621.254731	1	C31H41O13	100.00	621.255265	-0.5	-0.9	3.0	11.5	even	ok	M-H
		2	C28H33N10O7	77.97	621.253917	-0.8	-1.3	9.0	17.5	even	ok	M-H
		3	C27H37N6O11	29.95	621.252580	2.2	3.5	12.8	12.5	even	ok	M-H
		4	C32H37N4O9	36.50	621.256602	-1.9	-3.0	13.6	16.5	even	ok	M-H
		5	C25H25N20O	28.27	621.252569	2.2	3.5	15.3	23.5	even	ok	M-H
		6	C29H29N14O3	78.32	621.255254	0.5	0.8	16.5	22.5	even	ok	M-H
	622.257597	1	C20H36N11O12	26.57	622.255039	2.6	4.1	3.9	8.5	even	ok	M-H
		2	C23H44NO18	65.86	622.256387	1.2	1.9	9.1	2.5	even	ok	M-H
		3	C21H32N15O8	58.71	622.256377	1.2	2.0	14.7	13.5	even	ok	M-H
		4	C18H24N25O2	21.10	622.255029	2.6	4.1	15.8	19.5	even	ok	M-H
		5	C24H40N5O14	100.00	622.257725	0.1	0.2	16.2	7.5	even	ok	M-H
	623.260304	1	C13H35N16O13	20.46	623.257499	2.8	4.5	5.8	4.5	even	ok	M-H
		2	C14H31N20O9	51.00	623.258836	-1.5	-2.4	13.7	9.5	even	ok	M-H
		3	C11H23N30O3	16.78	623.257488	2.8	4.5	15.9	15.5	even	ok	M-H
		4	C17H39N10O15	100.00	623.260184	-0.1	-0.2	16.1	3.5	even	ok	M-H

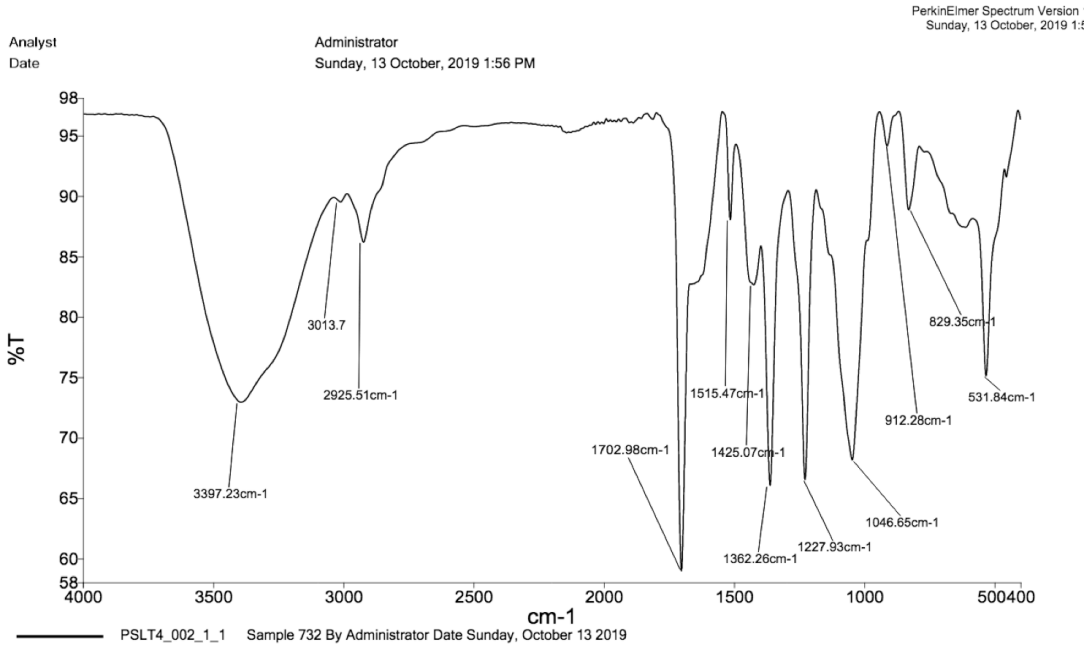

Appendix 79: HRESIMS (ESI-) and IR Spectra of Saccardianoside (**21**).

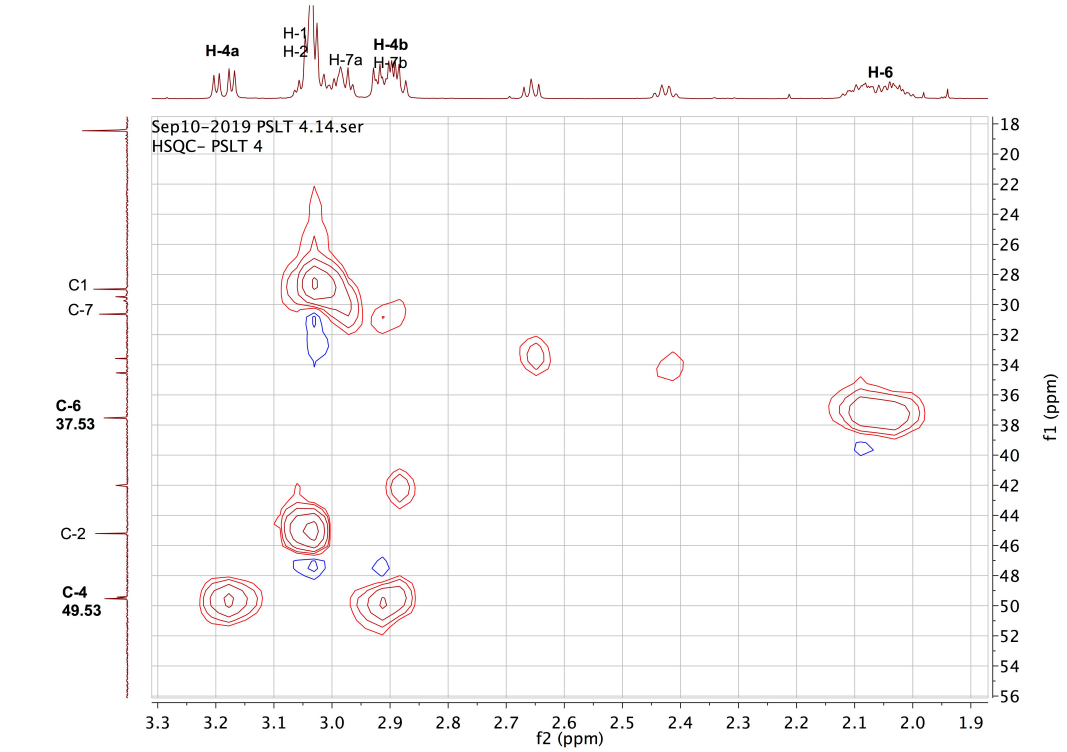

Appendix 80: Glycosidation Shift NMR Experiment of **21** (600 MHz, C_5D_5N).

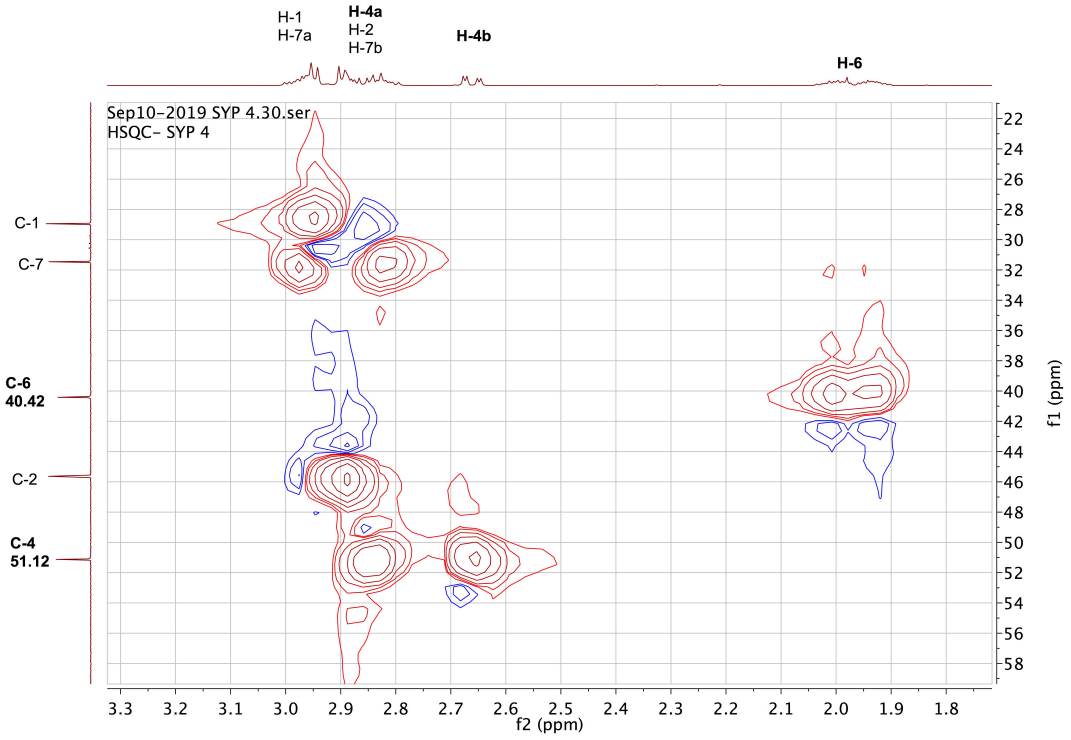

Appendix 81: Glycosidation Shift NMR Experiment of **23** (600 MHz, C_5D_5N).

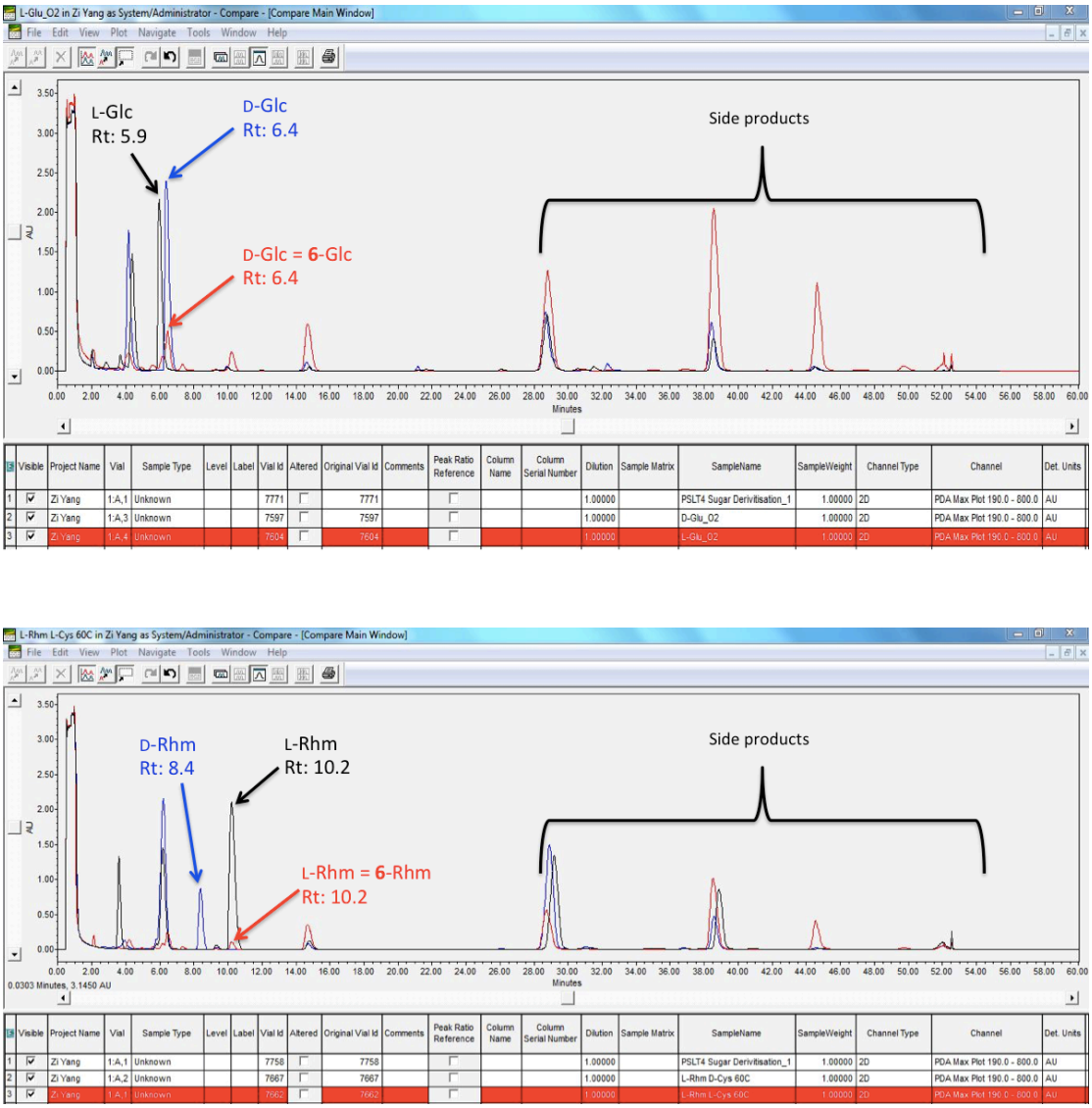

Appendix 82: HPLC Chromatogram of the Acid Hydrolysate of **21** following Arylthiocarbomyl-thiazolidine Derivatisation.

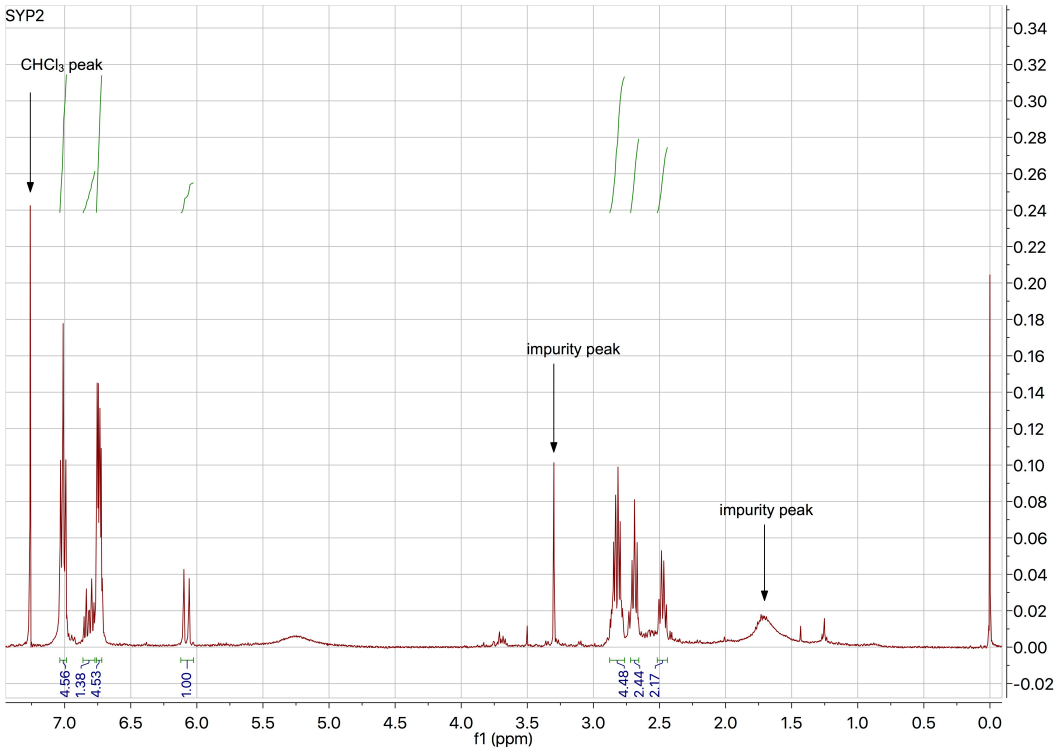

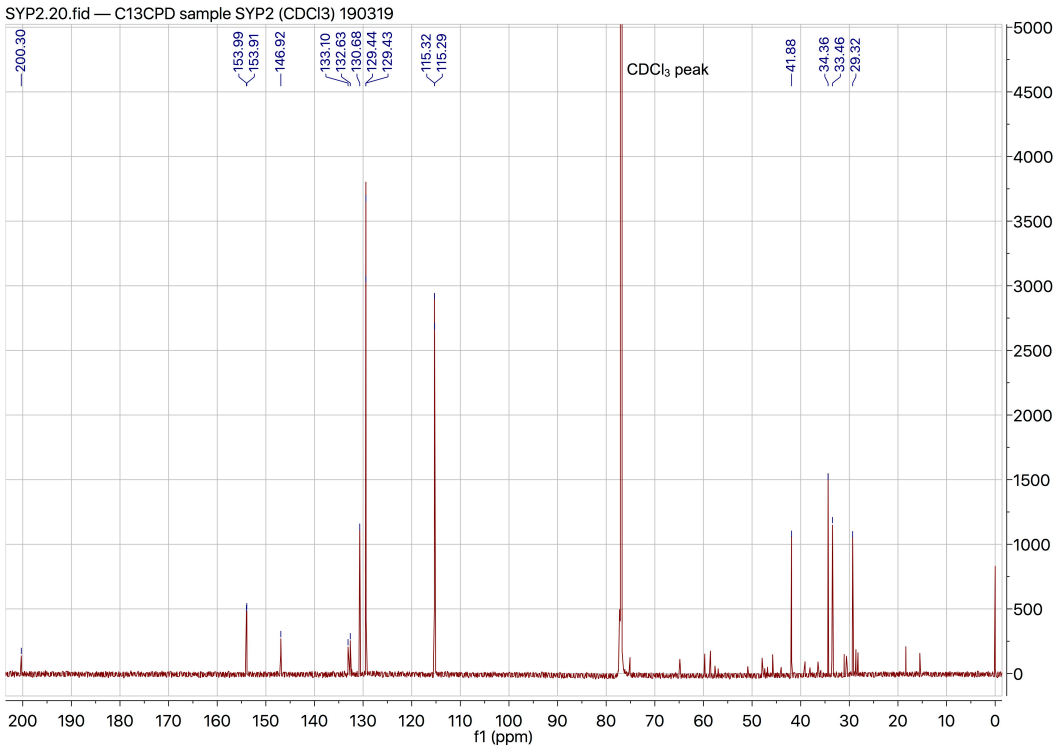

Appendix 83: ^{1}H and ^{13}C NMR Spectra of Platyphyllenone (**21**).

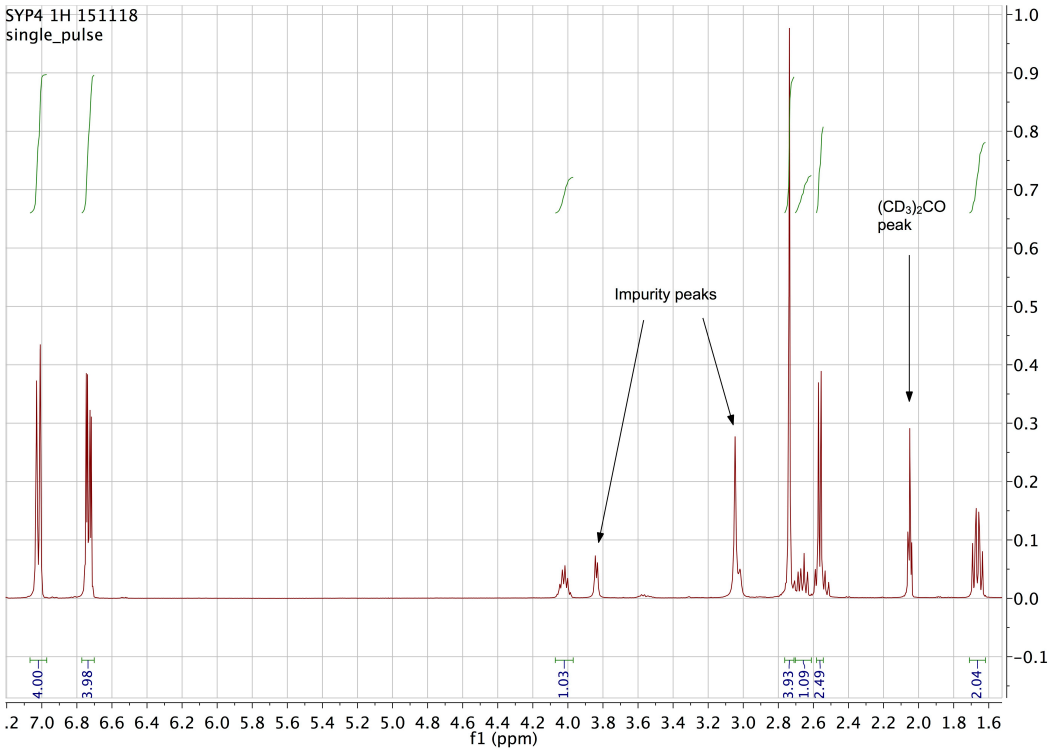

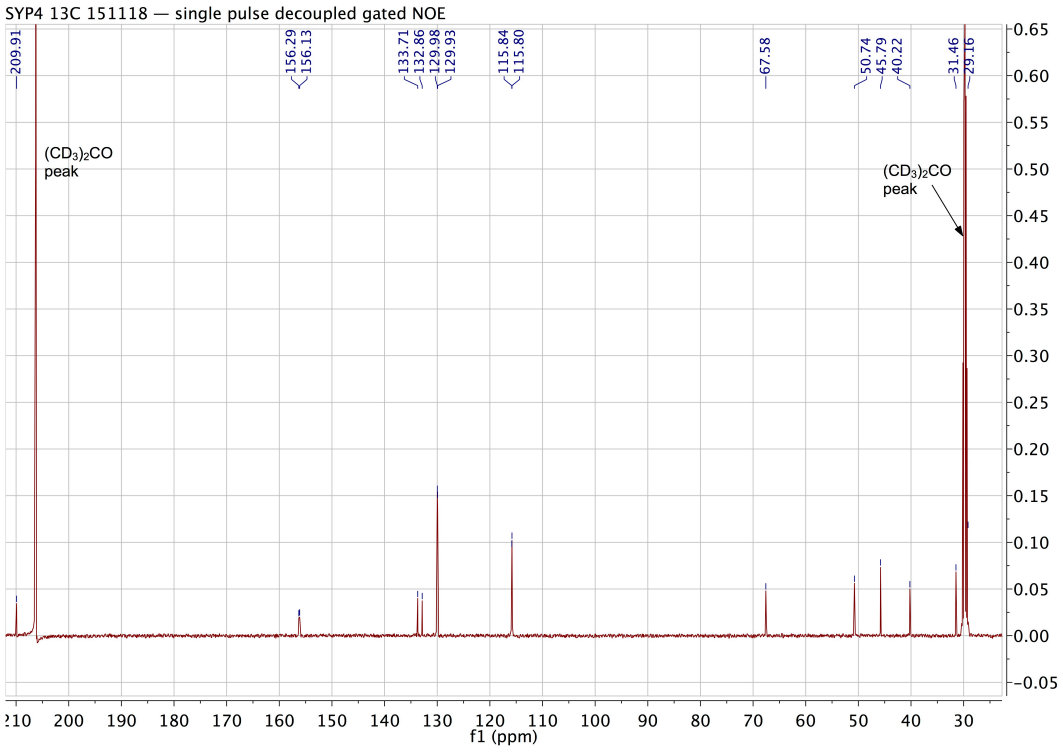

Appendix 84: ^{1}H and ^{13}C NMR Spectra of (±)-5-Hydroxy-1,7-bis(4-hydroxyphenyl)-3-heptanone (**23**).

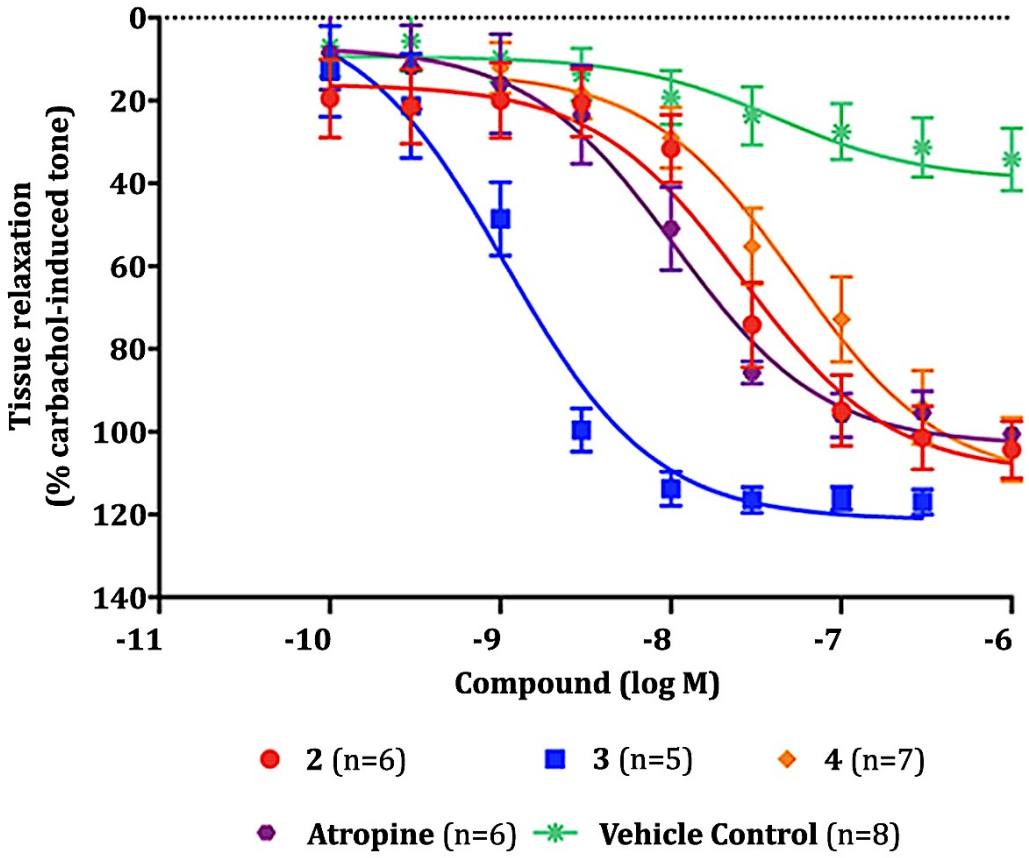

Appendix 85: Antispasmodic activity of alkaloids **2** – **4**, atropine and DMSO on rat isolated trachea.

Compound	E_{max} (%) (mean ± SEM) (*p*-value)[a]	EC_{50} (mean ± SEM)[b]
2	110.1 ± 9.0 (0.0001)	26.0 ± 5.2 nM
3	121.0 ± 3.3 (< 0.0001)	1.2 ± 0.2 nM
4	115.6 ± 3.4 (< 0.0001)	134.0 ± 71 nM
Atropine	102.1 ± 5.8 (0.0004)	10.1 ± 2.7 nM
Vehicle control (DMSO)	44.0 ± 5.8	1200 ± 700 nM

[a] Statistical analyses of test compounds vs vehicle control were performed using Student's unpaired t-test. E_{max} values are considered as statistically significant if *p*-value < 0.05.

[b] Statistical analyses were not performed on the EC_{50} of test compounds vs vehicle control because DMSO showed low E_{max}, as it is not considered as bioactive. The minor relaxation activity of DMSO could be due to non-specific solvent-tissue interactions.

Appendix 86: Potency and maximal response of the relaxation activity of alkaloids **2** – **4**, atropine and DMSO on rat isolated trachea.

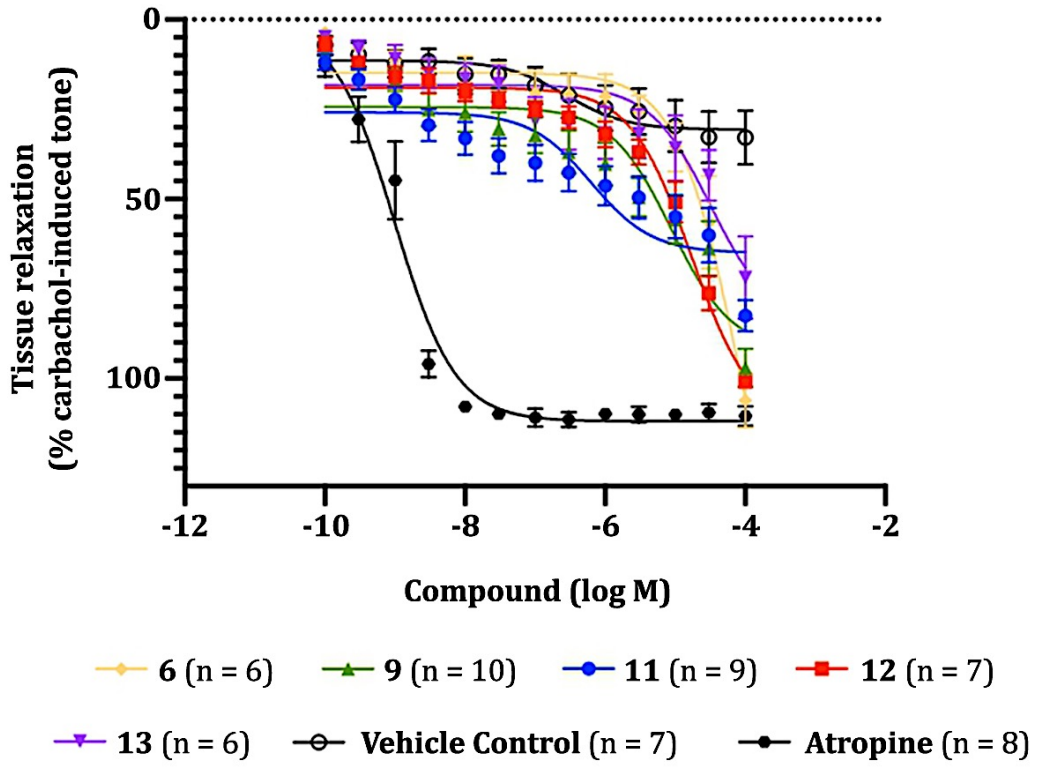

Appendix 87: Antispasmodic activity of alkaloids **6**, **9**, **11** – **13**, atropine and DMSO on rat isolated trachea.

Compound	E_{max} (%) (mean ± SEM) (*p*-value)[a]
6	106.1 ± 7.5 (< 0.0001)
9	97.0 ± 5.2 (< 0.0001)
11	82.46 ± 4.2 (< 0.0001)
12	100.9 ± 1.4 (< 0.0001)
13	71.9 ± 11.3 (0.0432)
Atropine	111.7 ± 1.7 (< 0.0001)
Vehicle control (DMSO)	30.7 ± 7.4

[a] Statistical analyses of test compounds vs vehicle control were performed using Student's unpaired t-test. E_{max} value is considered as statistically significant if *p*-value < 0.05.

Appendix 88: Maximal response of the relaxation activity of alkaloids **6**, **9**, **11** – **13**, atropine and DMSO on rat isolated trachea.

Compound*	IC_{50} ± SD (μM)								
	AsPC-1[a]	SW1990[a]	BxPC-3[a]	PANC-1[a]	MCF-7[b]	MDA-MB-468[c]	MDA-MB-231[c]	MCF-10A[d]	MRC-5[e]
11	>100	50.84 ± 2.11	80.4 ± 3.40	69.36 ± 3.33	NT	NT	NT	NT	79.31 ± 7.99
13	5.68 ± 0.49	10.85 ± 1.63	5.53 ± 0.24	2.30 ± 0.48	NT	NT	NT	NT	11.12 ± 1.14
14	3.43 ± 0.14	5.20 ± 0.24	2.17 ± 0.12	1.13 ± 0.24	NT	NT	NT	NT	4.15 ± 0.21
15	39.80 ± 3.94	23.48 ± 3.12	41.79 ± 79.4	40.84 ± 0.22	47.77 ± 1.34	32.73 ± 2.19	42.43 ± 2.77	80.44 ± 1.81	NT
16	15.47 ± 4.14	32.31 ± 1.91	70.93 ± 3.49	49.88 ± 2.92	38.64 ± 8.39	45.93 ± 4.43	43.31 ± 0.43	80.88 ± 1.72	NT
20	35.37 ± 1.15	29.26 ± 0.29	46.66 ± 1.14	20.76 ± 0.35	36.79 ± 0.50	16.62 ± 0.83	13.32 ± 0.11	91.77 ± 0.38	NT
22	30.47 ± 0.50	24.25 ± 2.00	28.41 ± 1.09	14.85 ± 1.09	20.02 ± 4.78	21.04 ± 4.21	19.99 ± 2.19	81.17 ± 1.20	NT
Curcumin	23.22 ± 0.90	19.53 ± 2.32	20.19 ± 0.89	18.51 ± 0.56	50.93 ± 2.31	17.35 ± 1.89	15.35 ± 2.10	80.93 ± 2.11	NT
Gemcitabine	29.11 ± 0.44	25.41 ± 0.79	25.92 ± 2.44	30.00 ± 5.11	NT	NT	NT	21.22 ± 2.31	35.12 ± 3.21
Cisplatin	NT	NT	NT	NT	8.99 ± 0.41	7.07 ± 0.12	6.22 ± 0.11	6.29 ± 0.17	NT

[a]Human pancreas adenocarcinoma
[b]Human breast adenocarcinoma (luminal breast cancer, ER+, PR+)
[c]Human breast adenocarcinoma (triple-negative breast cancer)
[d]Non-tumorigenic human breast cells
[e]Non-tumorigenic human lung fibroblast
* Three replicates were conducted for the cytotoxic bioassay of each compounds.
NT - Not tested

Appendix 89: Cytotoxic effects of **11**, **13 – 16**, **20**, **22** and positive controls on pancreatic and breast cancer cell lines.

Appendix 90: Methodology of Antispasmodic Bioassay.

Test Compounds and Krebs-Ringer Bicarbonate Solution: KCl and carbachol (Nacalai Tesque) were dissolved in purified water (ELGA PURELAB®) to prepare 100 mM stock solutions. Alkaloids **2** – **4**, **6**, **9**, **11** – **13** and atropine sulfate (positive control, muscarinic receptor antagonist) were dissolved in DMSO (vehicle) to prepare 100 mM stock solutions before being diluted down in purified water (final bath concentration of vehicle was < 0.2 % (v/v)). The Krebs-Ringer bicarbonate solution was freshly prepared daily following the composition (nM): NaCl 120, KCl 5.4, $MgSO_4.7H_2O$ 1.2, KH_2PO_4 1.2, $NaHCO_3$ 25, D-glucose 11.7, $CaCl_2$ 1.26 and gassed with 95% O_2, 5% CO_2.

Tissue Preparation: Ethical approval was obtained from the University of Nottingham's Animal Welfare and Ethics Review Body (UNMC12). All applicable international, national and/or institutional guidelines for the care and use of animals were followed. Male Sprague Dawley rats (235 **–** 440 g; 2 **–** 3 months old) purchased from University Putra Malaysia, were sacrificed on the day of experiment. Rat respiratory tract was removed and the trachea section was excised into 2 mm rings. Changes in muscle tension produced by tissue contraction were detected by a force transducer (MLTF050/ST, ADInstruments, US). Data were recorded by a PowerLab data acquisition system (LabChart v7.3.4) displayed on a computer. Muscle tension was expressed in milliNewtons (mN). Tissues were left to equilibrate to bath conditions for 30 minutes after the application of 9.8 mN tension. Following equilibration, all tissues were exposed twice to 60 mM KCl to assess tissue viability and to provide reference contractions for subsequent data

analysis. After the KCl was washed out and a stable basal tone was re-established, experiments were carried out as per the procedures below.

Antispamodic Effects of Alkaloids 2 – 4, 6, 9, 11 – 13: The tracheal segments were pre-contracted with 1 μM carbachol to elicit an approximate 80% of the 60mM KCl contracture response. Cumulative concentration-response curve was determined for each compound once the carbachol contraction has reached plateau. The degree of response (tissue relaxation) was measured as the tissue tension in increasing alkaloid concentrations. Tissue relaxation of compounds **2** – **4**, **6**, **9**, **11** – **13** and atropine sulfate (positive control) was expressed as a percentage of 1 μM carbachol-induced tone.

Statistical Analysis: Data were analysed and CRCs were generated using PRISM v7.0 (GraphPad software). All data were expressed as mean ± standard error of mean (SEM) of n number of animals. Maximum tissue relaxation response (E_{max}) and half maximal effective concentration of tissue relaxation (IC_{50}) were derived from non-linear regression analysis of the obtained individual concentration-response curves. Statistical analyses were performed using Student's unpaired t-test (two tailed, single variance). Results were considered statistically significant if p-value < 0.05.

Appendix 91: Methodology of Cytotoxic Bioassay.

Cell Lines and Cell Culture: A panel of human pancreatic (AsPC-1, BxPC-3, PANC-1 and SW 1990) and breast (MCF-7, MDA-MB-468 and MDA-MB-231) cancer cell lines, human normal lung fibroblast cells (MRC-5), and non-tumorigenic human breast cell (MCF-10A) was purchased from the American Type Culture Collection (ATCC). All cancer cells were maintained in RPMI 1640 medium with 10% fetal bovine serum, 100 IU/mL penicillin, and 100 μg/mL streptomycin (Sigma-Aldrich, St. Louis, MO, USA), while MRC-5 and MCF-10A cells were cultured in DMEM/F12 added with 5% horse serum, 20 ng/mL epidermal growth factor, 0.5 μg/mL hydrocortisone, 10 μg/mL insulin, 100 IU/mL penicillin, and 100 μg/mL streptomycin.All cells were maintained in an incubator at 37 °C and 5% carbon dioxide.

Luminescent Cell Viability Assay: Cell viability after treatment with **11**, **13** –**16**, **20**, **22**, curcumin, gemcitabine and cisplatin were determined using a CellTiter-Glo luminescent cell viability assay kit (Promega, Madison, WI, USA). All compounds were prepared in 100 mM DMSO as a stock solution and diluted to various concentrations (1.5 to 100 μM) using sterile phosphate buffer solution. Gemcitabine and cisplatin were tested at concentrations of 0.01 – 10 μM as a positive control in this assay. The cancer and non-cancer cells were seeded in 384-well opaque plates for 24 hours at a density of 1000 cells/well, followed by treatment with **11**, **13** – **16**, **20**, **22**, curcumin, gemcitabine and cisplatin for 72 h. Cells treated with 0.1% DMSO were used as negative controls. Luminescence reading was measured using a SpectraMax M3 Multi-Mode microplate reader (Radnor, PA, USA). The inhibitory concentration of 50% cell viability (IC_{50}) was

determined based on the luminescent reading of treated cells and cells treated with the negative control. A replicate of n = 3 was conducted for each test compounds.